

Displacement-Based Seismic Design of RC Wall-Frame Buildings and
Asymmetric Plan Buildings

by

Farrokh Fazileh

A thesis submitted to the Faculty of Graduate and Postdoctoral
Affairs in partial fulfillment of the requirements
for the degree of

Doctor of Philosophy

in

Civil Engineering

Carleton University
Ottawa, Ontario

© 2011

Farrokh Fazileh



Library and Archives
Canada

Published Heritage
Branch

395 Wellington Street
Ottawa ON K1A 0N4
Canada

Bibliothèque et
Archives Canada

Direction du
Patrimoine de l'édition

395, rue Wellington
Ottawa ON K1A 0N4
Canada

Your file *Votre référence*
ISBN: 978-0-494-81536-6
Our file *Notre référence*
ISBN: 978-0-494-81536-6

NOTICE:

The author has granted a non-exclusive license allowing Library and Archives Canada to reproduce, publish, archive, preserve, conserve, communicate to the public by telecommunication or on the Internet, loan, distribute and sell theses worldwide, for commercial or non-commercial purposes, in microform, paper, electronic and/or any other formats.

The author retains copyright ownership and moral rights in this thesis. Neither the thesis nor substantial extracts from it may be printed or otherwise reproduced without the author's permission.

In compliance with the Canadian Privacy Act some supporting forms may have been removed from this thesis.

While these forms may be included in the document page count, their removal does not represent any loss of content from the thesis.

AVIS:

L'auteur a accordé une licence non exclusive permettant à la Bibliothèque et Archives Canada de reproduire, publier, archiver, sauvegarder, conserver, transmettre au public par télécommunication ou par l'Internet, prêter, distribuer et vendre des thèses partout dans le monde, à des fins commerciales ou autres, sur support microforme, papier, électronique et/ou autres formats.

L'auteur conserve la propriété du droit d'auteur et des droits moraux qui protège cette thèse. Ni la thèse ni des extraits substantiels de celle-ci ne doivent être imprimés ou autrement reproduits sans son autorisation.

Conformément à la loi canadienne sur la protection de la vie privée, quelques formulaires secondaires ont été enlevés de cette thèse.

Bien que ces formulaires aient inclus dans la pagination, il n'y aura aucun contenu manquant.

**
Canada

Abstract

A displacement-based design of buildings for seismic forces is better able to meet the desired performance criteria than a force-based design. In the present work Displacement-Based Seismic Design (DBSD) procedures are developed for reinforced concrete wall-frame structures and structures with asymmetry in their plan. The buildings are designed to meet three performance criteria: the ductility demand should not exceed the ductility capacity, global P- Δ instability should not occur, and the drifts should remain within the limits that would minimize structural and non-structural damage. These performance criteria are satisfied by imposing limits on the ultimate displacement of the structures.

In the DBSD for reinforced concrete wall-frame structures simple empirical relations are used to estimate the yield curvature of the wall and yield and ultimate displacements of the structure. These estimates are refined during subsequent iterations through moment curvature and pushover analyses.

A parametric study of the seismic behaviour of single-storey systems forms the basis for the proposed DBSD for asymmetric plan buildings. It is shown that depending on the level of torsional stiffness in a structure, the first mode alone or the first two modes are sufficient to obtain reasonable estimates of the global yield and acceptable ultimate displacements.

Both DBSD procedures employ inelastic response spectrum in A–D format constructed for the acceptable ductility to represent the seismic demand. The demand spectrum is entered at the acceptable ultimate displacement in an equivalent single-degree-of-freedom system for obtaining an estimate of the design base shear. Further design iterations are required to get better estimates of the global yield and ultimate displacements. Such iterations are carried out until convergence is achieved in the design base shear. A multi-mode pushover analysis is then carried out to improve the estimates of internal forces in different structural elements. These estimates are used to design the structural elements.

The proposed DBSD procedures are applied in the seismic design of several wall-frame structures and plan asymmetric buildings. Nonlinear time-history analyses of the designed structures are carried out for their response to a series of spectrum compatible ground motions to assess the performance of the proposed DBSD procedures.

Acknowledgement

I would like to express my deepest appreciation to many people without whose support this work could not have been completed.

I owe my deepest gratitude to Professor Jag Mohan Humar. He supported me in many ways during my research. I am thankful for the opportunity to work with one of the elites in the field of Earthquake Engineering. This work has been enriched by his guidance, and has benefited by his many years of experience.

I would like to thank Carleton University for supporting me financially and providing me with a peaceful environment to study. Also I am thankful to the sponsors of “Indira Gandhi Fellowship” which helped me to alleviate some of my financial burdens.

My fellow researchers and friends made all these years a memorable chapter of my life. I appreciate their moral supports and wish them all great health, happiness and prosperity.

I would like to dedicate this thesis to my parents whose love, support, and blessings encouraged me all along this path from the very first day of my elementary school.

Farrokh Fazileh

Spring 2011, Ottawa, Canada

Table of Contents

| | |
|--|------|
| Abstract | ii |
| Acknowledgement | iv |
| Table of Contents..... | v |
| List of Tables | ix |
| List of Figures | xi |
| Notations | xvi |
| Acronyms | xxii |
| Chapter 1. Introduction | 1 |
| 1.1 General | 1 |
| 1.2 Performance based seismic design..... | 1 |
| 1.3 Displacement-based seismic design..... | 5 |
| 1.3.1 Nonlinear Static Procedures | 6 |
| 1.3.2 Capacity Spectrum Method (ATC-40) | 7 |
| 1.3.3 Coefficient method (FEMA 356) | 10 |
| 1.4 Literature on displacement-based seismic design..... | 13 |
| 1.5 Literature on DBSD of reinforced concrete structures | 15 |
| 1.6 Literature on torsional behaviour in asymmetric plan buildings | 18 |
| 1.7 Previous studies at Carleton University | 23 |
| 1.8 Objective and scope | 25 |
| 1.9 Layout of the Report | 27 |
| Chapter 2. Displacement-based design of hybrid wall-frame structures | 40 |
| 2.1 Introduction | 40 |
| 2.2 Estimation of yield and ultimate displacements..... | 40 |
| 2.2.1 Yield displacement..... | 40 |
| 2.2.2 Ultimate displacement..... | 45 |
| 2.3 Inflection height estimate..... | 46 |
| 2.4 Equivalent SDOF model | 48 |
| 2.5 Determination of inelastic response spectrum | 49 |

| | | |
|------------|---|-----|
| 2.6 | Capacity diagram and pushover analysis | 51 |
| 2.7 | Modal Pushover analysis | 53 |
| 2.8 | Displacement based seismic design procedure | 55 |
| Chapter 3. | Application of DBSD procedure for wall-frame structures..... | 66 |
| 3.1 | Introduction | 66 |
| 3.2 | Problem definition..... | 66 |
| 3.3 | DBSD of the five buildings..... | 67 |
| 3.3.1 | Inflection height | 68 |
| 3.3.2 | Wall yield and ultimate curvatures..... | 69 |
| 3.3.3 | Yield and ultimate displacement | 70 |
| 3.3.4 | Equivalent SDOF systems..... | 71 |
| 3.4 | Structural model | 73 |
| 3.5 | Pushover analysis | 75 |
| 3.6 | Multi-mode pushover analysis | 76 |
| 3.7 | Verification of DBSD for wall-frames structures | 78 |
| 3.7.1 | Selection of ground motions..... | 78 |
| 3.7.2 | Nonlinear time history analysis | 79 |
| 3.7.3 | Results | 80 |
| 3.7.4 | Verification..... | 81 |
| 3.8 | Summary and conclusions | 82 |
| Chapter 4. | Nonlinear seismic response of single-storey asymmetric plan buildings.. | 110 |
| 4.1 | Introduction | 110 |
| 4.2 | Asymmetric plan buildings | 110 |
| 4.3 | Analytical tools | 112 |
| 4.3.1 | BST ultimate surface | 112 |
| 4.3.2 | Incremental dynamic analysis (IDA) | 115 |
| 4.4 | Torsionally unrestrained and restrained systems | 116 |
| 4.5 | Modal decomposition..... | 118 |
| 4.6 | Different torsional systems | 119 |
| 4.6.1 | Torsionally stiff system T1..... | 120 |
| 4.6.2 | Torsionally similar system T2 | 121 |

| | | |
|------------|--|-----|
| 4.6.3 | Torsionally similar system T3 | 122 |
| 4.6.4 | Torsionally very flexible system T4..... | 122 |
| 4.7 | Angle of twist..... | 123 |
| 4.8 | Summary and conclusion | 125 |
| Chapter 5. | Displacement based seismic design of asymmetric plan buildings | 145 |
| 5.1 | Introduction | 145 |
| 5.2 | Angle of twist..... | 146 |
| 5.2.1 | Twist within the elastic limit..... | 147 |
| 5.2.2 | Twist within inelastic range | 148 |
| 5.2.3 | Effect of rotational mass..... | 150 |
| 5.2.4 | Proposed angle of twist | 154 |
| 5.3 | Equivalent yield displacement estimates | 155 |
| 5.4 | Equivalent ultimate displacements..... | 156 |
| 5.4.1 | Equivalent ultimate displacement as governed by ductility limit | 157 |
| 5.4.2 | Equivalent ultimate displacement estimate as controlled by drift limit | 157 |
| 5.4.3 | Equivalent ultimate displacement estimate as governed by the stability limit | 159 |
| 5.5 | Capacity Spectrum Method (CSM)..... | 159 |
| 5.6 | Modal pushover analysis..... | 162 |
| 5.7 | DBSD for asymmetric plan buildings | 164 |
| Chapter 6. | Case studies on DBSD of asymmetric plan buildings | 172 |
| 6.1 | Introduction | 172 |
| 6.2 | Torsionally stiff building | 172 |
| 6.2.1 | Problem definition..... | 172 |
| 6.2.2 | DBSD of torsionally stiff building | 173 |
| 6.2.3 | Multi-mode pushover analysis | 176 |
| 6.3 | Verification of DBSD for torsionally stiff system | 177 |
| 6.3.1 | Ground motions..... | 177 |
| 6.3.2 | Structural model | 178 |
| 6.3.3 | Results | 180 |
| 6.4 | Torsionally flexible Building | 181 |
| 6.4.1 | Problem definition..... | 181 |

| | | |
|-------------|--|-----|
| 6.4.2 | DBSD for torsionally flexible building | 182 |
| 6.4.3 | Multi-mode pushover analysis | 186 |
| 6.5 | Verification of DBSD for torsionally flexible system | 187 |
| Chapter 7. | Summary and conclusions | 203 |
| 7.1 | Summary | 203 |
| 7.1.1 | Summary of DBSD for wall-frame structures..... | 203 |
| 7.1.2 | Summary of DBSD for asymmetric plan buildings | 204 |
| 7.2 | Conclusions | 206 |
| 7.2.1 | Concluding remarks for DBSD of wall-frame structures..... | 206 |
| 7.2.2 | Concluding remarks related to DBSD of asymmetric plan buildings | 207 |
| 7.3 | Recommendations for future research | 209 |
| Appendix A. | Case Study 12-storey wall-frame structures..... | 211 |
| Appendix B. | Supplementary data on multi-mode pushover and nonlinear time-history analyses..... | 274 |
| Appendix C. | Case studies for asymmetric plan buildings..... | 292 |
| References | | 333 |

List of Tables

| | |
|---|-----|
| Table 1.1: Design earthquake levels proposed by Vision 2000 & FEMA 273 | 30 |
| Table 1.2: Improved effective parameters to be used in CSM | 31 |
| Table 1.3: Coefficients for use in equations for effective damping | 32 |
| Table 1.4: Coefficients for use in equations for effective periods | 33 |
| Table 2.1: Values of η for different steel and reinforced concrete sections suggested by Paulay (2000) | 57 |
| Table 3.1: Characteristics of the wall-frame buildings | 84 |
| Table 3.2: Estimates of DBSD parameters in different iterations of the five buildings..... | 85 |
| Table 3.3: Design parameters of the walls for the five buildings..... | 86 |
| Table 3.4: Details of the equivalent SDOF systems in the DBSD of the five buildings..... | 87 |
| Table 3.5: Acceptable ultimate displacements based on different design limits.... | 88 |
| Table 3.6: Modal characteristics for multi-modal pushover analyses | 89 |
| Table 3.7: Results of multi-mode pushover analyses for the five buildings studied | 90 |
| Table 3.8: Ground motions proposed by SAC for a probability of exceedance of 10% in 50 years for Los Angeles..... | 91 |
| Table 4.1: Characteristics of torsional restrained and unrestrained systems | 127 |
| Table 4.2: Characteristics of different torsional systems | 127 |
| Table 4.3: Dynamic properties of different torsional systems | 128 |
| Table 6.1: Details of the equivalent 2DOF systems for torsionally stiff building | 189 |
| Table 6.2: Dynamic parameters in multi-mode pushover analyses..... | 189 |

| | |
|--|-----|
| Table 6.3: Modal response parameters and their combination..... | 189 |
| Table 6.4: Specifications of the selected ground motions..... | 190 |
| Table 6.5: Nonlinear time history response parameters | 190 |
| Table 6.6 Details of the equivalent 2DOF systems for the first mode of torsionally flexible building..... | 190 |
| Table 6.7 Details of the equivalent 2DOF systems for the second mode of torsionally flexible building..... | 191 |
| Table 6.8: Dynamic parameters in multi-mode pushover analyses..... | 191 |
| Table 6.9: Modal response parameters and their combination..... | 191 |
| Table 6.10: Nonlinear time history response parameters | 192 |

List of Figures

| | |
|--|----|
| Figure 1.1: Minimum performance objectives (Vision 2000) | 34 |
| Figure 1.2: Inelastic seismic analysis procedures for various structural models and ground motion characterization (FEMA 440)..... | 35 |
| Figure 1.3: Bilinear idealization of pushover curve | 36 |
| Figure 1.4: ADRS showing effective period and damping parameters of equivalent linear system along with the capacity curve, as described in FEMA 440. | 37 |
| Figure 1.5: Types of Behaviour considered in improved CSM (FEMA 440)..... | 38 |
| Figure 1.6: Effective post yield stiffness (FEMA 356) | 39 |
| Figure 2.1: Components of the total displacement of wall..... | 58 |
| Figure 2.2: Different plastic hinge length relations for walls..... | 59 |
| Figure 2.3: Bilinear simulation a) moment-curvature relation b) capacity diagram | 60 |
| Figure 2.4: Idealized stress-strain relationships for A) unconfined concrete, B) reinforcing steel (Yavari 2001)..... | 61 |
| Figure 2.5: Capacity Spectrum Method Chopra and Goel (1999)..... | 62 |
| Figure 2.6: $R_y-\mu-T_n$ relations according to Krawinkler and Nassar for elasto-plastic force deformation relationship..... | 63 |
| Figure 2.7: Inelastic response spectrum for El Centro ground motion for $\mu=2.9$ | 64 |
| Figure 2.8: Wall-Frame plastic mechanism, and internal force distribution | 65 |
| Figure 3.1: Typical plan view of the wall-frame buildings | 92 |
| Figure 3.2: Design response spectrum and average of the spectra of 20 selected earthquakes | 93 |
| Figure 3.3: Normalised inflection height of the 5 wall-frame buildings | 94 |

| | |
|---|-----|
| Figure 3.4: Details of the longitudinal reinforcements for the final design of shear wall for the 12-storey building..... | 95 |
| Figure 3.5: Global yield displacement estimates..... | 96 |
| Figure 3.6: Ultimate displacement estimates..... | 96 |
| Figure 3.7: Capacity and demand diagrams for the 6-storey building for first and last iterations | 97 |
| Figure 3.8: Capacity and demand diagrams for the 9-storey building for the first and last iterations | 97 |
| Figure 3.9: Capacity and demand diagrams for the 12-storey building for the first and last iterations | 98 |
| Figure 3.10: Capacity and demand diagrams for the 15-storey building for the first and last iterations | 98 |
| Figure 3.11: Capacity and demand diagrams for the 20-storey building for the first and last iterations | 99 |
| Figure 3.12: Structural model for the 20-storey building and development of plastic hinges | 100 |
| Figure 3.13: Pushover curve and its bi-linear idealization for the 6-storey building | 101 |
| Figure 3.14: Pushover curve and its bi-linear idealization for the 9-storey building | 101 |
| Figure 3.15: Pushover curve and its bi-linear idealization for the 12-storey building | 102 |

| | |
|---|-------|
| Figure 3.16: Pushover curve and its bi-linear idealization for the 15-storey building | 102 |
| | |
| Figure 3.17: Pushover curve and its bi-linear idealization for the 20-storey building | 103 |
| | |
| Figure 3.18: Distribution of the maximum storey shear in the five buildings subjected to twenty ground motions | 104 |
| Figure 3.19: Distribution of the maximum inter-storey drifts in the five buildings subjected to twenty ground motions | 105 |
| Figure 3.20: Distribution of the maximum storey displacements in the five buildings subjected to twenty ground motions | 106 |
| Figure 3.21: Comparison of storey shears in multi-modal pushover analyses with the Mean of twenty Nonlinear Time-history Analyses..... | 107 |
| Figure 3.22: Comparison of inter-storey drift in multi-modal pushover analyses with the Mean of twenty Nonlinear Time-history Analyses..... | 108 |
| Figure 3.23: Comparison of storey displacements in multi-modal pushover analyses with the Mean of twenty Nonlinear Time-history Analyses..... | 109 |
| Figure 4.1: BST surface for a symmetric plan, from De La Llera et al (1995).... | 129 |
| Figure 4.2: Typical BST surfaces for plan asymmetric building | 130 |
| Figure 4.3: Typical IDA curves by Vamvatsikos and Cornell (2002) | 131 |
| Figure 4.4: BST surface and IDA results for torsionally unrestrained system (S1) | |
| | 132 |
| Figure 4.5: Base shear IDA curves for torsionally unrestrained system (S1) | 132 |
| Figure 4.6: BST surface and IDA results for torsionally restrained system (S2).. | 133 |

| | |
|--|-----|
| Figure 4.7: Base shear IDA curves for torsionally unrestrained system (S2) | 133 |
| Figure 4.8: BST surface and IDA results for torsionally restrained system (S3).. | 134 |
| Figure 4.9: Base shear IDA curves for torsionally unrestrained system (S3) | 134 |
| Figure 4.10: Modal response contributions for system T1 | 135 |
| Figure 4.11: Modal response contributions for system T2..... | 136 |
| Figure 4.12: Modal response contributions for system T3..... | 137 |
| Figure 4.13: Modal response contributions for system T4..... | 138 |
| Figure 4.14: Modal contribution of response of system T4 at flexible and stiff side edges of the building..... | 139 |
| Figure 4.15: Flexible plane response and the estimates based on angle of twist for system S1 | 140 |
| Figure 4.16: Flexible plane response and the estimates based on angle of twist for system S2 | 141 |
| Figure 4.17: Flexible plane response and the estimates based on angle of twist for system S3 | 142 |
| Figure 4.18: Uncoupled frequency ratios | 143 |
| Figure 4.19: Angle of twist for translation dominant mode | 144 |
| Figure 5.1: Plan view of torsionally balanced, system 1, and torsionally unrestrained, system 2 (Castillo et al 2001)..... | 168 |
| Figure 5.2: System rotation and nominal rotations (Castillo et al 2001)..... | 168 |
| Figure 5.3: Torsion factor as a function of normalized stiffness eccentricity and normalized stiffness ratio (Sommer and Bachmann 2005)..... | 169 |

| | |
|---|-----|
| Figure 5.4: Normalized modified eccentricity as a function of normalized stiffness eccentricity and normalized stiffness ratio (Sommer and Bachmann 2005) | 169 |
| Figure 5.5: Deformed shape corresponding to the first and second normalised mode shapes..... | 170 |
| Figure 5.6: DBSD procedure for asymmetric plan buildings..... | 171 |
| Figure 6.1: Plan layout of torsionally stiff system | 193 |
| Figure 6.2: Translational and normalised rotational components of the first six modes | 194 |
| Figure 6.3: Pushover curves for the first six modes | 195 |
| Figure 6.4: Target spectrum and the scaled spectra for five ground motions | 195 |
| Figure 6.5: Displacement-time histories..... | 196 |
| Figure 6.6: Base shear time histories..... | 197 |
| Figure 6.7: Plan view of torsionally flexible system | 198 |
| Figure 6.8: Translational and rotational components of the mode shapes | 199 |
| Figure 6.9: Pushover curves for the first six modes | 200 |
| Figure 6.10: Displacement-time histories..... | 201 |
| Figure 6.11: Base shear time histories..... | 202 |

Notations

| | |
|-----------------|---|
| $\mathbf{1}$ | Unit vector |
| α | Post-yield stiffness ratio |
| | Ratio of frame contribution to the base shear |
| | Strength ratio of the orthogonal planes |
| | Modification factor for plan rotation |
| α_i | Response modal contribution in i^{th} mode |
| β | Strength ratio parameter for parallel planes |
| β_{eq} | Equivalent damping ratio |
| Γ | Mass participation factor |
| Δ_{CM} | Displacement at center of mass |
| Δ_{fyr} | Yield displacement of the frame at roof |
| Δ_i | Displacement of plane i |
| δ_t | Maximum total displacement at roof level |
| δ_u | Ultimate displacement of SDOF |
| Δ_u | Ultimate displacement |
| Δ_{ucm} | Maximum displacement at the center of mass |
| Δ_{ui} | Maximum displacement of element i |
| Δ_{ui}^* | Equivalent ultimate displacement of plane i at center of mass |
| Δ_{wy} | Yield displacement of the wall |
| Δ_{wyr} | Yield displacement of the wall at roof |
| δ_y | Yield displacement of SDOF |
| Δ_y | Global yield displacement |

| | |
|---------------------------------|---|
| Δ_{yi}^* | Equivalent yield displacement of plane i at center of mass |
| ε_y | Yield strain of steel |
| η | Correction factor for effective yield curvature |
| θ_{fy} | Inter-storey yield rotation of the frame |
| θ_N | Nominal rotation in the plan |
| θ_n | Inter-storey drift ratio at n^{th} storey |
| θ_m | Nominal rotation for element i |
| θ_p | Plastic rotation in the wall plastic hinge |
| θ_t | Angle of twist resulting from stiffness eccentricity |
| θ_{vt} | Angle of twist resulting from strength eccentricity at ultimate state |
| κ | Adjustment factor for hysteretic behaviour |
| μ | Ductility |
| ρ | Mass radius of gyration |
| τ_i | Dynamic torque at time step i |
| $\varphi, \varphi_1, \varphi_n$ | Mode shape |
| φ_u | Curvature capacity of the wall |
| φ_y | Effective yield curvature of the wall |
| | Nominal yield curvature of the wall |
| φ'_y | First yield curvature of the wall |
| φ_y^n | Translational component of the mode shape at n^{th} storey |
| φ_θ^n | Rotational component of the mode shape at n^{th} storey |

| | |
|----------------------|---|
| φ_{yn} | Translational component of the n th mode shape |
| $\varphi_{\theta n}$ | Rotational component of the n th mode shape |
| Ψ | Angle of twist |
| Ω | Uncoupled torsional to translational frequency ratio |
| ω_y | Uncoupled translational frequency |
| ω_θ | Uncoupled torsional frequency |
| A | Elastic spectral acceleration |
| a_i | Stiffness coefficient for i th element |
| A_y | Spectral acceleration from inelastic design spectrum |
| b_i | Strength coefficient i th element |
| C_0 | Modification factor to relate maximum displacement of SDOF with MDOF |
| C_1 | Modification factor for to account for inelastic behaviour |
| C_2 | Modification factor to represent the effect of hysteretic shape |
| C_3 | Modification factor to account for P–Δ effect |
| D | Peak spectral displacement of the inelastic system |
| d | Effective depth of the beam |
| $\mathbf{D}(t)$ | Response vector |
| D_b | Depth of the beam |
| $e_{CR.}$ | Strength eccentricity |
| e_{max} | Maximum strength eccentricity |
| e_{min} | Minimum strength eccentricity |

| | |
|--------------------------|--|
| e_{rx}, e_{sx} | Stiffness eccentricity in x direction |
| e_{vx} | Strength eccentricity in the x direction |
| F | Strength of the plane |
| f_i | Lateral load at i^{th} floor |
| H | Height of the wall |
| | Total height of the structure |
| h_e | Wall inflection height |
| H_n | Heigh of n th storey |
| I_{On}^* | Modal static response for base torque |
| J | Total rotational inertia |
| $J_{R,\mu}$ | Ductile rotational stiffness |
| K | Stiffness of the plane |
| $K_{dynamic}$ | Dynamic rotational stiffness |
| K_e | Post-yield effective stiffness |
| K_i | Elastic initial stiffness |
| K_{static} | Static rotational stiffness |
| K_t | Torsional stiffness |
| l_b | Length of the beam |
| l_p | Wall plastic hinge length |
| l_w | Wall length |
| \mathbf{M}, \mathbf{m} | Mass matrix |
| M^* | Effective modal mass |
| M_n | Nominal flexural strength of the wall |

| | |
|---------------------|--|
| M_y | Strength of the wall at first yield |
| n | Number of storeys |
| R, R_y | Elastic strength ratio |
| r_k | Stiffness radius of gyration |
| T_{asym} | Torque arising from asymmetry |
| T_e | Effective period |
| T_{eq} | Equivalent period |
| T_i, T_n | Fundamental period of the structure |
| T_{\max} | Maximum torque |
| T_{\min} | Minimum torque |
| T_n | Natural period |
| T_{orth} | Total torque to be resisted by orthogonal planes |
| u_m | Maximum displacement |
| $u_{\phi,i}$ | Rotation at time step i |
| $ u_y _{\max}$ | Maximum translational response |
| $ u_\theta _{\max}$ | Maximum rotational response |
| V_b, V_{bn} | Base shear |
| V_{bn} | Base torque |
| V_{Ey} | Design base shear in y direction |
| V_f | Shear strength of the frame |
| V_i | Storey shear at i^{th} floor |
| V_w | Shear strength of the wall |
| W | Distance between the flexible and stiff planes |

| | |
|-------|--|
| x_i | Distance of plane i from the center of mass |
| z | Distance between the critical section and the point of contraflexure of the beam |

Acronyms

| | |
|--------|--|
| 2DOF | Two-Degree Of Freedom |
| ABSSUM | Absolute Summation |
| A-D | Acceleration-Displacement |
| ADRS | Acceleration Displacement Response Spectra |
| ATC | Applied Technology Council |
| BST | Base Shear Torque |
| C.M. | Center of Mass |
| CQC | Complete Quadratic Combination |
| CSM | Capacity Spectrum Method |
| DBSD | Displacement-Based Seismic Design |
| DDBD | Direct Displacement-Based Design |
| EPP | Elastic Perfect Plastic |
| FEMA | Federal Emergency Management Agency |

| | |
|-------|--|
| IDA | Incremental dynamic Analysis |
| MCE | Maximum Considered Earthquake |
| MDOF | Multi-Degree Of Freedom |
| MPA | Modal Pushover Analysis |
| NBCC | National Building Code of Canada |
| NEHRP | National Earthquake Hazards Reduction Program |
| NSP | Nonlinear Static Procedure |
| SDOF | Single-Degree Of Freedom |
| SEAOC | Structural Engineers Association of California |
| SRSS | Square root of sum of squares |
| UHS | Uniform Hazard Spectrum |

Chapter 1. Introduction

1.1 General

The force-based method of seismic design of structures, which is the basis of the seismic design provisions of most building codes, is considered as being unable to ensure a uniform level of protection against earthquakes. This is because damage is related to the induced displacements rather than the level of forces. Consequently, interest in a performance based method of design, which would ensure that the structure achieves a specified level of performance under specified earthquake hazard, is increasing. A displacement-based method of design is an important component of a more broad-based performance based design. The present work focuses on the displacement-based design of certain classes of structures. The essential concepts of performance based methods are described in the following sections. Also presented is the current state of the art on the displacement-based design procedures.

1.2 Performance based seismic design

Since the late 1980's and early 1990's and following the extensive economical loss due to structural and non-structural damage caused by a few moderate earthquakes in United States and Japan, performance based engineering has seen considerable development and has come to be recognized as the preferred methodology for the seismic design of structures. In seismic design, performance based engineering provides methods for the design, construction, and maintenance of all kinds of engineering structures, such that

their structural and non-structural elements are capable of achieving a defined level of performance when affected by a specified level of hazard due to earthquake.

In contrast with conventional seismic design, performance based seismic design – a component of performance-based engineering – is a general design philosophy in which the design criteria are expressed in terms of the achievement of stated performance levels when the structure is subjected to stated levels of seismic hazard. These design criteria, involving a combination of performance levels and earthquake levels, are called performance objectives. Minimum performance objective includes Basic Objective, which is the minimum acceptable performance for typical new buildings, and Essential, and Safety critical objectives which are minimum objectives for facilities such as hospitals, and nuclear processing facilities. Minimum performance objectives have been outlined in the Vision 2000 report produced by Structural Engineers Association of California SEAOC (1995) and are presented in Figure 1.1.

Performance level is stated in terms of the amount of acceptable damage sustained by a building when affected by earthquake ground motion. Collapse prevention, life safety, operational, and fully operational are the four performance levels as defined by Vision 2000 report. These levels are discrete points on a continuous scale describing the building's expected performance, or alternatively, how much damage, economic loss, and disruption may occur due to earthquake ground motion. FEMA 273 (1997) report, *Guidelines for the Seismic Rehabilitation of Building*, expresses the four performance levels and the corresponding state of damages as follows:

- 1) Operational: negligible structural and non-structural damage, occupants are safe during event, utilities are available, facility is available for immediate re-use (some cleanup required), and total loss is less than 5% of replacement value
- 2) Immediate occupancy: negligible structural damage, occupants safe during event, minor non-structural damage, building is safe to occupy but may not function, limited interruption of operations, and total loss is less than 15% of replacement value
- 3) Life safety, significant structural damage, some injuries may occur, extensive non-structural damage, building is not safe for reoccupancy until repaired, and total loss is less than 30% of replacement value
- 4) Collapse prevention, extensive (near complete) structural and non-structural damage, significant potential for injury but not wide scale loss of life, extended loss of use, repair may not be practical, and total loss is more than 30% of replacement value

These performance levels need to be quantified with some measurable response parameters like global displacement, inter-storey drift ratio, storey forces, or global ductility demand ratios. Structural and non-structural damages due to strong ground motion have strong correlation with inter-storey drift ratio. It is widely accepted that 0.2%, 0.5%, 1.5%, and 2.5% inter-storey drift limits should be imposed to ensure operational, immediate occupancy, life safety, and collapse prevention performance levels, respectively.

In performance based design, seismic hazard level is estimated by a probabilistic seismic hazard analysis based on the seismicity of the building location. Seismic hazard analysis describes the potential for dangerous earthquake-related natural phenomena such as ground shaking, fault rupture, or soil liquefaction. The design level of seismic hazard obtained by such an analysis is represented by Uniform Hazard Spectrum (UHS). In probabilistic approach to seismic hazard analysis, the hazard is expressed in terms of the value of a given design parameter, such as the peak ground acceleration or a spectral acceleration having a specific probability of exceedance in a given period of time. This is done after taking the three main sources of uncertainty into account, namely a) what is the distance of the epicentre of the earthquake from the site, b) what is the probability of occurrence of the maximum considered earthquakes (MCE), c) how does the ground motion attenuate as it propagates from the source to the site?

The MCE ground motion is defined as the maximum level of earthquake shaking that is considered as a reasonable value of hazard that normal structures should be designed to resist. The MCE ground motion maps developed by NEHRP 1997 provision for United States are based on seismic hazard maps, which are (1) 2%/50 year earthquake ground motion hazard maps for regions that have different ground motion attenuation relationships, and (2) deterministic ground motion maps in regions of high seismicity with the appropriate ground motion attenuation relationships for each region. There are four levels of earthquake ground motions considered for performance based design of structure; Frequent, Occasional, Rare, and Very Rare. Table 1.1 presents the chance of

exceedance and the return period for different earthquake levels as proposed by Vision 2000 report and FEMA 273.

Geological Survey of Canada has developed the MCE ground motion maps of Canada for 2% chance of exceedance in 50 years. The UHS constructed from spectral acceleration at 0.2, 0.5, 1.0 and 2.0 second periods forms the basis of the seismic provisions of the 2005 National Building Code of Canada (NBCC 2005).

1.3 Displacement-based seismic design

Seismic performance of a structure is strongly dependent on the damage suffered by it under the design earthquake. Since damage in structures results from inelastic displacement, assessment of the performance of an existing or new structure requires inelastic structural analysis to determine the magnitude of demand parameters in the structures. These demand parameters are used to compare the performance against the acceptance criteria.

There are five major demand parameters which can be predicted and controlled in performance based design: 1) storey forces, 2) global displacement, 3) inter-storey drift, 4) component distortion (e.g., deformation or curvature) 5) component forces. The first three are global parameters, and the latter two are local. Among these parameters, global displacement (e.g., roof level displacement) and inter-storey drift have been commonly used by the researchers and engineers. A design methodology which specifies acceptable level of displacements and/or drifts to measure performance is referred to as

displacement-based design. It is in fact a component of the performance based design methodology.

1.3.1 Nonlinear Static Procedures

As referred to above, displacement-based seismic deign (DSBD) is a design procedure in which the structure is designed to resist the inelastic displacement demand which is estimated by an inelastic seismic analysis. As summarized in Figure 1.2 extracted from FEMA 440 (2005), based on the level of details in the structural model and characterization of the design ground motions used in the analysis, several inelastic analysis procedures have been defined. Nonlinear dynamic analyses of the structural response to several ground motion records in which the structure is modeled as an assembly of nonlinear elements is assumed to provide the value of response parameters with a low level of uncertainty. However, on account of the high cost of computation, and difficulties in modelling, inelastic dynamic analysis is not often used in designing the structures.

Nonlinear static procedures (NSPs) have been widely used as the tools for estimating the inelastic seismic demand parameters. In general, these procedures use an equivalent single degree of freedom (SDOF) system to represent the actual MDOF system, and response spectra to represent the seismic ground motion. The NSP procedures provide estimate of the maximum global displacement demand (see Figure 1.2). NSPs can be categorized in two groups:

- 1) Equivalent linearization methods, which are based on the assumption that the maximum total displacement of a SDOF system can be estimated by the elastic response of a SDOF system with a longer period and a higher damping ratio.
- 2) Coefficient methods, which estimate the maximum total displacement by multiplying the elastic response by one or more coefficients derived empirically from a series of nonlinear dynamic analyses.

A version of Capacity Spectrum Method (CSM), which is documented in ATC-40 (1996) and belongs to the first category, and a coefficient method presented in FEMA 356 (2000) and its improved form in FEMA 440, which belongs to the second category, are discussed briefly here.

1.3.2 Capacity Spectrum Method (ATC-40)

The capacity spectrum method uses the secant stiffness at maximum displacement, u_m , to compute the period and relates the effective damping to the area under the hysteresis curve shown in Figure 1.3. An equivalent elastic SDOF system is used to estimate the maximum displacement of the actual structure. The equivalent period (T_{eq}) and damping ratio (β_{eq}) of the equivalent SDOF are obtained from:

$$T_{eq} = T_n \sqrt{\frac{\mu}{1 + \alpha\mu - \alpha}} \quad (1.1)$$

$$\beta_{eq} = 0.05 + \kappa \frac{2(\mu - 1)(1 - \alpha)}{\pi\mu(1 + \alpha\mu - \alpha)} \quad (1.2)$$

where, T_n is the fundamental period of the structure, α is the post-yield stiffness ratio of idealized pushover curve (see Figure 1.3), μ is the ductility factor, $\mu = u_m/u_y$, and κ is an adjustment factor to approximately account for characteristics of the hysteretic behaviour of reinforced concrete structures. The 0.05 on the right hand side of Equation 1.2 is the initial elastic viscous damping suggested for reinforced concrete buildings. As expressed in Equations 1.1 and 1.2, the effective parameters of equivalent SDOF system are functions of ductility, and since ductility is the object of analysis, the solution is to be found by iteration or graphical techniques.

Calculation of the maximum displacement demand consists of the following steps as illustrated in Figure 1.4:

- 1) Develop a relation between the base shear and the roof displacement under a selected lateral force distribution (pushover cure).
- 2) Convert the pushover curve to a capacity curve, by dividing the force by effective first mode mass, and the roof displacement by first mode participation factor times the value of first mode shape at roof.
- 3) Construct the Acceleration Displacement Response Spectra (ADRS) from elastic design spectra for 5% damping.
- 4) Plot the capacity curve and the demand spectrum together and find the displacement demand from the intersection of capacity and demand curves. Iterations are involved in this step based on the updated values of T_{eq} , and β_{eq} and are carried out until convergence is achieved.

- 5) Convert the displacement obtained in step 4 to the roof displacement and compare the component deformations against the limiting values for the specified performance level.

Several approximations are involved in the steps outlined above. These are related to the assumptions regarding section properties used in calculating T_n and the use of a very large viscous damping ratio, which according to Chopra and Goel (2000) can lead to significant underestimation of the maximum displacement when compared with that obtained from a nonlinear response history analysis for a wide range of periods. Moreover, iteration is time consuming and may sometimes lead to no solution or multiple solutions. Iwan et al. (2000) have reported that equivalent viscous damping defined as above gives satisfactory results only for a limited period range where a resonance type of response occurs.

FEMA 440 presents an improved procedure for equivalent linearization as a modification to the CSM according to ATC-40. In the improved CSM, the effective period and effective damping ratio of equivalent SDOF system are determined so that the difference between the maximum response of an actual inelastic system and its equivalent linear counterpart is minimized. The equations used to find the effective period, T_{eff} , and effective viscous damping, β_{eff} , are tabulated in Table 1.2, where T_0 and β_0 are elastic period and elastic viscous damping as shown in Figure 1.4.

Two sets of equations are presented in Table 1.2 to estimate the effective period and damping parameters, as defined in Figure 1.4, for different levels of the ductility of the system, one set for the cases where the hysteretic behaviour of the actual inelastic system is known and the other set in which it is unknown. When the hysteretic behaviour is known coefficients A to L can be found from Table 1.3 and Table 1.4 based on the behaviour of the system (bilinear behaviour, stiffness degrading, and strength degrading behaviour, see Figure 1.5).

1.3.3 Coefficient method (FEMA 356)

In contrast with CSM which uses secant stiffness to find the equivalent period, the coefficient method uses an effective stiffness which gives a much smaller effective period as obtained from:

$$T_e = T_i \sqrt{\frac{K_i}{K_e}} \quad (1.3)$$

where T_i is the elastic fundamental period, K_i is the elastic initial stiffness, and K_e is the yield related effective stiffness shown in Figure 1.6. The maximum total displacement at roof level, called target displacement in FEMA 356, can be estimated from:

$$\delta_t = C_0 C_1 C_2 C_3 \frac{T_e^2}{4\pi^2} g \quad (1.4)$$

where, C_0 is modification factor to relate spectral displacement of an equivalent SDOF system to roof displacement of the MDOF system, which can be taken as the first modal participation factor. C_1 is modification factor to relate the expected maximum displacements of an inelastic SDOF oscillator with elastic perfect plastic (EPP) behaviour to the displacement calculated for a linear elastic response. Factor C_1 is expressed as a function of the ratio (R) of the elastic strength demand to the calculated strength capacity, characteristics of the response spectrum, and the effective period. C_2 is modification factor to represent the effect of pinched hysteretic shape, stiffness degradation, and strength deterioration on maximum displacement response. The factor is obtained for different framing systems and structural performance levels. C_3 is modification factor to represent increased displacements due to second order geometric nonlinearity (P- Δ effect). For buildings with positive post yield stiffness C_3 is set equal to 1.0 and for buildings with negative post yield stiffness it is calculated from:

$$C_3 = 1.0 + \frac{|a|(R-1)^{3/2}}{T_e} \quad (1.5)$$

Coefficient method has been evaluated in FEMA 440 for a large number of SDOF systems with a wide range of periods of vibration, lateral strength, and hysteretic behaviour. The systems were subjected to relatively large number of earthquake ground motions (including near-field and far-field ground motions), and the errors in estimating the maximum displacement were quantified through statistical analysis. Some improvement has been proposed for the coefficients, based on the empirical data obtained for the mean value of the maximum displacement of the SDOF oscillators subjected to

ground motion records. It is suggested that coefficient C_1 can be calculated from the following simplified expression:

$$C_1 = 1.0 + \frac{R-1}{aT_e^2} \quad (1.6)$$

where a is equal to 130, 90, and 60 for site classes B, C, and D, respectively. For periods less than 0.2 sec, the value of the coefficient C_1 for 0.2 sec may be used, and for periods greater than 1.0 sec, C_1 may be assumed to be 1.0. According to FEMA 440 coefficient C_2 is to be calculated from the following regardless of the performance objective of the structure:

$$C_2 = 1.0 + \frac{1}{800} \left(\frac{R-1}{T_e} \right)^2 \quad (1.7)$$

For periods less than 0.2 sec, the value of the coefficient C_2 for 0.2 sec may be used, and for periods greater than 0.7 sec, C_2 may be assumed to be 1.0. The coefficient C_2 need only be applied where significant degradation of stiffness and/or strength exists in the structure. Coefficient C_3 is recommended to be eliminated and replaced with a limit on minimum strength required (maximum R) to avoid dynamic instability.

1.4 Literature on displacement-based seismic design

DBSD is a recent tool used in performance based design methodology. The concept of displacement-based seismic design has received much attention in recent years because such design focuses on displacement instead of force as the indicator of performance or damage indicator. Researchers have taken advantage of NSPs to estimate the maximum global displacement demand in structures, and the corresponding local effects on structural elements to design them properly.

Fajfar and Gaspersic (1996) developed a performance evaluation method, called N2 method, in which they used a simplified pushover analysis based on pre-assumed displacement shape to represent the MDOF system with an equivalent SDOF system and used an elastic demand spectrum to estimate the roof demand displacement and to calculate the cumulative damage index in reinforced concrete structures. In the N2 method, the effective period obtained from pushover analysis is used in the calculation of spectral acceleration and Newmark and Hall (1982) empirical $R_y-\mu-T$ relationship are utilized to estimate the inelastic displacement demand. The authors reported that the estimates of global responses for structures that vibrate primarily in their fundamental mode are reasonable, and predictions of local demand parameters (component deformations, energy dissipations, and damage indices) are adequate for design purposes. However, when the higher mode effects are important, the N2 method underestimates some response parameters.

Priestley, MJN. Kowalsky, MJ (2000) have implemented the CSM in their “Direct Displacement-Based Design” (DDBD), in which a limit on maximum displacement is used to determine the required properties of concrete buildings. The acceptable limit is obtained from a displacement profile and is selected to limit material strains or code specified drift limits. They show that the target displacement from DDBD for multi-storey frame building and wall structure are acceptable when compared with results from inelastic time-history analysis. DDBD overestimates the effective damping ratio, but at the same time the uncracked properties make structural components stiffer than is considered in this method; as a result, the higher damping ratio compensates for the use of more flexible structure, and reasonable displacement estimate is obtained.

Fajfar (1999) employed the inelastic demand spectra in CSM to estimate the seismic displacement demand on structures. Using a graphical procedure, Fajfar (1999) showed that displacement demand of a SDOF system can be obtained from the intersection of the idealized capacity diagram and the inelastic demand spectrum which is plotted either by using the Vidic et al. (1994) $R_y-\mu-T$ relationship or directly from time-history analysis of inelastic SDOF system. The N2 method was also formulated in the capacity spectrum format and it was shown that by reversing the steps in N2 method, a direct displacement-based design method can be obtained (see Fajfar 2000).

Chopra (1999) also recommends the use of constant-ductility design spectrum in CSM. He used the three well-known $R_y-\mu-T$ relationships: Newmark and Hall (1982), Krawinkler and Nassar (1992), and Vidic et al. (1994), in estimating the deformation

demand. All of the relationships provided similar results. Chopra reported that ATC-40 underestimated the deformation for a wide range of periods and ductility.

Chopra and Goel (2003) report that the use of linear elastic spectra with increased damping ratio (as recommended in DDBD) does not work well in comparison with an inelastic design spectrum derived using the Newmark-Hall relations. They demonstrate that the use of an inelastic design spectrum provides accurate values of the displacement and ductility demand and also a structural design that satisfies the design criteria for allowable plastic rotation. A similar approach is recommended by Xue (2001) and also by Xue and Chen (2003), namely to modify the DDBD to a non-iterative capacity-spectrum method without the linear approximation of hysteretic behaviour.

1.5 Literature on DBSD of reinforced concrete structures

Paulay (1998) presented the concept of strength dependent stiffness in reinforced concrete components. In contrast with the conventional assumption for stiffness of a reinforced concrete component which assumes the stiffness to be proportional to the component's cross-sectional dimensions, the stiffness is assumed to be equal to the slope of an equivalent bilinear simulation of force–displacement curve of the component. In the moment-curvature analysis of the rectangular walls, Paulay showed that the yield curvature is only related to the wall's length and the yielding strain of the reinforcements. Moreover, it is more or less independent of the reinforcement content and layout, concrete properties, and the intensity of axial load.

Priestley and Kowalsky (1998) also showed that for cantilever shear walls the yield curvature and ultimate curvature are insensitive to variations in axial load ratio, longitudinal reinforcement ratio, and distribution of reinforcement. The yield curvature can be defined as a function of wall length and the yield strain of reinforcing steel. They noted that generally the displacement ductility capacity of the wall structure is limited by the code drifts limit rather than by the curvature ductility capacity of the wall section.

Paulay (2001a) presented a new design procedure based on strength dependant stiffness. He showed that the yield displacement of different reinforced concrete elements can be calculated when the yield curvature of its section is known. It was postulated that the designer had the freedom to assign the strength to different lateral force-resisting components. This was in contrast to the conventional method in which the strength required in each of the lateral force-resisting elements was obtained based on stiffness calculated from cross-sectional dimensions.

Paulay (2001b) presented a displacement-based design method in which the maximum earthquake-induced displacement demand was obtained based on the maximum displacement capacity of the global structure. It was shown that the maximum displacement ductility capacity of a wall could be obtained from the acceptable drift ratio, maximum allowable steel strain, and the aspect ratio of the wall. Paulay noted that the displacement limit for the global structure would be determined before the design started. It was also shown that the freedom to assign the strength to the lateral force-resisting

components enabled the designer to choose the locations of the centres of strength and stiffness for a system. Therefore, the adverse effects of torsional phenomena could be mitigated or even eliminated.

Aschheim (2002) proposed a new seismic design method based on the yield displacement, which, he argued, was a more stable and more useful parameter in seismic design than the fundamental period of the structure. It was shown that the yield displacement of a structure responding in flexural mode was a function of the yield strain of the material, the height of the structure, the depth of the yielding members, the shape of the predominant mode of response, and the distribution of mass and stiffness throughout the structure. It was noted that the yield displacement was almost independent of strength and could be calculated early in the design process. Entering the equivalent SDOF yield displacement on the yield point spectra with allowable ductility the required strength could be calculated.

Paulay (2002a) presented a displacement-based design focused on wall-frame reinforced concrete structures. He showed that the displacement limits for ductile system to satisfy the performance criteria, could be estimated precisely before the design of the structure started. However, the displacement capacity of the critical elements could control the maximum acceptable displacement demand on the structure.

Sullivan et al. (2006) presented a direct displacement-based design procedure for frame-wall structures. Taking the interaction of the frame and the wall into account, a set

of expressions was proposed for displacement shape and equivalent viscous damping of frame-wall structure at maximum response. The authors stated that although the strength could be assigned arbitrary to the frame and wall, one could improve the design by altering the proportions of the shear assigned to the two segments. If a large fraction of the shear was assigned to the wall, one would have a heavily reinforced wall and lightly reinforced beams and columns at the end of design. On the other hand, if a large fraction of the shear was assigned to the frame, the height of the point of inflection would be lower. A low height for the point of inflection could impose a higher curvature ductility demand on the wall. When this was unacceptable, either the design storey drift would have to be reduced or a larger fraction of strength assigned to the wall.

1.6 Literature on torsional behaviour in asymmetric plan buildings

Asymmetric plan buildings experience torsional motion as well as translational motion when excited by ground motion. This coupled motion causes non-uniform seismic demand on structural elements that makes them highly vulnerable to damage due to earthquake forces. Therefore, study of the inelastic torsional behaviour in asymmetric plan building has been a subject of interest to many researchers. Elastic torsional seismic behaviour of asymmetric plan building has been investigated exhaustively and there is a consensus among the researcher on how asymmetric plan buildings respond to strong ground motion. Nevertheless, that is not the case for inelastic seismic response of asymmetric plan buildings.

In general, the elastic torsional response of asymmetric plan buildings to strong ground motions are governed by 1) eccentricity between the center of mass and center of stiffness, and 2) the ratio of uncoupled torsional to translational frequencies. The inelastic torsional response, on the other hand, is affected both by the stiffness and strength distribution in plan of the building; also the response is sensitive to how the structure enters into the inelastic range (Castillo et al 2001, Humar and Kumar 1999, and Myslimaj and Tso 2002). As a result, inelastic torsional response of asymmetric plan is strongly dependent on the characteristics of the input ground motion with a greater dispersion than the elastic response. Depending on the frequency content and the intensity of the input ground motion the inelastic rotation in the plan may be smaller or larger than the elastic rotation (Perus and Fajfar 2002).

One-storey models have been used widely as the main tool to investigate the inelastic torsional coupling in asymmetric plan buildings. Recently multi-storey buildings have been used to study more realistic behaviour of plan asymmetric buildings; however they are limited to only a few cases of real buildings. Several review papers (Rutenberg 1992 and 2002, and De Stefano and Pintucchi 2008) have summarized the state-of-the-art of inelastic torsional behaviour of structures. Here some of the most important works on the seismic response of asymmetric plan buildings are reviewed and their results are discussed.

The base shear and torque surface (BST) was introduced by De La Llera and Chopra (1995) as a useful tool to understand the behaviour of asymmetric plan buildings.

BST surface represents all combinations of shear and torque that applied statically lead to collapse of the structure. The shape of BST surface is a function of lateral and torsional strength of the system, the plan-wise strength distribution, and the strength eccentricity. It is shown that the nonlinear response of the building does not change if the global elastic properties and the global resisting capacities of the system remain the same. The BST surface and the use of it in understanding the behaviour of asymmetric plan buildings are discussed in more details in Chapter 4.

Trombetti and Conte (2005) developed a procedure, called “alpha method”, to estimate the maximum rotational response of single-storey base isolated structure under free and forced vibration. Alpha is a dimensionless parameter that is defined as being the product of the mass radius of gyration of the structure and the ratio of the maximum rotational to the maximum longitudinal displacement response developed by a one-storey eccentric system. It has been reported that alpha is weakly dependent on the excitation and strongly dependent on the stiffness eccentricity and the ratio of lateral to rotational uncoupled frequencies.

Pettinga et al (2006) studied the seismic response of a series of torsionally unrestrained and restrained single-storey structures under unidirectional earthquake loading focusing on the residual deformation due to torsional response. They report that for torsionally restrained systems, a reduction in the residual rotation of the plan can be obtained with a decrease in the level of torsional restraint. Moreover, it has been pointed

out that the ratio of the residual rotation in plan to the maximum rotation is a function of the ratio of lateral to rotational uncoupled frequencies

Perus and Fajfar (2005) investigated the response of torsionally stiff single storey structures with eccentric mass under bi-axial excitation. In general they found that the inelastic torsional response was qualitatively similar to elastic torsional response, and the displacement demand increased on the flexible side but decreased slightly with increasing plastic hinge deformation. It was shown that the displacement on the stiff side was dependent on several modes of vibration and the influence of the transverse ground motion. It was also mentioned that the reduction of the displacement on the stiff side due to torsion decreased with increasing plastic deformations.

Chopra and Goel (2004) extend the modal pushover analysis procedure to estimate the seismic demand on asymmetric plan buildings. In modal pushover analysis the displacement-controlled nonlinear static analysis of the structure is carried out for the effective earthquake forces obtained from the modal inertia force distribution, which in contrast to a symmetric plan building, includes two lateral forces and torque at each floor level. It has been reported that the accuracy of estimated seismic demand using the modal pushover analysis for unsymmetric plan building is similar to that for symmetric buildings. However, the same is not true when the elastic torsional and translational frequencies are close to each other.

Myslimaj and Tso (2005) studied the asymmetric plan buildings with strength dependent stiffness. They pointed out that if the strength in the plan is assigned in a way that the center of mass locates between the center of stiffness and center of strength, the inelastic rotation in the plan is minimized. They proposed a design-oriented strength allocation procedure to achieve such strength and stiffness eccentricities. Since this procedure will assign more strength to the flexible side of the structure rather than to the stiff side of the structure, it might not be feasible or economical in many real structures. For instance in wall structures the walls on the flexible side should be highly reinforced, while the walls on the stiff will have low axial reinforcement ratios. Aziminejad and Moghadam (2008) pointed out that the balanced location proposed by Myslimaj and Tso optimizes the response when all the lateral resisting elements are yielded, i.e. at life safety performance level. They reported that the proper distribution of strength is dependent on the ground motion level and the strength in a multi-storey structure can be properly assigned similar to one-storey system.

Sommer and Bachmann (2005) studied the dynamic torsional response of multi-storey asymmetric plan reinforced concrete wall structures with strength dependent stiffness. It was suggested that the strength could be assigned to the walls in proportion to the wall length powered by a factor between 1/2 and 2.0. The authors proposed a method to estimate the dynamic response of the building and the displacement profile of the building. This deformed shape along with a few empirical relations obtained from extensive numerical calculations of the dynamic torsional response of wall systems was used to propose a deformation-based seismic design method.

Fajfar et al. (2005) extended the N2 design method to asymmetric plan buildings, proposing that the results of 3D pushover analysis be combined with the results of a linear dynamic (spectral) analysis. It was stated that the linear dynamic analysis gave an upper limit estimate for torsional effects, which controls the target displacement, whereas the pushover analysis results defined the torsional amplifications. The MDOF system was transformed to equivalent SDOF system using the same deformed shape as in the case of planar systems. The result of the test structure suggested that the proposed method led to conservative results when compared with dynamic analysis.

De Stefano and Pintucchi (2010) conducted an extensive parametric study of a series of single-storey systems with moderate to large torsional stiffness. They pointed out that the procedure proposed by Fajfar to employ the elastic torsional response with pushover analysis results in the design of asymmetric plan building was valid only for a system with moderate torsional stiffness. That was mainly because for torsionally very stiff systems the inelastic torsional response was almost always greater than the elastic response and the displacement demand on the flexible side of the structure was much larger than the one obtained from the pushover analysis.

1.7 Previous studies at Carleton University

In the previous studies carried out at Carleton University, displacement-based seismic design procedure have been developed for symmetric concrete frame buildings, symmetric steel frame buildings and symmetric buildings with concrete shear walls.

These procedures employ a variant of the capacity spectrum method in which the demand is represented by an inelastic response spectrum plotted in the acceleration displacement format for a ductility that is determined from estimates of the yield displacement and acceptable ultimate displacement. Details of the procedures have been presented by Ghorbanie-Asl (2007), Humar and Ghorbanie-Asl (2005, 2006) and Humar et al (2006, 2010).

Humar and Ghorbanie-Asl (2005) introduced a practical displacement-based design procedure in which the maximum acceptable displacement demand on building structures was limited to the least of displacement capacity of the critical component, displacement dictated by performance criteria, and displacement limit to prevent P- Δ instability. Through examples of the design of several reinforced concrete, and steel moment-resisting frames as well as braced frames Ghorbanie-Asl (2007) showed that within a few iterations one could estimate the yield and ultimate displacement capacities of the system accurately.

Pina Burgos (2006) introduced a displacement-based design procedure with emphasis on reinforced concrete shear walls buildings having symmetric layout. In the proposed procedure empirical relations were used to estimate the yield displacement of the wall. The acceptable ultimate displacement was determined on the basis of the same three criteria as referred to in the preceding paragraph. At the preliminary design stage, a triangular shape was assumed for the first mode, while in further iterations the first mode

shapes calculated from an eigen value analysis was used to construct the equivalent SDOF system for the structure.

Elrodesly (2008) introduced a displacement-based design procedure for torsionally stiff reinforced concrete shear wall structures. The target displacement was calculated based on the code drift limit and ductility limit, and the higher mode effect was taken into account using the modal pushover analysis (MPA), as extended by Chopra and Goel (2004) for asymmetric plan buildings. The P– Δ effect was not considered. It was shown that the square root of sum of squares (SRSS) combination rule underestimated the base shear when compared to nonlinear time history analyses while the absolute summation (ABSSUM) led to a conservative estimate.

1.8 Objective and scope

The present study extends the DBSD procedure to the design of wall-frame buildings and torsionally unsymmetric buildings. The wall-frame buildings have not been studied earlier at Carleton and only a limited amount of work has been carried out on torsionally unsymmetric buildings. Studies related to wall-frame buildings exist in the literature but they are based on the equivalent linearization procedure and not on the capacity spectrum method proposed in this study. To the knowledge of the author, detailed studies on the DBSD of torsionally unsymmetric buildings have not been reported in the literature.

The wall-frame buildings studied here are symmetric in the plan area and are designed for the effect of earthquake loading in one direction. Torsional effects are

neglected in the development of DBSD for wall-frame buildings. The studies on torsionally unsymmetric buildings are limited to the case of independent rectangular shear walls. Walls of other shape, such as C-shaped walls or I-shaped walls have not been covered. Also, the study does not extend to core wall, buildings. In principle, the DBSD procedure developed here could be applied in the seismic design of a wide range of plan asymmetric buildings, however, further studies would be required to assess the effectiveness of the proposed method in the design of plan asymmetric plan buildings with different type of lateral resisting systems.

The following objectives are identified for the present study:

1. Review the performance based design philosophy and the guidelines for displacement-based design
2. Develop a displacement-based design procedure for reinforced concrete wall-frame structures that could be implemented in a design office.
3. Review the inelastic torsional response of asymmetric plan buildings in order to propose a straightforward procedure to estimate the maximum displacement demand on different structural and non-structural elements of such buildings.
4. Develop a displacement-based design procedure for plan irregular buildings specially for torsionally flexible structures
5. Evaluate the effectiveness of the proposed displacement-based design method for wall-frame structures and plan irregular structures by comparing the inelastic response of designed structures to a series of spectrum compatible ground motions.

1.9 Layout of the Report

An outline of this thesis is presented in the following:

Chapter 1 provides an overview of the existing performance based design philosophy and the displacement-based seismic design procedures, and their application in reinforced concrete structures. A review of the literature on inelastic torsional behaviour of asymmetric plan buildings is presented and some of the proposed design procedures are discussed.

Chapter 2 presents the theoretical background to the proposed approach for displacement-based design of wall-frame structures. Some empirical relations are employed to estimate the yield and ultimate displacement of reinforced concrete wall-frame structures. Also a simple procedure is proposed for estimating the inflection height at the preliminary design stage. Finally the step by step procedure for seismic design of wall-frame systems is presented.

In Chapter 3 the design of five reinforced concrete wall-frame buildings, 6, 9, 12, 15, and 20 storeys in height, according to the proposed DBSD is presented. Different design parameters that are evaluated within iterations of design are presented and discussed. Using nonlinear time-history analyses of the response of designed buildings to twenty spectrum compatible ground motions, the estimates of the maximum roof

displacement, maximum inter-storey drift ratio, and the base shear demand obtained by the proposed DBSD are evaluated.

Chapter 4 contains an overview of the tools available for investigating the inelastic torsional response of asymmetric plan buildings, such as the BST surface, incremental dynamic analysis, and modal decomposition method. Through several parametric studies the torsional behaviour of different torsionally unbalanced systems is studied and a simple procedure for estimating the maximum twist in the plan and the maximum displacement demands on structural members is proposed.

In Chapter 5 a DBSD procedure for asymmetric plan building is presented. The theoretical background for the proposed expressions for determining the maximum twist in the plan of the system and its comparison with some other proposals are discussed. Also, details related to the estimation of the equivalent yield and ultimate displacements for different design criteria are presented.

Chapter 6 describes two case studies. One torsionally stiff system and one torsionally flexible system are designed according to the proposed DBSD. Different iterations of the design are presented for both cases. The global response parameters for both the flexible and the stiff edge as well as at the center of mass of the systems are compared with the results obtained from nonlinear time-history analyses for a series of spectrum compatible ground motions.

Summary and conclusions of this work, as well as some recommendations for future works are presented in Chapter 7. Appendix A. of this report includes the details of the step-by-step design of 12-storey wall-frame building. Appendix B. presents complementary information for multi-mode pushover and nonlinear time history analyses of 6, 9, 15, and 20-storey wall-frame buildings. Details of the step-by-step design of both torsionally stiff and torsionally flexible buildings are presented in Appendix C.

Table 1.1: Design earthquake levels proposed by Vision 2000 & FEMA 273

| Design Earthquake Level | Vision 2000 | | FEMA 273 | |
|--------------------------------|----------------------|---------------|----------------------|---------------|
| | Chance of exceedance | return period | Chance of exceedance | return period |
| Frequent | 50% in 30 years | 43 years | 50% in 50 years | 72 years |
| Occasional | 50% in 50 years | 72 years | 20% in 50 years | 225 years |
| Rare | 10% in 50 years | 475 years | 10% in 50 years | 475 years |
| Very rare | 5% in 50 years | 970 years | 2% in 50 years | 2475 years |

Table 1.2: Improved effective parameters to be used in CSM

| Ductility | Hysteretic model known | |
|-------------------|--|---|
| | Effective viscous damping | Effective period |
| $1.0 < \mu < 4.0$ | $A(\mu - 1)^2 + B(\mu - 1)^3 + \beta_0$ | $[G(\mu - 1)^2 + H(\mu - 1)^3 + 1]T_0$ |
| $4.0 < \mu < 6.5$ | $C + D(\mu - 1) + \beta_0$ | $[I + J(\mu - 1) + 1]T_0$ |
| $\mu > 6.5$ | $E \left[\frac{F(\mu - 1) - 1}{[F(\mu - 1)]^2} \right] \left(\frac{T_{\text{eff}}}{T_0} \right)^2 + \beta_0$ | $\left\{ K \left[\sqrt{\frac{(\mu - 1)}{1 + L(\mu - 2)}} - 1 \right] + 1 \right\} T_0$ |

| Ductility | Hysteretic model unknown | |
|-------------------|---|---|
| | Effective viscous damping | Effective viscous damping |
| $1.0 < \mu < 4.0$ | $4.9(\mu - 1)^2 - 1.1(\mu - 1)^3 + \beta_0$ | $4.9(\mu - 1)^2 - 1.1(\mu - 1)^3 + \beta_0$ |
| $4.0 < \mu < 6.5$ | $14.0 + 0.32(\mu - 1) + \beta_0$ | $14.0 + 0.32(\mu - 1) + \beta_0$ |
| $\mu > 6.5$ | $19.0 \left[\frac{0.64(\mu - 1) - 1}{[0.64(\mu - 1)]^2} \right] \left(\frac{T_{\text{eff}}}{T_0} \right)^2 + \beta_0$ | $19.0 \left[\frac{0.64(\mu - 1) - 1}{[0.64(\mu - 1)]^2} \right] \left(\frac{T_{\text{eff}}}{T_0} \right)^2 + \beta_0$ |

Table 1.3: Coefficients for use in equations for effective damping

| Model | | $\alpha(\%)$ | A | B | C | D | E | F |
|-----------|------------|--------------|-----|-------|-----|------|----|------|
| Bilinear | hysteretic | 0 | 3.2 | -0.66 | 11 | 0.12 | 19 | 0.73 |
| Bilinear | hysteretic | 2 | 3.3 | -0.64 | 9.4 | 1.1 | 19 | 0.42 |
| Bilinear | hysteretic | 5 | 4.2 | -0.83 | 10 | 1.6 | 22 | 0.4 |
| Bilinear | hysteretic | 10 | 5.1 | -1.1 | 12 | 1.6 | 24 | 0.36 |
| Bilinear | hysteretic | 20 | 4.6 | -0.99 | 12 | 1.1 | 25 | 0.37 |
| Stiffness | degrading | 0 | 5.1 | -1.1 | 12 | 1.4 | 20 | 0.62 |
| Stiffness | degrading | 2 | 5.3 | -1.2 | 11 | 1.6 | 20 | 0.51 |
| Stiffness | degrading | 5 | 5.6 | -1.3 | 10 | 1.8 | 20 | 0.38 |
| Stiffness | degrading | 10 | 5.3 | -1.2 | 9.2 | 1.9 | 21 | 0.37 |
| Stiffness | degrading | 20 | 4.6 | -1.0 | 9.6 | 1.3 | 23 | 0.34 |
| Strength | degrading | -3 | 5.3 | -1.2 | 14 | 0.69 | 24 | 0.9 |
| Strength | degrading | -5 | 5.6 | -1.3 | 14 | 0.61 | 22 | 0.9 |

Table 1.4: Coefficients for use in equations for effective periods

| Model | | $\alpha(\%)$ | G | H | I | J | K | L |
|-----------|------------|--------------|------|--------|------|-------|------|-------|
| Bilinear | hysteretic | 0 | 0.11 | -0.017 | 0.27 | 0.09 | 0.57 | 0 |
| Bilinear | hysteretic | 2 | 0.1 | -0.014 | 0.17 | 0.12 | 0.67 | 0.02 |
| Bilinear | hysteretic | 5 | 0.11 | -0.018 | 0.09 | 0.14 | 0.77 | 0.05 |
| Bilinear | hysteretic | 10 | 0.13 | -0.022 | 0.27 | 0.1 | 0.87 | 0.1 |
| Bilinear | hysteretic | 20 | 0.1 | -0.015 | 0.17 | 0.094 | 0.98 | 0.2 |
| Stiffness | degrading | 0 | 0.17 | -0.032 | 0.1 | 0.19 | 0.85 | 0 |
| Stiffness | degrading | 2 | 0.18 | -0.034 | 0.22 | 0.16 | 0.88 | 0.02 |
| Stiffness | degrading | 5 | 0.18 | -0.037 | 0.15 | 0.16 | 0.92 | 0.05 |
| Stiffness | degrading | 10 | 0.17 | -0.034 | 0.26 | 0.12 | 0.97 | 0.1 |
| Stiffness | degrading | 20 | 0.13 | -0.027 | 0.11 | 0.11 | 1 | 0.2 |
| Strength | degrading | -3 | 0.18 | -0.033 | 0.17 | 0.18 | 0.76 | -0.03 |
| Strength | degrading | -5 | 0.2 | -0.038 | 0.25 | 0.17 | 0.71 | -0.05 |

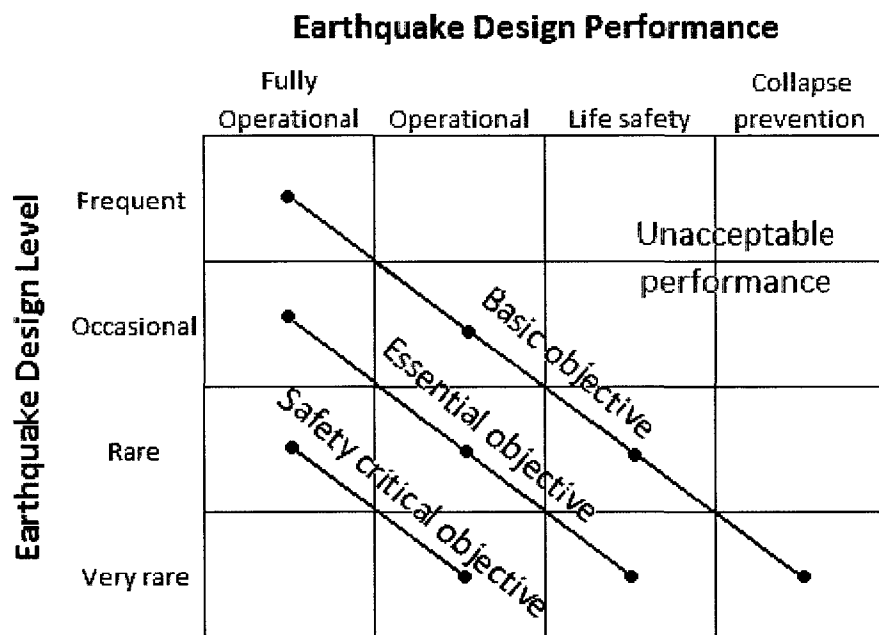


Figure 1.1: Minimum performance objectives (Vision 2000)

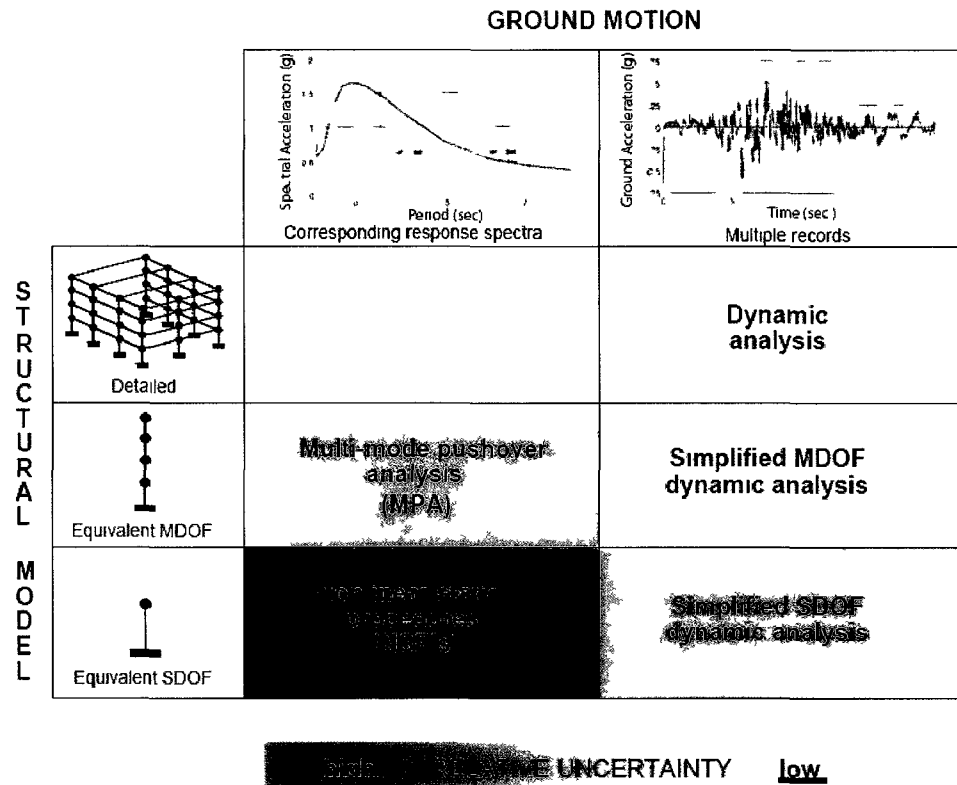


Figure 1.2: Inelastic seismic analysis procedures for various structural models and ground motion characterization (FEMA 440)

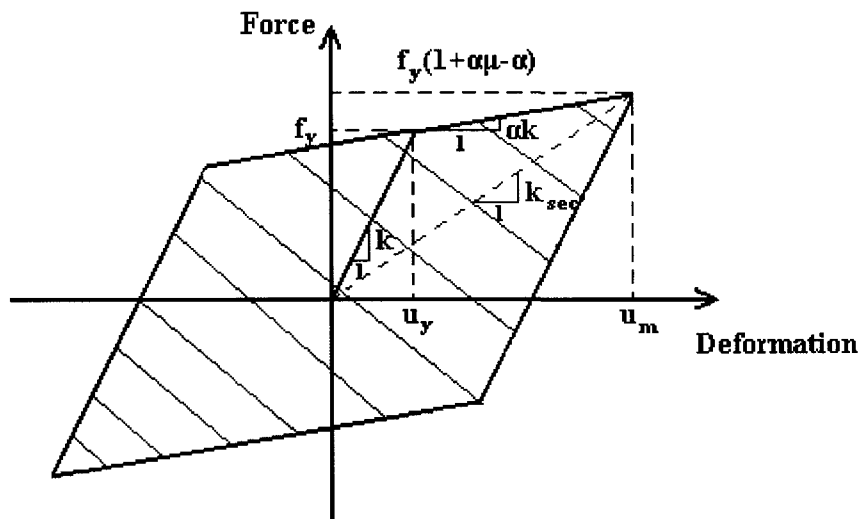


Figure 1.3: Bilinear idealization of pushover curve

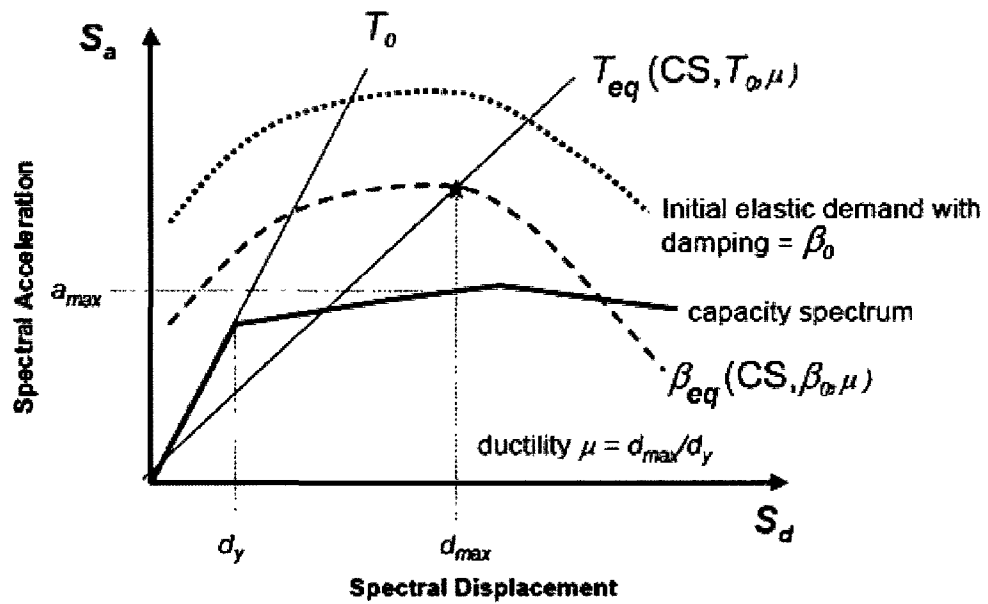
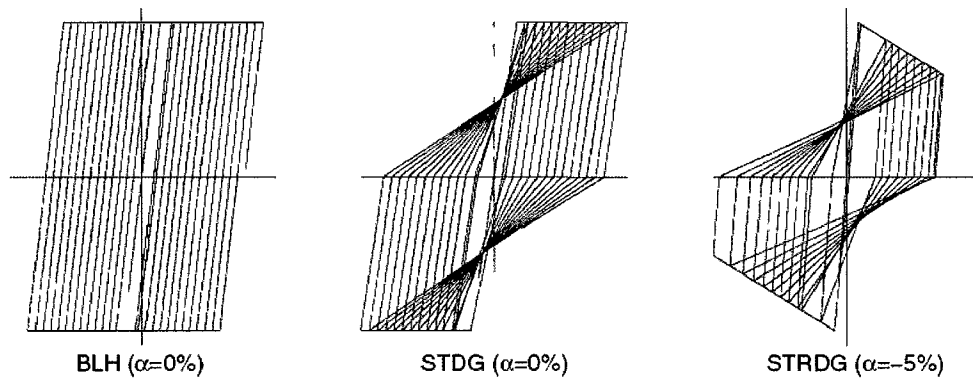
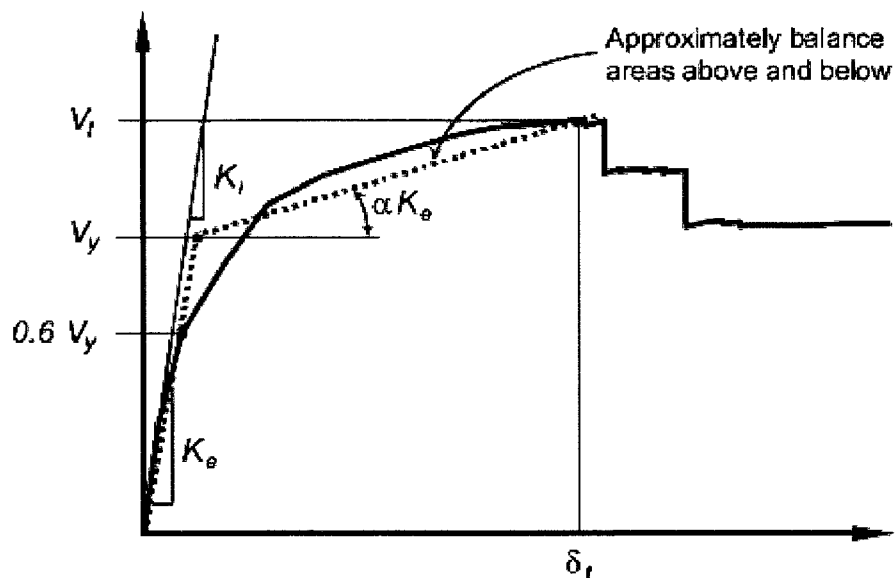


Figure 1.4: ADRS showing effective period and damping parameters of equivalent linear system along with the capacity curve, as described in FEMA 440.

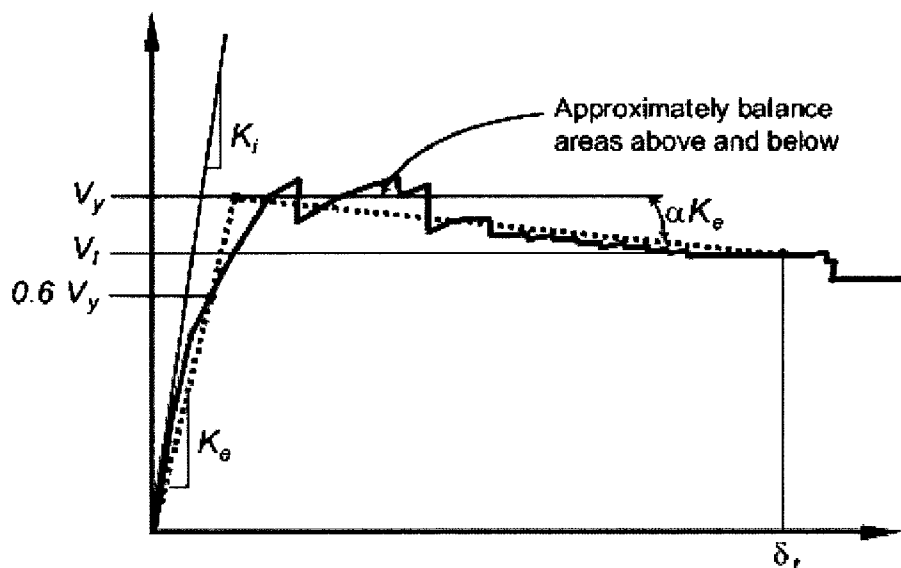


Types of inelastic behavior considered. BLH=Bilinear Hysteretic STDG=Stiffness Degrading, and STRDG=Strength Degrading.

Figure 1.5: Types of Behaviour considered in improved CSM (FEMA 440)



(a) Positive post-yield slope



(b) Negative post-yield slope

Figure 1.6: Effective post yield stiffness (FEMA 356)

Chapter 2. Displacement-based design of hybrid wall-frame structures

2.1 Introduction

A wall-frame system, also referred to as dual or hybrid system, is a structural system that uses both frames and walls to resist the earthquake induced actions in the structure. The seismic behaviour of a wall-frame structure is considerably different from that of a wall structure and a frame structure. The wall structures have flexural behaviour like a cantilevered beam and they can control the drifts at lower floor levels, while pure frame structures restrain deformation at upper floors. On combining these two systems a very efficient and economical system for resisting the earthquake forces is obtained.

Displacement-based seismic design method proposed earlier for reinforced concrete and steel frame structures by Humar and Ghorbanie-Asl (2005) is modified here for wall-frame structures. The method is based on approximate estimates of the ultimate and yield roof displacements and the related ductility capacity of the structure. However, if the code recommends a lower value for ductility capacity, it should be the one to be used in design. The details of the method are described in the following sections.

2.2 Estimation of yield and ultimate displacements

2.2.1 Yield displacement

The maximum permissible global displacement of a structural system can be estimated by using empirical relations, based on the mechanism of failure of that system. For instance, a shear wall forms a plastic hinge at its base when it is subjected to extensive lateral load.

Therefore, the maximum displacement demand of the wall can be estimated by decomposing the maximum displacement into yield displacement and inelastic displacement (see Figure 2.1) to obtain

$$\Delta_u = \Delta_{wy} + (h - l_p/2) \times \theta_p \quad (2.1)$$

where h is the height of the wall, θ_p is the plastic rotation at the plastic hinge at the base, Δ_{wy} is the roof level yield displacement of the wall and l_p is the length of plastic hinge in the wall. Several recommendations exist in the literature for the length of the plastic hinge in the walls; some relate it to both the length and the height of the wall, others suggest it is a function of the wall length alone. Various expressions for plastic hinge length are plotted in Figure 2.2 as a function of the aspect ratio of the wall. In this study the plastic hinge length of a wall is assumed to be half the length of the wall.

Since in frame-wall systems the ultimate lateral displacement is controlled by the wall, the lateral displacements at base yield are obtained by assuming that the curvature as well as moment in the wall varies in the shape of a triangle from zero at inflection height, h_e , to a maximum at the base, and that for $h > h_e$ the moment can be taken as negligible (see Figure 2.8). The displacements at the instant of the yielding at the base of the wall are then given by (Sullivan et al 2006):

$$\begin{aligned}\Delta_{wyi} &= \frac{\varphi_y h_i^2}{2} - \frac{\varphi_y h_i^3}{6h_e} \quad \text{for } h \leq h_e \\ \Delta_{wyi} &= \frac{\varphi_y h_e h_i}{2} - \frac{\varphi_y h_e^2}{6} \quad \text{for } h > h_e\end{aligned}\tag{2.2}$$

where h_i is the height of i^{th} storey, and φ_y is the effective yield curvature of the wall. As mentioned in the previous chapter the yield curvature of a section is a function of only the yield strain of steel, ε_y , and the length of the wall, l_w . At the preliminary design stage, the yield curvature is thus estimated using the following empirical equation:

$$\varphi_y = \eta \frac{\varepsilon_y}{l_w}\tag{2.3}$$

The value of η is not significantly affected by the ratio of the reinforcement or the arrangement of bars in a reinforced concrete section. It has been shown by Priestley (1998) that the values of η , summarized in Table 2.1, do not differ from exact ones by more than 10 to 15 percent. In this study the value of $\eta = 1.8$ is assumed as recommended by Paulay (2000).

Published research (Priestley 2003) has shown that the most appropriate linearization of moment-curvature relationships is by an initial elastic segment passing through “first yield” extrapolated to nominal flexural strength, M_n , and a post-yield segment connected to a point at the intersection of ultimate strength and the corresponding curvature. “First yield” of the section is defined as the moment, M_y and

curvature ϕ'_y when the reinforcement attains its tensile yield strain of ε_y , or the concrete extreme compression fibre attains a strain of 0.002, whichever occurs first. The nominal flexural strength M_n develops when the extreme compression fibre strain reaches 0.004, or the reinforcement tension strain reaches 0.015, whichever occurs first. Figure 2.3a shows a moment curvature relationship and the nominal yield curvature ϕ_y corresponding to nominal flexural strength. In this study the moment curvature relation for the wall is obtained using a MATLAB program developed by Yavari (2001).

In this program, Hognestad's model is used to define the idealized stress-strain relationship for unconfined concrete. As shown in Figure 2.4, the stress-strain curve follows the following equation up to a strain $\varepsilon_0 = 0.002$.

$$f_c = f_c' \left[\frac{2\varepsilon_c}{\varepsilon_0} - \left(\frac{\varepsilon_c}{\varepsilon_0} \right)^2 \right] \quad (2.4)$$

For $\varepsilon_c > \varepsilon_0$ the stress decreases linearly with strain reaching a value of $0.85f_c'$ at $\varepsilon = 0.0038$. The stress-strain relationship for reinforcement steel uses a trilinear model, consisting of a straight line from 0 strain to the yield strain ε_y , a yield plateau from ε_y , to the strain at onset of strain hardening, ε_s , and another straight line from the yield strength at ε_s to the ultimate strength.

The yield displacement of the frame at roof, Δ_{fyr} , may be taken as

$$\Delta_{fyr} = H \times \theta_{fy} \quad (2.5)$$

where H is the total height of structure, and inter-storey yield rotation of the frames, θ_{fy} is obtained assuming that all the beams have yielded at both ends and the curvature varies linearly from one end of the beam to the other. As recommended by Priestley (1998) θ_{fy} may be obtained from

$$\theta_{fy} = \frac{0.5 \varepsilon_y l_b}{D_b} \quad (2.6)$$

where l_b is the length of the beam, and D_b its depth.

The designer has the freedom to select the relative strengths of the wall and the frame to withstand the demand base shear V_b . The strength of the components may be assigned arbitrarily, and this freedom can be exploited to achieve more rational and economical design (Paulay 2002b). Once such assignment is made, the global yield displacement of the wall-frame system can be obtained from

$$\Delta_y = \frac{V_b}{V_w/\Delta_{wy_r} + V_f/\Delta_{fyr}} \quad (2.7)$$

where V_w , and V_f are the wall and frame strengths, respectively, and Δ_{wy_r} is the wall yield roof displacement (see Figure 2.3b).

2.2.2 Ultimate displacement

The acceptable ultimate displacement is the least of the following:

- 1) The roof displacement corresponding to inter-storey drift limit which is expected to prevent excessive non-structural damage. Rewriting Equation 2.1, the total displacement at level i is given by

$$\Delta_{ui} = \Delta_{wyi} + (h_i - l_p/2) \times \theta_p, \quad \theta_p = 0.025 - \frac{\varphi_y h_e}{2} \quad (2.8)$$

where as shown in Equation 2.8, θ_p , the plastic rotation at the base of the wall, is estimated by taking the difference between the maximum inter-storey drift limit and the yield rotation of the wall calculated from the assumption we made for the distribution of curvature in the wall (see Figure 2.1)

- 2) The roof displacement at which the ductility demand in any element of the structure reaches its ductility capacity. For instance, the displacement at roof at which the curvature demand in the wall reaches its capacity can be calculated as:

$$\Delta_{ur} = \Delta_{wyr} + (H - l_p/2) \times (\varphi_u - \varphi_y) \times l_p \quad (2.9)$$

where φ_u is the wall curvature capacity, and φ_y the yield curvature obtained from bilinear simulation of moment curvature analysis of the section (see Figure 2.3a).

3) The roof displacement limit beyond which P–Δ instability may result. The gravity loads on the structure tend to apply additional moment and shears on the structure when it experiences the earthquake induced lateral displacement; this is known as P–Δ effect. The P–Δ effect reduces the capacity of structures to withstand the earthquake forces and may lead to instability, therefore the lateral displacement should be limited so as to mitigate the risk of instability (Humar et al. 2006). It has been shown that P–Δ instability is prevented if the maximum displacement produced by the design earthquake lies in the region of positive slope of the pushover curve.

In preliminary design only the first of the above three limits is generally available; however, for subsequent design iterations more accurate ultimate displacement estimates can be calculated taking into account the ductility capacity of the system, and the P–Δ instability.

2.3 Inflection height estimate

An estimation of inflection height of the building is needed in Equation (2.2) to estimate the yield displacement of the wall-frame structure. At the preliminary design stage inflection height is estimated according to the following simple procedure. Assume that the contribution of the frames, in resisting the lateral loads has been assigned a value αV_b . Thus, the shears resisted by the walls and the frames is given by:

$$\begin{cases} V_{frames} = \alpha V_b \\ V_{walls} = (1 - \alpha) \times V_b \end{cases} \quad (2.10)$$

where the V_b is the base shear. The distribution of the lateral loads along the height of the building is assumed to be triangular. In that case, the lateral load f_i , at the i^{th} floor, of an n -storey building with equal storey heights will be:

$$f_i = \frac{2 \times i}{n(n+1)} V_b \quad (2.11)$$

Based on the assumption that the shear is constant along the height of the frames, the storey shear is given by:

$$V_i = \left[1 - \frac{i(i-1)}{n(n+1)} \right] V_b \quad (2.12)$$

The inflection height is the height where the moment in the wall becomes zero; therefore taking the moment of the lateral loads on the system and the resistant offered by the frames, which is represented by a point load at the top of the wall, we have

$$\sum_{i=1}^m \left[\frac{2(n-i+1)}{n(n+1)} [x - (i-1) \times h_i] V_b - \alpha V_b x \right] = 0 \quad (2.13)$$

where m is the number of storeys above the inflection point, and x is the distance from inflection point to the roof, which should lie in the range $(m-1) \times h_i \leq x \leq m \times h_i$. The, solution of Equation 2.13 gives the value of x from which the inflection height h_e is found as:

$$h_e = H - x \quad (2.14)$$

where H is the total height.

For subsequent iterations, the inflection height is determined when the base shear is distributed along the height in proportion to $\mathbf{M}\varphi$, where \mathbf{M} is the mass matrix and φ is mode shape.

2.4 Equivalent SDOF model

For the design of a MDOF system it must first be represented by an equivalent SDOF system. For that purpose a deformed shape for the structure should be selected. In preliminary design this is taken as the ultimate displacement estimate at each level as obtained from Equation 2.2; however, for subsequent iterations the first mode shape of structure may be used. Assuming vector φ to be the normalised deformed shape the dynamic parameters can be calculated from

$$\Gamma = \frac{\varphi^T \mathbf{M} \mathbf{1}}{\varphi^T \mathbf{M} \varphi} \quad (2.15)$$

$$L = \varphi^T \mathbf{M} \mathbf{1} \quad (2.16)$$

$$M^* = \frac{(\varphi^T \mathbf{M} \mathbf{1})^2}{\varphi^T \mathbf{M} \varphi} \quad (2.17)$$

where $\mathbf{1}$ is a unit vector, Γ is the participation factor and M^* is the effective mass. The ultimate displacement δ_u , and yield displacement δ_y of the SDOF system are obtained by dividing the ultimate and yield displacements of MDOF by Γ to give

$$\delta_y = \frac{\Delta_y}{\Gamma} \quad (2.18)$$

$$\delta_u = \frac{\Delta_u}{\Gamma} \quad (2.19)$$

where it is assumed that φ has been normalized such that its roof level element is 1.

2.5 Determination of inelastic response spectrum

As shown in Figure 2.5c, the methodology described here uses the inelastic response spectrum in acceleration displacement format to represent the seismic demand on an equivalent SDOF system. Such a spectrum can be obtained by carrying out a nonlinear response analysis or by a suitable modification of the elastic response spectrum (see Figure 2.5d).

Starting from a uniform hazard spectrum for the site, the peak spectral displacement of the inelastic system can be determined from

$$D = \frac{\mu}{R_y} \left(\frac{T_n}{2\pi} \right)^2 A \quad (2.20)$$

where A is the elastic spectral acceleration at natural period T_n , and R_y is the yield strength reduction factor. Using Equation 2.20 the inelastic spectrum can be plotted in the Acceleration versus Displacement (A-D) format provided a relationship between $R_y-\mu-T_n$ is available

Several recommendations regarding the $R_y-\mu-T_n$ relations to be used in the calculation of inelastic response spectrum are available in the literature. In the present study we use Krawinkler–Nassar relations to obtain the inelastic demand spectrum (Krawinkler and Nassar 1992). These relations are given by

$$c = \frac{T_n^a}{1 + T_n^a} + \frac{b}{T_n} \quad (2.21)$$

$$R_y = [c(\mu - 1) + 1]^{1/c}$$

where T_n is the period of the SDOF system and a and b are parameters that depend on the force-displacement relationship for the system. For an elasto-plastic force-displacement relationship $a = 1$, and $b = 0.42$. Figure 2.6 shows the relationship between R_y and the

period for different values of μ . It would be noted that for long periods and low values of μ , R_y becomes very close to μ .

The relationships developed by Krawinkler and Nassar as well as other similar relationships provide good results only when averaged over a number of ground motions. Considerable scatter may exist between the true inelastic spectrum of an individual ground motion and the spectrum obtained by modifying the elastic spectrum by one of the recommended relationships. As an example Figure 2.7 shows two inelastic response spectra for El Centro ground motion for a ductility ratio of 2.9, one obtained by nonlinear analysis and the other by modifying the elastic spectrum using Krawinkler Nassar relationships. As can be seen the inelastic response spectrum obtained from the modified elastic response spectrum provides a good match only in the low period range. However, generating the inelastic response spectrum in each iteration of design for the ductility obtained in that iteration is very time consuming and not practical for use in design. In addition, the design spectrum itself is not obtained from a single event but is an average of several ground motions that are representative of the seismicity of the site. Thus, even though the inelastic response spectrum obtained by modifying the elastic spectrum is approximate, it is appropriate for use in design.

2.6 Capacity diagram and pushover analysis

Having determined the acceptable ultimate displacement of the SDOF system the corresponding spectral acceleration (A_y) is obtained from the inelastic acceleration-

displacement response spectrum by entering the latter at displacement δ_u . The base shear is then given by

$$V = M^* A_y \quad (2.22)$$

This base shear is distributed over the height of building in proportion to $M\varphi$. Assuming that the shear assigned to the frame acts as a point load at the roof level on the wall, the resulting moment demand on the wall is determined. The design of the walls and the frames sections are then updated, also, a new estimate for the inflection height of the structure is obtained.

Next, a nonlinear pushover analysis including the P- Δ effect is carried out for a lateral force distribution proportional to the first mode inertial forces, $M\varphi_1$. Pushover analysis is a nonlinear multi-step static analysis of structure. In such an analysis the structure is subjected to a selected lateral load pattern. The load magnitude is increased in steps until the target displacement at specific height of structure is reached. With the increase in the magnitude of the loading, weak links and failure modes of the structure are found. Plotting the base shear of structure in such an analysis, versus the target displacement a force-deformation relationship for the structure is obtained which is called pushover curve (see Figure 2.5a).

The resulting pushover curve is idealized as recommended by FEMA 356 to estimate the yield displacement. The ultimate displacement limit to preclude P- Δ

instability may be assumed to be that corresponding to a 5% to 10% decrease in strength of the structure. Based on the updated displacement estimates and hence the ductility capacity, a new inelastic spectrum is constructed and a new base shear estimate is obtained. If the difference between the updated base shear and the one from the previous iteration is small, the design process is assumed to have converged. If that is not the case, the new base shear is distributed along the height to update the member forces and their reinforcements, and the remaining steps repeated.

2.7 Modal Pushover analysis

Modal pushover analysis (MPA) is now used to obtain better estimates of the seismic demand parameters. In such an analysis the seismic demand is determined by a superposition of the demand in a number of lower order modes. The modal demand is in turn determined by a pushover analysis using the inertia force distribution for the given mode. It is assumed that the higher modes remain elastic, and the target displacement for each of the higher modes is obtained using:

$$D = \Gamma \frac{T^2}{4\pi^2} A \quad (2.23)$$

where Γ is the modal participation factor, T is the period, and A is the elastic spectral acceleration. Combining these ‘modal’ demands in the first two or three modes using the standard square root of the sum of squares (SRSS) provides an estimate of the total seismic demand in the inelastic systems, (Chopra 2002). When applied to elastic systems, the MPA procedure is shown to be equivalent to standard response spectrum analysis.

Theoretically, modal superposition and SRSS are not valid methods of analysis for a nonlinear structure, but the results obtained by MPA provide reasonably accurate estimates of the true response, provided certain conditions are satisfied. The SRSS rule is used when the frequencies of the MDOF system are spaced apart, however, for closely spaced frequencies where there is more chance of coupling between modes complete quadratic combination (CQC) rule is used. For two adjacent modes, if the ratio between them lies between 0.5 and 2.0 those modes are assumed to be coupled.

Using the results of MPA, an estimate of shear forces in the wall and frame components is obtained. In addition, the curvature ductility demand on the plastic hinges at the base of the walls and columns as well as at the end of beams can be calculated. For this purpose, plastic hinge length of the beams and columns are needed. Several recommendations for the plastic hinge length of beams and columns are available in the literature; most suggest it is a function of the effective depth of the section, d , and the distance between the critical section and the point of contraflexure, z , which can be assumed to be half of the span. In the present study the following relation suggested by Mattock (1967) will be used.

$$l_p = 0.5d + 0.05z \quad (2.24)$$

2.8 Displacement based seismic design procedure

The steps involved in the displacement-based design of a structure can be summarized as follows:

- 1) Based on the selected ratio of the base shear carried by the frames to the total base shear, estimate the inflection height from Equations 2.10 through 2.14.
- 2) Calculate the yield displacement of the walls and the frames and the corresponding global yield displacement using Equations 2.1 through 2.3 and Equations 2.5 through 2.7 for a preliminary design of the wall-frame structure.
- 3) Calculate the acceptable ultimate displacement of the roof considering the three limiting criteria - inter-storey drift, ductility demand, and instability prevention - using Equations 2.8 and 2.9, (instability criteria is not available at preliminary design stage).
- 4) Form the equivalent SDOF system based on the ultimate deformed shape and calculate its yield and ultimate displacements.
- 5) Construct the inelastic response spectrum for the ductility determined from the yield and ultimate displacements determined in step 4. Obtain the spectral acceleration corresponding to the acceptable ultimate displacement of SDOF using Equations 2.18 and 2.19 and calculate the base shear.
- 6) Design the structural elements for the induced base shear, and update their sectional properties.

- 7) Carry out nonlinear pushover analysis for first mode inertial force distribution.
Update the yield and ultimate displacement estimates based on the results of pushover analysis, and moment curvature relations of the designed sections.
- 8) Repeat steps 2 through 7 until the design base shear converges.
- 9) At this stage, the calculated base moment in the wall can be used as an acceptable estimate for design, however a modal pushover analysis is needed to estimate the shear and ductility demand in the walls and frames accurately.

Table 2.1: Values of η for different steel and reinforced concrete sections suggested by Paulay (2000)

| 1 | 2 | 3 | 4 | 5 | 6 | 7 | 8 | 9 |
|----------------------------|-----|---------------|---------------|---------------|---------------|---------------|---------------|---------------|
| Section Geometry | | | | | | | | |
| Strain Pattern | | | | | | | | |
| Stress pattern at Ultimate | | | | | | | | |
| η | 3.0 | ≈ 2.3 | ≈ 2.7 | ≈ 2.0 | ≈ 1.8 | ≈ 1.4 | ≈ 1.4 | ≈ 1.8 |

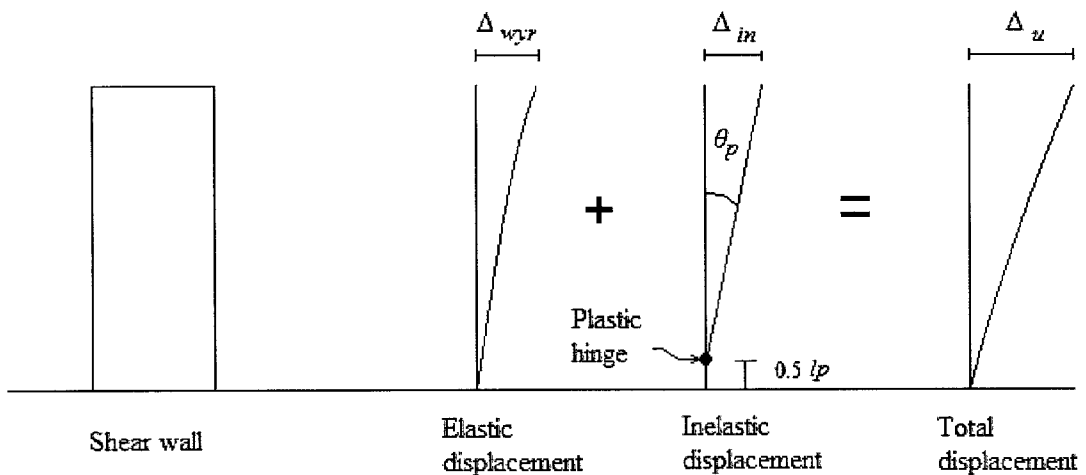


Figure 2.1: Components of the total displacement of wall

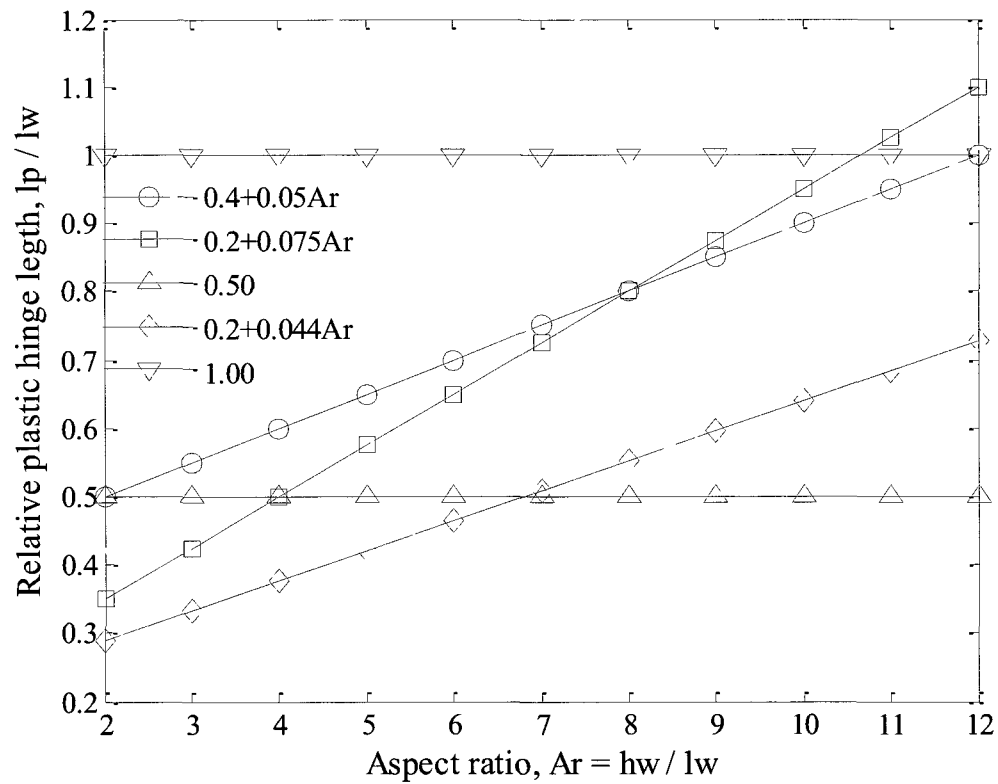


Figure 2.2: Different plastic hinge length relations for walls

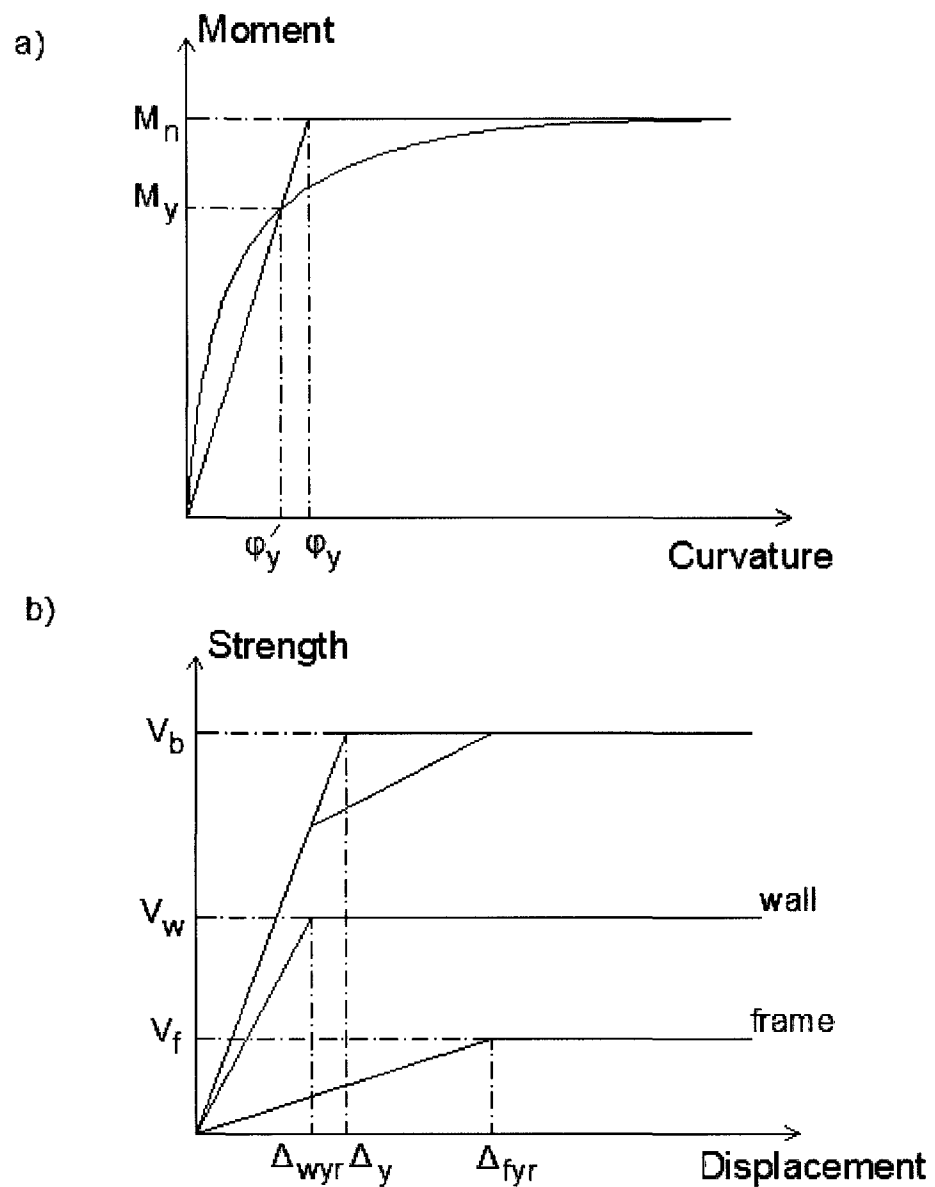


Figure 2.3: Bilinear simulation a) moment-curvature relation b) capacity diagram

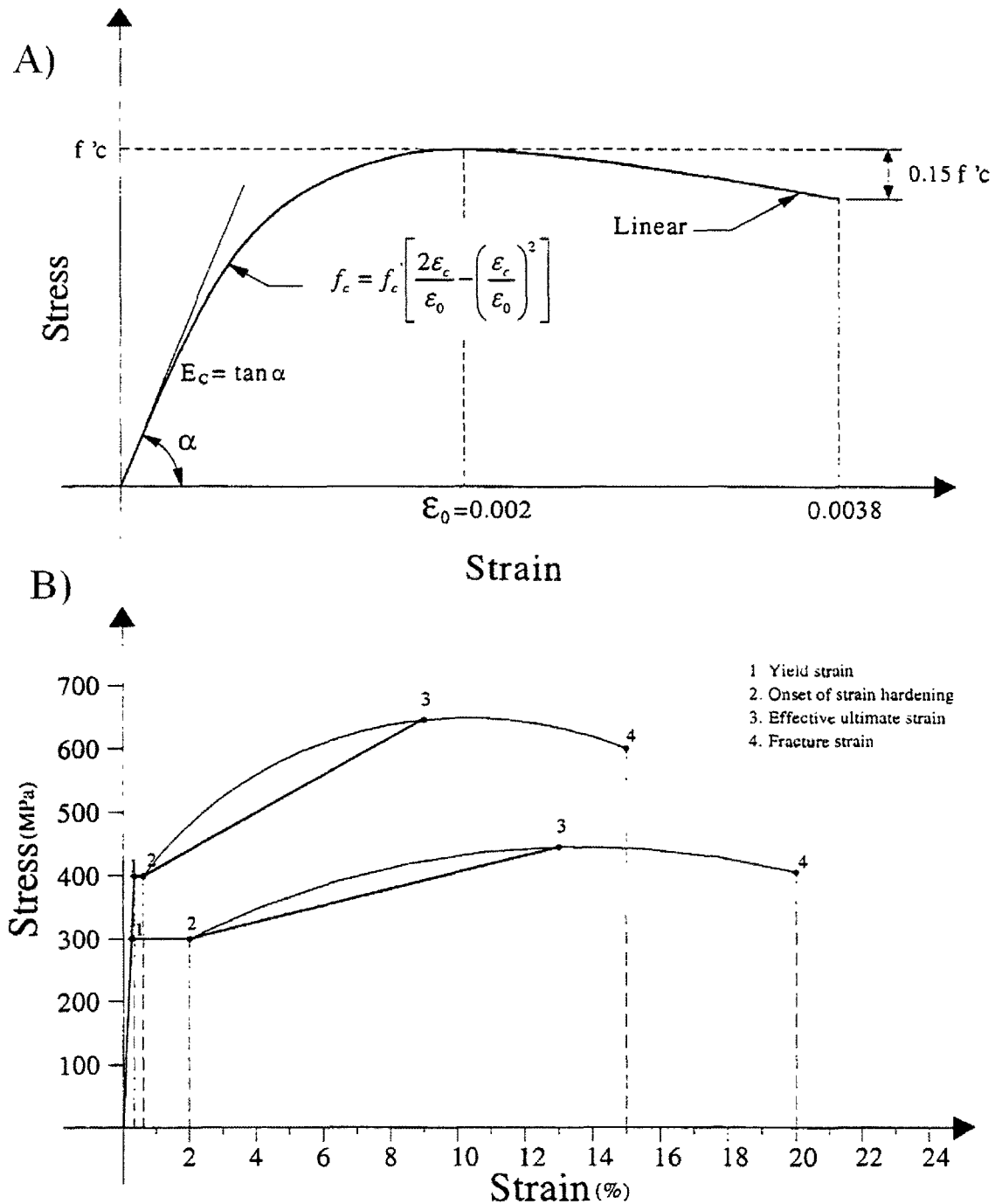


Figure 2.4: Idealized stress-strain relationships for A) unconfined concrete, B) reinforcing steel (Yavari 2001)

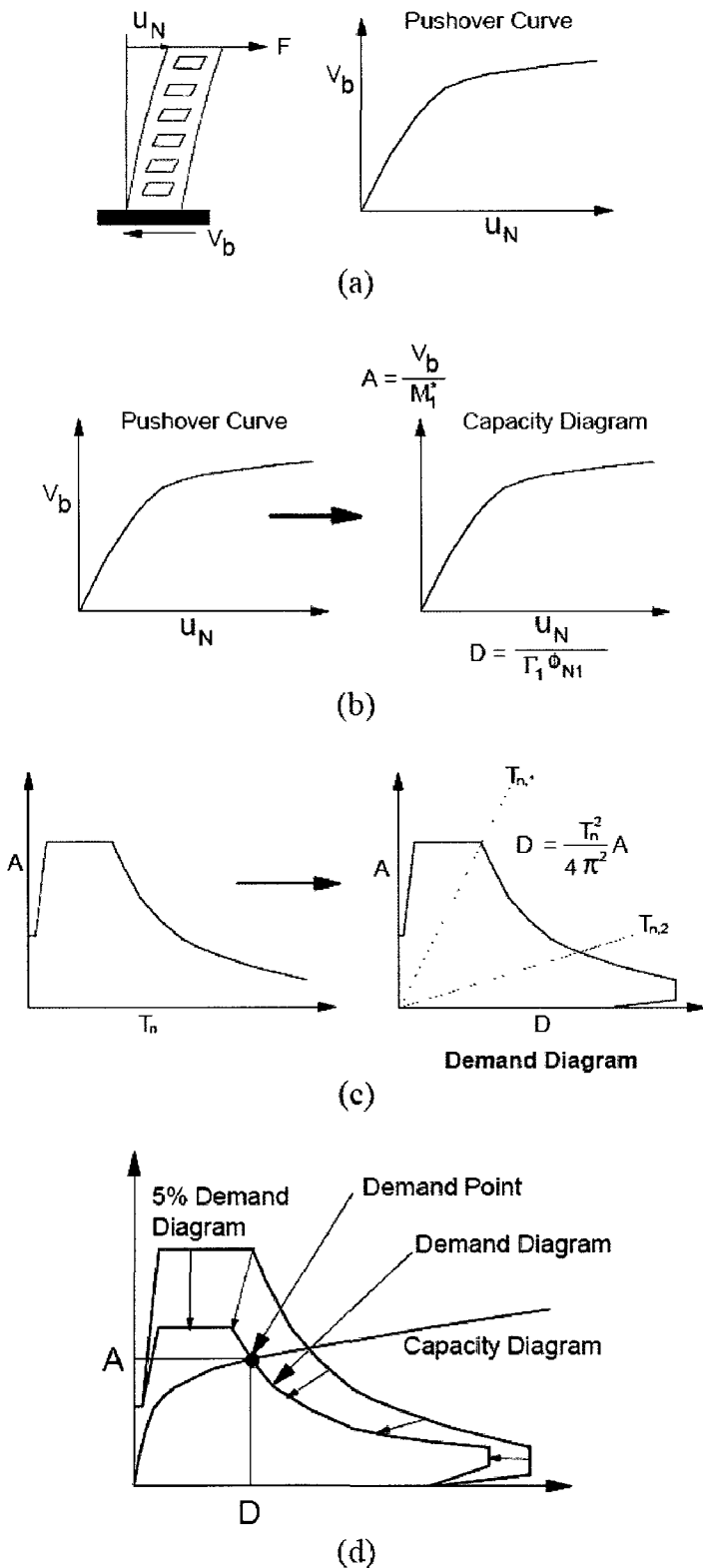


Figure 2.5: Capacity Spectrum Method Chopra and Goel (1999)

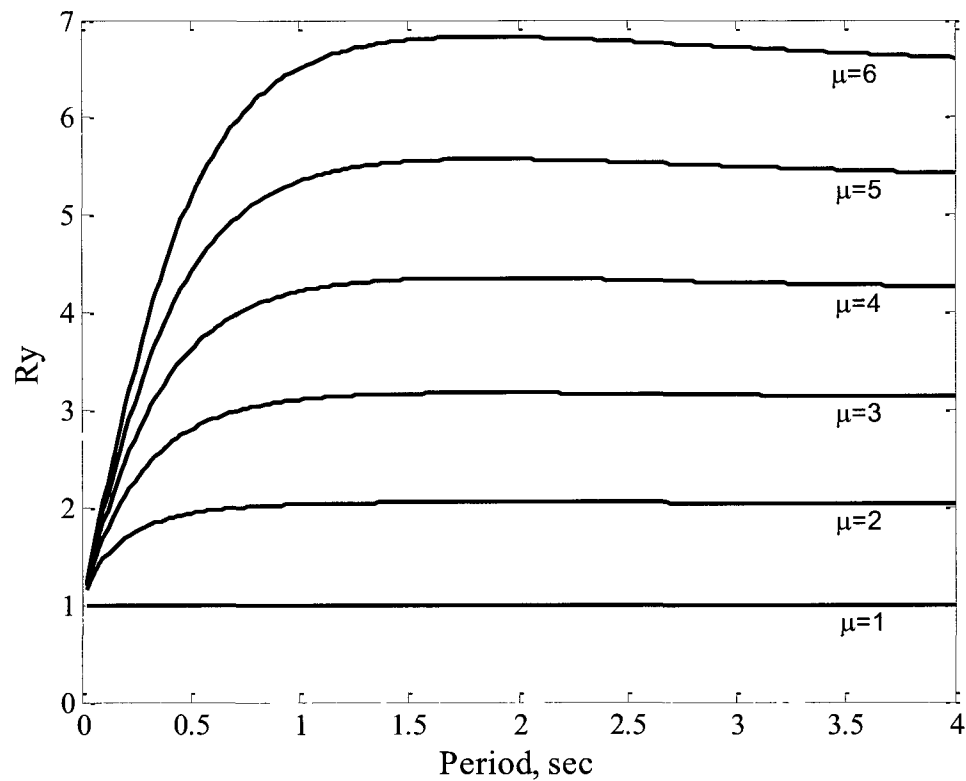


Figure 2.6: $R_y-\mu-T_n$ relations according to Krawinkler and Nassar for elasto-plastic force deformation relationship

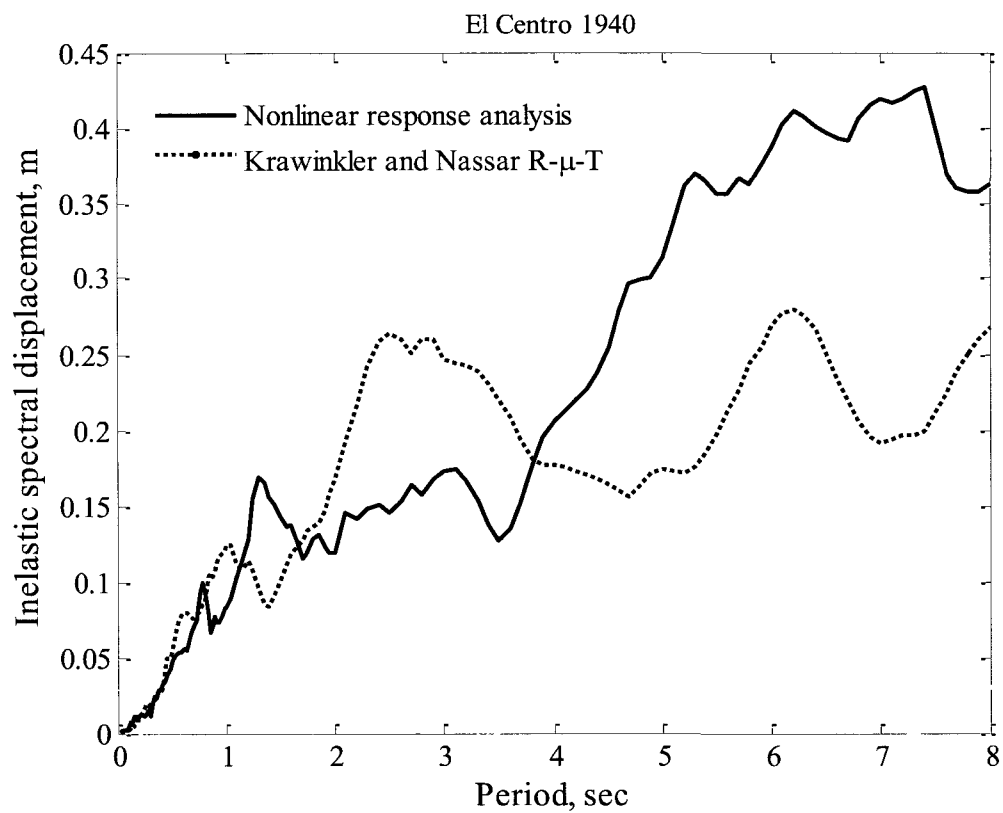


Figure 2.7: Inelastic response spectrum for El Centro ground motion for $\mu=2.9$

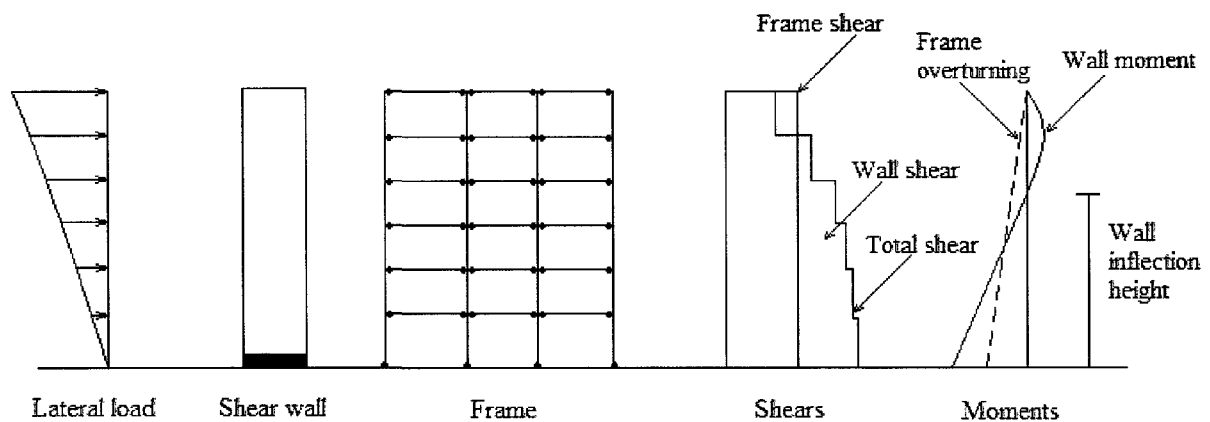


Figure 2.8: Wall-Frame plastic mechanism, and internal force distribution

Chapter 3. Application of DBSD procedure for wall-frame structures

3.1 Introduction

In order to assess the performance of the design process outlined in Chapter 2 it is implemented in the design of a series of reinforced concrete wall-frame buildings. A symmetric plan is selected to enable two-dimensional analysis and to focus on the wall-frame interaction. The structure is assumed to be located in the city of Los Angeles, where extensive research has been carried out to evaluate the seismic hazard and to develop appropriate ground motions. However, the method is effective irrespective of the nature of seismic hazard as long as a design response spectrum is available or can be developed. In this chapter the results of these designs and their verification based on nonlinear dynamic analysis of the structures for their response to 20 spectrum compatible ground motions are presented and discussed. A detailed step-by-step DBSD of the 12-storey building is presented in Appendix A.

3.2 Problem definition

A series of 6, 9, 12, 15, and 20-storey hybrid wall-frame buildings whose plan is shown in Figure 3.1 are designed based on the proposed DBSD procedure to examine the effectiveness of the method. For all of the buildings studied here, the height of first storey is 4.85 m; the other stories are each 3.65 m in height. There are six equal 8-meter bays along the East-West direction, and three equal 8-meter bays along the North-South direction. The lateral resistance in the North-South direction is provided by two shear walls and two frames as shown in Figure 3.1. Dimensions of the walls, columns and

beams for all five buildings are shown in Table 3.1. The dead load on all floors and the roof is 5.8 kN/m^2 . The live load on the floors is 2.4 kN/m^2 . The snow load on roof is taken as 2.2 kN/m^2 . The load combination of $D+0.5L$ is used to calculate the gravity loads at the base of columns and walls given in Table 3.1. The strength of concrete is 30 MPa and the steel yield strength is 400 MPa.

The buildings are designed for an earthquake having a 10% chance of exceedance in 50 years for the city of Los Angeles represented by the target response spectrum shown in Figure 3.2. The structures are designed for earthquake forces in the N-S direction neglecting the accidental torsion effect.

3.3 DBSD of the five buildings

The iterative DBSD procedure described in the previous Chapter is implemented to design the five aforementioned wall-frame buildings. For all five cases, the preliminary design process started with the use of empirical relations for estimating the wall yield curvatures, yield displacement and ultimate displacement of the wall-frame system for the 2.5% drift limit, which leads to a base shear estimate and a design for structural elements. For all cases studied, the design converges after two iterations, i.e. the difference in the estimated base shear in two consecutive iterations became very small. After the DBSD using empirical deformed shape has converged another iteration of design is carried out with pushover analysis using the first mode force distribution, from which the ultimate displacement for $P-\Delta$ instability limit and drift limits are obtained.

The equivalent SDOF system is constructed using the first mode shape rather than the empirical deformed shape.

In the following sections DBSD parameters in different iterations of each of the buildings are discussed in detail.

3.3.1 Inflection height

As mentioned earlier, estimating the inflection height is the first step in the DBSD of wall-frame systems. Equation 2.2 shows that the yield displacement of the walls depends on the height of the inflection point in the walls. At preliminary design stage the height of the inflection point is calculated by the procedure described in Chapter 2 and using Equations 2.10 through 2.14. However, in subsequent iterations where the lateral loads are distributed along the height in proportion to the floor displacements according to the assumed deformed shape or the first mode shape, the inflection height is obtained from the moment diagram for the walls.

Figure 3.3 shows the inflection height as a fraction of the total height for each of the five wall-frame systems. As can be seen from this figure, and the third column of Table 3.2, the inflection height varies from 65% to 80% of the total height of the structures. It is interesting to note that with an increase in the number of storeys the normalised inflection height decreases, which indicates that the negative moment region covers a larger portion of the wall for tall buildings than for short buildings.

3.3.2 Wall yield and ultimate curvatures

At the preliminary design stage, the yield curvature of the walls is obtained from simple empirical relations as described in Chapter 2. However, in subsequent iterations, the ultimate and yield curvatures of the walls are obtained using moment-curvature analyses of the designed sections. In the design process, it is assumed here that the concrete is unconfined and the ultimate capacity of a section is reached when concrete strain is 0.004. This is a design choice and the proposed DBSD can be implemented for any other value of ultimate concrete strain.

Table 3.3 shows the details of the wall design for the five buildings in each iteration of design. The third column in the table shows the concentrated and distributed reinforcements in the wall in mm^2 . The minimum distributed reinforcement in the walls is shown as 200@200 representing two layers of 100 mm^2 each at a spacing of 200 mm. Figure 3.4 shows the detail of the designed wall for 12-storey building at the last iteration of the design. The fourth column shows the nominal flexural strength as described in Chapter 2. The fifth and sixth columns of Table 3.3 show the yield and ultimate curvatures of the walls for different design iterations. It will be noted that the variation in these parameters from one iteration to the next iteration is negligible. Moreover, the yield curvature as estimated using the empirical relation at the beginning of preliminary stage is quite accurate, the difference between the estimated yield curvature in the preliminary design stage and the second iteration being less than 6% for all buildings, and even smaller for taller buildings with longer walls.

3.3.3 Yield and ultimate displacement

The estimated yield and ultimate displacements are presented in the fourth and fifth columns of Table 3.2, respectively. The global yield displacement at the preliminary design stage and in the first and second iterations is estimated from Equation 2.7, where the yield displacement of wall and frames are calculated using the empirical relations presented in Equations 2.2 through 2.4 and 2.6. However, when a pushover analysis is carried out the yield displacement is obtained from the pushover curve. This is discussed further in Section 3.5. The yield displacement estimates in the second iterations, and those obtained from the pushover analyses are plotted in Figure 3.5 against the number of storeys for the five different wall-frame structures. As can be seen the two values are very close.

As explained in Chapter 2, the ultimate displacement of wall-frame systems are controlled by the ultimate displacement of the wall and the latter is estimated using Equation 2.1. At the preliminary design stage the plastic rotation of the wall, θ_p , is determined from the code-prescribed drift limit of 0.025. In subsequent iterations estimates of acceptable plastic rotations based on the ductility limit are also available and are seen to govern the design. Ductility capacity remains the critical criterion in estimating the ultimate displacement even when pushover analyses are carried out and the ultimate displacement limit that would preclude P– Δ instability and the ultimate displacement below which the code-prescribed drift limit would not be exceeded are found.

Figure 3.6 shows the ultimate displacement estimates in the second iteration and those obtained from pushover analyses. In calculating the ultimate displacement of the wall from Equation 2.1 an estimate of the yield displacement is needed. At the stage of preliminary design and in the subsequent iterations this is obtained from Equation 2.2. However, after a pushover analysis is carried out the yield displacement of the wall element as determined from such an analysis is used. The ultimate displacements estimated by empirical relations are about 1% to 9% different from those obtained from the pushover analyses, the difference being smaller for low-rise building than for high-rise ones.

3.3.4 Equivalent SDOF systems

The equivalent SDOF systems are constructed using an assumed deformed shape for the structure and Equations 2.15 through 2.19. In the preliminary design and the first two iterations, the displaced shape is assumed to be the ultimate displacement of the wall given by Equation 2.1. In the final iteration the displaced shape is assumed to be that given by the first mode shape.

The main parameters of the equivalent SDOF for the five buildings are tabulated in Table 3.4 for different iterations. The mass participation factors, Γ , are listed in the first column, and the modal masses, M^* , in the second column. As can be seen the mass participation factor increases as the height of structure increases. It would also be noted that for each building, there are only small variations in the participation factors and modal masses from one iteration to another; however, in the final iteration in which a

pushover analysis is carried out and the first mode shape is used to determine the equivalent SDOF system there is a change of about 5%. This shows that the deformed shapes assumed in the preliminary and the first two iterations are acceptable design choices.

In Table 3.4, δ_y and δ_u are, respectively, the yield and ultimate displacements of SDOF calculated using Equation 2.18 and 2.19. The ductility demand, μ , is the same as that obtained by dividing the acceptable ultimate displacement of the system by the global yield displacement. It would be noted that the ductility demand and the ultimate displacement of the equivalent SDOF system have the most pronounced effect on the spectral acceleration, S_a , and the estimated base shear demand, V .

Figure 3.7 through 3.10 show the capacity demand diagrams for the first and last design iterations for the five buildings. It may be noted that the last iteration uses the information obtained from pushover analysis. In general, the estimates for spectral acceleration and the base shear demand increase from the preliminary design to consecutive iterations for all five cases, while the ductility demand decreases (see Table 3.4). This can be mainly due to decrease in acceptable ultimate displacement estimate in consecutive iterations where the ductility limit governs the design while in the preliminary design stage the design is dictated by the code prescribed drift limit.

It is also interesting to note that as the number of stories increases within the five case studies, DBSD converges with a smaller ductility demand. In each case the design

ductility is governed by the ultimate concrete strain limit of 0.004 on the compression fibres of the wall sections. It is evident that in order to achieve the high ductility values recommended by seismic design codes for moderately ductile and ductile wall sections, confinement is required to increase the acceptable ultimate strain of concrete. It is also noted that while confinement will increase the value of ductility capacity, the full code prescribed values for ductile wall sections would not be realized because the drift limit and P- Δ instability limit would start to govern.

3.4 Structural model

As shown in the plan view of the building in Figure 3.1 the buildings being studied are symmetrical about an axis parallel to the N-S direction. This permits the building structures to be modeled as a two-dimensional model in program DRAIN 2DX. The model consists of one frame and one wall that are constrained to each other at each floor level. This model is used for pushover analysis, multi-modal pushover analyses, and the nonlinear dynamic analyses.

The walls and the columns are modeled with element TYPE 2 in program D2DX (Prakash et al 1993) which is a beam column element with plastic hinges at both ends and is capable of including the P- Δ effect. Based on the concept of strong columns and weak beams, the columns should be designed to remain elastic except at their base where they will yield. The walls are also expected to yield only at their base. Therefore, in modeling both the walls and the columns the moment capacity at the base is assigned based on the moment curvature analyses of the sections while for the higher levels large values are

assigned to the capacities of the wall and the columns so that plastic hinges will form only in the beams. The beams are modeled with element TYPE 1 (Prakash et al 1993) which has zero-length plastic hinges at both ends.

In both elements TYPE 1 and 2 the interaction of axial load and bending moment is not considered, i.e. the flexural resistance of the element is independent of the magnitude of axial load. However, the flexural resistance assigned to an element is determined from a moment-curvature analysis which includes the effect of gravity load incident from the tributary area of the element. Gravity loads applied on the models consist of two parts: 1) gravity load from the tributary areas of the frames which is directly applied on the frames, and 2) the remaining portion of the total floor gravity loads, which is applied on the walls to account for the secondary moment or P- Δ effects.

The structural model of the 20-storey building is shown in Figure 3.12 which indicates the plastic hinge patterns at seven steps of a pushover analysis of the building. The plastic hinges are shown with filled circles when yielding happens at them. As can be seen from the figure, the base of the wall and the roof beams are the first to yield, followed by the bases of the columns. Next to yield are the plastic hinges at the ends of the beams on the side away from the direction in which the building is being pushed. Finally, the plastic hinges of the beams at the near side yield.

3.5 Pushover analysis

For each of the five buildings a pushover analysis using a first mode force distribution is carried out after the base shear obtained from an assumed deformed shape has converged. When a pushover analysis is carried out, the ultimate displacements corresponding to all three limiting criteria can be obtained as explained in Chapter 2. Such ultimate displacements corresponding to ductility limit, 0.025 drift limit, and 5% drop in maximum base shear due to P–Δ effect, are shown in the second, third and fourth columns of Table 3.5, respectively. In all cases the ductility limit governs the design with a large margin.

The pushover curves are shown in Figure 3.13 through 3.16 in red lines. Bi-linear idealizations of the pushover curves are shown in blue lines in the same set of figures. The idealized curve is obtained by drawing a horizontal line through the 95% value of the maximum strength and then connecting it by a straight line to the origin such that the positive and negative areas between the idealized curve and the actual pushover curve are equal. The intersection of these two straight lines is used as the global yield displacement of the system. The ultimate displacements to prevent P–Δ instability, displacement corresponding to the maximum base shear, and the global yield displacements are indicated by dashed lines in Figure 3.13 through 3.16.

The governing ultimate displacement, the global yield displacement and the corresponding ductility demand are shown in Table 3.2. Comparing these results with the ones obtained from iterations using the empirical deformed shape one can conclude that

the empirical relations are capable of estimating the yield and ultimate displacements of wall-frame structures fairly accurately. A similar conclusion can be drawn by reviewing the characteristic parameters of SDOF systems within iterations and after running the pushover analyses, as tabulated in Table 3.4.

3.6 Multi-mode pushover analysis

Multi-mode pushover analyses are carried out to obtain a better estimate of the element forces. Table 3.6 shows dynamic characteristics of the first four modes. Multi-mode pushover analyses are carried out for the first four modes, where the summation of the modal masses covers more than 90% of the total mass. The first mode pushover is carried out up to the ultimate displacements for each building. It is first assumed that the building remains elastic in higher modes; as a result the target displacement for each of the higher modes is obtained using Equation 2.23.

During analyses it was found that for all of the five buildings studied, the structure in fact, became inelastic in the second mode when pushed to the target displacement determined under the assumption of elastic response. In addition, the roof displacement was observed to change direction as the structure was pushed under the second mode load distribution. In order to capture the response of structure in the second mode, target displacement at a lower storey was therefore used. This displacement increases monotonically with the lateral load. An iterative procedure must be used to determine the target displacement, as explained in the following paragraph.

The first estimate of target displacement for the lower storey is obtained based on the elastic deformed shape of structure under lateral loading of $M\phi_2$. The obtained pushover curve is then transformed to equivalent SDOF space by dividing the base shear by M_2^*g and the displacement at the selected lower storey by second mode participation factor as well as by the value of the second mode shape at that storey. This transformed pushover curve is plotted on inelastic demand spectrum in A-D format with $\mu=1$. From the intersection of the two curves, i.e. the performance point, a new value for ductility is estimated. Now a new inelastic demand spectrum is plotted with the transformed pushover curve to estimate the ductility demand from the performance point. This process is repeated till the ductility calculated for the performance point obtained graphically is close enough to the ductility used to construct the inelastic demand spectrum. Table 3.6 lists the inelastic target displacement for second mode pushover analyses as well as the elastic target displacements for third and fourth mode pushover analyses. Ductility demands for second modes and other dynamic characteristics of the higher modes for all five cases are also tabulated in Table 3.6.

The results obtained from these multi-mode pushover analyses are given in Table 3.7. The modal values of the response parameters are combined using the SRSS rule. Such combinations for maximum roof displacements, base shears, and inter-storey drift ratios for first three and four modes are shown in Table 3.7. There is negligible difference between the three-mode combination and four-mode combination for maximum roof displacement and inter-storey drifts, where the first mode makes dominant contribution to the total response. However, higher modes make significant contribution to the base

shear. The change in the base shear estimate by adding the fourth mode is about 0.05% for the 6-storey building and 7.07% percent for the 20-storey building.

3.7 Verification of DBSD for wall-frames structures

In order to verify the accuracy of the design procedure proposed for wall-frame structures, nonlinear time history analysis of the designed structure are carried out for its response to a set of ground motions. Nonlinear response of structures is highly dependent on the characteristics of the input ground motion, such as, frequency content, duration, and phase angle. Therefore, a set of ground motions that are representative of the seismicity of the building location is needed to compare the response of the designed structures with the estimated demands in DBSD.

3.7.1 Selection of ground motions

Two types of ground motions are usually employed in the time history analyses of the structures: 1) scaled ground motions obtained from earthquake shaking, and 2) synthetic ground motions obtained from probabilistic seismic hazard analysis of seismically active zone. Ground motions from large earthquakes that are recorded on a site condition similar to that of the building location are preferred because attenuation of large ground motions is strongly dependent on the site condition and also on the magnitude, while the attenuation relations that are used in generating ground motions from seismic hazard analysis are normally developed from data obtained during small earthquakes.

In this study, a set of 20 ground motion records developed by Somerville et al. (1997) that are compatible with the uniform hazard spectrum having 10 % chance of exceedance in 50 years for Los Angeles are used. The ground motions and their scaling factors are listed in Table 3.8. The ground motions are scaled so as to minimize the weighted squared error between the spectral acceleration of the scaled ground motion and target spectrum at four different periods, namely 0.3, 1.0, 2.0, and 4.0 seconds with weighting factors of 0.1, 0.3, 0.3, and 0.3, respectively. The response spectra of these ground motions and the target design response spectrum are shown in Figure 3.2. Although the response spectrum for an individual ground motion is not close to the target design spectrum, the average of all twenty response spectra is quite compatible with the design spectrum (see Figure 3.2)

3.7.2 Nonlinear time history analysis

One hundred nonlinear time history analyses are carried out for the set of twenty ground motions on the five models developed in Drain 2DX for pushover analyses of the five wall-frame structures. As explained in Section 3.4, elastic properties of beams, columns and the walls are found using a simple bilinear elasto-plastic model based on properties determined through a moment-curvature analysis of the section. Potential plastic hinges in all structural elements are concentrated at the end of the elements, and the properties of the hinges are also based on the moment-curvature analyses of the sections. Rayleigh damping is employed to achieve 5% damping in the first two modes of each building, using the corresponding coefficients for the mass and stiffness matrices. Structures are analyzed using the same time step as that of the input ground motion record as tabulated

in Table 3.8. In each analysis envelopes of the element forces, storey shears, storey displacements, and inter-storey drift ratios are recorded for further processing and comparison.

3.7.3 Results

The maximum storey shears, maximum inter-storey drift ratios, and maximum storey displacements response of all five buildings to the twenty ground motions are presented in Appendix A. Figure 3.18 through 3.19 show the box plot distributions of the maximum storey shears, maximum inter-storey drift ratios, and maximum storey displacements along the height. The red lines in the box represent the median value for each storey and the box extends from the upper quartile to the lower quartile of the responses. In cases where the red line is not located in the middle of the box there is an indication of skewness in the distribution of response. The whiskers – the lines extending beyond the boxes – extend up to 1.5 times the upper and lower quartiles and a red plus sign identifies an outlier. An outlier is defined as data point that lies beyond 1.5 times the upper or lower quartiles.

When compared to the storey displacements and inter-storey drifts, shown Figures 3.18 and 3.19 there is less dispersion in the storey shears that are presented in Figure 3.18. For all three global parameters shown in Figure 3.18 through 3.19 the dispersions in the responses increase as the number of stories increase. This is mainly because of the nonlinear behaviour of the structure and different contribution of the higher modes for different ground motions. It is noted that there exist one or two outliers

out of the range of 1.5 times the upper quartile in the responses, which is due to the high dispersion in the input ground motions (see Figure 3.2)

3.7.4 Verification

In order to compare the results of the nonlinear time history analyses with the results obtained from the proposed DBSD procedure, the ratio between the estimated parameter and the Mean of the Nonlinear Time-history Analyses (MNTA) of the twenty ground motion is calculated. If this ratio is greater than one, it means that the proposed procedure is over-estimating that parameter, and if the value of this ratio is less than one that parameter is under-estimated by the proposed DBSD.

Figures 3.20 through 3.22 show the distribution of the aforementioned ratios for storey shears, inter-storey drifts, and storey displacements along the height of the buildings. In these figures the ratios calculated for first mode pushover analyses are shown with dashed lines, while the ratios calculated for the SRSS of four modes are shown with solid lines. It can be seen in Figure 3.21 that first mode pushover analyses under-estimates the storey shears while the SRSS of four modes accurately predicts the storey shear along the height of the buildings.

The inter-storey drifts are over-estimated at the mid-height of the buildings as shown in Figure 3.22, and slightly under-estimated at roof levels. It is also interesting to note that for fifteen and twenty-storey buildings higher modes make significant contribution to the inter-storey drifts, especially at the roof level, while higher modes

have negligible contribution at lower floors and for shorter buildings. Storey displacements are over-estimated in all five buildings, and the over-estimation increases as the number of stories increases (see Figure 3.23). This over-estimation is mainly due to nonlinear nature of the response of wall-frame structure to different ground motions. Note that, in general, higher modes make almost no contribution to the roof displacements however for tall building they make a small contribution in the lower storey displacements.

3.8 Summary and conclusions

It has been shown that simple empirical relations can be used to estimate the yield and ultimate displacement of wall-frame systems in the seismic design of such structures. The estimated design parameters, such as ductility and base shear demands, obtained from these relations are quite close to the ones obtained from the first mode shape of the structure.

When comparing with nonlinear time-history analyses, the proposed DBSD provides a conservative estimate of the storey displacements and acceptable estimates for inter-storey drift ratios which are needed for detailed design of the structural members. The storey shear estimates are fairly accurate all along the height of the structures while the inter-storey drifts are slightly under-estimated at roof levels and over-estimated at the lower floors. The inter-storey drifts are accurate around the point of inflection, where the maximum inter-storey drifts of wall-frame structures are recorded.

In general, the storey displacements are over-estimated when comparing with dynamic analyses. The over-estimation of storey displacements is rooted in the uncertainty inherent in the use of empirical equations to estimate the maximum displacements. This phenomenon has been reported by other researchers as summarized in FEMA 440, and is a common attribute of nonlinear static procedures. There is also approximation embedded in employment of $R-\mu-T$ relations to construct inelastic response spectra, as was discussed in Chapter 2 in detail.

In conclusion, the proposed DBSD for wall-frame structure is a fast converging procedure and requires only a few design iterations. It shows good promises to be used in the design office, where the use of nonlinear dynamic analysis in the design of a structure would not be the preferred choice of the designers. Also, use of simple empirical relations in a straightforward procedure makes the proposed DBSD a practical tool in the seismic design of wall-frame structures.

Table 3.1: Characteristics of the wall-frame buildings

| | 6-storey | 9-storey | 12-storey | 15-storey | 20-storey |
|--|-----------|-----------|-----------|-----------|-----------|
| Beams, width x depth (mm) | 400 x 500 | 400 x 550 | 400 x 600 | 400 x 650 | 400 x 700 |
| Interior columns (mm) | 600 x 600 | 650 x 650 | 700 x 700 | 750 x 750 | 800 x 800 |
| Exterior columns (mm) | 600 x 600 | 650 x 650 | 700 x 700 | 750 x 750 | 800 x 800 |
| Walls, length (mm) | 5000 | 5500 | 6000 | 7000 | 8000 |
| Walls, thickness (mm) | 400 | 400 | 400 | 400 | 400 |
| Interior columns, gravity load DL+0.5LL (kN) | 2846.4 | 4341.77 | 5903.6 | 7535.3 | 10258.2 |
| Exterior columns, gravity load DL+0.5LL (kN) | 1531.7 | 2352 | 3222.9 | 4148.36 | 5695.4 |
| Walls, gravity load DL+0.5LL (kN) | 3708.3 | 5501.32 | 7856.4 | 10378 | 14571.3 |

Table 3.2: Estimates of DBSD parameters in different iterations of the five buildings

| | | Normalised inflection height | Yield displacement Δ_y (m) | Ultimate displacement Δ_u (m) | Ductility demand μ |
|------------|---------------|------------------------------|-----------------------------------|--------------------------------------|------------------------|
| 6 -Storey | preliminary | 0.7836 | 0.147 | 0.515 | 3.498 |
| | 1st iteration | 0.7983 | 0.143 | 0.463 | 3.246 |
| | 2nd iteration | 0.7991 | 0.141 | 0.460 | 3.256 |
| | Pushover | - | 0.157 | 0.464 | 2.954 |
| 9- Storey | preliminary | 0.7142 | 0.259 | 0.763 | 2.942 |
| | 1st iteration | 0.7345 | 0.254 | 0.624 | 2.460 |
| | 2nd iteration | 0.7383 | 0.253 | 0.622 | 2.458 |
| | Pushover | - | 0.238 | 0.612 | 2.573 |
| 12- Storey | preliminary | 0.6756 | 0.381 | 1.009 | 2.650 |
| | 1st iteration | 0.7042 | 0.387 | 0.772 | 1.993 |
| | 2nd iteration | 0.7127 | 0.391 | 0.773 | 1.977 |
| | Pushover | - | 0.37 | 0.734 | 1.984 |
| 15 Storey | preliminary | 0.6638 | 0.502 | 1.253 | 2.497 |
| | 1st iteration | 0.6865 | 0.501 | 0.913 | 1.822 |
| | 2nd iteration | 0.6958 | 0.509 | 0.920 | 1.809 |
| | Pushover | - | 0.531 | 0.989 | 1.862 |
| 20 Storey | preliminary | 0.6469 | 0.691 | 1.654 | 2.393 |
| | 1st iteration | 0.6690 | 0.713 | 1.194 | 1.675 |
| | 2nd iteration | 0.6786 | 0.724 | 1.207 | 1.667 |
| | Pushover | - | 0.708 | 1.106 | 1.563 |

Table 3.3: Design parameters of the walls for the five buildings

| | | Reinforcement (mm ²) | M _n (kNm) | ϕ_y (1/m) | ϕ_u (1/m) |
|-----------|---------------------------|----------------------------------|----------------------|----------------|----------------|
| 6-storey | Preliminary | 200@200 | 12830 | 6.862E-04 | 7.203E-03 |
| | 1 st iteration | 2 layers 1200 + 200@200 | 16520 | 6.770E-04 | 7.152E-03 |
| | 2 nd iteration | 2 layers 1200 + 200@200 | 16520 | 6.770E-04 | 7.152E-03 |
| 9-storey | Preliminary | 200@200 | 13526 | 6.249E-04 | 5.335E-03 |
| | 1 st iteration | 2 layers 2000 + 200@200 | 26320 | 6.202E-04 | 5.311E-03 |
| | 2 nd iteration | 2 layers 2000 + 200@200 | 26320 | 6.202E-04 | 5.311E-03 |
| 12-storey | Preliminary | 200@200 | 26310 | 5.924E-04 | 4.017E-03 |
| | 1 st iteration | 3 layers 2000 + 200@200 | 38003 | 5.988E-04 | 4.000E-03 |
| | 2 nd iteration | 3 layers 2000 + 200@200 | 38003 | 5.988E-04 | 4.000E-03 |
| 15-storey | Preliminary | 200@200 | 43930 | 5.013E-04 | 3.125E-03 |
| | 1 st iteration | 2 layers 2000 + 200@200 | 53520 | 5.059E-04 | 3.126E-03 |
| | 2 nd iteration | 2 layers 2000 + 200@200 | 53520 | 5.059E-04 | 3.126E-03 |
| 20-storey | Preliminary | 200@200 | 57410 | 4.586E-04 | 2.320E-03 |
| | 1 st iteration | 3 layers 2800 + 200@200 | 80630 | 4.642E-04 | 2.319E-03 |
| | 2 nd iteration | 3 layers 2800 + 200@200 | 80630 | 4.642E-04 | 2.319E-03 |

Table 3.4: Details of the equivalent SDOF systems in the DBSD of the five buildings

| | | Γ | M* (tonne) | δ_y (m) | δ_u (m) | μ | S_a (g) | V (kN) |
|-----------|---------------------------|----------|------------|----------------|----------------|-------|-----------|---------|
| 6 Storey | preliminary | 1.395 | 4077.9 | 0.106 | 0.369 | 3.498 | 0.0658 | 2632.2 |
| | 1 st iteration | 1.396 | 4068.9 | 0.102 | 0.332 | 3.246 | 0.0863 | 3444.7 |
| | 2 nd iteration | 1.396 | 4069.4 | 0.101 | 0.329 | 3.256 | 0.0869 | 3469.1 |
| | Pushover | 1.407 | 3680.9 | 0.112 | 0.329 | 2.954 | 0.0977 | 3527.9 |
| 9 Storey | preliminary | 1.434 | 6034.7 | 0.181 | 0.532 | 2.942 | 0.0357 | 2113.45 |
| | 1 st iteration | 1.437 | 5990.1 | 0.176 | 0.434 | 2.460 | 0.0677 | 3978.3 |
| | 2 nd iteration | 1.437 | 5989.3 | 0.176 | 0.432 | 2.458 | 0.0698 | 4099.9 |
| | Pushover | 1.444 | 5460.7 | 0.165 | 0.423 | 2.573 | 0.0702 | 3760.6 |
| 12 Storey | preliminary | 1.456 | 8120.6 | 0.262 | 0.693 | 2.650 | 0.031 | 2469.6 |
| | 1 st iteration | 1.462 | 79885 | 0.265 | 0.528 | 1.993 | 0.0552 | 4325.9 |
| | 2 nd iteration | 1.463 | 7982.8 | 0.267 | 0.528 | 1.977 | 0.0557 | 4361.9 |
| | Pushover | 1.459 | 7426.9 | 0.254 | 0.503 | 1.984 | 0.0581 | 4233.1 |
| 15 Storey | preliminary | 1.470 | 10357.0 | 0.342 | 0.853 | 2.497 | 0.0271 | 2753.4 |
| | 1 st iteration | 1.476 | 10167.7 | 0.34 | 0.619 | 1.822 | 0.0521 | 5196.7 |
| | 2 nd iteration | 1.477 | 10154.6 | 0.344 | 0.623 | 1.809 | 0.0521 | 5190 |
| | Pushover | 1.449 | 9712.3 | 0.367 | 0.682 | 1.862 | 0.0462 | 4405.9 |
| 20 Storey | preliminary | 1.485 | 14053.1 | 0.466 | 1.114 | 2.393 | 0.0219 | 3012.2 |
| | 1 st iteration | 1.492 | 13686.0 | 0.477 | 0.800 | 1.675 | 0.0442 | 5928.9 |
| | 2 nd iteration | 1.493 | 13662.0 | 0.485 | 0.808 | 1.667 | 0.0439 | 5890.4 |
| | Pushover | 1.472 | 13070.2 | 0.481 | 0.751 | 1.563 | 0.0506 | 6487.9 |

Table 3.5: Acceptable ultimate displacements based on different design limits

| | Ultimate roof displacement, m | | |
|-----------|-------------------------------|-------------------|-----------------|
| | Ductility limit | 0.025 Drift limit | P-Δ for 5% drop |
| 6 Storey | 0.464 | 0.56 | 0.93 |
| 9 Storey | 0.612 | 0.82 | 0.92 |
| 12 Storey | 0.734 | 1.05 | 1.04 |
| 15 Storey | 0.989 | 1.27 | 1.36 |
| 20 Storey | 1.106 | 1.71 | 1.80 |

Table 3.6: Modal characteristics for multi-modal pushover analyses

| | | First mode | Second mode | Third mode | Fourth mode |
|-----------|---------------------------------|------------|-------------|------------|-------------|
| 6 Storey | M^*/M_{total} | 0.708 | 0.1961 | 0.0625 | 0.0237 |
| | Γ | 1.406 | 0.5996 | 0.3286 | 0.2204 |
| | T (sec) | 2.111 | 0.3770 | 0.1370 | 0.0700 |
| | μ | 2.954 | 1.58 | 1.00 | 1.00 |
| 9 Storey | $D_{\text{target}} \text{ (m)}$ | 0.464 | 0.0200 | 0.0012 | 0.00013 |
| | M^*/M_{total} | 0.687 | 0.1862 | 0.0661 | 0.0314 |
| | Γ | 1.444 | 0.6493 | 0.3488 | 0.2437 |
| | T (sec) | 3.123 | 0.5897 | 0.2177 | 0.1117 |
| 12 Storey | μ | 2.573 | 1.80 | 1.00 | 1.00 |
| | $D_{\text{target}} \text{ (m)}$ | 0.611 | 0.0510 | 0.0040 | 0.00058 |
| | M^*/M_{total} | 0.681 | 0.1768 | 0.0656 | 0.0331 |
| | Γ | 1.459 | 0.6856 | 0.3670 | 0.2590 |
| 15 Storey | T (sec) | 4.150 | 0.8250 | 0.3100 | 0.1600 |
| | μ | 1.984 | 1.70 | 1.00 | 1.00 |
| | $D_{\text{target}} \text{ (m)}$ | 0.734 | 0.0900 | 0.0092 | 0.0015 |
| | M^*/M_{total} | 0.689 | 0.1603 | 0.0634 | 0.0331 |
| 20 Storey | Γ | 1.449 | 0.6885 | 0.3879 | 0.2668 |
| | T (sec) | 5.491 | 1.1930 | 0.4664 | 0.2434 |
| | μ | 1.862 | 1.40 | 1.00 | 1.00 |
| | $D_{\text{target}} \text{ (m)}$ | 0.989 | 0.1491 | 0.0205 | 0.0039 |
| 20 Storey | M^*/M_{total} | 0.673 | 0.1648 | 0.0636 | 0.0334 |
| | Γ | 1.472 | 0.7262 | 0.4169 | 0.2763 |
| | T (sec) | 6.347 | 1.3200 | 0.5080 | 0.2640 |
| | μ | 1.563 | 1.47 | 1.00 | 1.00 |
| | $D_{\text{target}} \text{ (m)}$ | 1.106 | 0.1786 | 0.0255 | 0.0051 |

Table 3.7: Results of multi-mode pushover analyses for the five buildings studied

| | | (1) | (2) | (3) | (4) | (5) | (6) |
|-----------|-----------------|------------|-------------|------------|-------------|--------------|--------------|
| | | First Mode | Second Mode | Third Mode | Fourth Mode | SRSS 3 Modes | SRSS 4 Modes |
| 6 Storey | Base shear (kN) | 3409.8 | 6826.6 | 2987.6 | 256.6 | 8194.8 | 8198.8 |
| | Roof Disp. (m) | 0.460 | 0.014 | 0.0012 | 0.00013 | 0.460 | 0.460 |
| | Maximum drift | 0.02096 | 0.00122 | 0.00036 | 0.00001 | 0.021 | 0.021 |
| 9 Storey | Base shear (kN) | 3829.4 | 7817 | 5593 | 3644 | 10346.2 | 10969.1 |
| | Roof Disp. (m) | 0.611 | 0.051 | 0.004 | 0.001 | 0.613 | 0.613 |
| | Maximum drift | 0.01903 | 0.00347 | 0.00007 | 0.00026 | 0.01935 | 0.01935 |
| 12 Storey | Base shear (kN) | 4329.0 | 9003.4 | 7581.2 | 4126.8 | 12541.0 | 13202.5 |
| | Roof Disp. (m) | 0.730 | 0.054 | 0.0092 | 0.0015 | 0.732 | 0.732 |
| | Maximum drift | 0.01773 | 0.00308 | 0.00088 | 0.0004 | 0.01802 | 0.01802 |
| 15 Storey | Base shear (kN) | 5207.8 | 9404 | 9107 | 5302 | 14089.3 | 15053.9 |
| | Roof Disp. (m) | 0.989 | 0.149 | 0.021 | 0.004 | 1.000 | 1.000 |
| | Maximum drift | 0.02006 | 0.00161 | 0.00239 | 0.00053 | 0.02027 | 0.02027 |
| 20 Storey | Base shear (kN) | 6415.6 | 11682.0 | 11340.4 | 6954.8 | 17499.5 | 18830.9 |
| | Roof Disp. (m) | 1.100 | 0.111 | 0.0255 | 0.0051 | 1.106 | 1.106 |
| | Maximum drift | 0.01654 | 0.00281 | 0.00175 | 0.00049 | 0.01686 | 0.01687 |

Table 3.8: Ground motions proposed by SAC for a probability of exceedance of 10% in 50 years for Los Angeles

| EQ code | Description | M | Distance (km) | Scale Factor | Number of Points | Time Step (sec) | PGA (g) |
|----------------|-------------------------------------|----------|--------------------------|-------------------------|-----------------------------|----------------------------|--------------------|
| La01 | fn Imperial Valley, 1940, El Centro | 6.9 | 10.0 | 2.01 | 2674 | 0.020 | 0.46 |
| La02 | fp Imperial Valley, 1940, El Centro | 6.9 | 10.0 | 2.01 | 2674 | 0.020 | 0.68 |
| La03 | fn Imperial Valley, 1979, Array #05 | 6.5 | 4.1 | 1.01 | 3939 | 0.010 | 0.39 |
| La04 | fp Imperial Valley, 1979, Array #05 | 6.5 | 4.1 | 1.01 | 3939 | 0.010 | 0.49 |
| La05 | fn Imperial Valley, 1979, Array #06 | 6.5 | 1.2 | 0.84 | 3909 | 0.010 | 0.30 |
| La06 | fp Imperial Valley, 1979, Array #06 | 6.5 | 1.2 | 0.84 | 3909 | 0.010 | 0.23 |
| La07 | fn Landers, 1992, Barstow | 7.3 | 36.0 | 3.20 | 4000 | 0.020 | 0.42 |
| La08 | fp Landers, 1992, Barstow | 7.3 | 36.0 | 3.20 | 4000 | 0.020 | 0.43 |
| La09 | fn Landers, 1992, Yermo | 7.3 | 25.0 | 2.17 | 4000 | 0.020 | 0.52 |
| La10 | fp Landers, 1992, Yermo | 7.3 | 25.0 | 2.17 | 4000 | 0.020 | 0.36 |
| La11 | fn Loma Prieta, 1989, Gilroy | 7.0 | 12.0 | 1.79 | 2000 | 0.020 | 0.67 |
| La12 | fp Loma Prieta, 1989, Gilroy | 7.0 | 12.0 | 1.79 | 2000 | 0.020 | 0.97 |
| La13 | fn Northridge, 1994, Newhall | 6.7 | 6.7 | 1.03 | 3000 | 0.020 | 0.68 |
| La14 | fp Northridge, 1994, Newhall | 6.7 | 6.7 | 1.03 | 3000 | 0.020 | 0.66 |
| La15 | fn Northridge, 1994, Rinaldi RS | 6.7 | 7.5 | 0.79 | 2990 | 0.005 | 0.53 |
| La16 | fp Northridge, 1994, Rinaldi RS | 6.7 | 7.5 | 0.79 | 2990 | 0.005 | 0.58 |
| La17 | fn Northridge, 1994, Sylmar | 6.7 | 6.4 | 0.99 | 3000 | 0.020 | 0.57 |
| La18 | fp Northridge, 1994, Sylmar | 6.7 | 6.4 | 0.99 | 3000 | 0.020 | 0.82 |
| La19 | fn North Palm Springs, 1986 | 6.0 | 6.7 | 2.97 | 3000 | 0.020 | 1.02 |
| La20 | fp North Palm Springs, 1986 | 6.0 | 6.7 | 2.97 | 3000 | 0.020 | 0.99 |

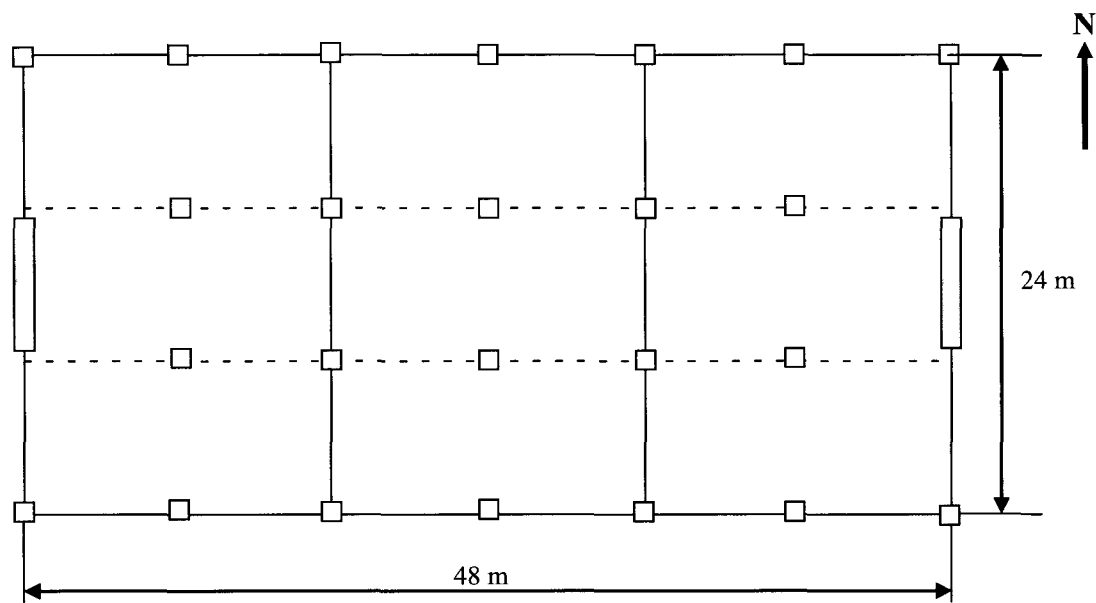


Figure 3.1: Typical plan view of the wall-frame buildings

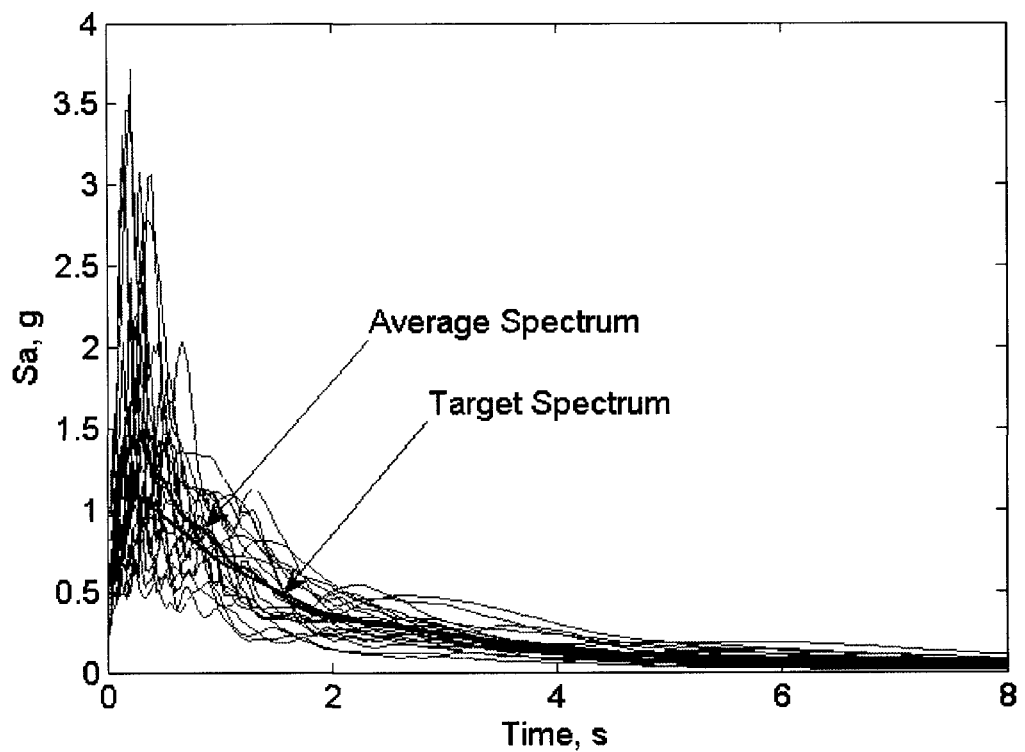


Figure 3.2: Design response spectrum and average of the spectra of 20 selected earthquakes

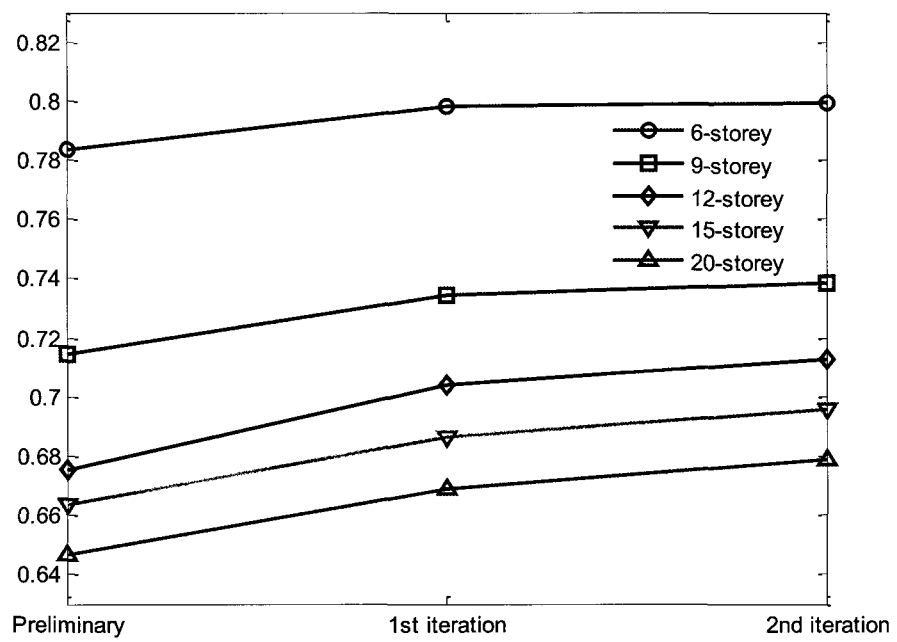


Figure 3.3: Normalised inflection height of the 5 wall-frame buildings

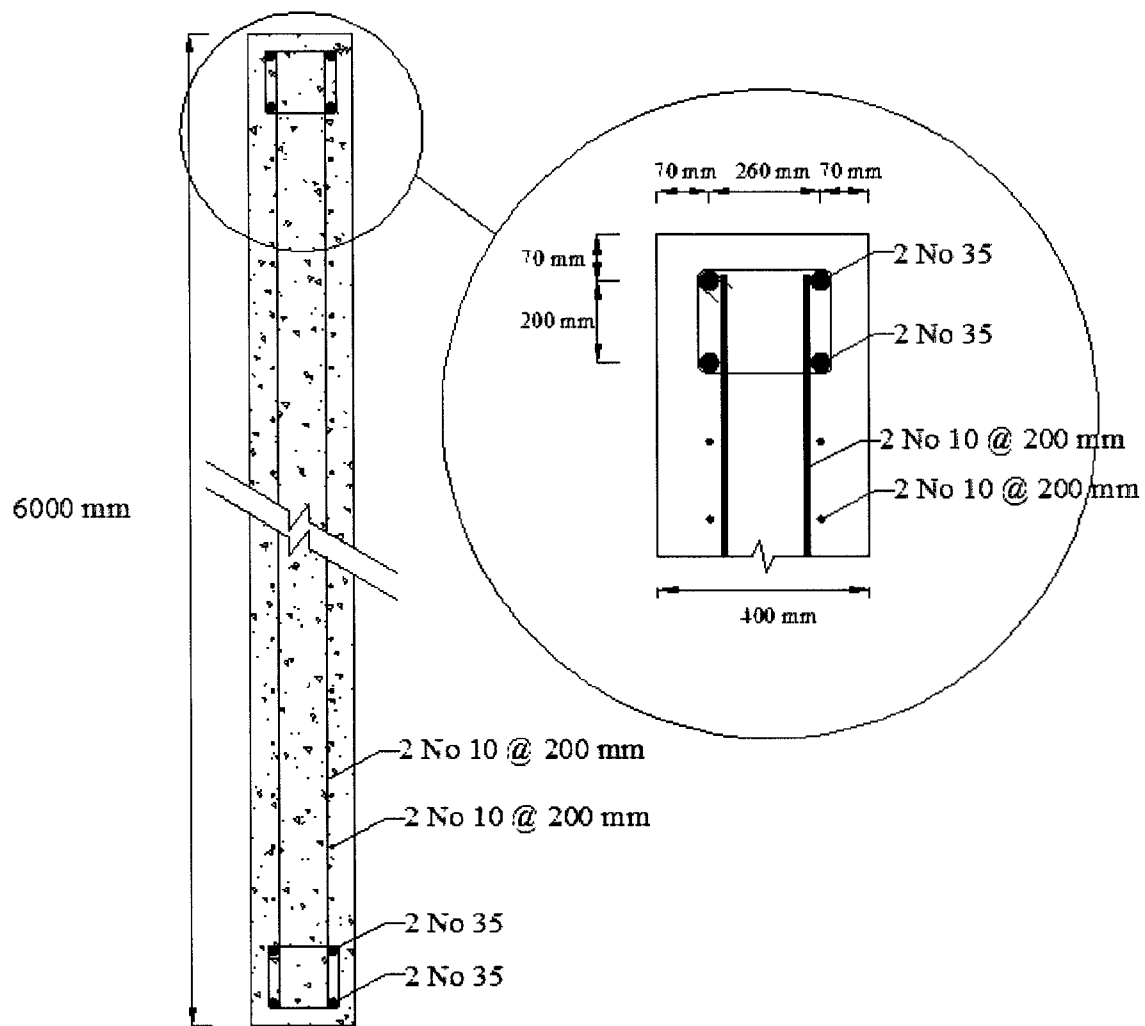


Figure 3.4: Details of the longitudinal reinforcements for the final design of shear wall for the 12-storey building

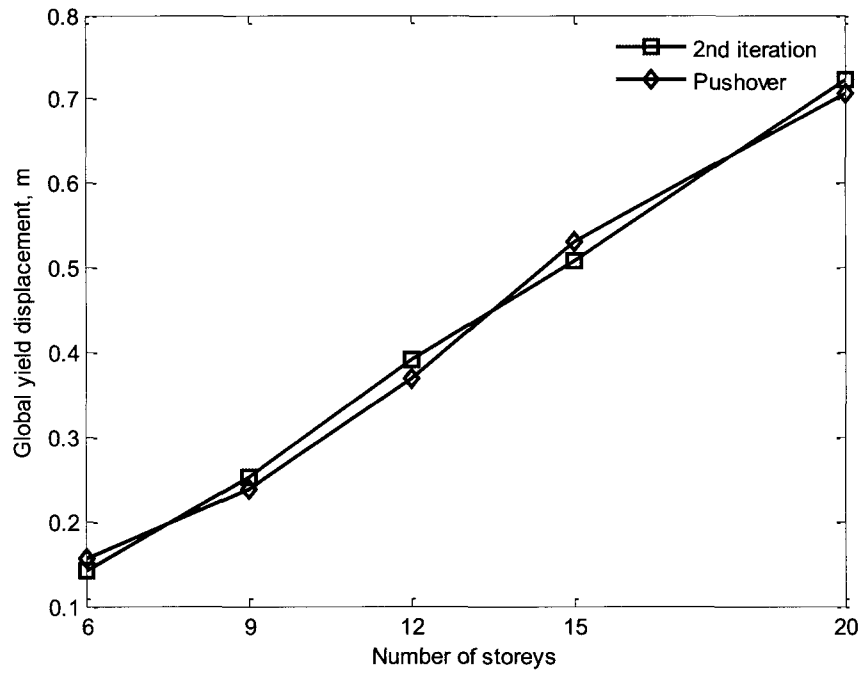


Figure 3.5: Global yield displacement estimates

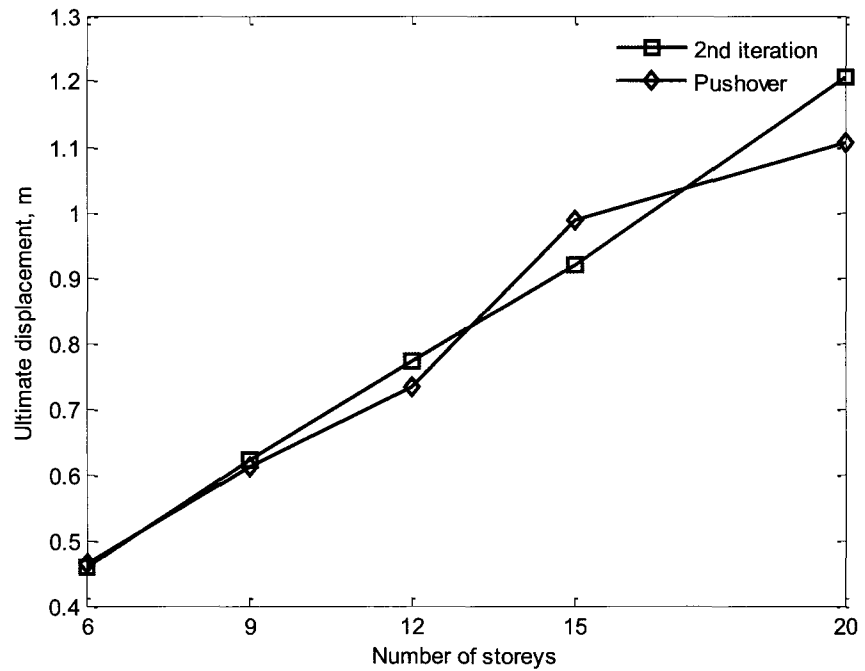


Figure 3.6: Ultimate displacement estimates

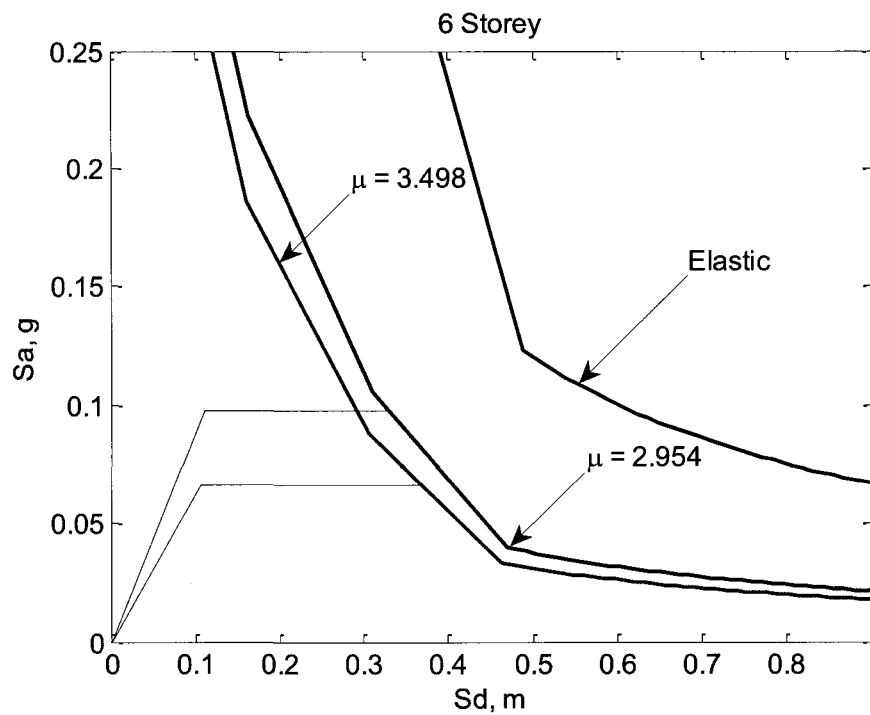


Figure 3.7: Capacity and demand diagrams for the 6-storey building for first and last iterations

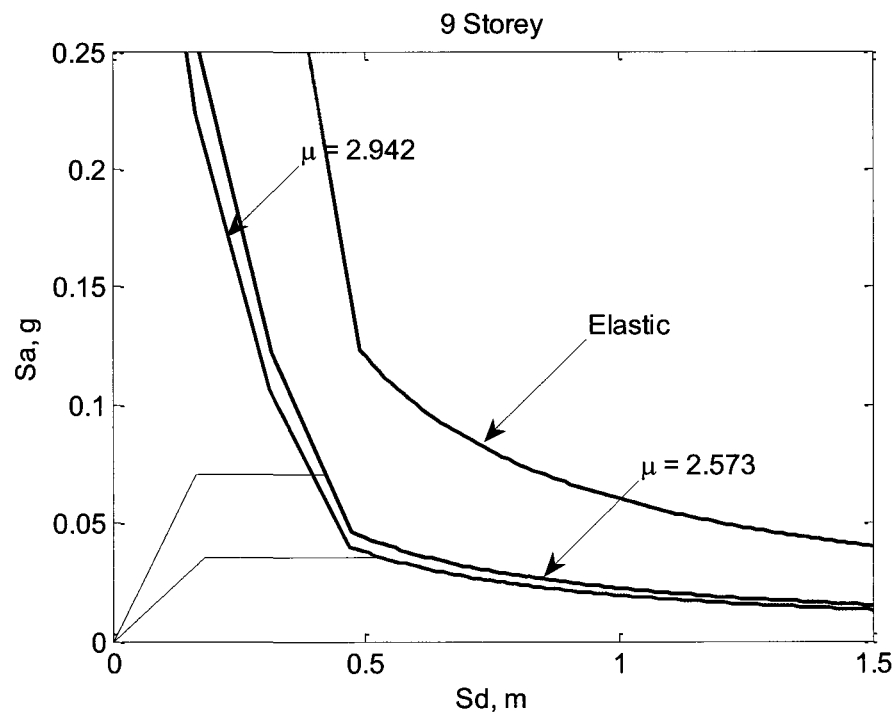


Figure 3.8: Capacity and demand diagrams for the 9-storey building for the first and last iterations

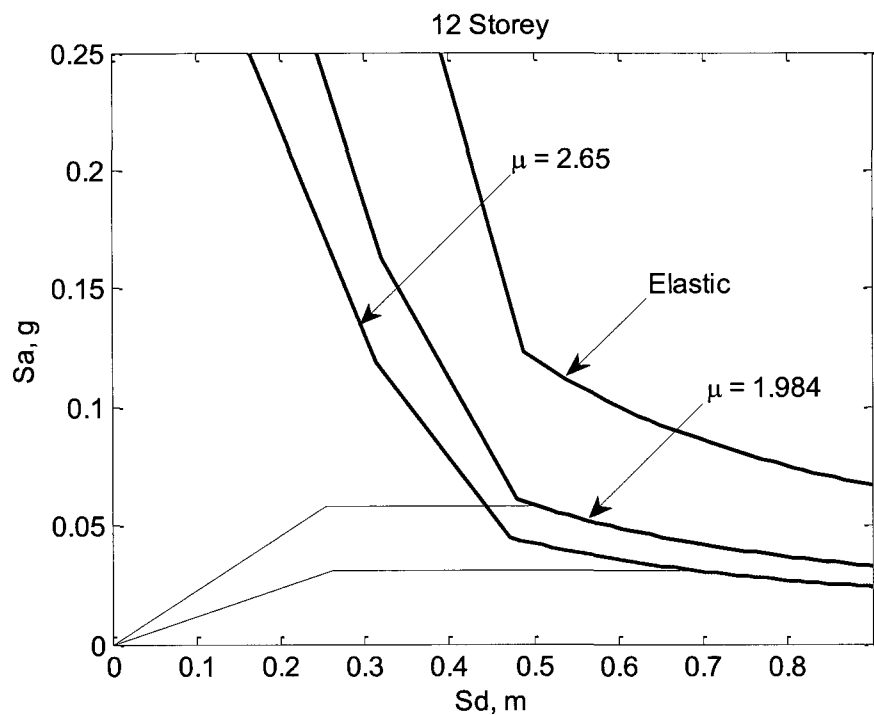


Figure 3.9: Capacity and demand diagrams for the 12-storey building for the first and last iterations

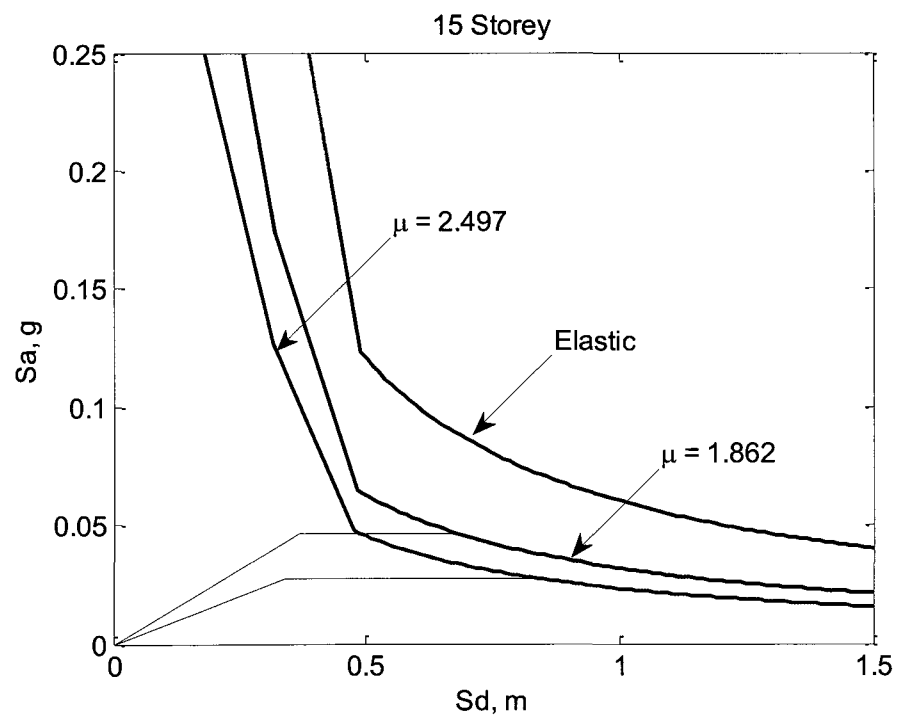


Figure 3.10: Capacity and demand diagrams for the 15-storey building for the first and last iterations

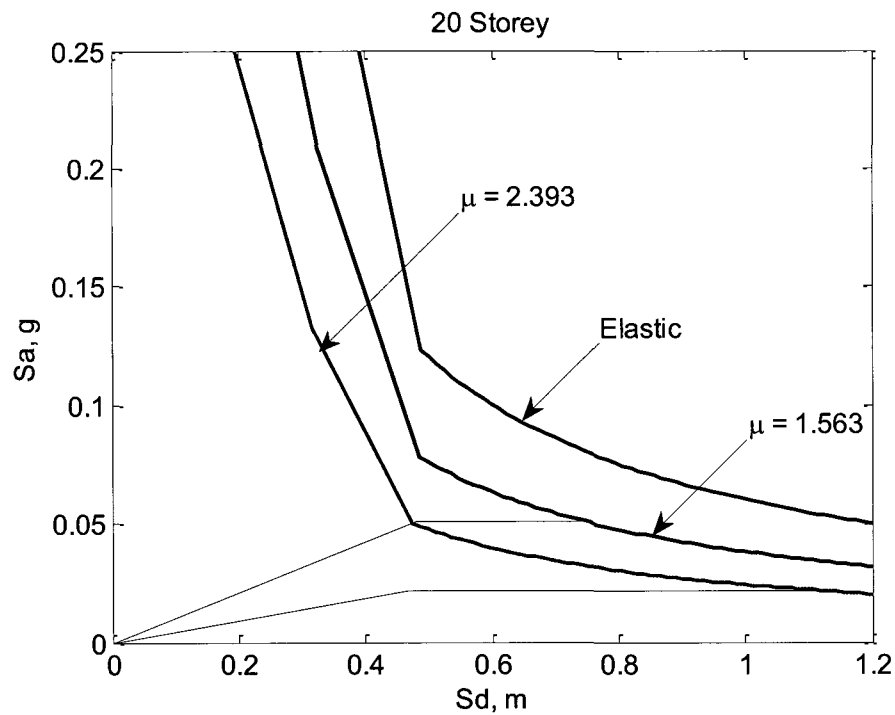


Figure 3.11: Capacity and demand diagrams for the 20-storey building for the first and last iterations

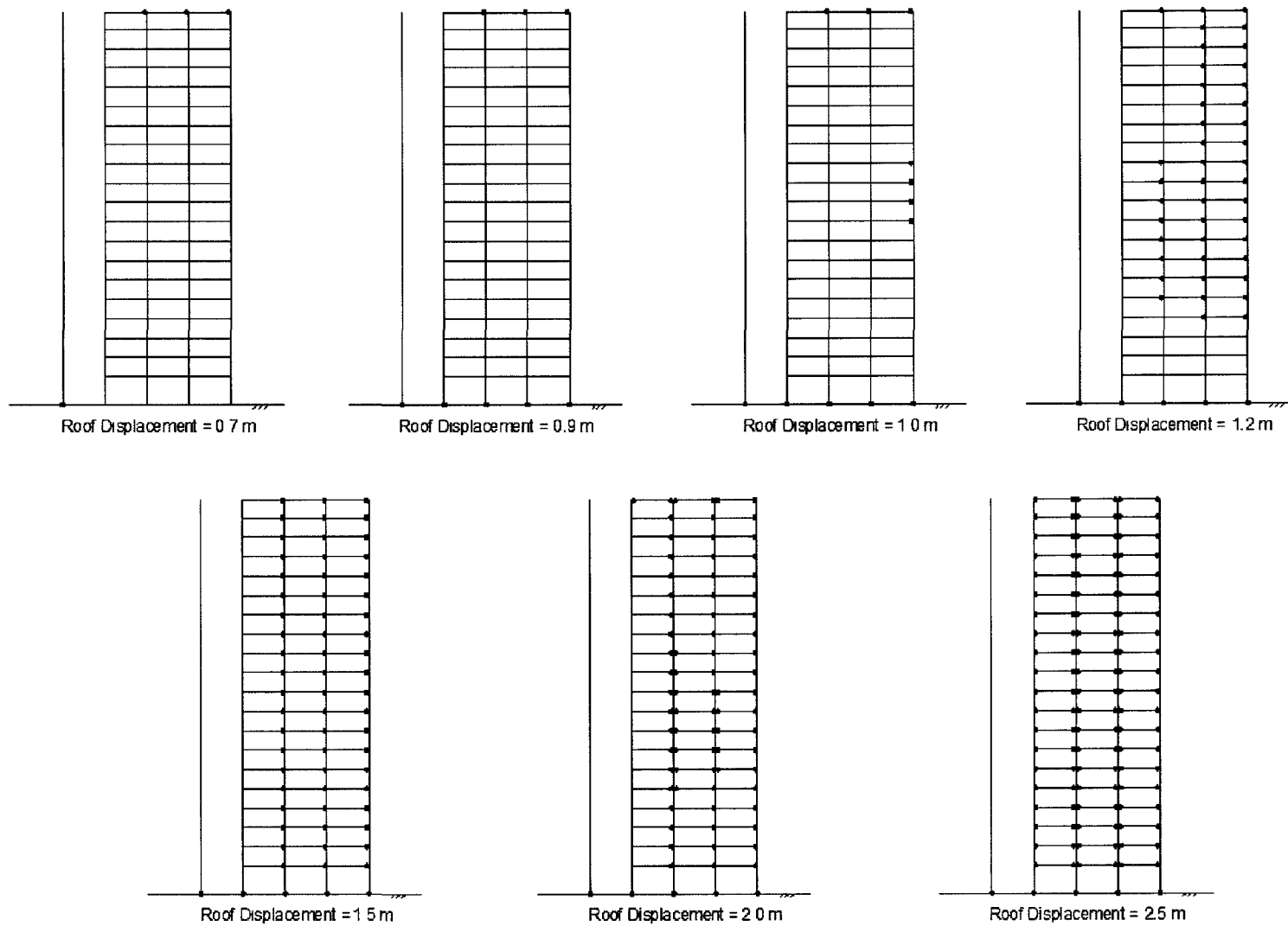


Figure 3.12: Structural model for the 20-storey building and development of plastic hinges

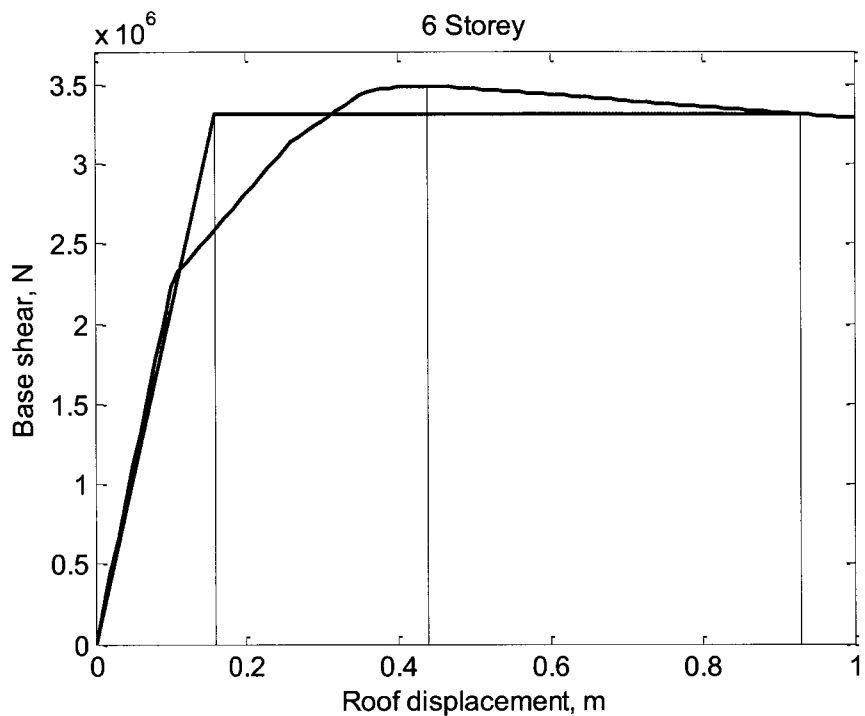


Figure 3.13: Pushover curve and its bi-linear idealization for the 6-storey building

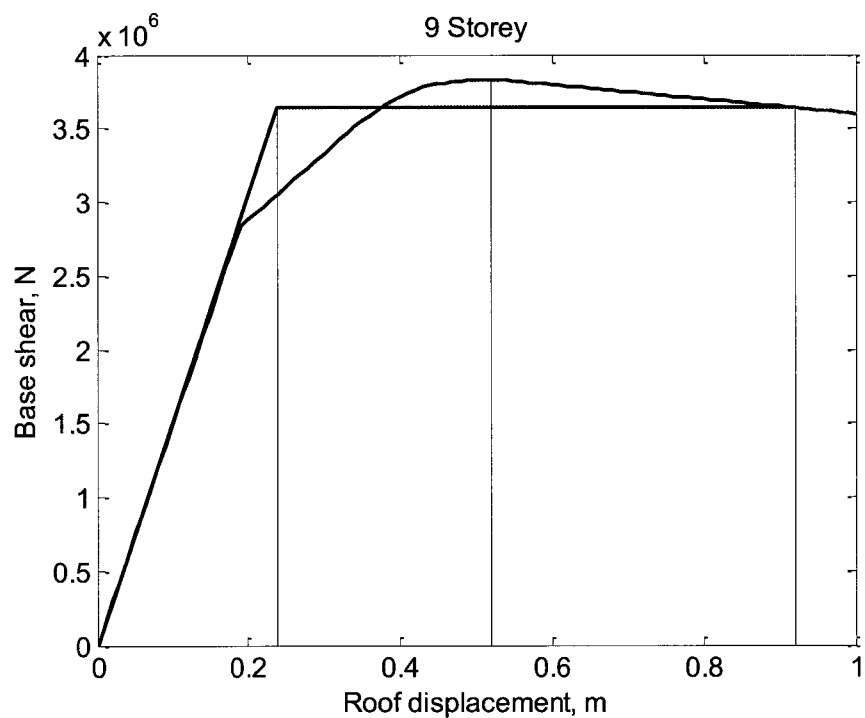


Figure 3.14: Pushover curve and its bi-linear idealization for the 9-storey building

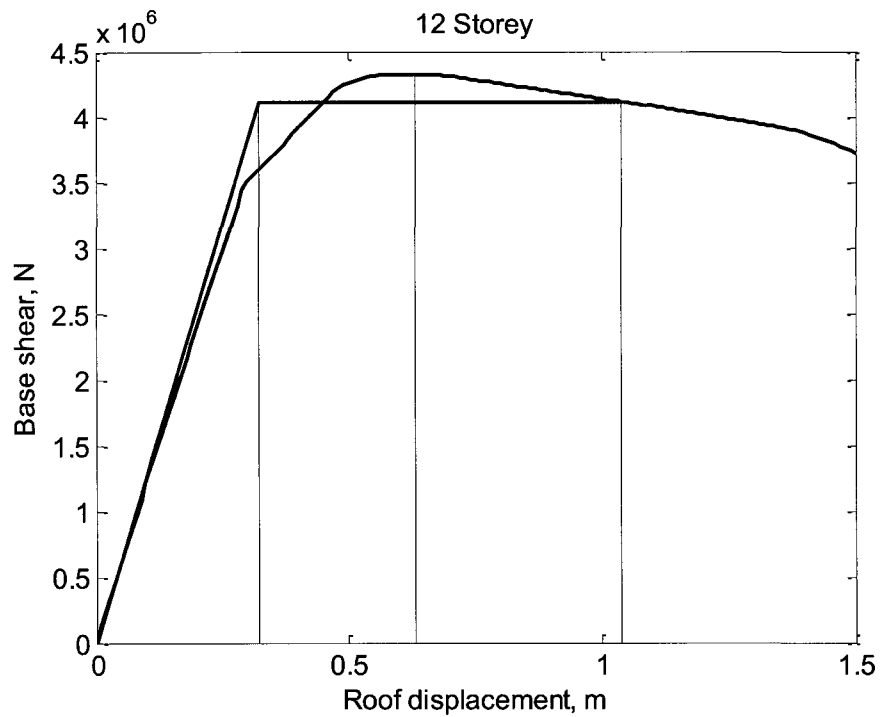


Figure 3.15: Pushover curve and its bi-linear idealization for the 12-storey building

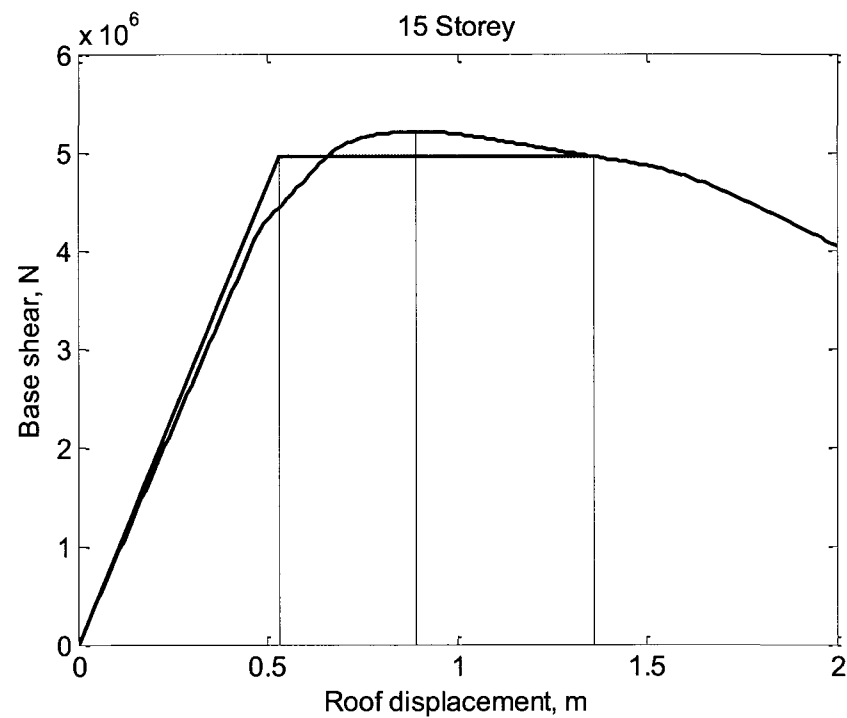


Figure 3.16: Pushover curve and its bi-linear idealization for the 15-storey building

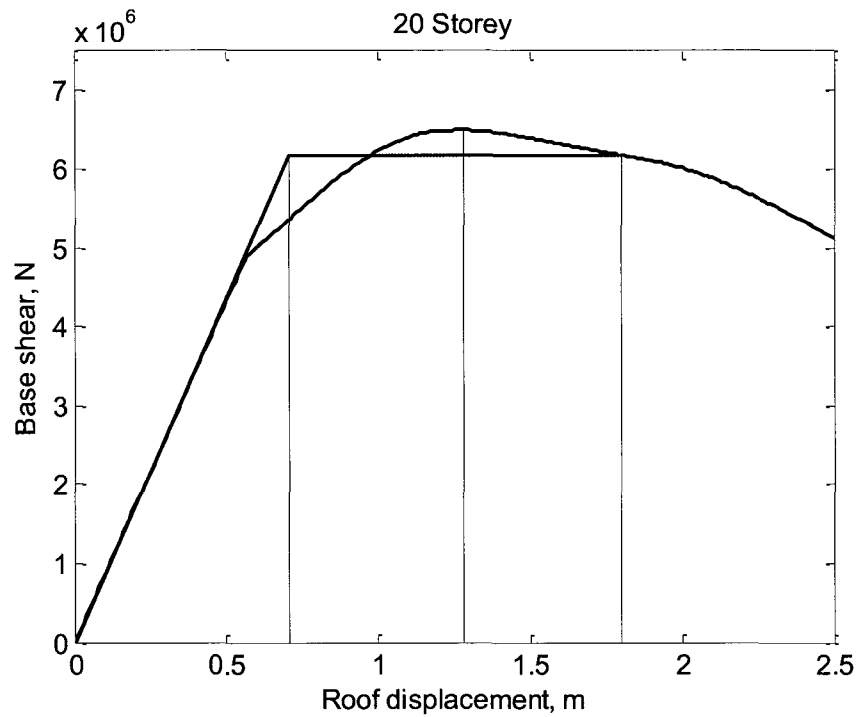


Figure 3.17: Pushover curve and its bi-linear idealization for the 20-storey building

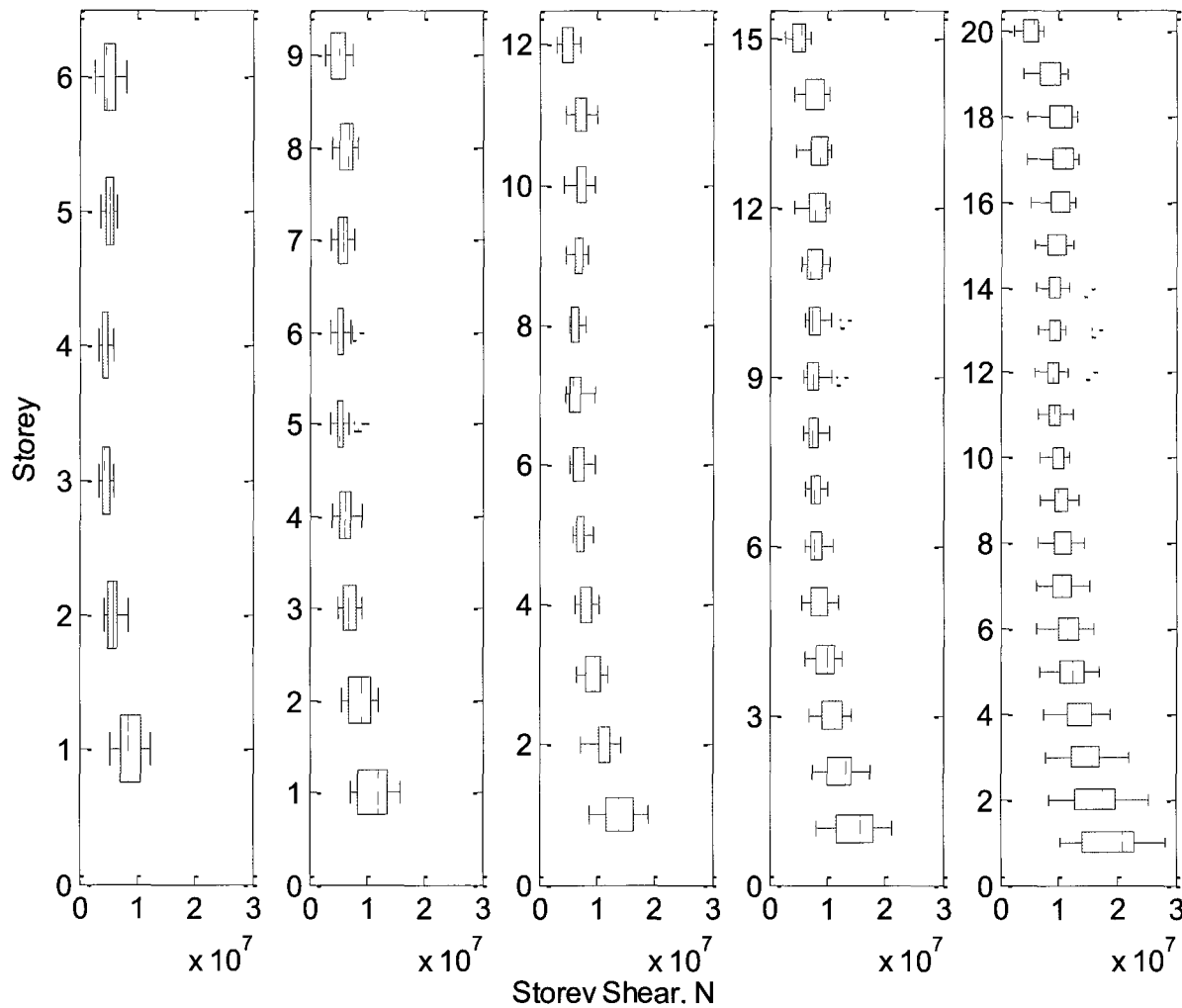


Figure 3.18: Distribution of the maximum storey shear in the five buildings subjected to twenty ground motions

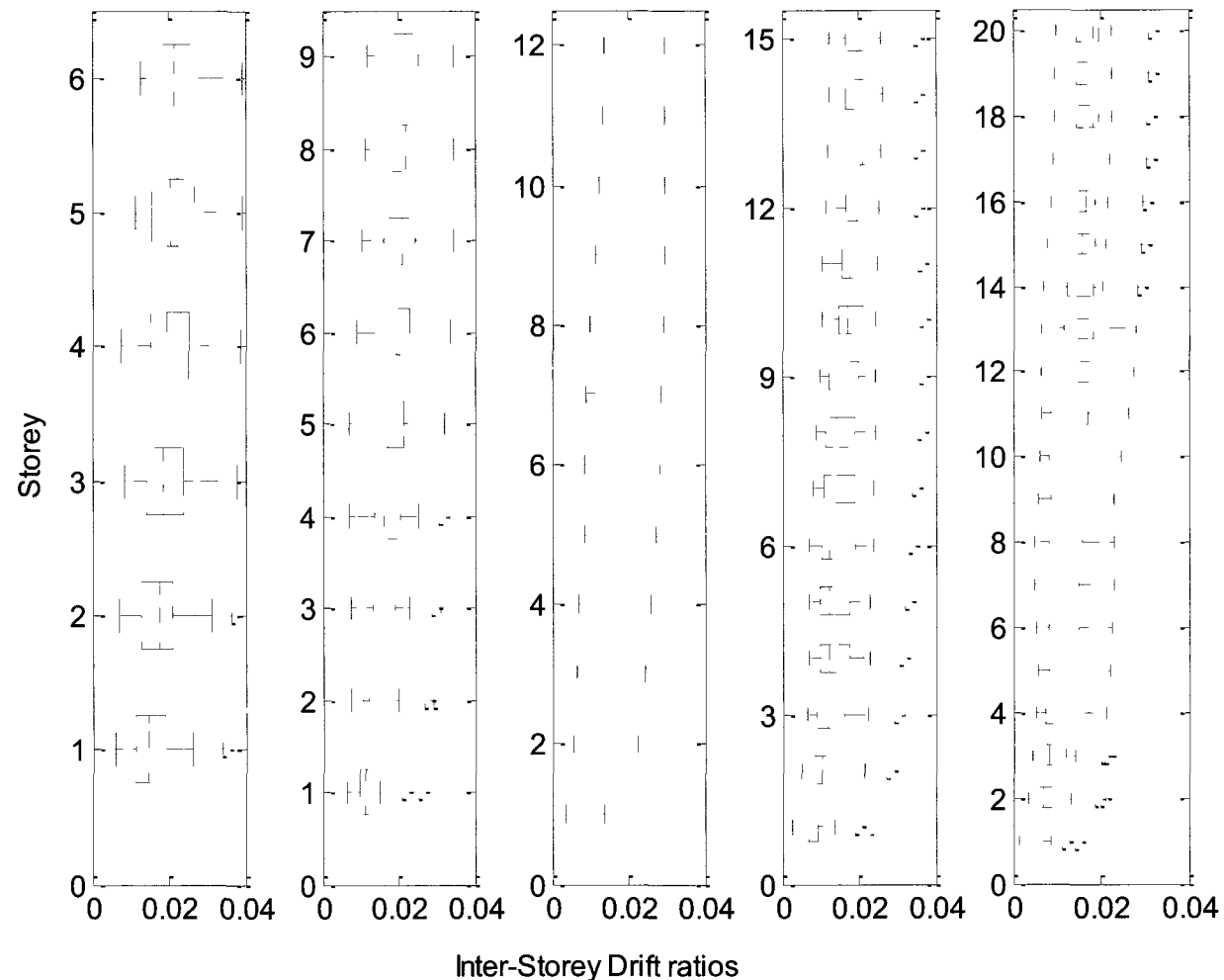


Figure 3.19: Distribution of the maximum inter-storey drifts in the five buildings subjected to twenty ground motions

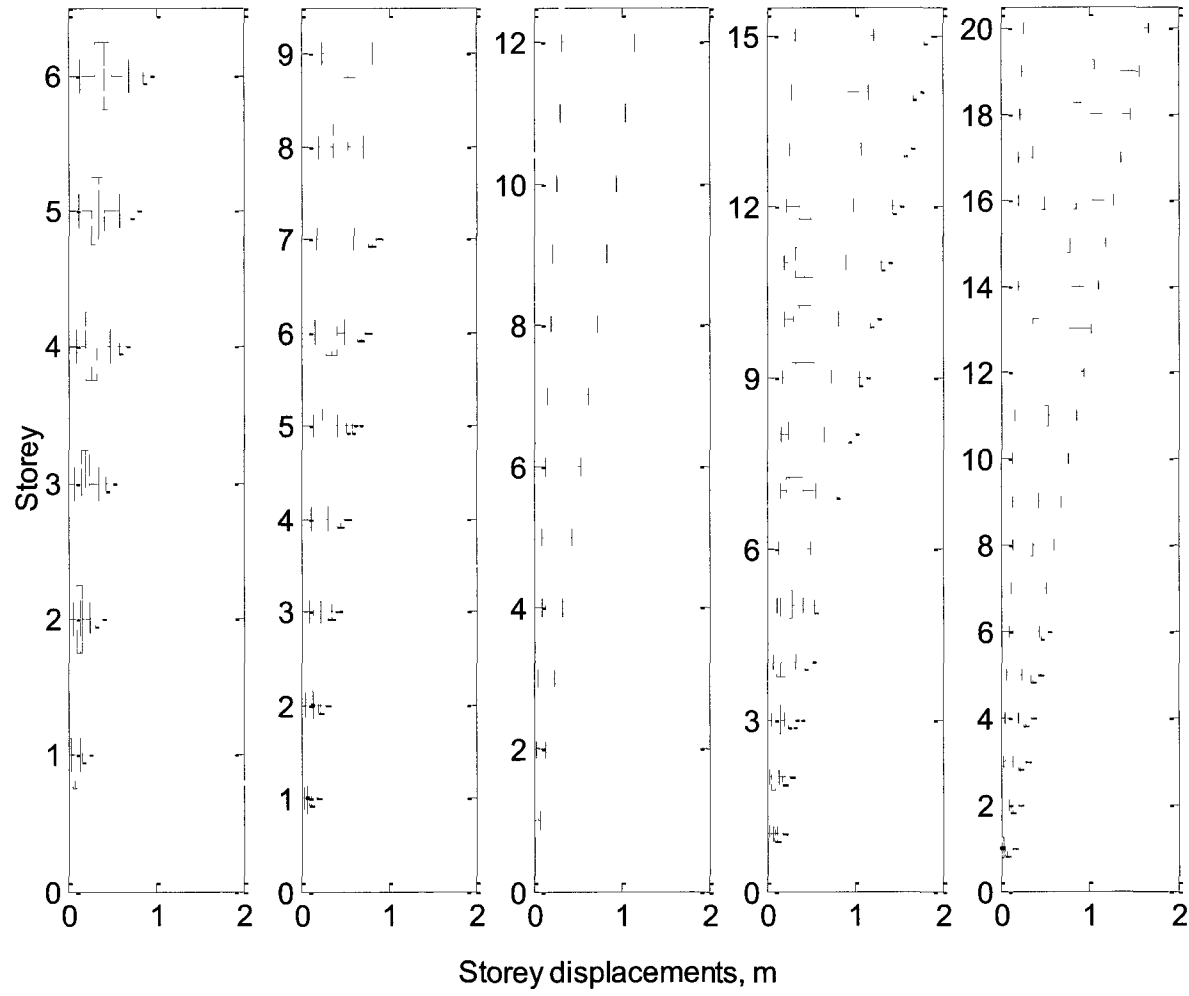


Figure 3.20: Distribution of the maximum storey displacements in the five buildings subjected to twenty ground motions

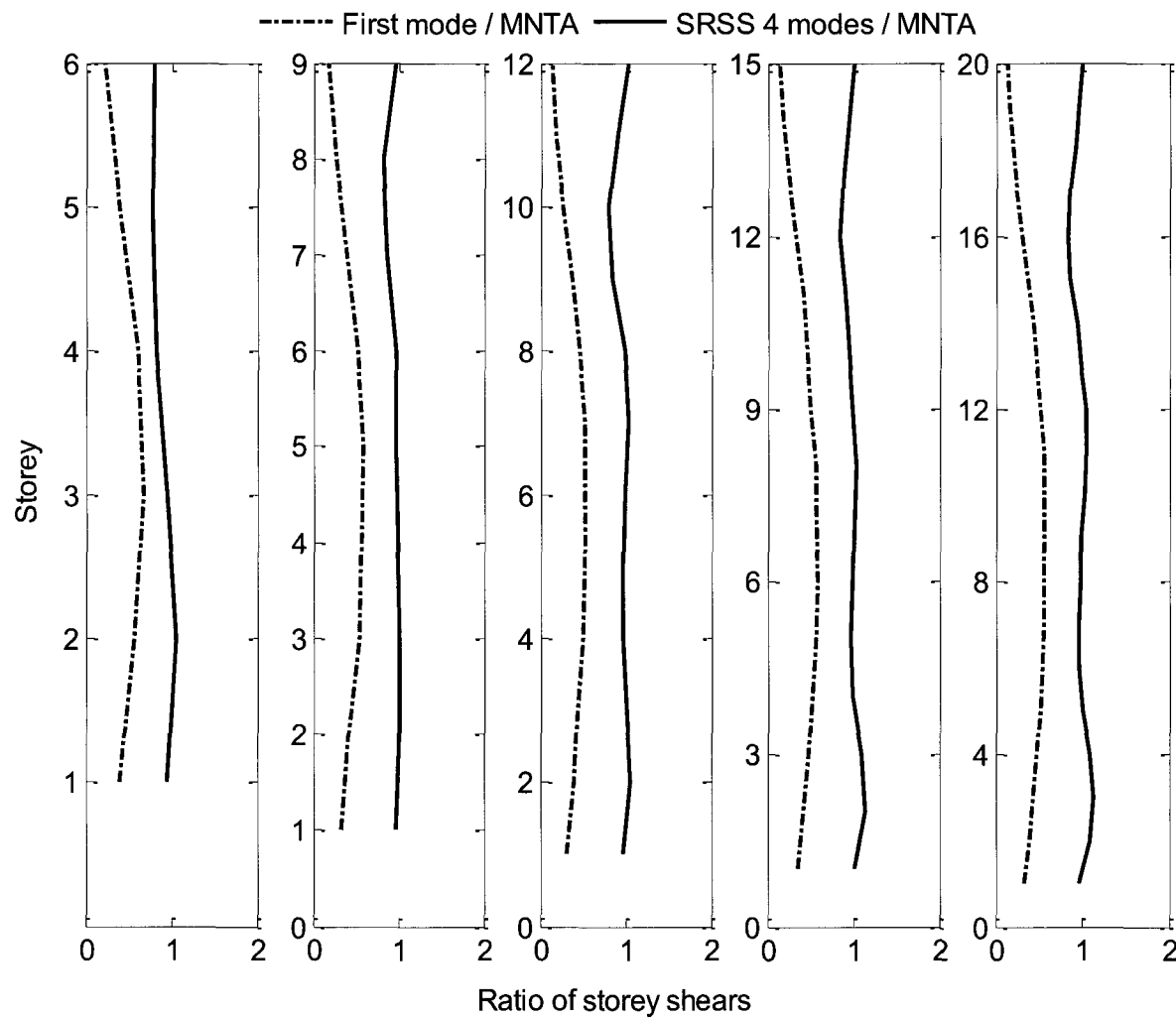


Figure 3.21: Comparison of storey shears in multi-modal pushover analyses with the Mean of twenty Nonlinear Time-history Analyses

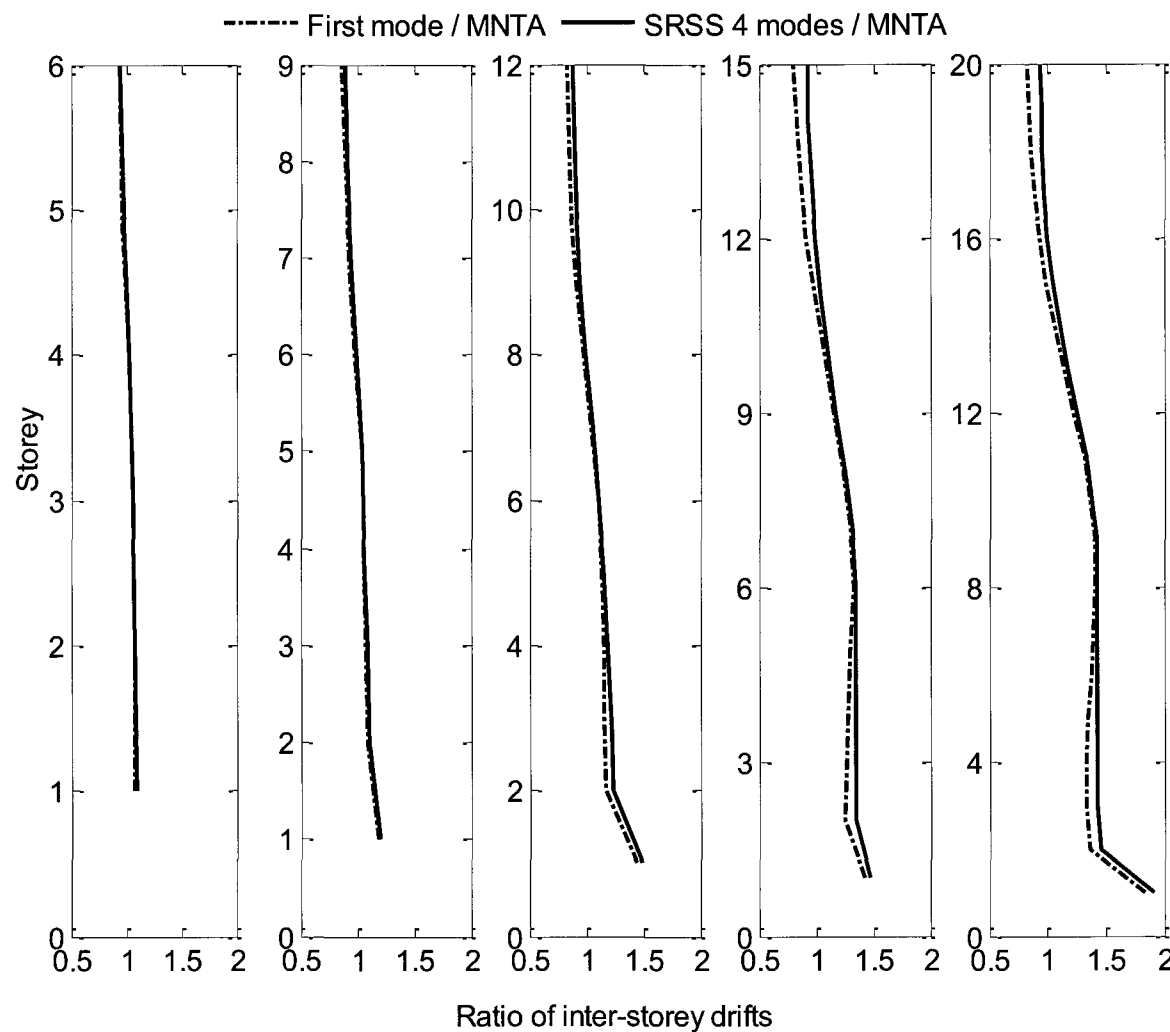


Figure 3.22: Comparison of inter-storey drift in multi-modal pushover analyses with the Mean of twenty Nonlinear Time-history Analyses

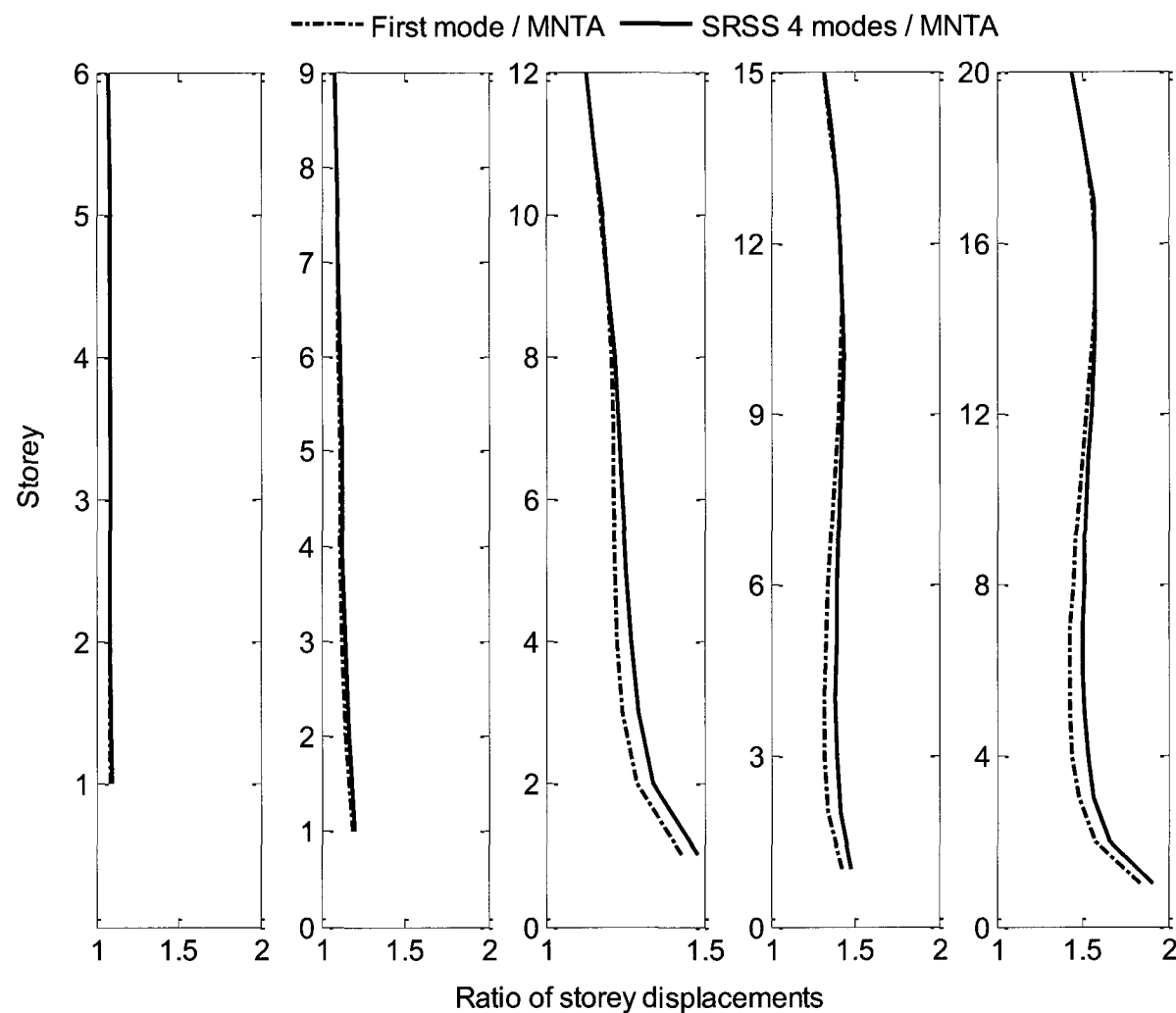


Figure 3.23: Comparison of storey displacements in multi-modal pushover analyses with the Mean of twenty Nonlinear Time-history Analyses

Chapter 4. Nonlinear seismic response of single-storey asymmetric plan buildings

4.1 Introduction

Asymmetry in the plan of a structural system has been a subject of study for the past few decades and researchers have paid significant attention to the effect of torsion in the response of structural systems. Even though designers prefer symmetrical structural layout, irregularity and asymmetry may be dictated by functional and aesthetic demands, or may result from irregularity in mass distribution due to occupancy needs. In practice, unsymmetry in structural layout and/or distribution of mass is quite common.

Currently, building codes contain forced-based design provisions to account for the effect of torsion in the structure when it is subjected to lateral excitation. These provisions are based on the studies on elastic response of asymmetric plan systems. A limited amount of work has been done on the performance based design of asymmetric plan buildings based on inelastic response of such structures. In this chapter, inelastic seismic response of asymmetric plan is studied for different torsionally unbalanced systems and a suggested method of estimating the maximum rotation in the plan of such structures due to torsional response is presented.

4.2 Asymmetric plan buildings

Asymmetric plan buildings experience coupled translational and torsional motion, when excited laterally. Such response of the system causes non-uniform demand on different resisting element of the structure, which makes a building with asymmetric plan

vulnerable to damage. Therefore, a study of the inelastic torsional behaviour of such systems is essential for developing a performance based design procedure.

Asymmetric plan buildings can be categorized into three groups based on the level of coupling between the translational and torsional contributions to the seismic response.

- 1) *Torsionally stiff*: It is a system in which the first torsion dominant mode has a period that is considerably shorter than the first translation dominant mode. First mode dominates the lateral displacement motion of such a system and is weakly coupled with torsion.
- 2) *Torsionally similar*: In such system the translation and torsion dominant modes have close modal periods. The lateral and torsional motions are similar in magnitude and they are strongly coupled.
- 3) *Torsionally flexible*: It is a system in which the first mode is torsion dominant, and the period of the second mode which is translation dominant is considerably shorter than that of the torsion dominant mode.

The presence of resisting planes perpendicular to the planes in the direction in which the response of the structure is being studied has a marked influence on the response. Systems in which orthogonal resisting planes exist are usually referred to as torsionally restrained systems. A system in which such planes do not exist is called torsionally unrestrained. The response of an asymmetric plan building is strongly dependent on whether the system is torsionally restrained or unrestrained.

In this chapter, base shear torque (BST) surface, incremental dynamic analysis (IDA), pushover analysis, and modal decomposition technique are used to investigate the inelastic response of asymmetric plan buildings to lateral excitation. First, these tools are briefly described, and then using such tools the responses of single-storey torsionally restrained and unrestrained systems are investigated. Finally, three different types of torsionally unbalanced systems are studied.

4.3 Analytical tools

4.3.1 BST ultimate surface

The in-plane strength distribution has significant effect on the nonlinear response of asymmetric plan buildings. De La Llera et al (1995) showed that a surface representing the base shear versus torque relationship at collapse is an effective means of describing the effect of in-plane distribution of the strengths. This surface can be generated by the set of base shear and torque combinations that correspond to different collapse mechanisms.

Figure 4.1 shows the plan view of a system consisting of a total of 5 resisting planes in x, and y direction. Since all the planes have identical strengths and stiffness the system is symmetric in plan in both directions. On the right side of Figure 4.1 the BST surface for this system is shown for excitation in y direction. The outer surface shows the sets of base shear and torque combinations that can cause a mechanism, while the inner surface separates the elastic domain from the inelastic domain. Point P1 represents a

mechanism in which all walls in the y direction have yielded but there is no rotation in the system. On the other hand, point P2 represents failure of the system due to pure torsion while the base shear is zero. For points along the line AB three planes in the y direction have yielded in the same direction. For points lying on the line CD both orthogonal planes have yielded, but in opposite directions. For points on line BC some planes have yielded while others have not.

The BST surface is point symmetric with respect to the origin of the base shear and torque axis. In other words similar mechanism can be developed by changing the direction of the pair of base shear and torques in the first quadrant. Several parameters can affect the shape of a BST surface as explained briefly here:

- 1) Lateral capacity: Lateral capacity in y direction, is provided by only the three planes in the y direction. With an increase in the lateral capacity, while the torsional capacity remains constant, line CD in Figure 4.1 will be longer and the BST surface will be skewed along the Vy axis.
- 2) Torsional capacity: Torsional capacity of the system arises from two sources, a) strength of the orthogonal walls, and b) strength of the edge planes. With an increase in either of these two sources, line AB in Figure 4.1 will be longer and the BST surface will be skewed along the T axis.
- 3) Strength distribution: The planar distribution of strength can also affect the shape of the BST surface. If the strengths are distributed symmetrically the BST will be a hexagon similar to the one shown in Figure 4.1. In cases where there is

unsymmetry in the distribution of strengths the BST surface will be skewed along a line parallel to the line AH. A typical BST surface for a plan asymmetric building is shown in Figure 4.2.

Let us consider an asymmetric plan building as shown in Figure 4.2. The building has 5 planes providing lateral resistance in X and Y directions. The stiffness of plane "i" is defined as $a_i \times k$, where $k = 5961.3$ kN/m and its strength is $b_i \times f$, where f is set to be 44.4 kN. It is assumed that strength is dependent on stiffness, $a_i = b_i$, and the center of rigidity (CR) coincides with the center of strength (CS). The distance between the center of mass (CM) and the center of strength is denoted as e_{CR} . Assuming that $b_3 = b_5$ and b_2 is greater than both b_1 and b_4 , e_{CR} can be obtained as follows (see Figure 4.2):

$$e_{CR} = \frac{b_2 - b_4}{(b_1 + b_2 + b_4)} * w/2 \quad (4.1)$$

where, w is the distance between the flexible and stiff planes as shown in Figure 4.2.

When the maximum base shear is developed (due to yielding of the three planes in y direction) based on the direction of the floor twist two different torques can be developed at which the orthogonal planes have also yielded (namely T_{min} and T_{max}), where,

$$T_{\min} = (b_2 - b_3 - b_4) * f * w/2 \rightarrow e_{\min} = \frac{(b_2 - b_3 - b_4)}{(b_1 + b_2 + b_4)} * w/2 \quad (4.2)$$

$$T_{\max} = (b_2 + b_3 - b_4) * f * w/2 \rightarrow e_{\max} = \frac{(b_2 + b_3 - b_4)}{(b_1 + b_2 + b_4)} * w/2 \quad (4.3)$$

Let b_2 and b_4 be given and b_3 varied. Then based on the value of b_3 , T_{\min} can be positive, zero, or negative. When T_{\min} is zero, the corresponding eccentricity, e_{\min} , will be zero. Therefore if the strength of orthogonal walls is assigned so that $T_{\min} = 0$, we have:

$$e_{\min} = 0 \rightarrow (b_2 - b_3 - b_4) = 0 \rightarrow b_3 = b_2 - b_4 \quad (4.4)$$

4.3.2 Incremental dynamic analysis (IDA)

Incremental dynamic analysis is a powerful tool in understanding the nonlinear behaviour of structural systems. The use of IDA has become feasible because the computer processing power has grown during the last decade. IDA involves nonlinear dynamic analysis of the structure for a series of ground motion intensities. IDA can be run for one or multiple records to get a better understanding of the nonlinear behaviour of the system.

IDA can provide good understanding of the variation of response and the nature of structural response as the intensity of ground motion increases. The most important advantage of IDA over pushover analysis is that it provides an estimate of the dynamic capacity of the global structural system. Recently, FEMA guidelines have adopted IDA as the state-of-the-art method for evaluating the collapse capacity of the structures. A set of typical IDA curves for 30 ground motions is shown with solid and dashed lines in Figure 4.3. IDA curves plot a response parameter versus the intensity of the ground

motion; in this case the maximum inter-storey drift ratio is used as the monitoring response parameter.

4.4 Torsionally unrestrained and restrained systems

Consider the system shown in Figure 4.2(a). When $b_3 = b_5 = 0$ the system is torsionally unrestrained, and the BST surface is the one shown with dashed line in Figure 4.2(b). Such a system would exist if the X direction resisting planes lie at the center of mass. Torsionally unrestrained systems are very vulnerable to seismic damage. This is mainly because when the flexible plane yields the center of rotation moves to the stiff edge and this greatly increases the displacement demand on the flexible plane.

Table 4.1 shows the characteristics of one torsionally unrestrained (S1) and two torsionally restrained systems (S2-S3) studied here. Use of Equation (4.1) gives $e_{C,R} = b/8$ for all three systems. The value of b_3 which makes T_{min} equal to zero works out to 0.75 (system S2). In order to investigate the torsional behaviour of the selected systems, incremental dynamic analyses are carried out for 0.1, 0.2, 0.4, 0.6, .8, 1.0, 1.5, 2.0, 2.5, and 3.0 times the El Centro ground motion.

Figure 4.4 shows the BST surface for S1 and the values of Vy-Torque pairs, while Figure 4.5 shows the IDA curves for base shear. The data points Figure 4.4 show the base shear-torque pair, at the instant maximum displacement demand is reached in the flexible edge plane, stiff edge plane, and the center plane, while, the data points in Figure 4.5 show the base shear at those instants. As the intensity of the ground motion increases the

response moves from elastic to inelastic. In the elastic domain, the maximum displacement demands for all three planes correspond to the same Vy-Torque pair, which means that the maximum displacement demand is achieved at the same deformed configuration. However, in the inelastic domain maximum displacement demand for each plan corresponds to a different deformed configuration. It is interesting to note that the maximum displacement demand on the flexible plane as well as the center plane occurs when the maximum lateral strength of the system has not been mobilized, i.e. the stiff plane has not yielded. On the other hand, the maximum displacement demand in the stiff plane corresponds to the state when all three planes have yielded.

The strength of the orthogonal plane in system S2 has been selected to make T_{min} equal to zero. This strength is also the minimum orthogonal strength required to keep the orthogonal walls in the elastic range at the instant when the maximum lateral strength is reached. For orthogonal wall strengths that make T_{min} negative, the orthogonal walls remain elastic, when the maximum lateral strength in the y direction is reached. For orthogonal wall strengths that make T_{min} positive, the orthogonal walls yield when the maximum strength in the y direction is reached. By examining the BST surface and IDA curves for system S2, shown in Figure 4.6, and Figure 4.7 it can be noted that with an increase in the intensity of ground motion the maximum displacement demands in all three planes are reached in the same displacement configuration, the one corresponding to T_{min} . The maximum displacement demand in the stiff plane always corresponds to the T_{min} configuration, as can be seen for the numbers assigned to the different ground motion scale factors and entered in Figure 4.6 and 4.7.

In system S3, the strengths of orthogonal planes as well as their stiffnesses are twice as much as in system S2. Figure 4.8 shows the BST surface and the IDA results and Figure 4.9 shows the corresponding IDA curves for the base shear of this system. It can be seen that as in the case of system S2, the base shear torque pairs at the instant of maximum displacement demand in each of the three planes merge at the configuration corresponding to T_{min} . However, in contrast to system S2, for the system S3 this configuration is the defining configuration for maximum displacement demand in all three planes, the flexible edge, the central and the stiff edge (see Figure 4.9).

In summary, if we provide sufficient orthogonal resistance to make T_{min} to be non-positive, the maximum lateral capacity of the system can be achieved and the deformed shaped corresponding to the development of T_{min} can be taken as the ultimate deformed shape.

4.5 Modal decomposition

As mentioned earlier, the torsional and lateral responses of an asymmetric plan building are coupled. The relative contribution of the different modes to the total response does, however, vary with the characteristics of the system. In order to investigate the contribution of individual modes in the lateral seismic response of asymmetric buildings, we take advantage of modal decomposition method. Let $\mathbf{D}(t)$ be the time dependent global response vector of order 2 (containing the lateral and torsional component of the response). The system is strained into the inelastic range hence the modal responses are

coupled. Even then, the predominant response may be in a single mode. To verify this we decompose the response into modal components as follows:

$$\mathbf{D}(t) = \alpha_1(t)\varphi_1 + \alpha_2(t)\varphi_2 \quad (4.5)$$

where φ_i is the i^{th} mass orthonormal elastic mode shape. Coefficients on the right hand side are obtained from:

$$\alpha_i(t) = \varphi_i^T \mathbf{MD}(t) \quad (4.6)$$

and represent the modal contributions to the response. We use this modal decomposition process to investigate different torsional systems.

4.6 Different torsional systems

As mentioned in Section 4.2, a torsional system can be categorized as torsionally stiff, torsionally flexible or torsionally similar. Here we define four systems each with a plan similar to the plan shown in Figure 4.2. For all these systems $k = 5961.3 \text{ kN/m}$; $m = 113.25 \text{ tonne}$; $I = 3950.0 \text{ tonne.m}^2$; $f = 44.4 \text{ kN}$, and $a_i = b_i$ for all values of i . The characteristics of these systems are shown in Table 4.2. Parameter w defines the distance of edge resisting planes in y direction from the center of mass; for systems T1 and T2 it is equal to the parameter, b , but for systems T3 and T4 it is reduced to 12.0 m, and 6.0 m, respectively, to represent systems with central cores.

Table 4.3 shows the dynamic properties of systems T1 to T4, including the eigenvalues and mode shapes. The first component of each mode shape is the translational element while the second represents the torsional element. The mode shapes are also shown schematically in the last row of the table. System T1 is torsionally stiff since its eigenvalues are well separated, and its first mode is predominantly translational. System T2 is torsionally similar since its eigenvalues for the first and second modes are fairly close. System T3 is also a torsionally similar system since its first and second mode shapes are very similar to each other. System T4 is torsionally very flexible system because its first and second eigenvalues are well separated and the first mode is torsionally dominant.

Nonlinear time history analyses are carried out on these systems for El Centro ground motion to examine their nonlinear response histories and the modal components of the response.

4.6.1 Torsionally stiff system T1

The first and second mode components of global Y direction displacement at the centre, stiff, and flexible planes of system T1 are shown in Figure 4.10. It can be seen that the first mode makes the major contribution to the response, while the second mode has negligible contribution in the response. For the flexible edge, the signs of the two terms of the first mode are opposite which makes the displacement caused by them at the flexible edge to be additive. For the stiff edge, the contribution to the displacement from the first two terms of mode 1 are opposite in sign, yet the lateral displacement from the

first term is so much larger than that from the second term that the first mode still dominates the response.

4.6.2 Torsionally similar system T2

An examination of the global displacement in y direction at the centre plane shown in Figure 4.11 reveals that the first mode, which is torsional in this case, makes a small yet significant contribution, while the second mode, which is translational, makes the major contribution. The contributions of the two modes to the displacement of flexible edge are also shown in Figure 4.11. In this case, the predominant contribution is from the first mode. This is because the shape of mode vector is such that the sign of torsion term is opposite to that of the translational term. Thus, the translational and torsional components add up at the flexible edge. For the stiff edge displacements both modes make significant contributions. It is evident from these examples that if one wants to represent the response of the structure by just one mode, the first mode will usually give fairly reasonable results for a structure that is torsionally stiff. For a structure that is torsionally more flexible the error in using just one mode is larger. Also, for some planes the torsional mode controls the maximum displacement while the translational mode controls the displacement for other planes.

4.6.3 Torsionally similar system T3

The displacements contributions of first and second mode for flexible, central and stiff planes are shown in Figure 4.12. It can be noticed that both modes contribute equally in the response of the center plane. While the response of the stiff plane is dominated by the

second mode, the first mode dominates the response of the flexible plane. Therefore, the response in first mode does not provide an appropriate representation of the system's response. Evidently, for torsionally similar systems the first two modes should be considered simultaneously.

4.6.4 Torsionally very flexible system T4

The contributions of first and second modes to the displacement responses are shown in Figure 4.13. In this case, all displacements are controlled by the second mode. In fact, the magnitudes of first mode contribution in the displacements are quite small for all planes. It may be noted that the displacements are measured at the wall locations not at the edges of the plan. The displacement limit of 0.025 may also apply to the edges to prevent non-structural damage as well as distress to structural components that are not considered part of the SFRS. The edge displacements are shown in Figure 4.14. Mode 2 still dominates the response, although for the flexible edge the contribution from the torsional mode is quite significant.

In summary, the displacement response of central, flexible and stiff planes is generally dominated by the response of the translation dominant mode. For a torsionally stiff system, the first mode is translation dominant while for a torsionally flexible system the second mode is usually translation dominant. However, for a torsionally similar system both modes should be considered in estimating the displacement demand in each plane.

4.7 Angle of twist

We define the angle of twist (Ψ) as the torsional component of the mode shape when it is normalized by the mode's translational component. The displacement of each plane can then be derived from the simple formula:

$$\Delta_i = \Delta_{C.M.} (1 + x_i \Psi) \quad (4.7)$$

where, Δ_i is the displacement of plane i , x_i is the distance of plane i from the center of mass and $\Delta_{C.M.}$ is the displacement at center of mass.

Consider again the systems S1, S2, and S3. The flexible edge responses of these systems to 0.1, 0.2, 0.4, 0.6, 0.8, 1.0, 1.5, 2.0, 2.5, and 3.0 times the El Centro ground motion are compared with the estimates obtained from Equation (4.7) in Figure 4.15 through 4.17. It is observed that for different ground motion levels and different systems, Equation (4.7) provides estimates that are very close to their response values and in all cases are greater than the actual response. It is worth mentioning that for scale factors (SF) up to 1.0, the estimates are very accurate, however the accuracy of the estimates decreases as the SF increases and as the system becomes less torsionally restrained.

In order to investigate the changes in the angle of twist, Ψ , as defined above for the translational dominant mode, with changes in the characteristics of the plan asymmetric systems, a parametric study for the system shown in Figure 4.2 is carried out. It is assumed that $b_1 = b_4 = (1-\beta)$, $b_2 = (1+2\beta)$, and $b_3 = b_5 = \alpha$ where, α varies from 0 to

3.0 in steps of 0.25 and β from 0.05 to 0.5 in steps of 0.05. For an asymmetric system, the uncoupled frequency ratio is calculated as follows:

$$\Omega = \frac{\omega_\theta}{\omega_y} \quad (4.8)$$

where, ω_θ and ω_y are uncoupled torsional and translational frequencies, respectively. If Ω is much greater than 1 the system is torsionally stiff, if it is much smaller than 1, the system is torsionally flexible, and if it is close to 1 the system is torsionally similar. Figure 4.18 shows the values of Ω for different values of α and β . As will be seen from Figure 4.18, all cases with Ω ranging from 0.63 to 1.67 have been covered, and the region with Ω close to one is shown with green contour.

The variation of the angle of twist is shown in Figure 4.19, from which it is noted that the value of Ψ increases significantly in the region where Ω is close to 1. In regions away from $\Omega = 1$, the value of Ψ is less than 0.1, while in the region where Ω is close to 1 it goes up to 0.25. The importance of the value of Ψ becomes evident when reference is made to Equation (4.7); the greater the value of Ψ , the greater will be the amplification of the displacement at the edge planes. For instance, if $\Psi = 0.1$, and a plane is located at the edge in Figure 4.2 where $x_i = 9.15$, the displacement demand on such a plane as obtained from Equation (4.7) will be 1.915 times the displacement demand of the plane located at the center of mass. For a value of Ω greater than 1.2, which represents a torsionally stiff system, the value of Ψ is less than 0.05 (see Figure 4.19).

4.8 Summary and conclusion

Using BST surfaces it is shown that there are two ultimate deformed shape configurations when the total capacity of the resisting plane of an asymmetric plan building is mobilized during its seismic response to strong ground motions. These two configurations correspond to two points on the BST surface called the T_{\max} and T_{\min} . Simple relations are developed for the required orthogonal strength for which the response of the structure in IDA for response to strong ground motion converges to a configuration corresponding to the T_{\min} on BST surface.

Modal decomposition of torsional response of several torsionally unbalanced systems reveals the contributions of the first and second modes to the displacement of the flexible and stiff edges as well as of the center of mass of these structures. It is observed that the first mode dominates the response for all three planes in torsionally stiff system. However for torsionally similar and flexible systems the second mode contributes significantly in the response and in some cases dominates the response. Therefore, it is recommended that for seismic design of torsionally similar and flexible structures both the first and second mode deformed shapes should be considered in estimating the displacement demand on different resisting planes.

The angle of twist in the plan of asymmetric plan building is defined as the rotational component of the design mode shape when normalized by the mode's translational component. This angle can be used to estimate the response of the flexible and the stiff planes from the response of the central plane. Through a few case studies for

torsionally restrained and unrestrained system subjected to increasing intensity ground motion, it is shown that the estimates based on the use of the angle of twist are fairly accurate.

It is observed that for a wide range of 2DOF systems, the defined angle of twist for the translational dominant mode has its highest value for 2DOF systems in which the uncoupled rotational frequency is close to the uncoupled translational frequency. Torsionally stiff systems and torsionally very flexible systems have relatively small angles of twist for their translational dominant modes. These observations are used in the DBSD procedure for torsionally unbalanced structures described in the next Chapter.

Table 4.1: Characteristics of torsional restrained and unrestrained systems

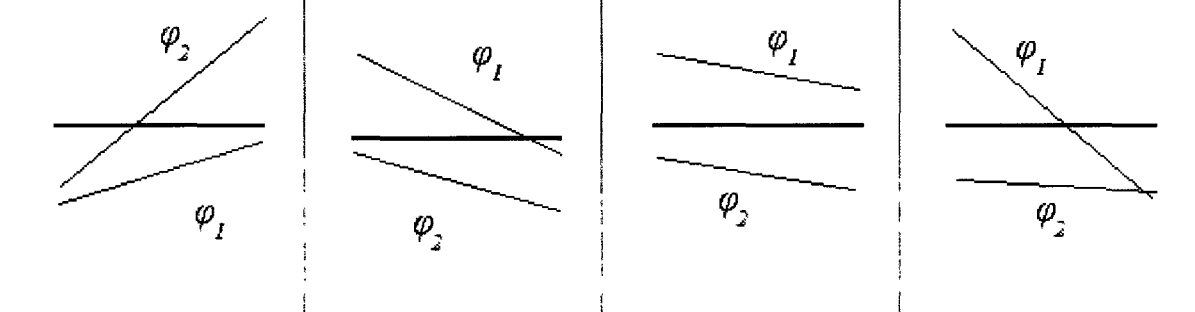
| Systems | b_1 | b_2 | $b_3=b_5$ | b_4 |
|-----------------|-------|-------|-----------|-------|
| Unrestrained S1 | 0.75 | 1.50 | 0.00 | 0.75 |
| Restrained S2 | 0.75 | 1.50 | 0.75 | 0.75 |
| Restrained S3 | 0.75 | 1.50 | 1.50 | 0.75 |

Table 4.2: Characteristics of different torsional systems

| Systems | b_1 | b_2 | $b_3=b_5$ | b_4 | w, m |
|---------|-------|-------|-----------|-------|--------|
| T1 | 0.75 | 1.50 | 1.00 | 0.75 | 18.3 |
| T2 | 3.00 | 1.00 | 0.00 | 0.75 | 18.3 |
| T3 | 0.75 | 1.50 | 1.00 | 0.75 | 12.0 |
| T4 | 0.75 | 1.50 | 1.00 | 0.75 | 6.0 |

Table 4.3: Dynamic properties of different torsional systems

| T1 Torsional stiff | | T2 Torsional Flex. | | T3 Torsional Similar | | T4 Torsional very Flex. | |
|-----------------------|-------------|-----------------------|-------------|-------------------------|-------------|----------------------------|-------------|
| λ_1 | λ_2 | λ_1 | λ_2 | λ_1 | λ_2 | λ_1 | λ_2 |
| 139.89 | 365.49 | 210.63 | 260.58 | 113.3 | 194.0 | 34.1 | 161.2 |
| φ_1 | φ_2 | φ_1 | φ_2 | φ_1 | φ_2 | φ_1 | φ_2 |
| -0.0901 | 0.0266 | 0.0432 | -0.0835 | 0.0628 | -0.0699 | 0.0150 | -0.0928 |
| 0.0045 | 0.0153 | -0.0141 | -0.0073 | -0.0118 | -0.0106 | -0.0157 | -0.0025 |
| Ψ_1 | Ψ_2 | Ψ_1 | Ψ_2 | Ψ_1 | Ψ_2 | Ψ_1 | Ψ_2 |
| -0.05 | 0.575 | -0.326 | 0.087 | -0.188 | 0.152 | -1.05 | 0.027 |



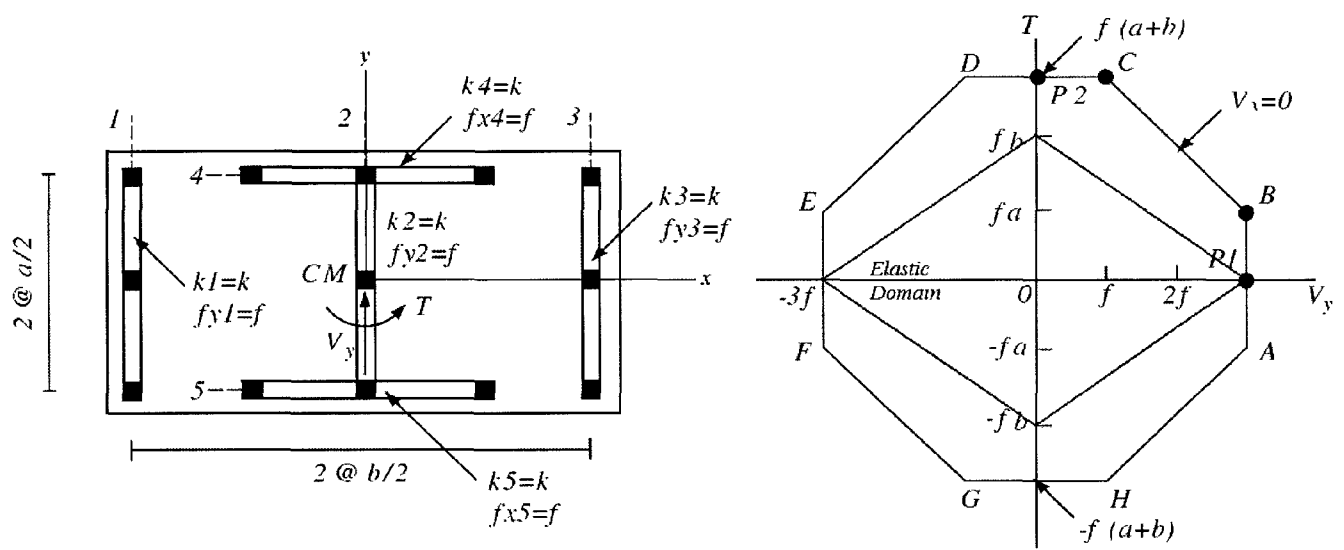


Figure 4.1: BST surface for a symmetric plan, from De La Llera et al (1995)

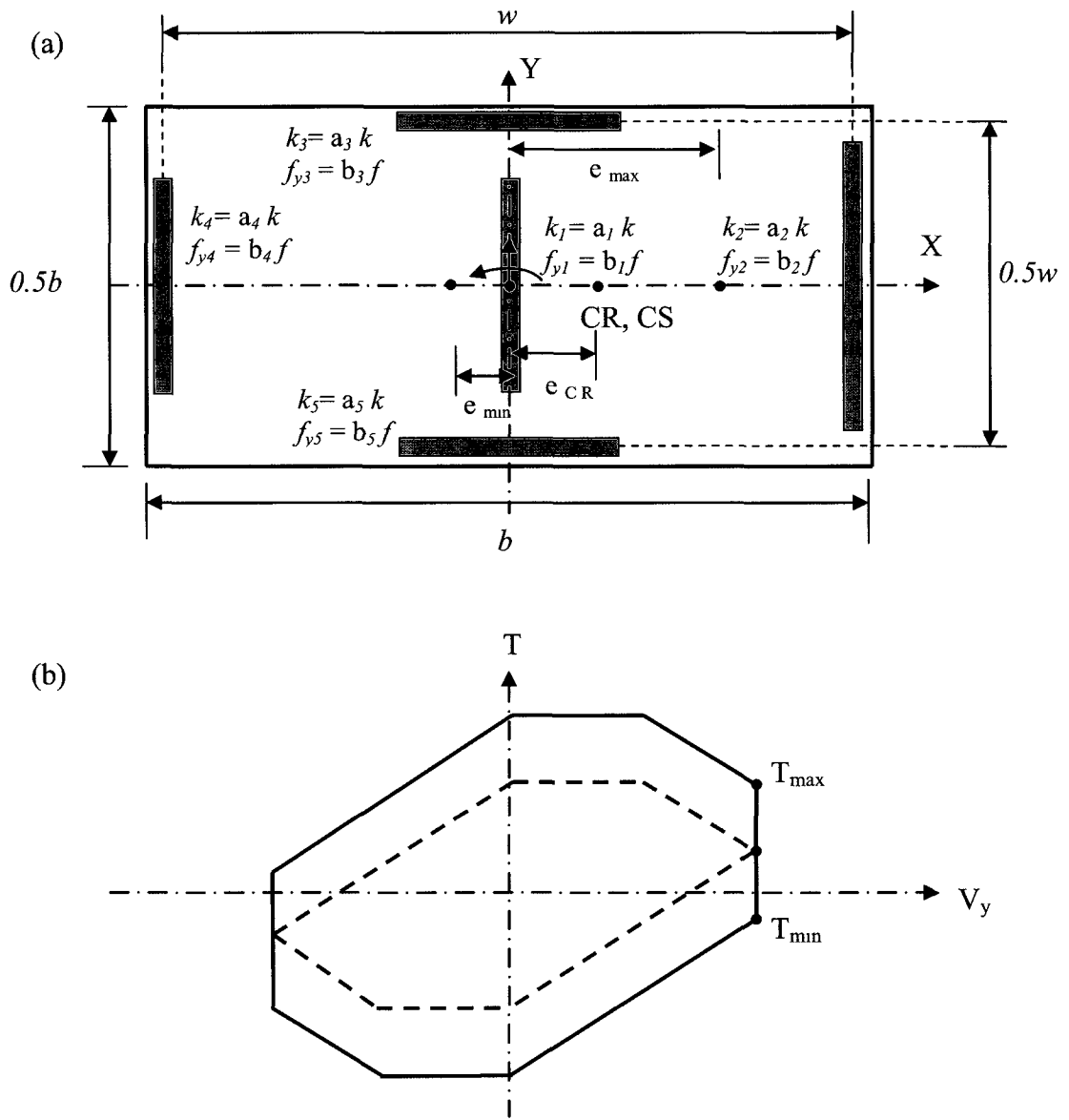


Figure 4.2: Typical BST surfaces for plan asymmetric building

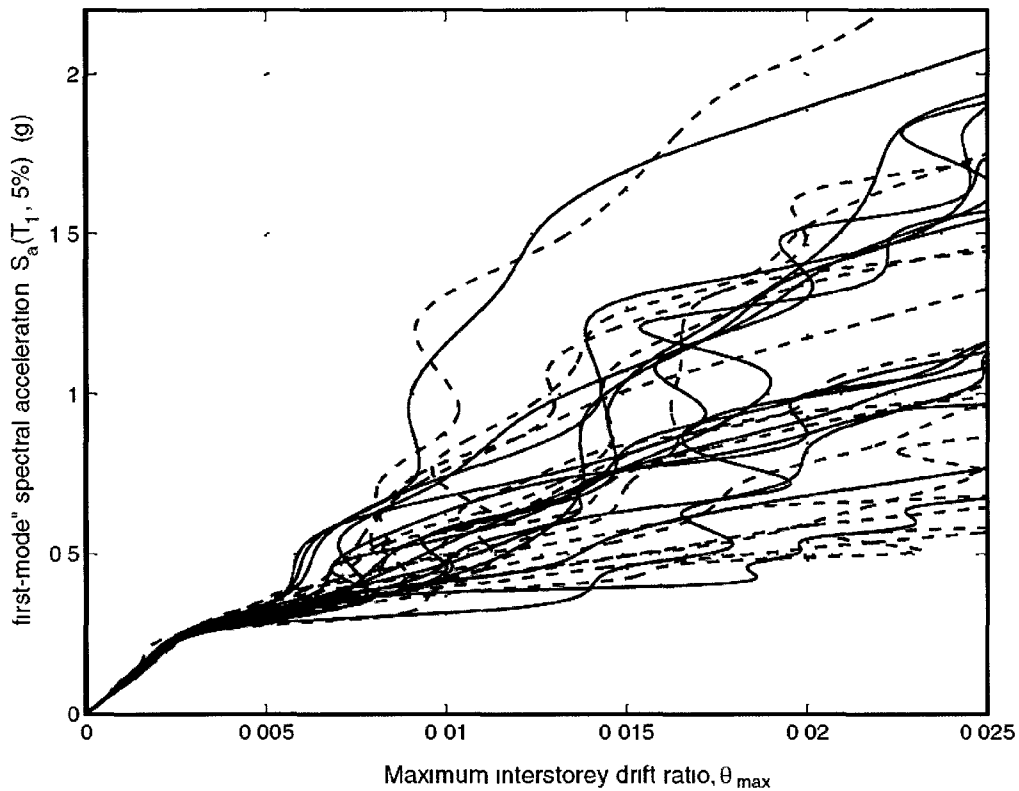


Figure 4.3: Typical IDA curves by Vamvatsikos and Cornell (2002)

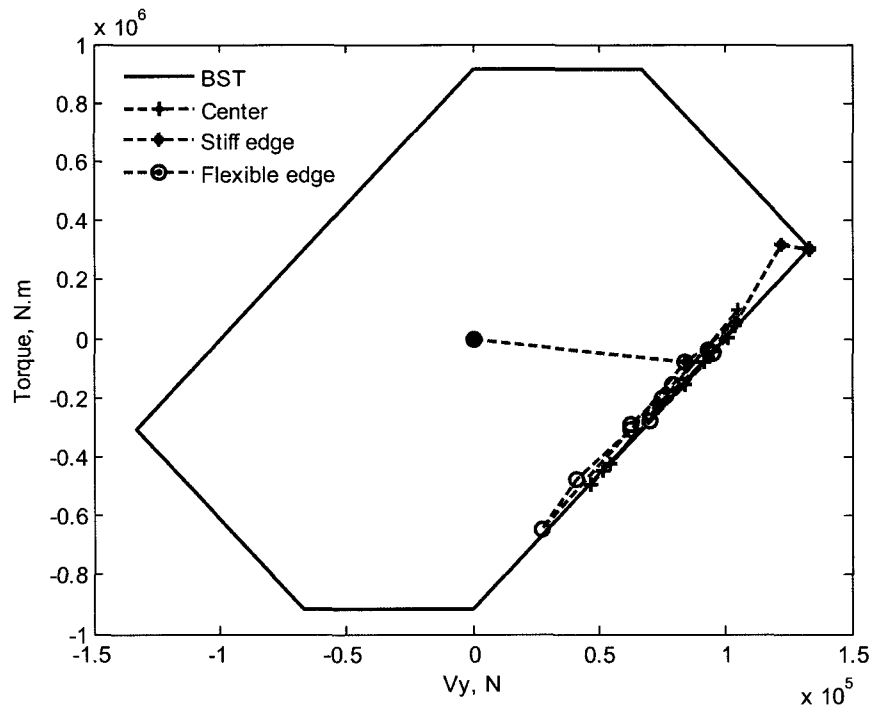


Figure 4.4: BST surface and IDA results for torsionally unrestrained system (S1)

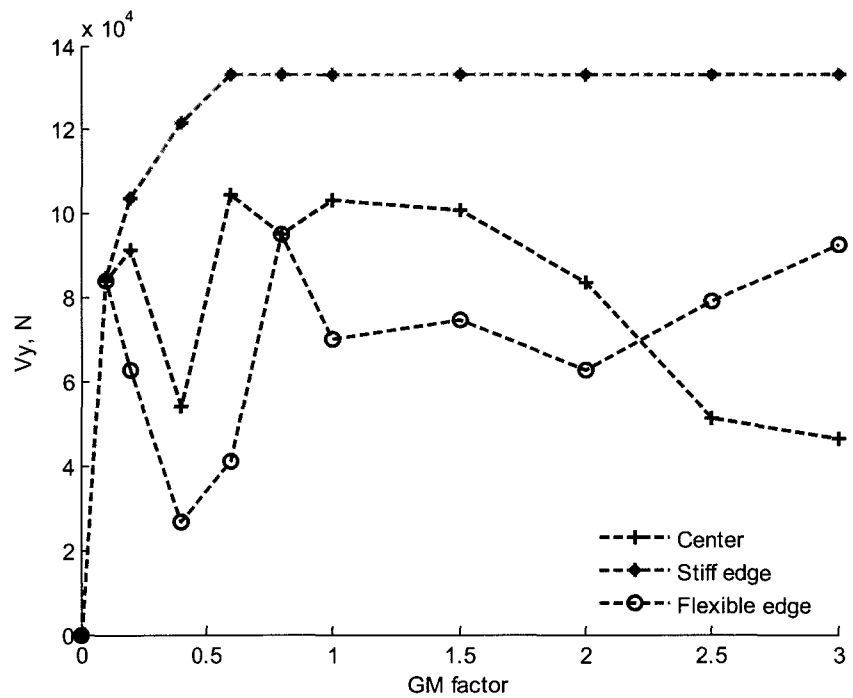


Figure 4.5: Base shear IDA curves for torsionally unrestrained system (S1)

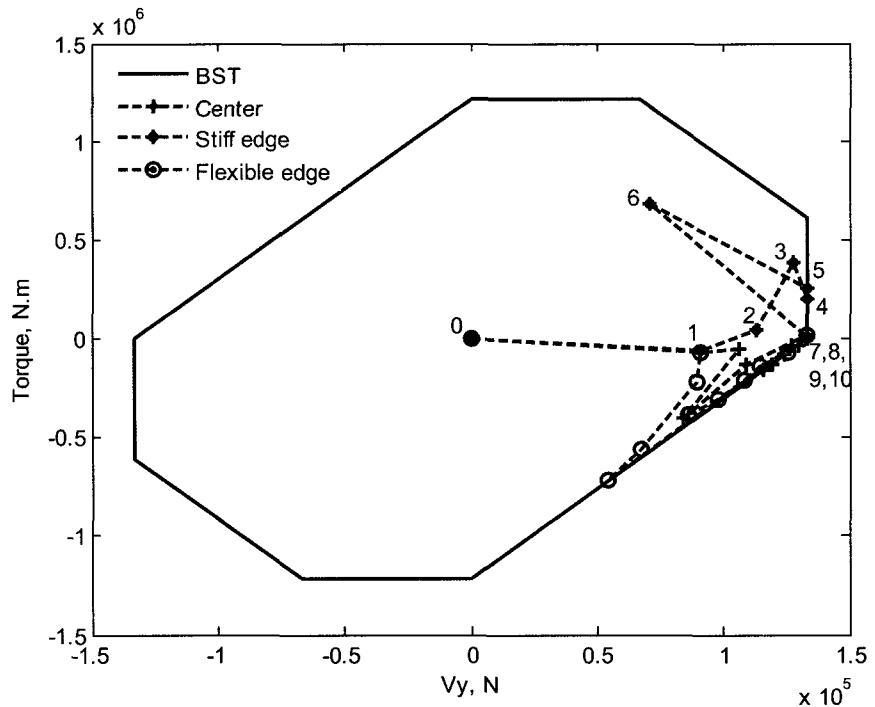


Figure 4.6: BST surface and IDA results for torsionally restrained system (S2)

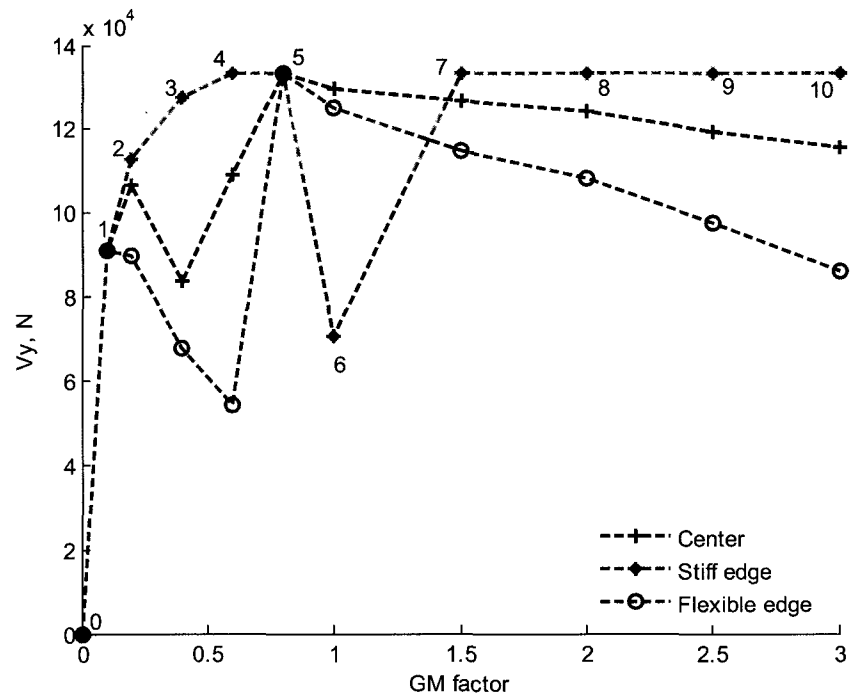


Figure 4.7: Base shear IDA curves for torsionally unrestrained system (S2)

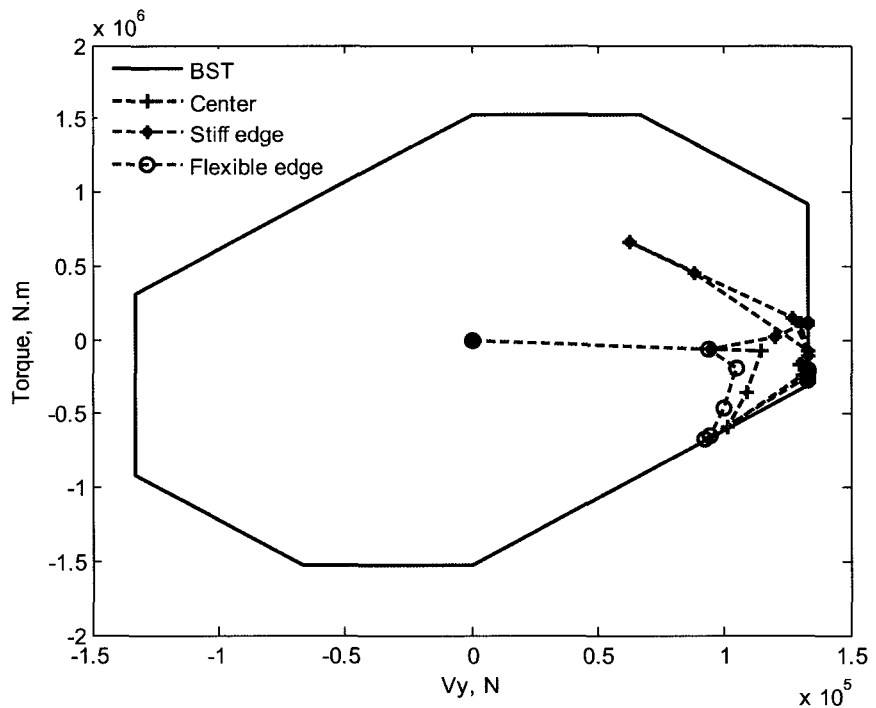


Figure 4.8: BST surface and IDA results for torsionally restrained system (S3)

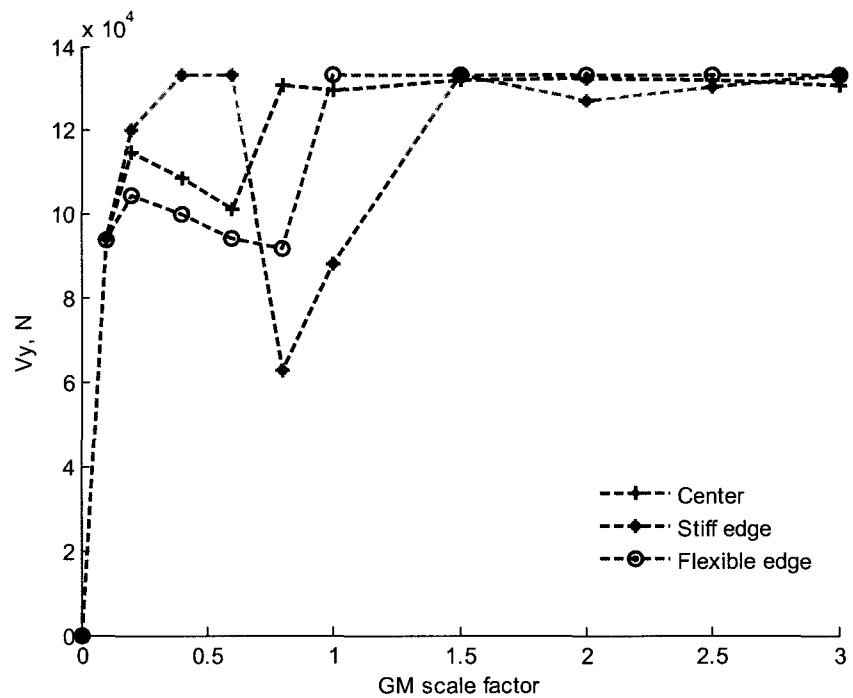


Figure 4.9: Base shear IDA curves for torsionally unrestrained system (S3)

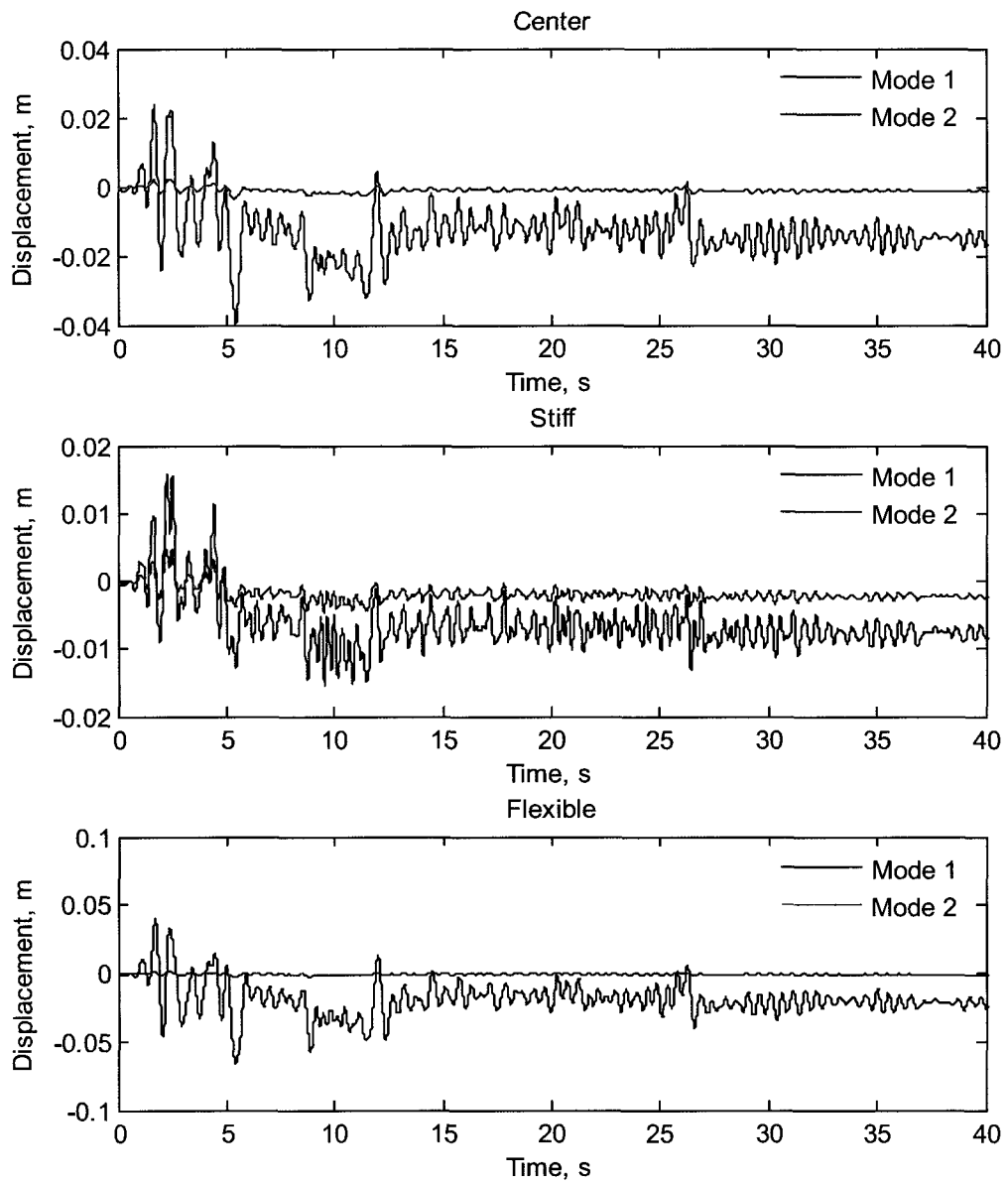


Figure 4.10: Modal response contributions for system T1

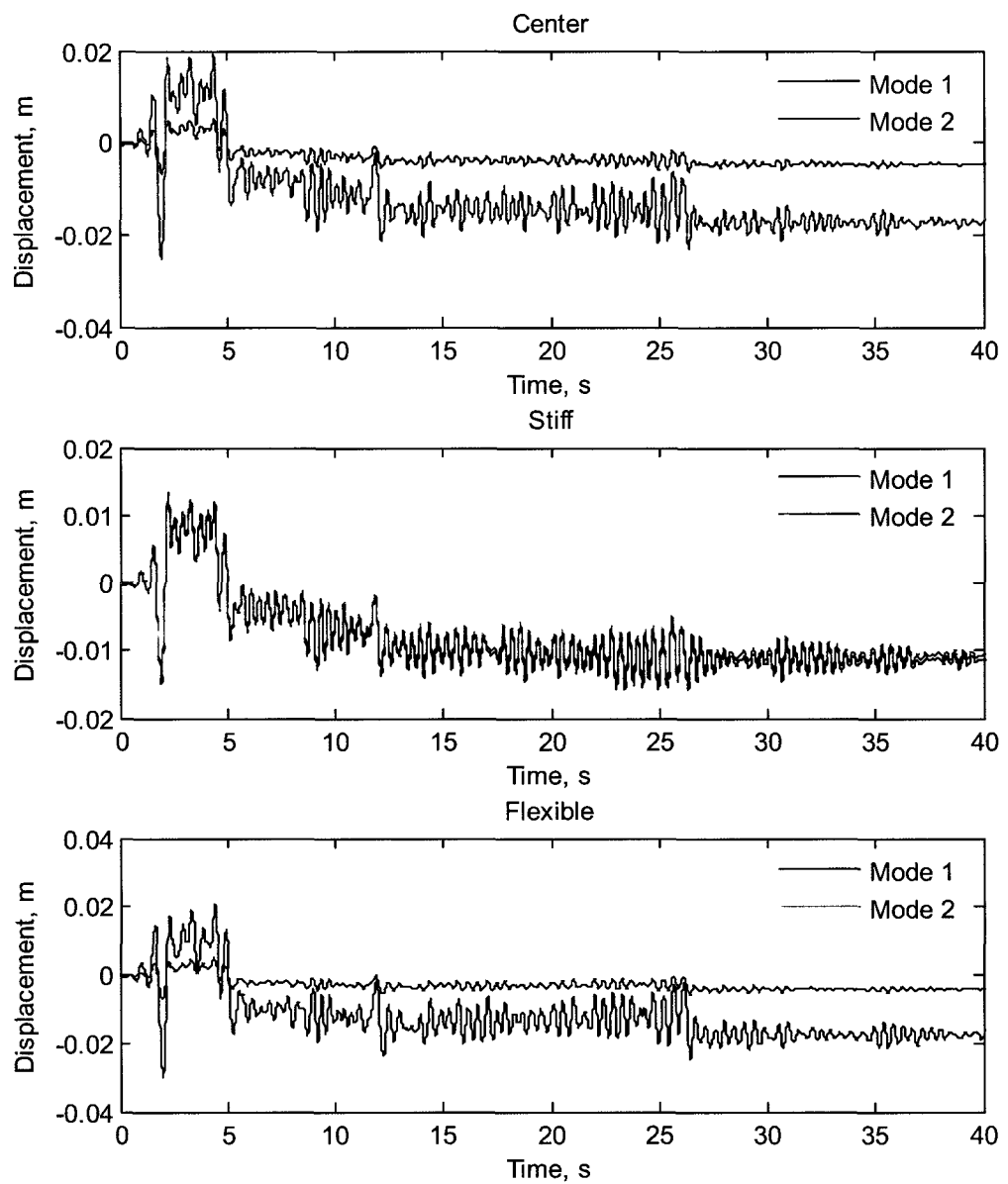


Figure 4.11: Modal response contributions for system T2

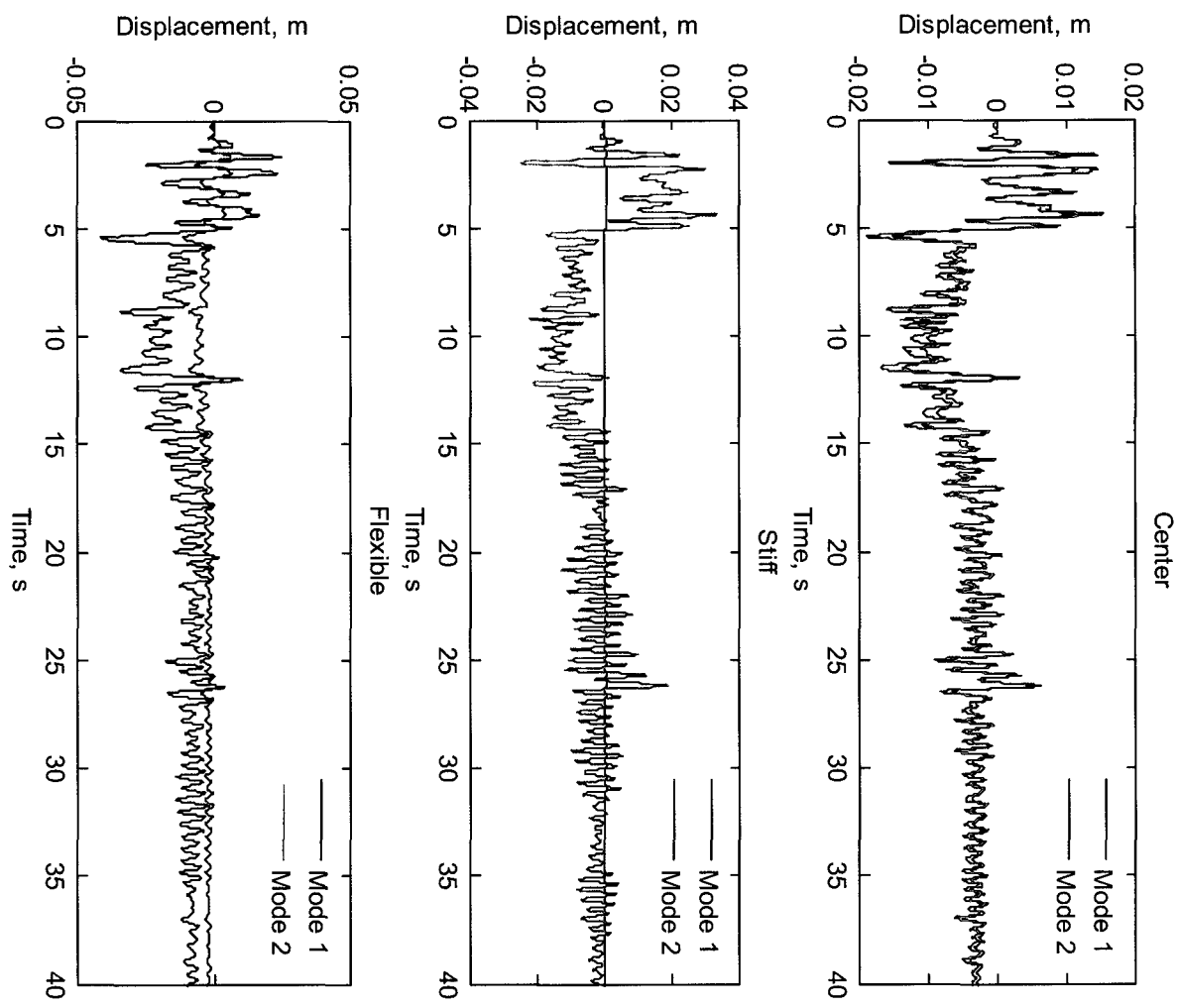


Figure 4.12: Modal response contributions for system T3

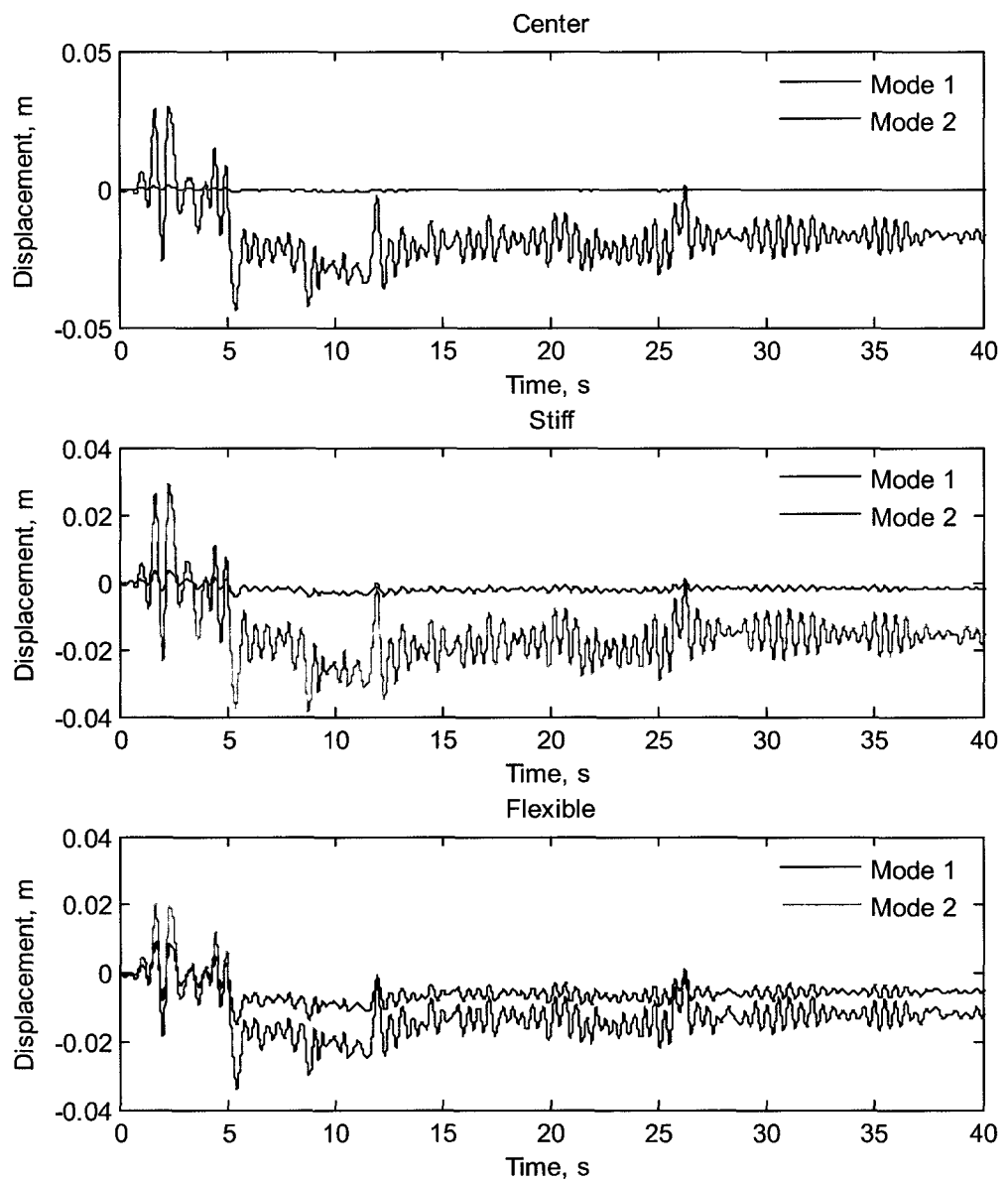


Figure 4.13: Modal response contributions for system T4

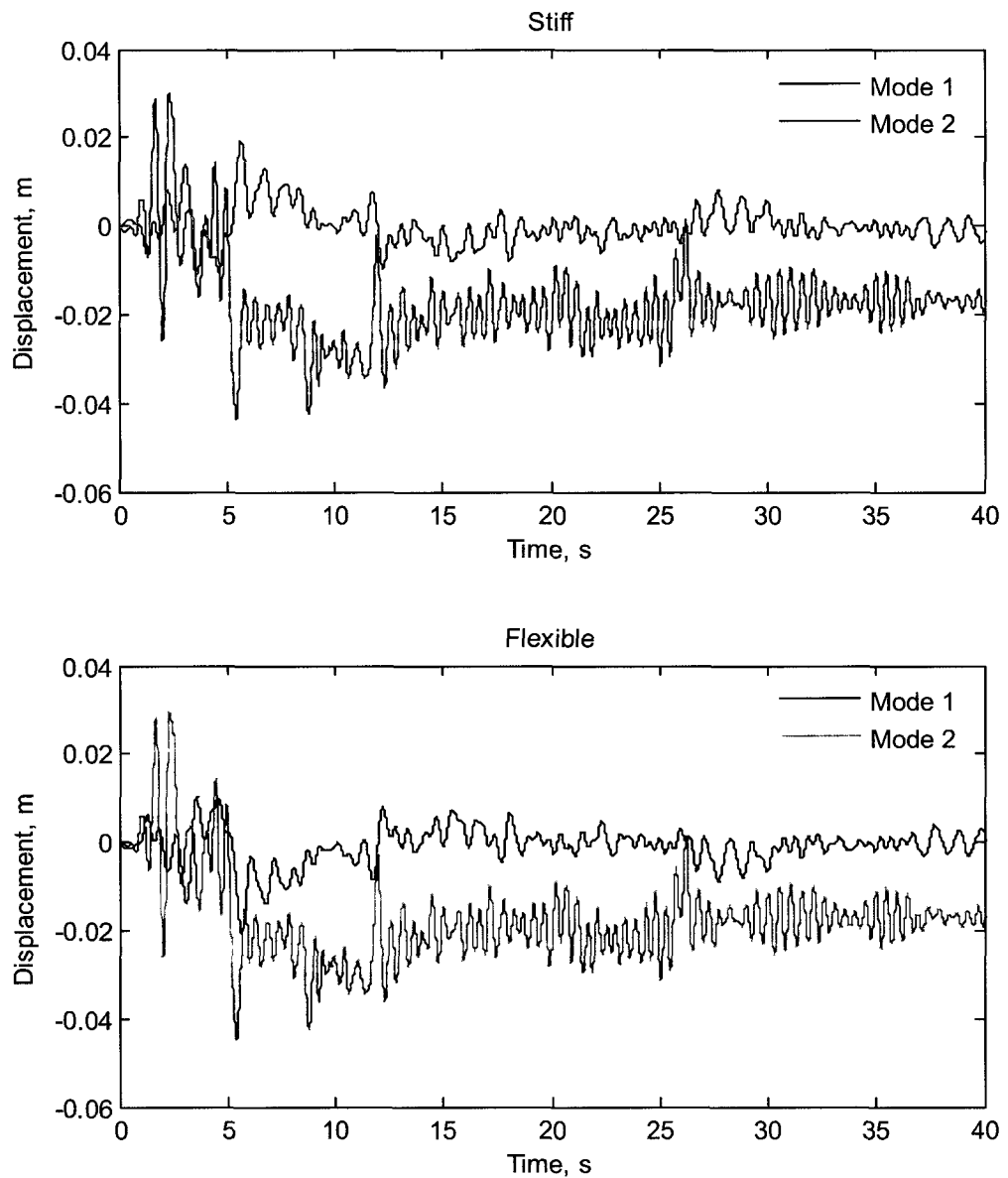


Figure 4.14: Modal contribution of response of system T4 at flexible and stiff side edges of the building

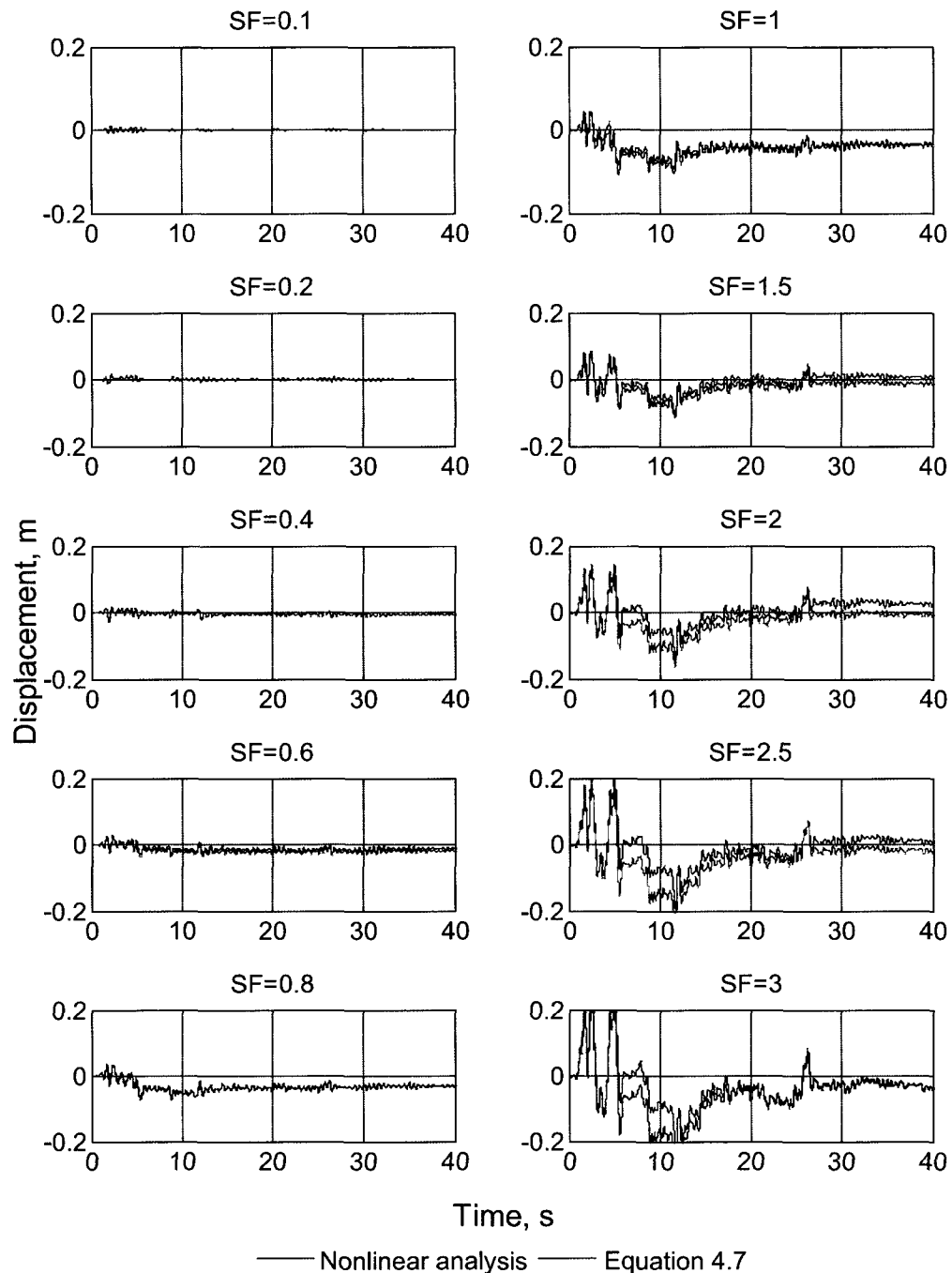


Figure 4.15: Flexible plane response and the estimates based on angle of twist for system S1

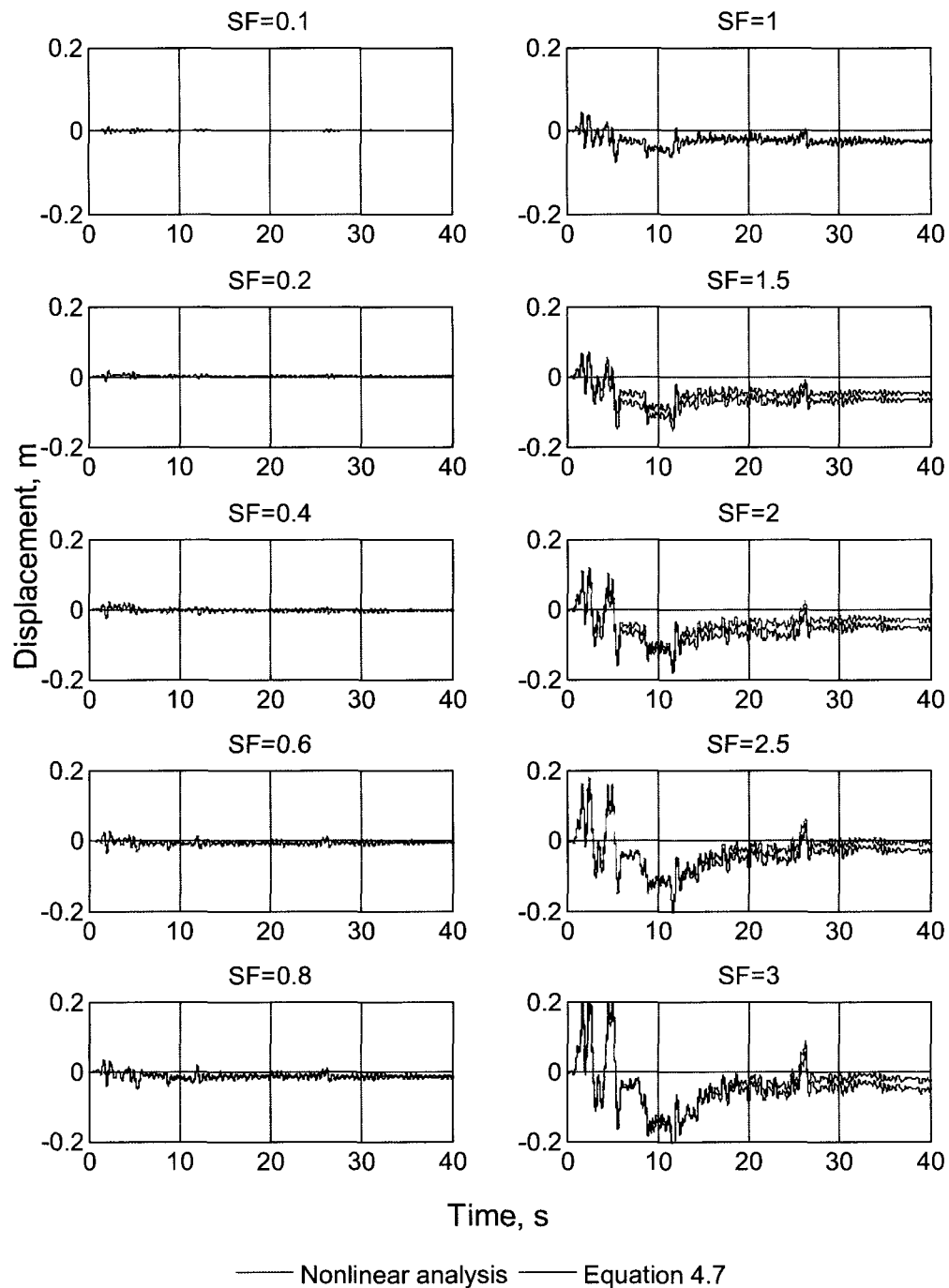


Figure 4.16: Flexible plane response and the estimates based on angle of twist for system S2

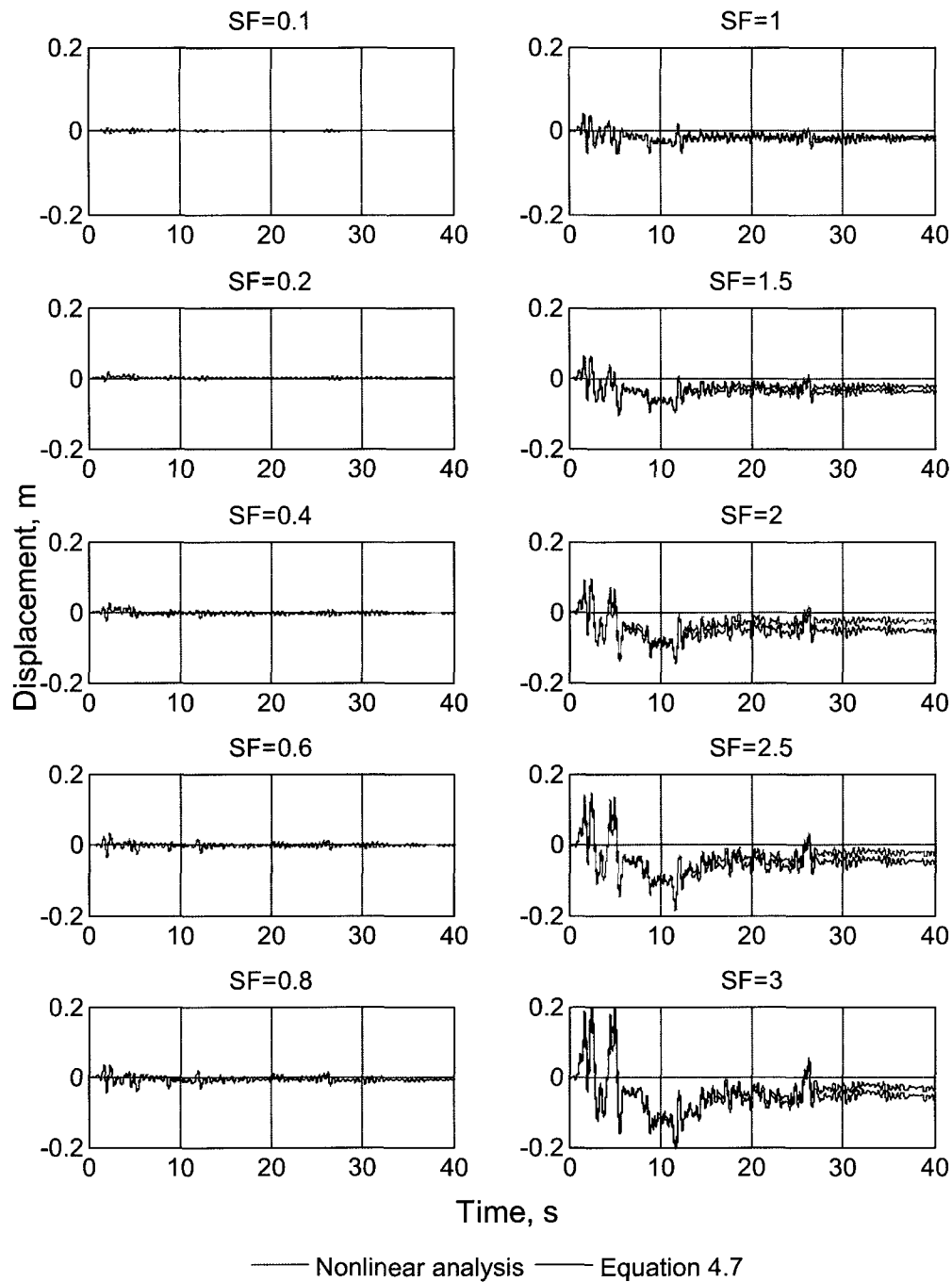


Figure 4.17: Flexible plane response and the estimates based on angle of twist for system S3

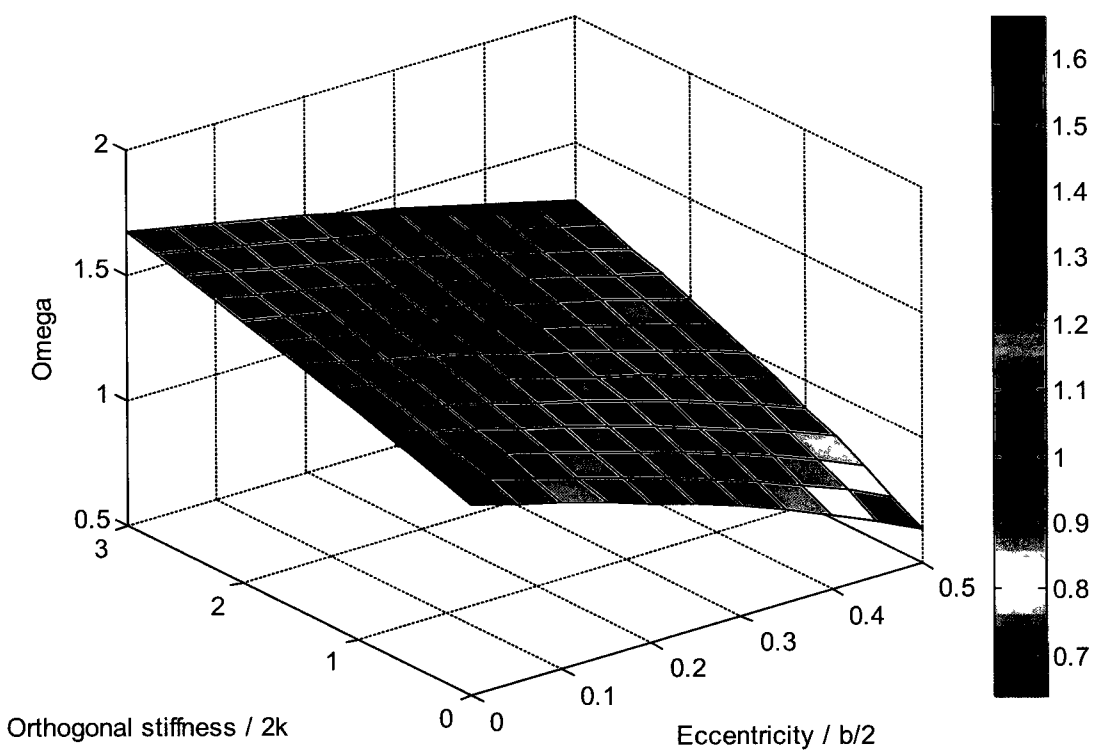


Figure 4.18: Uncoupled frequency ratios

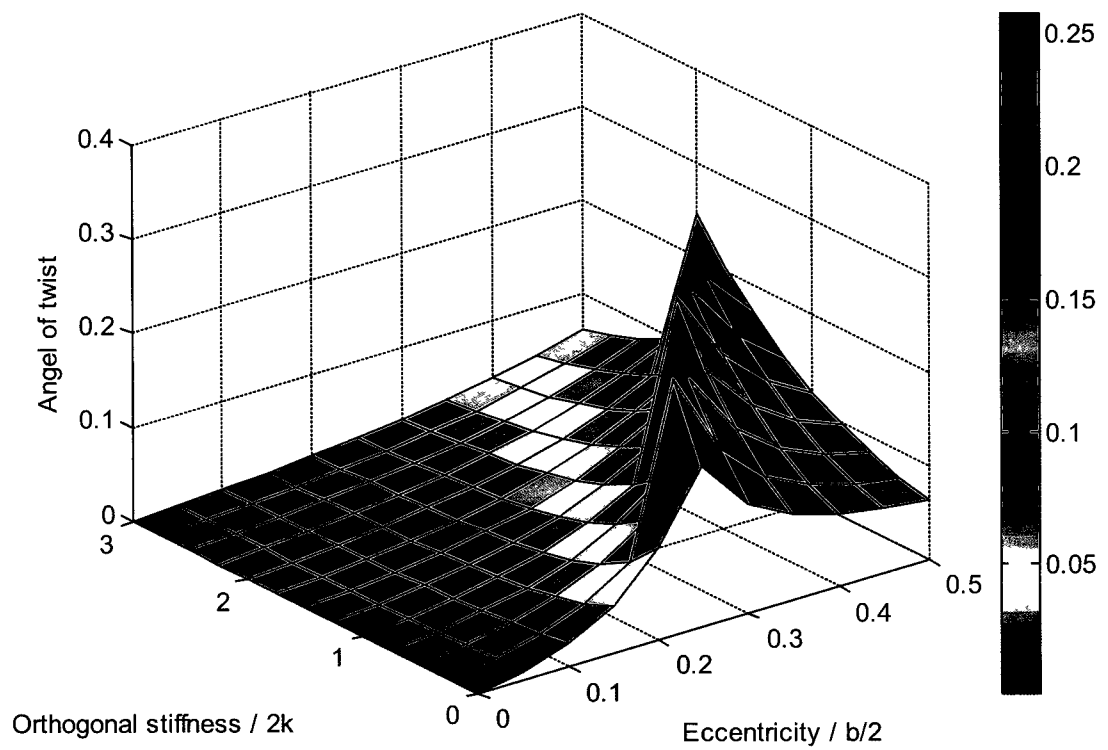


Figure 4.19: Angle of twist for translation dominant mode

Chapter 5. Displacement based seismic design of asymmetric plan buildings

5.1 Introduction

Force-based seismic design of asymmetric plan buildings commonly takes into account a combination of stiffness eccentricity due to asymmetry in the layout of the lateral resisting members, mass eccentricity due to non-uniform mass distribution, and accidental eccentricity due to variation in stiffness and/or mass from that assumed in the design. Accidental eccentricity is considered to provide protection against uncertainty in locating the center of mass and center of stiffness. This consideration appears to be inconsistent with other aspects of seismic design where higher uncertainties exist when compared to that in the distribution of the mass and stiffness in the plan of structures. In force-based design a building is considered asymmetric if the center of mass and the center of stiffness do not coincide. However, even when the centers of mass and stiffness coincide, there may be strength eccentricity in the plan. In such a case, the building will experience torsion beyond the first yield in the lateral resisting elements.

It has been shown by many researchers that dynamic elastic torsional response of structures is mainly controlled by stiffness eccentricity, while the inelastic torsional response, especially close to ultimate limit state, is dominated by the strength eccentricity (Humar and Kumar 1998, Castillo et al 2001). It is known that the designer has the freedom to assign the strength within the resisting elements; therefore, if the strength eccentricity is reduced or eliminated the stiffness eccentricity may have only limited effect on the inelastic response of the structure. It may, however, be noted that the designer may not always have the freedom to reduce or eliminate completely the strength

eccentricity. For instance, when designing reinforced concrete members, one must respect the code restrictions on the maximum reinforcement ratios, which place a cap on the maximum strength that can be assigned to a member.

In summary when accounting for torsion the role of accidental eccentricity is minor as compared to the effect of eccentricity in strength and this fact should be accounted for in design. In this chapter, some recent recommendations for estimating the torsional response of structures with asymmetry in their plan are discussed. Also, a new displacement based seismic design procedure based on the use of angle of twist proposed in the previous chapter is presented.

5.2 Angle of twist

The inelastic torsional response of structures to strong ground motion has been of great interest. This is mainly because the ability of a structural system to withstand strong ground motion depends on its ductility and its capacity to dissipate energy. The demand on these capacities is related to the displacements and drifts experienced by the system. At the same time, when the translational response to strong motions is highly coupled with the torsional response, the displacements in the lateral resisting elements increase significantly.

The challenge in DBSD for asymmetric plan building is to estimate the displacement demand on different lateral resisting elements or planes. In order to estimate the displacement demands on different resisting planes, one needs to calculate

the maximum twist in the structure caused by asymmetry in plan. Attempts to estimate the maximum twist of an asymmetric plan building due to its seismic torsional vibration have been reported in the literature and many of such studies are based on the analysis of a SDOF system. Following is a brief review of these attempts and also a recommendation to be implemented in the proposed displacement based seismic design (DBSD) for asymmetric plan buildings.

5.2.1 Twist within the elastic limit

The conventional approach to assess the torsional effect in asymmetric plan building is to calculate the member force taking into account the stiffness eccentricity. The angle of twist resulting from stiffness eccentricity is obtained from:

$$\theta_t = \frac{e_{rx} V_{Ey}}{K_t} \quad (5.1)$$

where θ_t is the angle of twist in the plan, V_{Ey} is the design base shear in y direction, e_{rx} is the stiffness eccentricity in x direction, and K_t is the torsional stiffness. Torsional stiffness comprises two components: one contributed by orthogonal planes and another by parallel planes, as given by the following expression

$$K_t = \sum (x_i - e_{rx})^2 k_{yi} + \sum y_j^2 k_{xj} \quad (5.2)$$

where k_{yi} is the stiffness of the i^{th} plane parallel to the y axis and x_i its x distance from the origin of the x and y coordinates, usually taken as the center of mass. Similarly k_{xj} is the

stiffness of the i^{th} plane parallel to the x axis and y_j its y distance from the origin. Equations (5.1) and (5.2) are strictly valid only for a static analysis.

5.2.2 Twist within inelastic range

A common approach for estimating the twist at ultimate state is to calculate the induced torque due to strength eccentricity divided by the torsional stiffness contributed by orthogonal planes. This is based on the assumption that when all the resisting elements in the direction of ground motion have reached their ultimate strength, their stiffness will be zero, while the orthogonal planes are still elastic. The angle of twist is given by (Paulay 1998)

$$\theta_{vt} = \frac{e_{vx} V_{Ey}}{\sum y_j^2 k_{xy}} \quad (5.3)$$

where e_{vx} is the strength eccentricity in the x direction and the ground motion is assumed to act parallel to the y axis. Both equations (5.1) and (5.3) are valid for static loading. Dynamic response of the structure may lead to larger rotations in the plan.

In the Direct Displacement-based design (DDBD) procedure proposed by Priestley (2007) a nominal rotation in plan, θ_N , is calculated from a relation similar to the equation (5.1):

$$\theta_N = \frac{e_{rx} V_{Ey}}{J_{R,\mu}} \quad (5.4)$$

where, the $J_{R,\mu}$ is the ductile rotational stiffness, modified from the elastic rotational stiffness using the system ductility of μ_{sys} for systems with eccentricity in both directions as:

$$J_{R,\mu} = \sum \frac{k_{yi}}{\mu_{sys}} (x_i - e_{rx})^2 + \sum k_{yj} (y_j - e_{ry})^2 \quad (5.5)$$

Note that while the elastic stiffness of orthogonal elements, namely those parallel to the x direction is used, only the effective (secant) stiffness of elements in the y direction is used, since the latter are subjected to significant ductility demand. The nominal rotation that is obtained from the above relation is then used to estimate the displacement demand on different elements using:

$$\Delta_i = \Delta_{CM} + \theta_N (x_i - e_{vx}) \quad (5.6)$$

where, Δ_{CM} is the displacement at center of mass, and e_{vx} is the strength eccentricity in the x direction. It is worth mentioning that in the calculation of ductile rotational stiffness in DDBD, stiffness eccentricity is used, while in estimating the displacement demands on different elements the strength eccentricity is used. Also equation (5.6) is based on the assumption that the plan rotates about the center of strength.

5.2.3 Effect of rotational mass

Beside the strength eccentricity, rotational mass of the asymmetric plan building also affects the rotation response of the system. When the mass is uniformly distributed over the plan area, an assumption commonly made, the rotational mass is only a function of total mass and plan dimensions.

Castillo et al (2001) studied the response of a torsionally unrestrained system, system 2, shown in Figure 5.1b to a generated ground motion seeded from the N-S component of El Centro earthquake of 1940 and matched to the New Zealand standard design spectrum. In Figure 5.1 CM, CV, and CR stand for center of mass, center of strength, and center of stiffness, respectively. The results of a parametric study on system 2 showed that the maximum rotation in plan of the torsionally unbalanced system was dependent on strength eccentricity and rotational mass. Figure 5.2 a, shows the variation of the maximum rotation in plan of system 2 with different rotational mass, marked as $0.85 r_0$, r_0 , and $1.2 r_0$ where, r_0 is the mass radius of gyration for a square plan system. It can be seen that with increase in the rotational mass while the lateral mass remained constant, the rotation in plan decreased (see Figure 5.2 a).

The authors noted that the maximum displacements of elements 1 and 2 and the center of mass (Figure 5.1), did not occur at the same instant of time, nor were these displacements reached when the maximum system rotation developed. Noting this behaviour they proposed that the nominal rotation for element i , θ_{ni} which relates the

displacements of element i to the displacement developed at the center of mass be calculated from:

$$\theta_m = \frac{\Delta_{ucm} - \Delta_{ui}}{x_i} \quad (5.7)$$

where, Δ_{ucm} is the maximum displacement at the center of mass, and Δ_{ui} is the maximum displacement of element i . As can be seen in Figure 5.2 b and c, the calculated nominal rotations, according to equation (5.7), are less than the system rotation obtained from the dynamic analysis, shown in Figure 5.2a.

Pettinga et al (2008), noted that, as demonstrated by Humar and Kumar (1999) and Castillo et al (2001), the rotational mass inertia provides the plan with significant resistant against the rotation. Using an energy balance method they proposed to make allowance for dynamic restraint by adjusting the rotational stiffness of the system. The rotation of the system could thus be found from:

$$\theta = \frac{e_v V_E}{K_{static} + K_{dynamic}} \quad (5.8)$$

where, K_{static} is the static rotational stiffness, and the $K_{dynamic}$ is the dynamic rotational stiffness, and e_v is the strength eccentricity. The dynamic rotational stiffness is then calculated using the time history response of the system to a half sine excitation as:

$$K_{dynamic} = \frac{\tau_i^2}{\tau_i(u_{\phi,i} - u_{\phi,i-1}) - 1/2 K_x(r_k^2 + e_r^2)(u_{\phi,i}^2 - u_{\phi,i-1}^2)} \quad (5.9)$$

where, τ_i is dynamic torque at time step i , $u_{\phi,i}$ is rotation at time step i , r_k is stiffness radius of gyration, e_r is the stiffness eccentricity, and K_x is lateral stiffness. It was also noted that $K_{dynamic}$ was generally positive, and therefore added to the static stiffness, however, it was quite feasible that dynamic stiffness as expressed above could produce negative values. Physically this can be interpreted as the rotational inertia acting to increase the diaphragm twist.

Sommer and Bachmann (2005) defined a torsion factor, ψ , corresponding to the ratio of the element of first coupled eigenmode of the building in direction which earthquake was considered to the corresponding element of the fictitious uncoupled eigenmode. The torsional factor is obtained from:

$$\psi = \frac{1}{2} \left(1 + \frac{K_t m}{K_x J} + \frac{e_{sx}^2 m}{J} - \sqrt{\left(1 + \frac{K_t m}{K_x J} + \frac{e_{sx}^2 m}{J} \right)^2 - 4 \frac{K_t m}{K_x J}} \right) \quad (5.10)$$

in which, K_t is the torsional stiffness at the center of stiffness, K_x is the total stiffness in x direction, J is the total rotational inertia about the center of mass, and e_{sx} is the stiffness eccentricity in x direction. Figure 5.3 shows the values of torsion factor versus normalized stiffness eccentricity. Based on this torsion factor, an eccentricity, e_{dyn} with respect to center of mass is defined for earthquake equivalent lateral force as:

$$e_{dyn} = -\frac{J(1-\psi)}{me_{sx}} \quad \text{where} \quad -\frac{e_{dyn}}{e_{sx}} \leq 1 \quad (5.11)$$

The corresponding displacement profile obtained from a static analysis when applying the design based shear at e_{dyn} , relates the displacement profile to the first eigenmode and is most important. When the second eigenmode is as important as the first eigenmode, or it is more important than first eigenmode $-e_{dyn}/e_{sx}=1$ is used, see Figure 5.4. The negative sign is to show that e_{dyn} is on the opposite direction of the center of stiffness.

Trombetti and Conte (2005) carried out an extensive analytical and numerical study on linear elastic single storey building with three degrees of freedom and eccentricity in both directions. They proposed a method called ALPHA method, in which the maximum rotation in plan is calculated as:

$$|u_\theta|_{max} = \alpha \frac{|u_y|_{max}}{\rho} \quad (5.12)$$

where, ρ is the mass radius of gyration and $|u_\theta|_{max}$ and $|u_y|_{max}$ are, respectively, the maximum rotational and lateral response of the system. They found that the upper bound for α is unity. Therefore, the maximum rotational response due to free vibration caused by an imposed initial deformation is limited to the maximum lateral response divided by the mass radius of gyration. In the case of un-damped free vibration, α can be found from

$$\alpha_u = \frac{\sqrt{48F^2}}{\sqrt{1+48F^2}} \quad (5.13)$$

The subscript u stands for un-damped free vibration, and F is defined as

$$F = \frac{e_r}{\Omega^2 - 1} \quad (5.14)$$

where, e_r is the stiffness eccentricity and Ω is the ratio of the uncoupled rotational frequency to the uncoupled translational frequency.

5.2.4 Proposed angle of twist

Prediction of maximum angle of twist is required in DBSD to estimate the maximum displacement demand on different structural elements. As evident from the literature review presented in the previous sections, developing a simple closed-form relation for the maximum angle of twist is impractical, when both the nonlinear behaviour and the dynamic rotational mass effect are considered. This is mainly because the maximum rotation of the building under earthquake excitation does not occur at the same time as the maximum lateral displacement at the center of mass. However, use of the maximum twist as obtained from an elastic analysis is reasonable because it has been shown by many researchers that the ratio between the maximum rotation in the plan to the displacement at center of mass is almost always smaller in the case of a dynamic nonlinear response than in the case of a dynamic linear response, (Perus and Fajfar 2002, and 2005, Sommer and Bachmann 2005).

Based on the foregoing, in this study, the angle of twist (Ψ) is defined as being equal to the torsional component of the translation dominant elastic mode shape when it is normalised by its translational component, an approach similar to what was proposed for a SDOF system in the previous chapter. For a MDOF system the translational and rotational components of the mode shapes at roof level are used to define the angle of twist. Figure 5.5 shows the deformation shapes corresponding to normalised first and second mode. For a torsionally unbalanced system, the first mode shape deforms in such a way that the flexible side of the building has a larger displacement than the stiff side, while in the second mode the displacement at stiff edge is greater than that at the flexible side. In the proposed design process for torsionally stiff system the angle of twist based only on the first mode will be used, but for torsionally similar and flexible systems the angle of twist calculated for both the first and the second mode will be considered in estimating the displacement demands. In other words for torsionally stiff system the design mode is the first mode, whereas the design mode for the torsionally similar and flexible structures is the more critical of the first two modes. This is explained in more details in the following sections.

5.3 Equivalent yield displacement estimates

The yield displacement of different resisting elements (walls or frames) in an asymmetric plan building can be estimated using empirical relations as was discussed in the DBSD of wall-frame systems. Since the lateral and torsional responses are coupled in asymmetric plan buildings, the yield displacements of individual walls will be reached at different

displacements of center of mass. The displacement at the center of mass at the instant plane i yields, Δ_{yi}^* , is obtained from:

$$\Delta_{yi}^* = \frac{\Delta_{yi}}{1 + x_i \Psi} \quad (5.15)$$

where, Δ_{yi} is the yield displacement of plane i , and x_i is the distance of plane i , from the center of mass. Based on the proportion of the base shear that is assigned to the individual planes, the global yield displacement can be estimated as follows:

$$\Delta_y = \frac{\sum V_i}{\sum (V_i / \Delta_{yi}^*)} \quad (5.16)$$

where, V_i is the shear assigned to plane i . This yield displacement estimate will be used in the preliminary design. During subsequent iterations the global yield displacement will be obtained from the pushover analysis.

5.4 Equivalent ultimate displacements

As in the case of wall-frame systems, the ultimate displacement of an asymmetric plan buildings is assumed to be the minimum of the lateral displacements under which 1) the compressive strain in concrete would not exceed 0.004, 2) the maximum drift ratio along the height would not exceed the code specified limit of 0.025, and 3) the reduction in shear capacity of the system due to P-Δ effect would not be more than 5% of the maximum shear capacity, so as to prevent instability in the system.

5.4.1 Equivalent ultimate displacement as governed by ductility limit

The ultimate displacement of a plane that can be attained without exceeding its ductility limit can be calculated using simple empirical relations. The corresponding displacement at the center of mass is given by:

$$\Delta_{ui}^* = \frac{\Delta_{ui}}{1 + x_i \Psi} \quad (5.17)$$

where, Δ_{ui} is the ultimate displacement of plane i , as controlled by its ductility capacity. The ultimate displacement of the system as governed by the ductility capacities of the resisting planes will be the minimum of all Δ_{ui}^* .

5.4.2 Equivalent ultimate displacement estimate as controlled by drift limit

In asymmetric plan buildings, the maximum drift occurs at the edge of the building. For minimizing the damage to non-structural components this drift should be limited to the value prescribed in the codes. In those cases where a lateral resisting element is located at the edge of the building, the drifts can be estimated using empirical relations similar to those for wall-frame systems. However if the lateral resisting elements are not located at the boundary of the building, the maximum acceptable displacement to prevent the drifts from exceeding the drift limit is calculated using the mode shapes at the stage of preliminary design, and from a pushover analysis in the subsequent iterations.

At the stage of preliminary design, mode shapes are obtained from the relative stiffness of the resisting elements. When the mode shapes become available, the displacements at the edge of the building for each floor can be calculated. The drift ratio at n^{th} storey, θ_n , is then obtained by taking the difference between the displacements of n^{th} and $(n-1)^{\text{th}}$ floors divided by the n^{th} storey height, H_n as:

$$\theta_n = \frac{(\varphi_y^n + x \varphi_\theta^n) - (\varphi_y^{n-1} + x \varphi_\theta^{n-1})}{H_n} \quad (5.18)$$

where x is the distance of the edge of the building from the center of mass, φ_y^n is translational component of the mode shape at n^{th} storey, and φ_θ^n is the rotational component of the mode shape at n^{th} storey. The ultimate displacement at the center of mass that would produce a drift ratio of 0.025, is then calculated from:

$$\Delta_u = \frac{0.025}{\theta_n} \varphi_y^n \quad (5.19)$$

For torsionally stiff systems, the maximum drift always occurs at the flexible edge of the building, and the first mode shape is used to calculate the equivalent ultimate displacement as controlled by the drift limit. For torsionally similar and flexible systems, ultimate displacement at which the drift at the flexible edge will reach its acceptable limit is calculated using the first mode, while the ultimate displacement at which the drift at the stiff edge will reach its acceptable limit is calculated using the second mode shape.

In subsequent iterations where pushover analyses are carried out, the drifts are recorded for both the flexible and the stiff edges of the building. The equivalent ultimate displacement at center of mass is the minimum displacement where the recorded drift in any plane reaches the code specified drift limit.

5.4.3 Equivalent ultimate displacement estimate as governed by the stability limit

The ultimate displacement to prevent instability caused by P–Δ effect is obtained from a pushover analysis, in which the controlling parameter is the displacement at the center of mass of the system. The equivalent ultimate displacement as controlled by the stability limit is the displacement at which a 5 to 10% drop in the base shear capacity of the system is observed. A value of 5% has been used in the present study.

5.5 Capacity Spectrum Method (CSM)

As in the DBSD procedure for wall-frame systems, the capacity spectrum method which employs the inelastic spectrum to estimate the seismic demand is used in the design of asymmetric system as well. The first step in CSM is to construct an equivalent SDOF system which represents the MDOF system. For asymmetric plan building an equivalent 2-degree-of-freedom (2DOF) system which considers the rotational inertia is used to represent the MDOF system. The equivalent 2DOF system for n^{th} mode is constructed using the lateral components, φ_{y_n} , and rotational components, φ_{θ_n} , of n^{th} mode shape. The dynamic properties of equivalent 2DOF are calculated from

$$L_n = \varphi_{yn}^T \mathbf{m} \mathbf{1} \quad (5.20)$$

$$M_n = [\varphi_{yn}^T \ \varphi_{\theta n}^T] \begin{bmatrix} \mathbf{m} & \\ & \mathbf{I}_o \end{bmatrix} \begin{Bmatrix} \varphi_{yn} \\ \varphi_{\theta n} \end{Bmatrix} \quad (5.21)$$

$$\Gamma_n = \frac{L_n}{M_n} \quad (5.22)$$

$$M_n^* = \frac{(L_n)^2}{M_n} \quad (5.23)$$

$$I_{On}^* = \Gamma_n \varphi_{\theta n}^T \mathbf{I}_o \mathbf{1} \quad (5.24)$$

where, for a system with N storeys, $\mathbf{1}$ is a unit vector of size Nx1, \mathbf{m} is an N by N matrix containing the storey masses, and \mathbf{I}_o is an N by N matrix containing the storey rotational masses. I_{On}^* is the modal static response for base torque. The ultimate lateral displacement δ_u , and yield displacement δ_y of the 2DOF system for n^{th} mode are obtained by dividing the ultimate and yield displacements of MDOF by Γ_n to give

$$\delta_{yn} = \frac{\Delta_y}{\Gamma_n} \quad (5.25)$$

$$\delta_{nu} = \frac{\Delta_u}{\Gamma_n} \quad (5.26)$$

Having determined the ultimate displacement of the 2DOF system for n^{th} mode the corresponding spectral acceleration (A_{yn}) is obtained from the inelastic acceleration displacement response spectrum for ductility calculated for the ultimate and yield displacements obtained from (5.25) and (5.26). The base shear and the base torque for n^{th} mode are then given by

$$V_{bn} = M_n^* A_{yn} \quad (5.27)$$

$$T_{bn} = I_{On}^* A_{yn} \quad (5.28)$$

where, A_n is spectral acceleration for n^{th} mode.

The design base shear is distributed among the resisting planes in proportions determined by the designer. The resulting actions of these lateral forces and the accompanying gravitational loads are used to design the resisting planes along the axis of asymmetry. The base torque on the other hand is assumed to be resisted by orthogonal planes. The demand on orthogonal planes is thus calculated from

$$T_{\text{orth}} = T_{bn} + T_{\text{asym}} \quad (5.29)$$

where, T_{orth} is the total torque to be resisted by orthogonal planes, and T_{asym} is the torque arising from asymmetry created when assigning the base shear to resisting planes.

It should be noted here that for torsionally stiff system, the base shear and base torque based on the first mode shape are used, however, for torsionally similar and flexible systems both the first and second modes are determined and the structure designed for the more critical case. This design leads to an updated estimate of section properties and global displacements.

5.6 Modal pushover analysis

Modal pushover analysis for asymmetric plan building is carried out according to the method proposed by Chopra and Goel (2004). A pushover analysis is carried out for each mode for the modal force distribution s_n given by

$$s_n = \begin{Bmatrix} s_{yn} \\ s_{\theta n} \end{Bmatrix} = \Gamma_n \begin{Bmatrix} \mathbf{m} \varphi_{yn} \\ \mathbf{I}_{On} \varphi_{\theta n} \end{Bmatrix} \quad (5.30)$$

where, s_{yn} is a Nx1 vector containing the lateral forces along the y axis at each floor level, and $s_{\theta n}$ is a Nx1 vector containing the rotational torques at each floor level. These forces and torques are applied at the center of mass and displacement control is also applied at the center of mass.

First mode pushover analysis is carried out in each iteration of design using the updated section properties to obtain the global yield displacement, as well as the ultimate displacement that will not cause instability in the structure, and the ultimate displacement at which the drift will still remain within the code prescribed drift limit. The global yield displacement and the ultimate displacement that will preclude instability are obtained from a pushover curve which provides a relationship between the total base shear and the roof displacement at the center of mass. The drift ratios at the boundaries of the structure are recorded at each step of the pushover analysis, so that one can obtain the displacement at center of mass when the first recorded drift ratio reaches the code drift limit of 0.025.

Multi-mode pushover analysis is carried out after the design process has converged to get better estimates of the element internal forces. The results of first mode pushover analysis when pushed up to the ultimate displacement obtained in the last iteration of the design are combined with the results of the higher mode pushover analysis when at the instant the elastic displacement demands calculated from the following expression is reached.

$$D_n = \Gamma_n \frac{T_n^2}{4\pi^2} A_n \quad (5.31)$$

where, D_n is the target displacement for n^{th} mode, and T_n is the period of the n^{th} mode. It is assumed that the structure remains elastic in the higher modes pushover analysis and this assumption is verified within the analysis. If this assumption is found not to be valid, an iterative process similar to the one explained in DBSD of wall-frame structure is used to find the performance point from inelastic capacity demand curves.

Although in the first mode pushover analysis the structure is pushed deep into the nonlinear zone, the results obtained from multi-mode pushover analysis can be combined using either the SRSS rule or the CQC rule. The CQC rule is more reliable when periods of different modes are close to each other. It is apparent that this combination would provide only an approximate estimate of the coupled response of the higher modes; however, comparison of the results from a nonlinear dynamic analysis with combined results of multi-mode pushover analysis shows that the multi-mode pushover analysis can

provide an acceptable estimate of the seismic demand on asymmetric plan building as well.

5.7 DBSD for asymmetric plan buildings

The proposed DBSD procedure for asymmetric plan buildings is shown in Figure 0.6.

The design procedure starts with the design of the planes along the axis of symmetry also referred to here as the orthogonal direction. Since the structure is assumed to be symmetric in the orthogonal direction there is no torsion induced due to lateral vibration in that direction. The orthogonal planes can therefore be designed by using a procedure similar to that proposed for wall-frame structures. The structure is next designed along the axis of asymmetry. During iterations for the design of planes along the axis of asymmetry, the demand on orthogonal planes due to rotation of the floor is calculated. If the capacities of the designed orthogonal planes are less than the calculated demand on them, they are re-designed, if not the iterations continue until convergence is achieved in the design of planes along the axis of asymmetry. The steps in the DBSD of planes along the axis of asymmetry are outlined in the following:

- 1) Estimate the yield curvature, and corresponding yield displacement for each resisting plane.
- 2) Select the proportions in which the base shear will be assigned to each resisting plane.

- 3) Calculate the angle of twist based on the design mode shape(s) obtained from an eigen value analysis of the structure based on the relative stiffness of various planes.
- 4) Calculate equivalent yield displacement for each plane at the center of mass using equation (5.15).
- 5) Estimate the global yield displacement according to the calculated equivalent yield displacements and the base shear assigned to each resisting plane using equation (5.16).
- 6) Obtain the deformed shape of structure for the design mode shape(s), and calculate the drift ratio at critical edge of the building associated with each design mode shape using equation (5.18).
- 7) Calculate the equivalent ultimate displacement at the center of mass using equation (5.17) for each resisting plane so that the drift at that resisting plane reaches the code specified drift limit. The ultimate displacement is the least of ultimate displacement for each plane.
- 8) Calculate the ductility demand for design mode shape(s) by dividing the ultimate displacement calculated in step 7 by yield displacement calculated in step 5.
- 9) Construct the 2DOF system using equations (5.20) through (5.26) for each design mode.
- 10) Construct the inelastic demand spectrum in A-D format for the ductility calculated in step 8, and find the corresponding spectral acceleration for ultimate displacement calculated by equation (5.26).

- 11) Estimate the base shear and the base torque using the spectral acceleration obtained in step 10 for each design mode using the equations (5.27) and (5.28).
- 12) Design the structure for the design mode which has the most critical combination of base shear and base torque.
- 13) Assign the design base shear to resisting planes, and calculate the shear demand on orthogonal planes. The shear demand on orthogonal planes is calculated for the total torque to be resisted by orthogonal planes that is calculated from equation (5.29).
- 14) Check if the orthogonal walls need to be re-designed.
- 15) Estimate the yield and ultimate displacements as controlled by the ductility limit of each plane now using the designed section properties.
- 16) Obtain the mode shapes and the corresponding angles of twists.
- 17) Calculate the equivalent yield and ultimate displacements at the center of mass.
- 18) Estimate the global yield displacement and the ultimate displacement as controlled by the ductility limit.
- 19) Run push over analysis for design mode(s). Then find the global yield displacements and the ultimate displacement to prevent P- Δ instability as well as the ultimate displacements at the center of mass at which the drifts at the boundaries would not exceed the drift limit for each of the design mode.

- 20) Calculate the ductility demand by selecting the ultimate displacement which is the least of the three limits described above and dividing it by the global yield displacement obtained from the pushover curve for each design mode pushover analysis.
- 21) Construct the 2DOF system using equations (5.20) through (5.26) for each design mode.
- 22) Construct the inelastic demand spectrum in A-D format for the ductility calculated in step 20, and find the corresponding spectral acceleration for ultimate displacement calculated by equation (5.26).
- 23) Estimate the base shear and the base torque using the spectral acceleration obtained in step 22 for each design mode.
- 24) If the calculated design base shear is not close to the one calculated in step 11, continue the iteration from step 12 to step 23 until convergence is achieved.

On achieving convergence in the design of planes along the axis of asymmetry a multi-mode pushover analysis is carried out for first few modes to cover at least 90% of the total mass of the building in order to get a better estimate of the shear demand on the structural elements., Shear reinforcement in the planes is determined from these shear estimates.. This concludes the DBSD of asymmetric plan buildings.

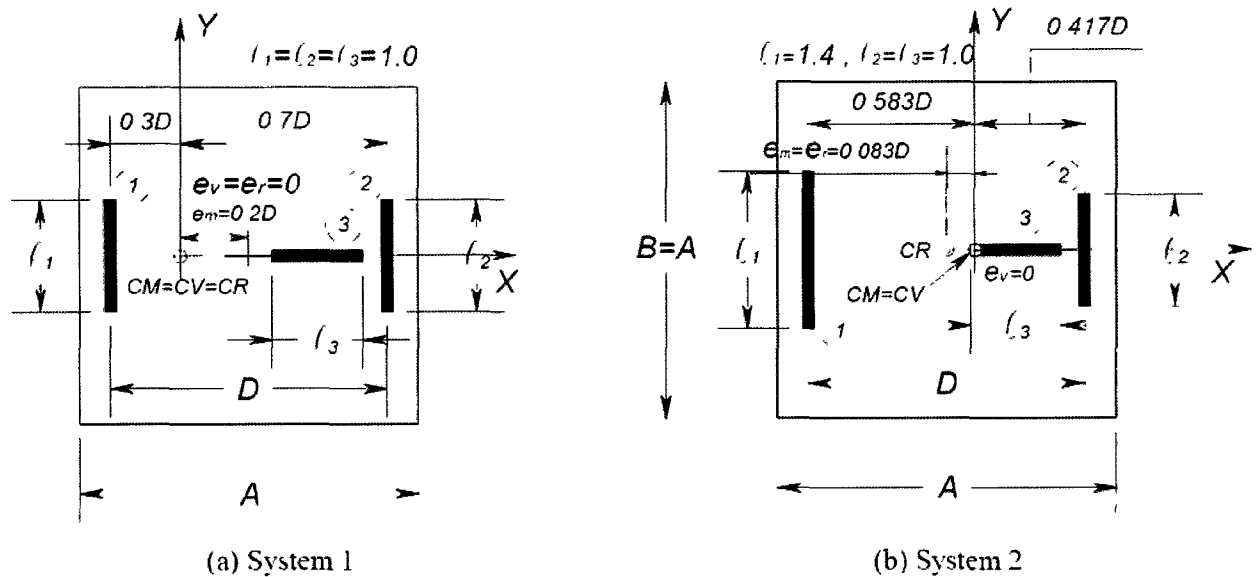


Figure 5.1: Plan view of torsionally balanced, system 1, and torsionally unrestrained, system 2 (Castillo et al 2001)

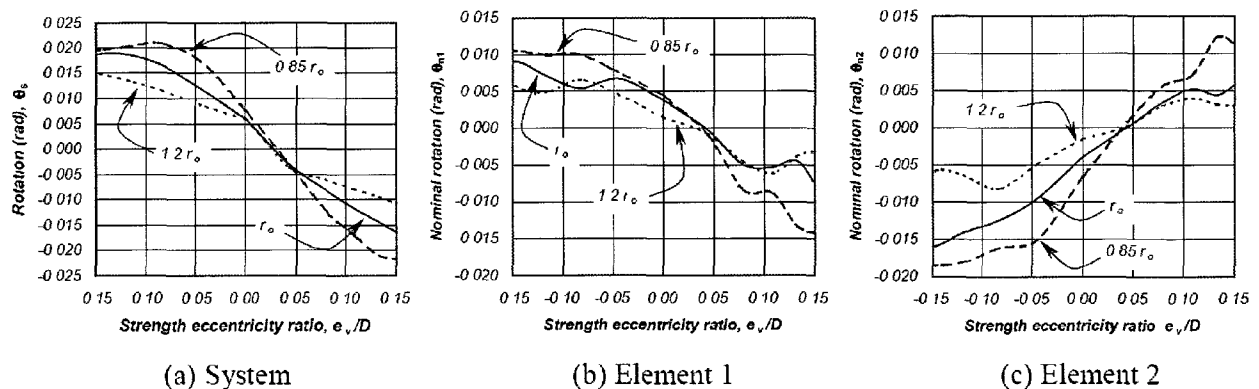


Figure 5.2: System rotation and nominal rotations (Castillo et al 2001)

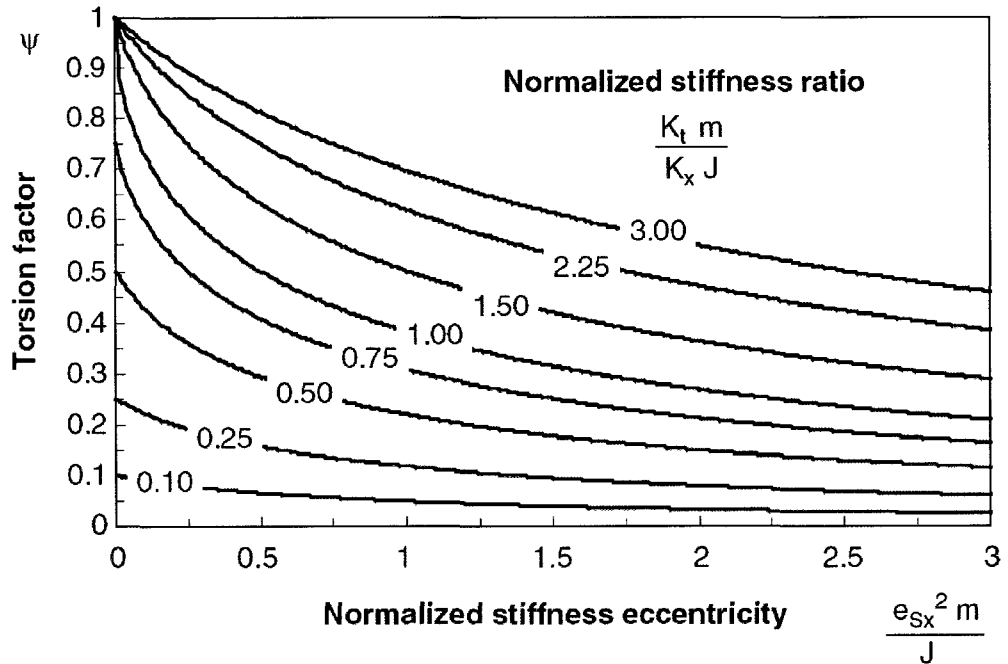


Figure 5.3: Torsion factor as a function of normalized stiffness eccentricity and normalized stiffness ratio (Sommer and Bachmann 2005)

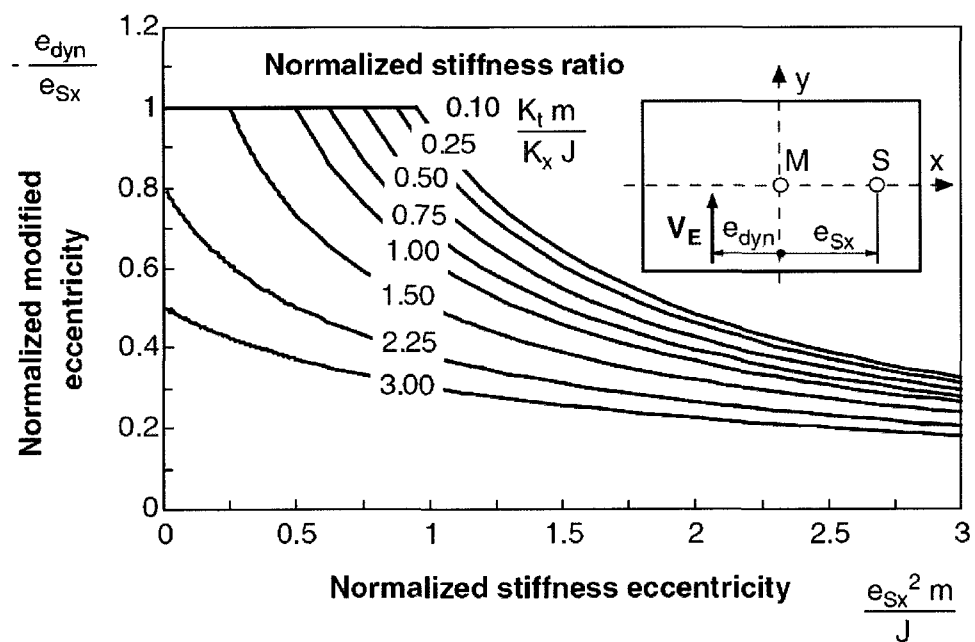


Figure 5.4: Normalized modified eccentricity as a function of normalized stiffness eccentricity and normalized stiffness ratio (Sommer and Bachmann 2005)

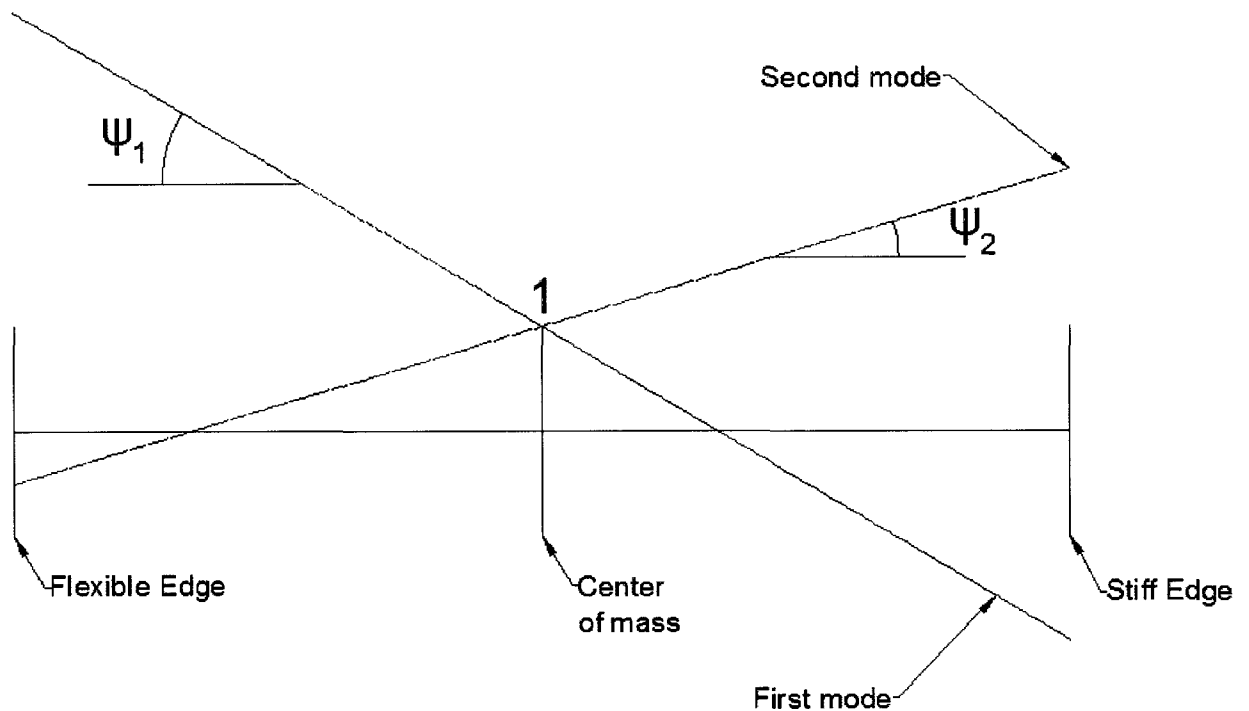


Figure 5.5: Deformed shape corresponding to the first and second normalised mode shapes

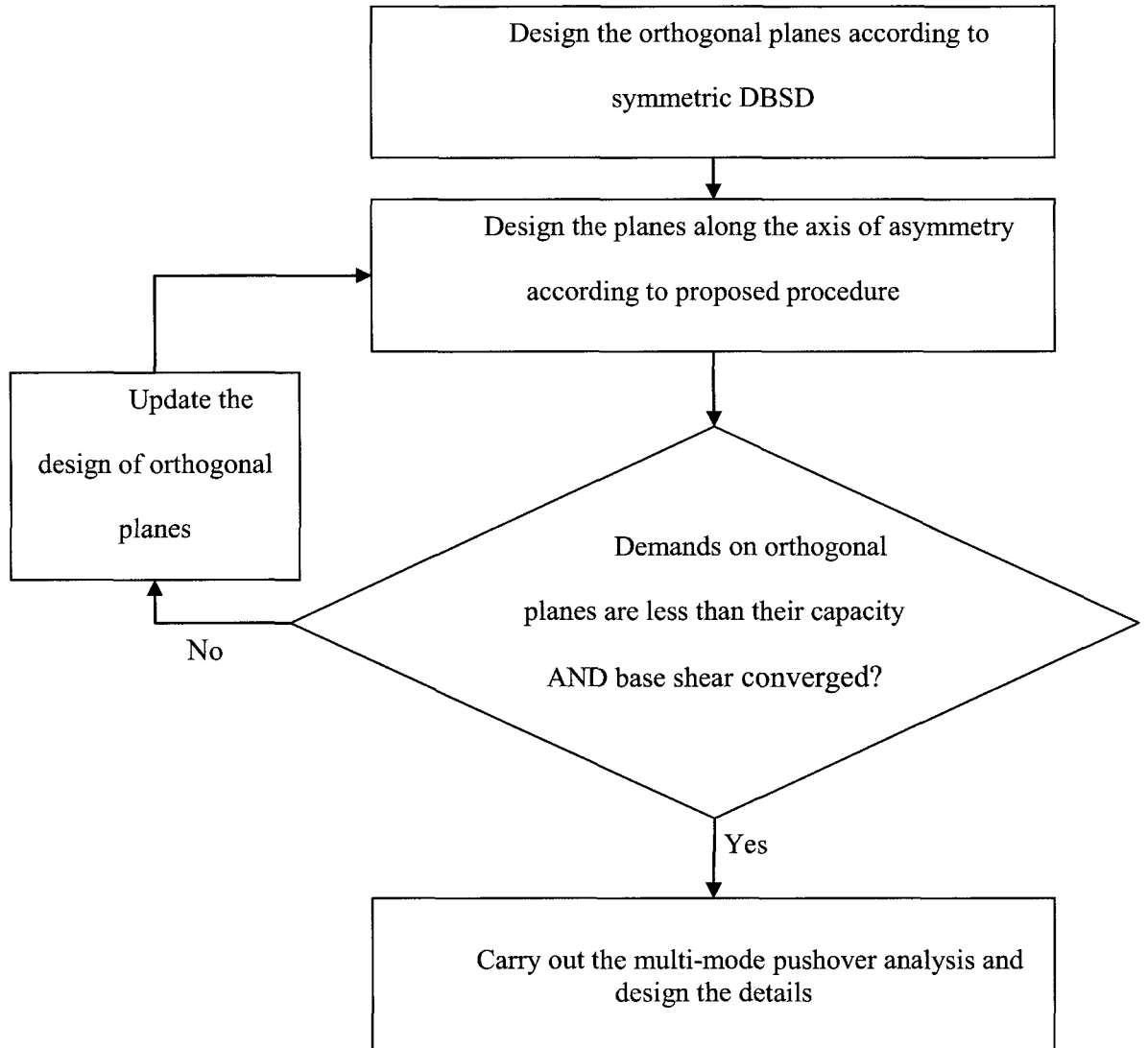


Figure 5.6: DBSD procedure for asymmetric plan buildings

Chapter 6. Case studies on DBSD of asymmetric plan buildings

6.1 Introduction

This chapter presents the DBSD of two 12-storey buildings with asymmetry in their plans. The design is carried out according to the proposed DBSD procedure for asymmetric plan buildings. The lateral resisting elements in these two systems are distributed in plan in such a way that one of the systems falls into the torsionally stiff category and the other into the torsionally flexible category. The DBSD for both the torsionally stiff and the torsionally flexible systems are presented. In each case the presentation includes the results of nonlinear dynamic analyses to verify the ability of the proposed method in predicting the seismic demands on structural elements at both the local and global levels. A detailed step-by-step DBSD of the two buildings is presented in Appendix C.

6.2 Torsionally stiff building

6.2.1 Problem definition

Plan view of 12-storey torsionally stiff building is shown in Figure 6.1. The floor dimension is 36 meter along the X axis, and 24 meter along the Y axis. The lateral resistance is provided by two 6.0 m by 0.4 m walls in the X direction and three walls in the Y direction. Of the Y direction walls the west and center walls are 5.0 m by 0.4 m, while the east wall is 7.0 m by 0.4 m. The building is located in the city of Vancouver and the design spectrum is obtained from the uniform hazard spectrum for 2% chance of exceedance in 50 years for Vancouver, which is provided in NBCC 2005.

6.2.2 DBSD of torsionally stiff building

6.2.2.1 DBSD of the planes along the axis of symmetry

The orthogonal planes have significant effect on the behaviour of asymmetric plan buildings, since they contribute to rotational strength and stiffness of the system. Therefore a comprehensive design procedure for asymmetric plan buildings should include the design for orthogonal planes as well as the planes in the principal direction of design earthquake. As explained in previous Chapter, DBSD of asymmetric plan buildings starts with the design of orthogonal planes using DBSD procedure for symmetric buildings. After the orthogonal planes are designed, the planes along the axis of unsymmetry will be designed.

During iterations for the design of planes along the axis of unsymmetry, demand on orthogonal walls is calculated and compared with their capacity. Orthogonal planes are re-designed if the calculated demand on orthogonal plane is greater than the designed capacity. For torsionally stiff building studied here, the calculated demands in different iterations remain less than the capacity of the 6.0 m walls in the orthogonal direction and the initial design of these walls is found to be adequate.

6.2.2.2 DBSD of planes along the axis of unsymmetry

Once the orthogonal resisting planes have been designed, planes along the axis of asymmetry can be designed according to the procedure proposed in Chapter 5. The

preliminary design process starts with the use of empirical relations to estimate the yield and ultimate displacements of the individual walls for the 2.5% drift limit. Relative stiffness of the walls is used to find the first mode shape of the building. For torsionally stiff building, the first mode shape alone is considered to be the design mode shape. The angle of twist corresponding to the first mode shape is employed to estimate the global yield and ultimate displacements at the center of mass. The base shear and base torque are then estimated using an equivalent 2DOF system constructed for the first mode. The structural walls are designed for the combined action of the base shear and base torque.

Further iterations are carried out using the updated estimates of the yield and ultimate displacements. DBSD of torsionally stiff building along the axis of unsymmetry converged after two iterations. In the following sections DBSD parameter values obtained in different iterations are discussed in detail.

6.2.2.2.1 Yield and ultimate displacements

The first step in estimating the global yield displacement is to obtain the yield displacement of each wall using empirical relations for the wall yield curvature, and yield displacement. The global yield displacement is then estimated using the equivalent yield displacement of individual walls at the center of mass. For torsionally stiff building, the angle of twist corresponding to first mode shape of the building is used to obtain the equivalent yield displacement of each wall at the center of mass. At the preliminary design stage, it is assumed that the base shear is distributed in proportion to the walls length. As a result, relative stiffness of the walls are related to the square of their lengths.

Using initial values of stiffnesses relative to 6-m orthogonal wall, the mode shapes are obtained and the equivalent yield displacement at the center of mass determined for each wall. The global yield displacement is calculated from these equivalent yield displacements.

In further iterations, global yield displacements are calculated using both the empirical relations and the first mode pushover curves. The global yield displacements estimated from empirical relations in the preliminary, first and the second iterations are 0.509 m, 0.459 m and 0.456 m compared to the global yield displacement obtained from the pushover curve that is 0.445 m for both the first and the second iterations. The yield displacement obtained from the pushover curve is used in the calculation of ductility demand of the building.

At the preliminary design stage, acceptable ultimate displacement can only be calculated using the code prescribed drift limit. The ultimate displacement for each resisting plane along the axis of unsymmetry is calculated, then using the angle of twist for the first mode shape, the equivalent ultimate displacement at the center of mass is found. The least of the calculated equivalent ultimate displacements is used to find the ductility demand on the buildings.

Further iterations of design are carried out using the results of pushover analysis of the building for lateral forces and torques distributed along the height in accordance with the first mode shape. Such an analysis provides the ultimate displacements corresponding

to the P– Δ instability limit and drift limits. For both the first and the second iterations, it is observed that ultimate displacement of the torsionally stiff building is controlled by the P– Δ instability limit.

6.2.2.2.2 Equivalent 2DOF systems

The equivalent 2DOF systems are constructed using the first mode shape for the building. The values of the main parameters of the equivalent 2DOF obtained during preliminary design and further iterations are tabulated in Table 6.1. As can be seen, the DBSD has converged in two iterations, and the base shear estimate of 2550.8 kN in the second iteration, is very close to the base shear capacity of 2586 kN. Also the shear demand on each of the orthogonal walls, V_{orth} , is smaller than the shear capacity of 734.85 kN.

6.2.3 Multi-mode pushover analysis

In order to get a better estimate of the shears a multi-mode pushover analysis is carried out next. Figure 6.2 shows the first 6 mode shapes of the system. The first, third, and the fifth modes are translation dominant while the second, fourth and sixth modes are torsion dominant. The first mode mass participation is only 60.20% of total mass, therefore higher modes should be considered as they may contribute significantly to the structural response.

We carry out a multi mode pushover analysis to investigate the higher mode contribution for the first six modes, for which the sum of modal masses is 92.21% of the total mass. The first mode pushover is carried out up to the maximum target displacement

of 0.594 m as calculated earlier. It is assumed that the structure remains elastic for higher modes, however this assumption will be verified during the pushover analysis for each mode. The target displacements in the pushover analysis for higher modes are obtained from Equation (5.29) and are shown in Table 6.2. Other dynamic properties for the first six mode are also shown in Table 6.2.

For each of these six modes a pushover analysis using the force distribution proportional to $M\phi$ is carried out to reach the target displacement. The pushover curves for these analyses are shown in Figure 6.3. As was expected the first mode pushover causes the structure to be displaced into the nonlinear range, but the structure remains elastic as it is pushed to the target displacement in the higher modes. It should be noted that the odd numbered modes contribute significantly to the base shear while the even numbered modes do not. We combine the modes to get the estimate of the base shear, roof displacement at the center of mass, angle of twist at roof level, and the maximum inter-storey drift ratio (see Table 6.3).

6.3 Verification of DBSD for torsionally stiff system

6.3.1 Ground motions

Nonlinear time history analyses are carried out to validate the design procedure. Five ground motions are selected from a set of ground motions that are compatible with the uniform hazard spectrum specified in the National Building Code of Canada 2005 for the west coast of Canada. The ground motions are selected from a group of 30 ground motions for site class C developed by Atkinson (2009). The process used for selecting the

ground motions is also the same as suggested by Atkinson (2009). In this process, the ratios of the target spectrum value to the elastic spectrum value for each of the 30 records are calculated over the period interval of 0.8 to 6.0 seconds, for every 0.005 second. Then the average and standard deviation of these ratios for every ground motion are calculated. The five ground motions that have the smallest standard deviations in their ratios are selected. Each is then scaled by the mean of its sampled ratios. Table 6.4 shows the specifications of the selected ground motions. As can be seen from Table 6.4 all scaling factors are within the acceptable range of 0.5 to 2.0. The peak ground accelerations reported in Table 6.4 are after scaling. The spectra of the five ground motions and their average are shown in Figure 6.4. It can be noticed that the spectra of the five records as well as their mean are quite close to the target design spectrum. The dispersion between the spectra of the individual records and the design spectrum is greater in the low period ranges, while there is a better match for longer periods.

6.3.2 Structural model

Reinforced concrete is a composite material with a very complex nonlinear behaviour. That is mainly because the concrete has completely different stress-strain relationships in compression and tension. Steel on the other hand, has varying nonlinear behaviour as it enters the yield plateau and then the stress hardening region. Moreover, the effect of cracked section, stress concentration at the tip of the cracks and the bar slip of reinforcements introduce additional nonlinearity in a reinforced concrete section. A number of different models have been described in the literature to model the response of reinforced concrete sections. Some of these models take into account the

strength/stiffness degradation experienced during cyclic loading. In the present study, nonlinear dynamic analyses of the buildings designed according to the DBSD procedure for their response to spectrum compatible ground motions are carried out primarily for comparing the results of such analyses with the corresponding estimates obtained during DBSD. For this purpose a simple bilinear elasto-plastic model based on properties determined through a moment-curvature analysis of the section is used in the nonlinear dynamic analysis. Nonetheless, more detailed model of the studied structure could be implemented in future studies.

The nonlinear dynamic analyses of the torsionally stiff building studied here are carried out using the OpenSees program (Mazzoni et al, 2007). The shear walls in both X and Y directions shown in Figure 6.1 are modeled using the elastic beam-column element available in OpenSees. The elastic moments of inertia of these elements are set to be equal to the effective moments of inertia of the walls found from the moment curvature analyses of the walls taking the effect of the gravity axial load into account. The potential plastic hinges in the walls are placed at the base of the walls and are modeled using zero-length elements with elasto-plastic behaviour. The properties of the zero-length elements are also specified using the results of moment curvature analyses of the walls, which provide the yield curvatures and yield moments of the walls.

The effect of second order forces, also referred to as P- Δ effect, is included in nonlinear dynamic analyses. The gravity loads from the self weight of the floors and structural elements are applied on the walls in both the X and Y directions in proportion

to the plan tributary areas of the walls. OpenSees updates the stiffness matrices of the walls taking the P- Δ effect at each step of the analysis.

Damping ratio has significant effect on the dynamic response of the structures to strong ground motions. In this study a Rayleigh damping is used and the value of the critical damping is set at 5% for the first and the third modes.

6.3.3 Results

The roof displacement response of the system to these ground motion is shown in Figure 6.5. It will be noted that during the first 20 seconds of the response there is not much movement, which is because the generated records have a 20 second lag. In general the flexible edges displacements are larger. There are some instances when the stiff edge displacement is greater than the flexible edge displacement but the maximum displacement always occurs on the flexible edge. This implies that the assumption we have made about the response of the system being dominated by the first mode is a valid assumption.

Figure 6.6 shows the time history of the base shear of the system for different ground motions. As can be observed from Figure 6.6 and Table 6.5 the record M7C1N5 which has the smallest PGA produces the smallest base shear demand.

The main global response parameters of the system are summarised in the Table 6.5. The CQC combination of base shear estimate of 10,286 kN is about 8% greater than

the average of the values obtained from five ground motion nonlinear time history analyses, namely 9,520.72 kN. The roof displacement estimate of 0.5983 m obtained from the multi-mode analysis is about 3% smaller than the average of five nonlinear time history analyses, which is 0.6161 m.

The maximum drifts at the flexible edge of the buildings are also shown in Table 6.5. The CQC combination of six modes estimates the maximum drifts to be 2.449% which is 4% more than the average of five nonlinear time history analyses of 2.358%. Moreover, the mean value of drift at flexible edge for nonlinear time history analyses is less than the code limit of 2.5%. In conclusion, the results of nonlinear time history analyses show that the proposed DBSD estimates the response parameters fairly well for a torsionally stiff system.

6.4 Torsionally flexible Building

6.4.1 Problem definition

Consider the 12 storey building, whose plan view is shown in Figure 6.7. This building is similar to the torsionally stiff system in respect of all the dimensions, applied gravity loads, and material properties. However, the edge walls are located closer to the center of the mass, so that the torsional stiffness is reduced and the structure becomes torsionally flexible. The torsionally flexible building is also assumed to be located in the city of Vancouver. The design spectrum is obtained from the uniform hazard spectrum for 2% chance of exceedance in 50 years for Vancouver, which is provided in NBCC 2005.

6.4.2 DBSD for torsionally flexible building

A detailed step-by-step DBSD of the torsionally flexible building is presented in Appendix C. In this section, highlights of the design procedure as well as some of the important assumptions and findings are discussed.

6.4.2.1 DBSD of the planes along the axis of symmetry

As explained in Chapter 5, the proposed DBSD of asymmetric plan buildings starts with the design of orthogonal planes. The orthogonal planes for torsionally flexible system are identical to the ones for torsionally stiff system. The only difference is that the axial gravity loads on the walls in the torsionally flexible building are smaller than those in the torsionally stiff building. This is because of a change in the plan layout and tributary areas of the walls. As a result of these changes, the orthogonal walls in torsionally flexible system end up with slightly more concentrated reinforcement at the end of the DBSD of resisting planes along the axis of symmetry.

Moreover, at the end of the preliminary design of planes along the axis of unsymmetry of torsionally flexible building, it is found that the demand on orthogonal wall to resist the combination of the dynamic torque and the torque induced due to assignment of the base shear to different resisting planes is greater than the capacity provided during initial design. As a consequence, the orthogonal walls have to be re-designed.

6.4.2.2 DBSD of planes along the axis of unsymmetry

DBSD of resisting planes along the axis of unsymmetry for torsionally flexible building is similar to that for torsionally stiff building as discussed in Section 6.2.2.2, with the following exceptions: (1) the design mode shape may be different and (2) the ultimate displacement as governed by the code prescribed drift limit is calculated to ensure that drifts at the periphery of the plan are less than the drift limit.

As explained in Chapter 4, for a torsionally stiff building only the first mode shape is used to estimate the displacement demand on the different resisting planes. However for a torsionally flexible building both the first and the second mode are considered in the design process. The DBSD of the torsionally flexible building converged after one iteration of design. In the following sections the various parameter values obtained in a DBSD are discussed in more details.

6.4.2.2.1 Yield and ultimate displacements

The first mode of the torsionally flexible building is found to be torsion dominant and the second mode is translation dominant. The deformed configuration based on the first mode shape imposes larger relative displacement on the flexible side while that in the second mode imposes larger relative displacement on the stiff side. The angles of twist calculated from the first mode and the second mode shape are different in sign. This influences the calculation of equivalent yield and ultimate displacements at the center of mass.

In preliminary design, empirical relations are used to estimate the yield curvature and the yield displacement of each individual wall and its equivalent at the center of mass for both the first mode and second mode deformed configurations. Global yield displacements for the two mode shape configurations are then calculated. It should be noted that at the preliminary stage, the mode shapes are obtained using the relative stiffnesses of the walls, as in the case of the torsionally stiff building.

In the first iteration, the global yield displacements for the first and second modes are obtained from the first and second mode pushover curves of the building rather than from empirical relations. The pushovers are carried out for the modal distribution of lateral forces and torques along the height of the building.

At the preliminary design stage the acceptable ultimate displacement can be found only for the code prescribe drift limit. Since the lateral resisting planes are not located at the edge of the building, the ultimate displacements for the first and second modes are calculated to ensure that drifts at the edge of the building would not exceed the 0.025. It is of interest to note that the ultimate displacement for the first mode is governed by the drift at the flexible edge, while the ultimate displacement for the second mode is dictated by the drift at the stiff edge.

In the first iteration, the ultimate displacement is obtained so as to satisfy all three criteria considering both the first and second modes. The ultimate displacement as governed by the ductility limit is found for each wall and its equivalent at the center of

mass is calculated for each mode shape deformed configuration. The least of the equivalent ultimate displacements for the three walls as governed by their ductility capacity is taken as the ductility related ultimate displacement for the mode being considered. The ultimate displacement limit to prevent P- Δ instability is obtained from the pushover curves for the first and second modes. The ultimate displacement dictated by the drift limit is also found from the pushover analysis. Again drifts at the flexible edge are found to dictate the acceptable ultimate displacement in the first mode while the ultimate displacement in the second mode is dictated by the drifts at the stiff edge.

6.4.2.2.2 Equivalent 2DOF systems

The equivalent 2DOF systems are constructed using the first and the second mode shapes for the building. The main parameters of the equivalent 2DOF for the preliminary design and further iterations are tabulated in Table 6.6 and 6.7 for the first and the second modes, respectively. As can be seen, the DBSD has converged in one iteration, and the base shear and base torque for the first mode govern the design since they are much larger than the base shear and torque for the second mode. The ductility demand calculated for the first mode, which is torsion dominant, is very close to one. That means the structure is designed to be very close its elastic state.

The demand on each of the orthogonal walls calculated in the preliminary design for the first mode is 1020.7 kN, which is greater than the orthogonal wall capacity of 734.85 kN. Therefore, the orthogonal walls are re-designed at the end of the preliminary design to resist this demand. The demand on orthogonal walls calculated in the first

iteration is very close to the re-designed section capacity, and the base shear and base torque have converged, therefore the DBSD of resisting planes along the axis of unsymmetry is assumed to have converged.

6.4.3 Multi-mode pushover analysis

Figure 6.8 shows the first 6 mode shapes of the system. The first, third, and the fifth modes are translation dominant while the second fourth and sixth modes are torsion dominant. The first mode mass participation is only 44.21% of the total mass, therefore higher modes should be considered as they would make significant contribution to the structural response.

We carry out a multi mode pushover analysis to investigate the higher mode contribution. The first mode pushover is carried out to the maximum target displacement of 0.430 m, and the second mode to the maximum displacement of 0.30 m, as calculated earlier. It is assumed that the structure remains elastic for higher modes, however this assumption will be verified during the pushover analysis for such modes. The target displacements for pushover analysis for modes three and higher are obtained from elastic design spectrum. For each of these six modes a pushover analysis using the force distribution proportional to $M\phi$ is carried out to reach the target displacement as calculated in Table 6.8.

As will be noted from Figure 6.9 the structure remains elastic as it reaches the target displacement in the 3rd, 4th, 5th, and the 6th mode pushover analyses. The structure

has lower capacity in the second mode as compared to that in the first mode. Combination of modes up to the eighth mode covers 95.89% of total mass. SRSS and CQC combination rules is used to get the estimates of the base shear, roof displacement at the center, angle of twist at roof level and the maximum inter-storey drift ratio (see Table 6.9). Higher modes have significant effect in the estimate of the base shear, while the effect of higher mode on drifts and displacements are negligible.

6.5 Verification of DBSD for torsionally flexible system

Nonlinear time history analyses are carried out to verify the accuracy of the proposed DBSD for torsionally flexible structures. The same set of ground motions as selected in Section 6.3 is used as the input. The characteristics of these ground motions are shown in Table 6.4 and the response spectra for the individual ground motions as well as the target design spectrum are shown in Figure 6.4.

The roof displacement response of the system to these ground motion is shown in Figure 6.10. It will be noted that during the first 20 seconds of the response there is not much movement, which is because the generated records have a 20 second lag. In general the flexible edges displacements are larger; however, there are instances when the stiff edge displacement is larger. This implies that the assumption we made that the response of the system is dominated by one or other of the first two modes is a valid assumption.

Figure 6.11 shows the time history of the base shear of the system for different ground motions. As can be seen in Figure 6.11 and Table 6.10 the record M7C1N5 which has the smallest PGA produces the smallest base shear demand.

The main global response parameters of the system are summarised in the Table 6.10. The CQC combination of base shear estimate of 9,681.3 kN is very close to the average of five ground motion nonlinear time history analysis of 9,266.3 kN. Also, the roof displacement of 0.6012 m as estimated by multi-mode pushover analyses is close to the average of five nonlinear time history analyses, namely 0.6732 m (see Table 6.9 and Table 6.10).

The maximum drifts at the flexible and stiff edges of the buildings are also shown in Table 6.10. It will be noted that, in general, the drifts at flexible edge are larger than those at the stiff edge. However for M7C1N5 and M7C1N7 where the maximum rotations in the plan are smaller than those for the other three records, the maximum drifts at the flexible and stiff edges are close to each other. Finally, it is of interest to note that the average drifts at both the flexible and the stiff edges are less than the code limit of 2.5 percent.

Table 6.1: Details of the equivalent 2DOF systems for torsionally stiff building

| | Γ | M^* (tonne) | δ_y (m) | δ_u (m) | μ | S_a (g) | V_b (kN) | T_b (kN.m) | V_{orth} (kN) |
|---------------------------|----------|------------------|----------------|----------------|-------|-----------|------------|-----------------|---------------------------|
| Preliminary | 1.488 | 5118.5 | 0.342 | 0.413 | 1.207 | 0.06474 | 3250.8 | 10,659.1 | 687.94 |
| 1st iteration | 1.363 | 4677.7 | 0.326 | 0.403 | 1.234 | 0.0646 | 2964.4 | 11,241.6 | 690.73 |
| 2 nd iteration | 1.370 | 4701.9 | 0.325 | 0.434 | 1.335 | 0.0553 | 2550.8 | 9,373.74 | 581.88 |

Table 6.2: Dynamic parameters in multi-mode pushover analyses

| Dynamic Parameters | First mode | Second mode | Third mode | Fourth mode | Five mode | Sixth mode |
|-------------------------|------------|-------------|------------|-------------|-----------|------------|
| M^*/M_{total} | 0.6020 | 0.0521 | 0.1841 | 0.0159 | 0.0624 | 0.0054 |
| Γ | 1.3702 | 0.1186 | 0.6624 | 0.0574 | 0.3377 | 0.0292 |
| T (sec) | 4.22 | 2.74 | 0.67 | 0.44 | 0.24 | 0.16 |
| S_a (g) | 0.0553 | 0.1466 | 0.5990 | 0.8083 | 1.0511 | 1.1000 |
| D_{target} (m) | 0.594 | 0.0325 | 0.0446 | 0.0022 | 0.0051 | 0.0002 |

Table 6.3: Modal response parameters and their combination

| | Base shear (kN) | Roof displacement at C.M (m) | Rotation at roof level | Maximum drift (%) |
|----------|--------------------|---------------------------------|---------------------------|----------------------|
| 1st mode | 2,586.9 | 0.594 | 0.0112 | 2.2677 |
| 2nd mode | 565.4 | 0.0325 | 0.0093 | 0.4191 |
| 3rd mode | 7,558.2 | 0.0446 | 0.0010 | 0.7187 |
| 4th mode | 972.3 | 0.0022 | 0.0006 | 0.1052 |
| 5th mode | 6,172.9 | 0.0051 | 1.17×10^{-4} | 0.1930 |
| 6th mode | 489.31 | 0.0002 | 5.13×10^{-5} | 0.0178 |
| SRSS | 8,008.6 | 0.59656 | 0.01459 | 2.4155 |
| CQC | 10,286 | 0.59826 | 0.01496 | 2.4486 |

Table 6.4: Specifications of the selected ground motions

| Record ID | Distance, km | Scaling factor | PGA, g |
|-----------|--------------|----------------|--------|
| M7c1N1 | 16.4 | 0.87581 | 0.4571 |
| M7c1N5 | 17.1 | 1.3239 | 0.3185 |
| M7c1N7 | 10.2 | 0.76673 | 0.4596 |
| M7c1N26 | 18.1 | 0.818 | 0.4219 |
| M7c1N30 | 15.2 | 0.72668 | 0.3726 |

Table 6.5: Nonlinear time history response parameters

| | Maximum base shear (kN) | Maximum roof disp. at C.M (m) | Maximum rotation at roof | Maximum drift (%) |
|---------|-------------------------|-------------------------------|--------------------------|-------------------|
| M7C1N1 | 7,770.6 | 0.5997 | 0.01576 | 2.571 |
| M7C1N5 | 5,469.8 | 0.3745 | 0.01006 | 1.557 |
| M7C1N7 | 11,498 | 0.7386 | 0.01474 | 2.746 |
| M7C1N26 | 9,732.2 | 0.7531 | 0.01963 | 2.960 |
| M7C1N30 | 13,133 | 0.6144 | 0.01658 | 2.093 |
| Average | 9,520.72 | 0.6161 | 0.01535 | 2.358 |

Table 6.6 Details of the equivalent 2DOF systems for the first mode of torsionally flexible building

| Γ | M^* (tonne) | δ_y (m) | δ_u (m) | μ | S_a (g) | V_b (kN) | T_b (kN.m) | V_{orth} (kN) |
|---------------|------------------|----------------|----------------|-------|-----------|------------|-----------------|--------------------|
| Preliminary | 0.9893 | 3326.1 | 0.372 | 0.397 | 1.070 | 0.0755 | 2,463.5 | -22,527 |
| 1st iteration | 1.0062 | 3452.6 | 0.417 | 0.427 | 1.023 | 0.0735 | 2,489.4 | -21,536 |

Table 6.7 Details of the equivalent 2DOF systems for the second mode of torsionally flexible building

| | Γ | M^* (tonne) | δ_y (m) | δ_u (m) | μ | S_a (g) | V_b (kN) | T_b (kN.m) | V_{orth} (kN) |
|---------------|----------|------------------|----------------|----------------|-------|-----------|---------------|-----------------|---------------------------|
| Preliminary | 0.5196 | 1782.9 | 0.398 | 0.523 | 1.320 | 0.0467 | 819.79 | 13,934 | 642.07 |
| 1st iteration | 0.4827 | 1656.3 | 0.518 | 0.622 | 1.200 | 0.0432 | 701.93 | 12,658 | 580.05 |

Table 6.8: Dynamic parameters in multi-mode pushover analyses

| Dynamic Parameters | First mode | Second mode | Third mode | Fourth mode | Five mode | Sixth mode |
|-------------------------|------------|-------------|------------|-------------|-----------|------------|
| M^*/M_{total} | 0.4421 | 0.2121 | 0.1352 | 0.0649 | 0.0458 | 0.022 |
| Γ | 1.0062 | 0.4827 | 0.4864 | 0.2334 | 0.2479 | 0.119 |
| T (sec) | 4.613 | 3.999 | 0.734 | 0.637 | 0.262 | 0.227 |
| S_a (g) | 0.0735 | 0.0432 | 0.6322 | 0.8409 | 1.0703 | 1.1000 |
| D_{target} (m) | 0.430 | 0.300 | 0.0360 | 0.0147 | 0.0043 | 0.0016 |

Table 6.9: Modal response parameters and their combination

| | Base shear (kN) | Roof displacement at C.M (m) | Rotation at roof level | Maximum drift flexible edge | Maximum drift stiff edge |
|----------|--------------------|---------------------------------|---------------------------|-----------------------------------|--------------------------------|
| 1st mode | 2179 | 0.43 | -2.14×10^{-2} | 0.025 | 0.0013 |
| 2nd mode | 1657 | 0.30 | 3.16×10^{-2} | -0.0077 | 0.025 |
| 3rd mode | 5262 | 0.036 | -1.93×10^{-3} | 0.0083 | 6.99E-05 |
| 4th mode | 2950 | 0.015 | 1.65×10^{-3} | -0.0018 | 0.0053 |
| 5th mode | 4527 | 0.0043 | -2.63×10^{-4} | 0.0024 | -9.76E-06 |
| 6th mode | 2155 | 0.0016 | 2.09×10^{-4} | -0.00047 | 0.0013 |
| 7th mode | 1520 | 0.0007 | -3.64×10^{-5} | 0.0004 | 1.52E-06 |
| 8th mode | 887.4 | 0.0003 | 3.18×10^{-5} | -9.45E-05 | 0.000272 |
| SRSS | 8492.4 | 0.52578 | 0.03825 | 0.027615 | 0.025623 |
| CQC | 9681.3 | 0.60124 | 0.03190 | 0.025026 | 0.026051 |

Table 6.10: Nonlinear time history response parameters

| | Base shear (kN) | Roof disp. at C.M (m) | Maximum rotation at roof | Maximum drift at flexible edge | Maximum drift at stiff edge |
|---------|--------------------|-----------------------|--------------------------|--------------------------------|-----------------------------|
| M7C1N1 | 6,987.6 | 0.5779 | 0.01475 | 0.02187 | 0.01498 |
| M7C1N5 | 6,531.4 | 0.4048 | 0.01072 | 0.01505 | 0.01261 |
| M7C1N7 | 10,220 | 0.7012 | 0.01193 | 0.02388 | 0.02024 |
| M7C1N26 | 8,218.4 | 0.8763 | 0.01670 | 0.03245 | 0.01797 |
| M7C1N30 | 14,374 | 0.8056 | 0.02001 | 0.02762 | 0.01973 |
| Average | 9,266.3 | 0.6732 | 0.01482 | 0.02418 | 0.01711 |

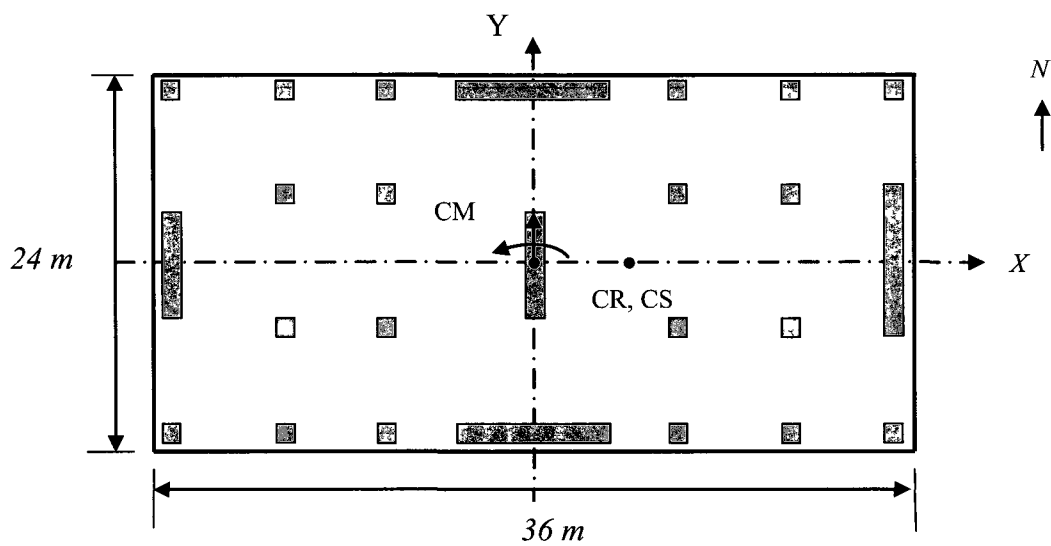


Figure 6.1: Plan layout of torsionally stiff system

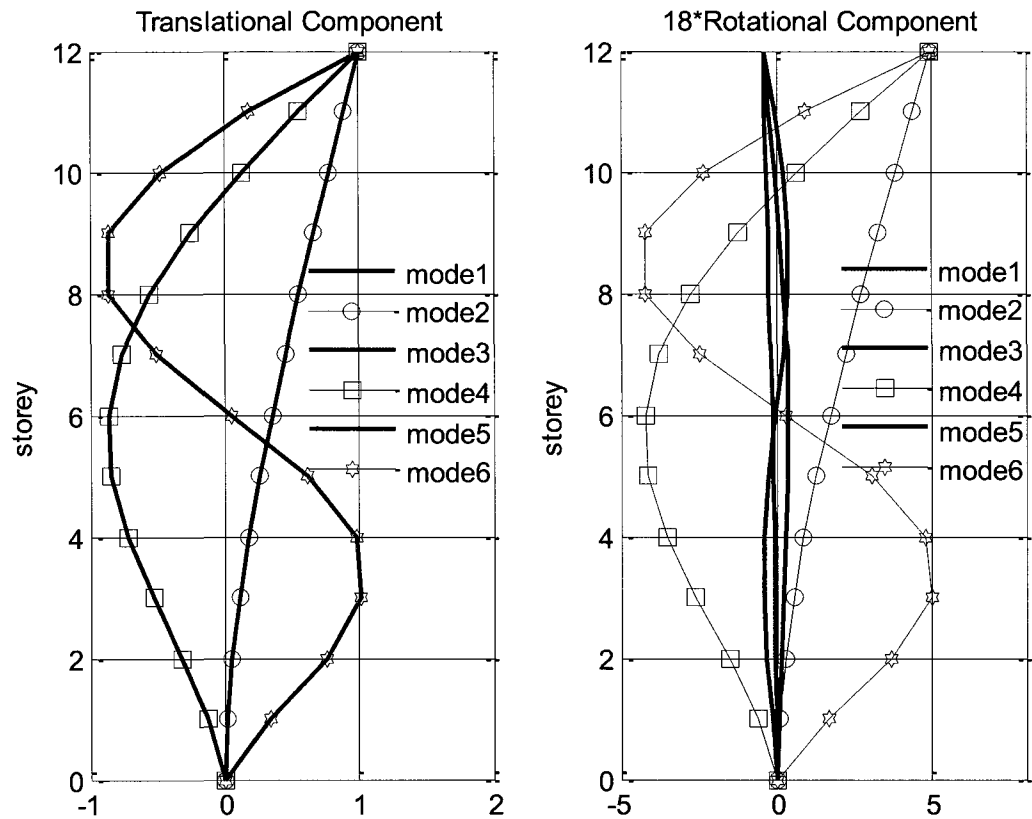


Figure 6.2: Translational and normalised rotational components of the first six modes

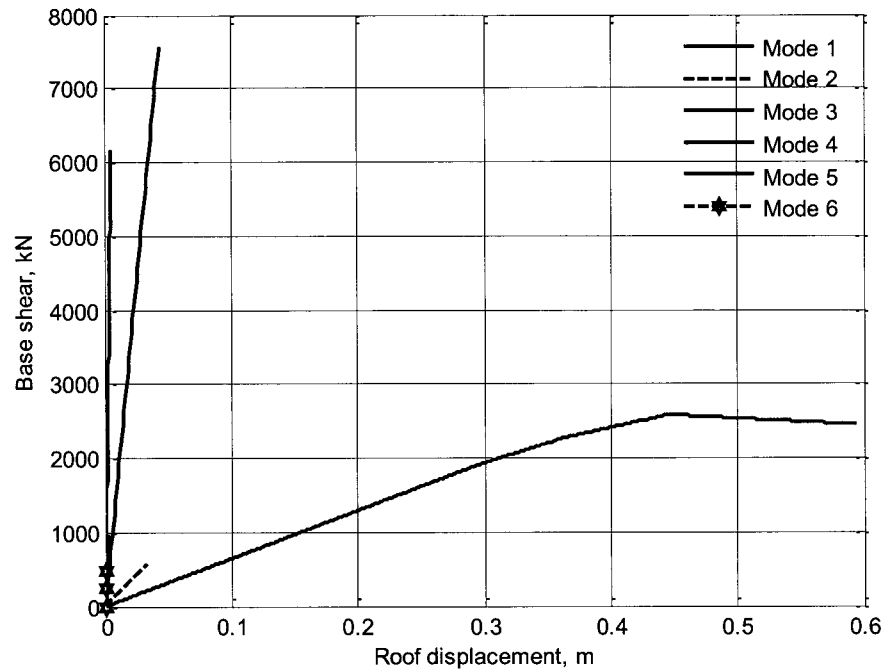


Figure 6.3: Pushover curves for the first six modes

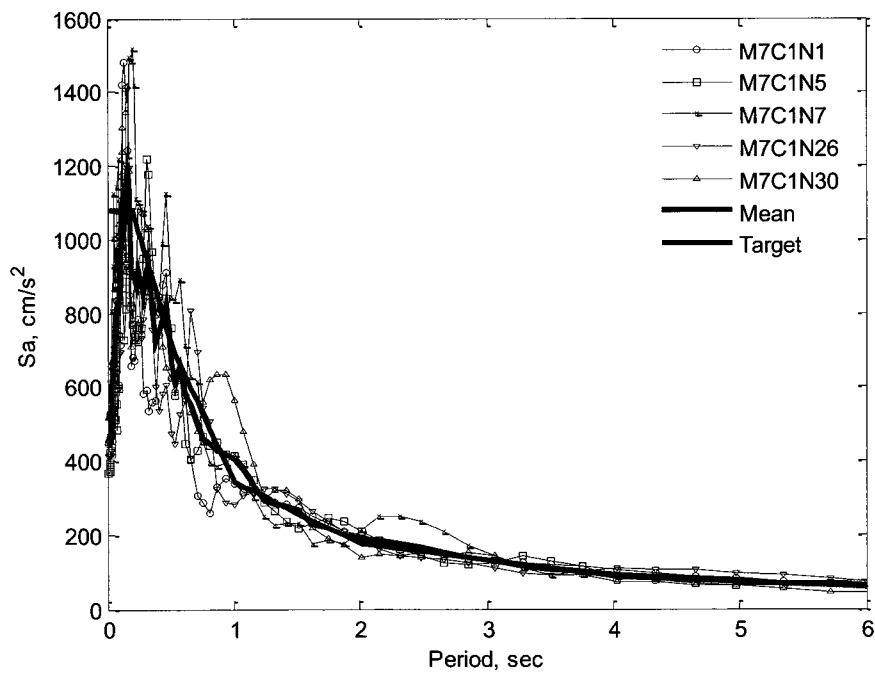


Figure 6.4: Target spectrum and the scaled spectra for five ground motions

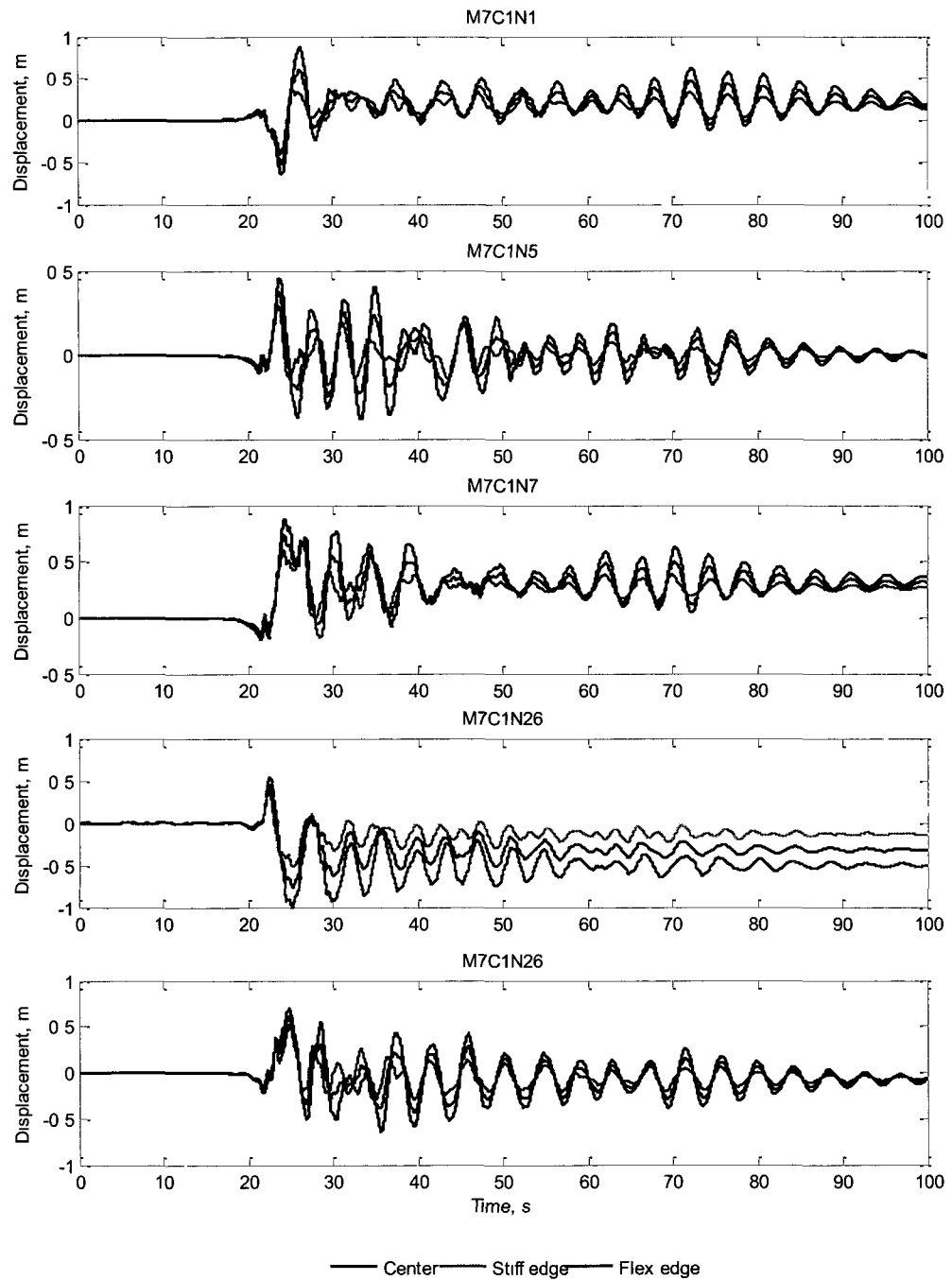


Figure 6.5: Displacement-time histories

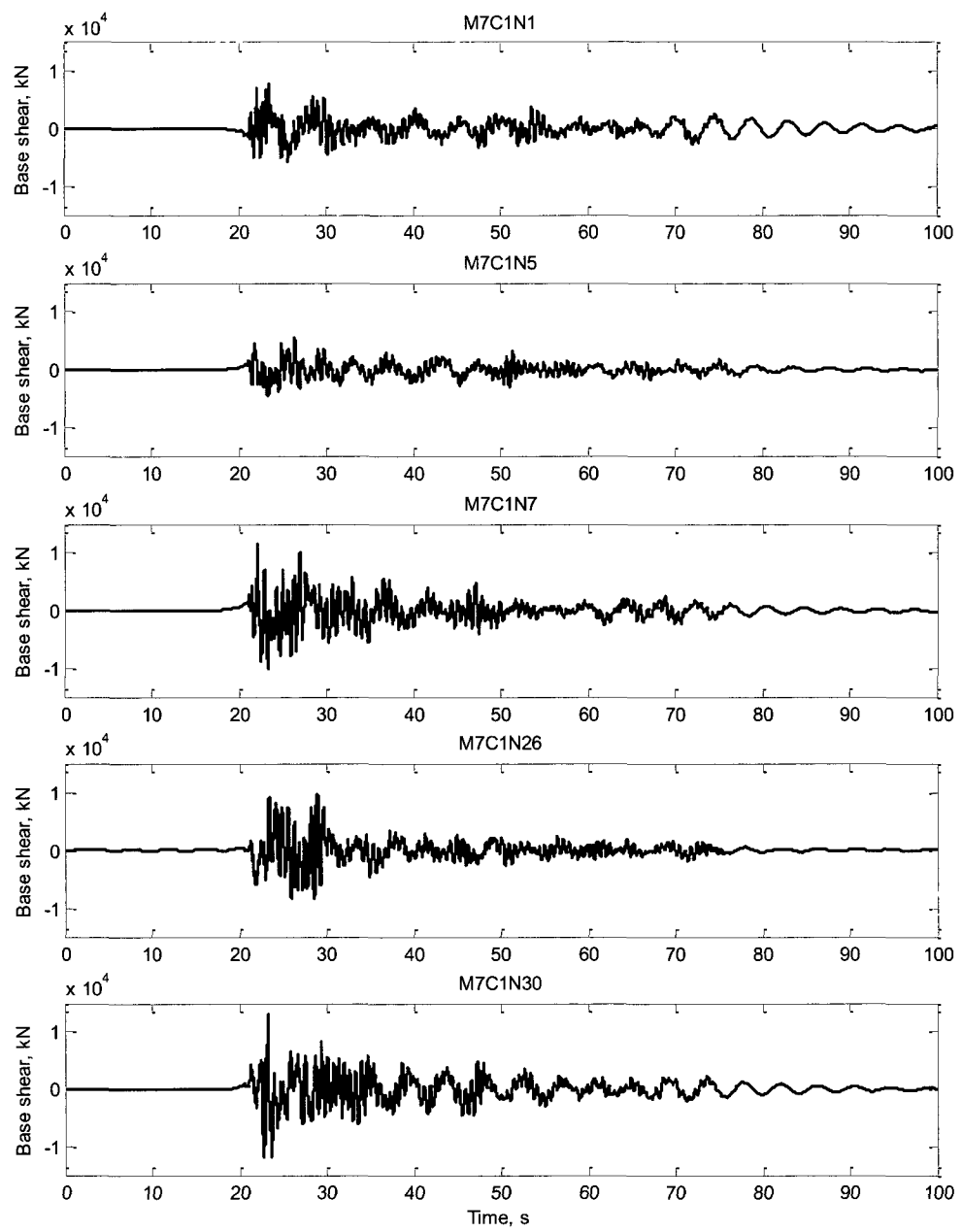


Figure 6.6: Base shear time histories

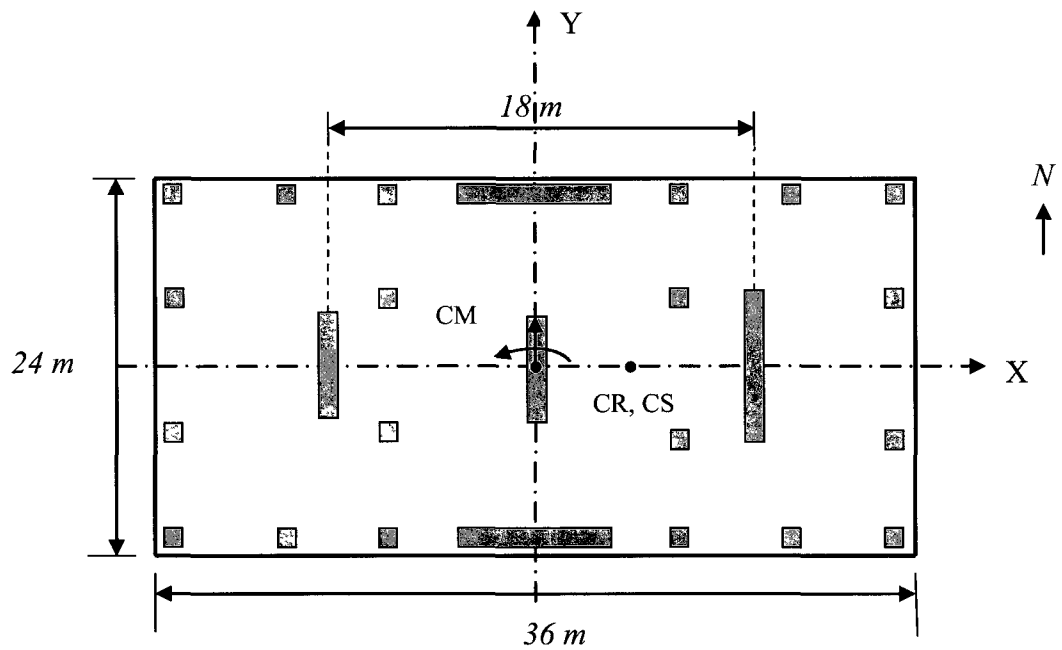


Figure 6.7: Plan view of torsionally flexible system

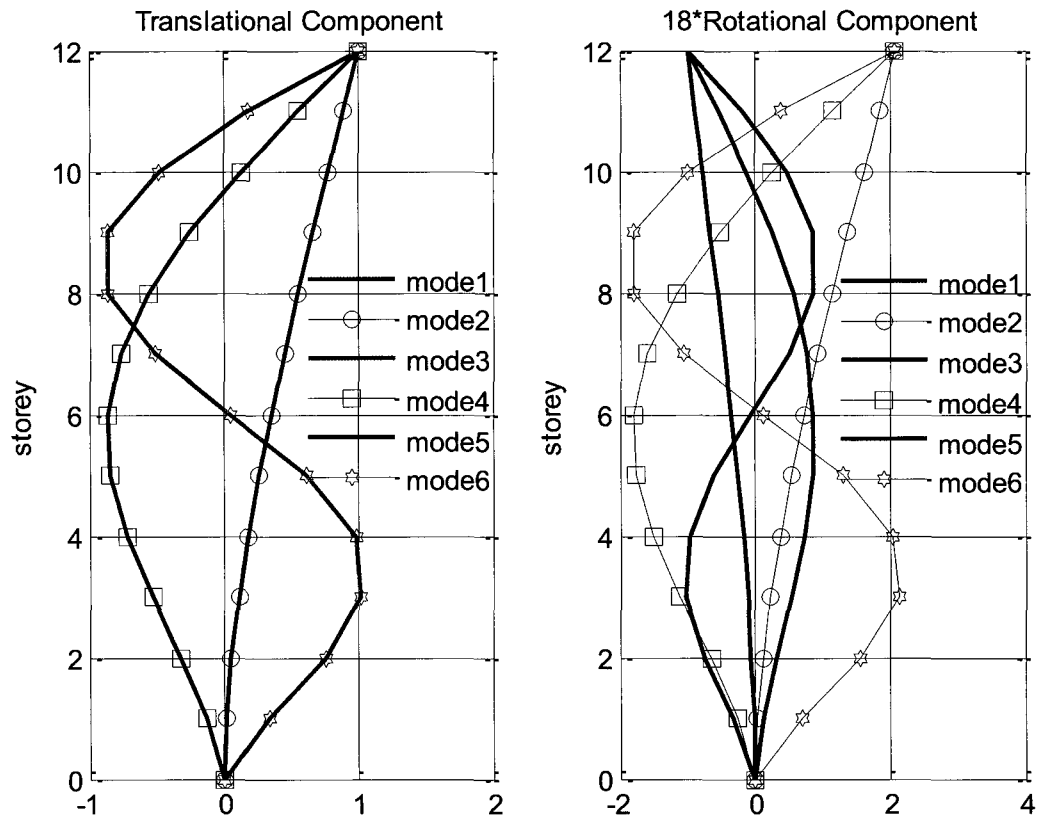


Figure 6.8: Translational and rotational components of the mode shapes

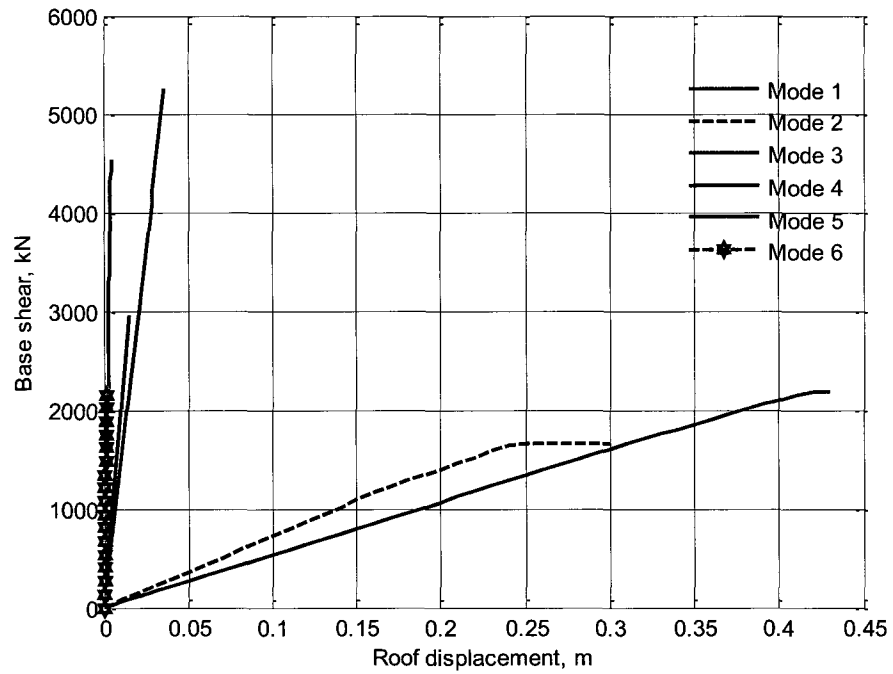


Figure 6.9: Pushover curves for the first six modes

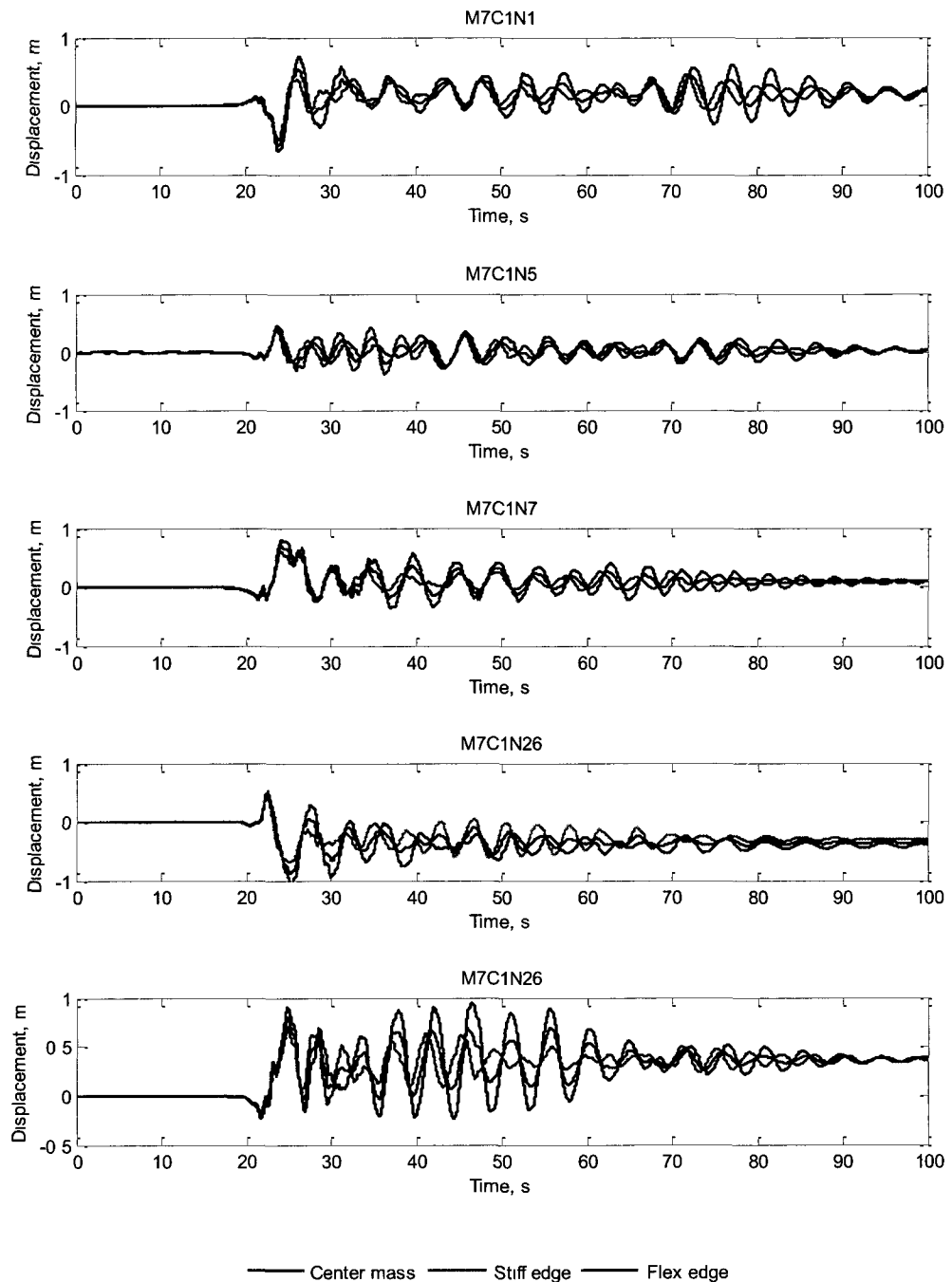


Figure 6.10: Displacement-time histories

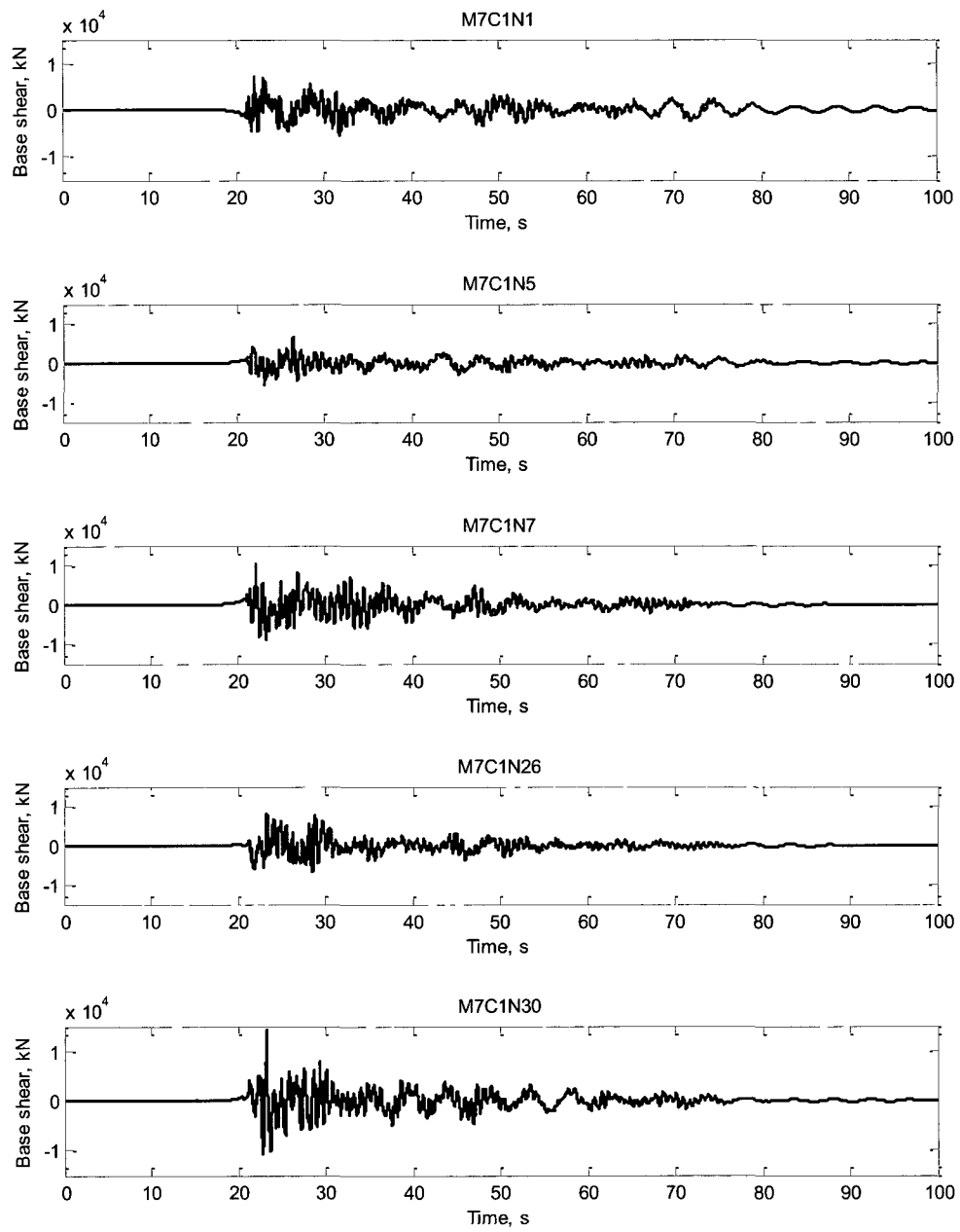


Figure 6.11: Base shear time histories

Chapter 7. Summary and conclusions

7.1 Summary

Two iterative DBSD procedures are presented: one for symmetric plan reinforced concrete wall-frame structures and the other for asymmetric plan reinforced concrete shear wall buildings. The study related to the DBSD of asymmetric plan buildings is limited to the case of individual reinforced concrete shear walls of rectangular section. Although, in principle the proposed method could be extended to structural systems consisting of shear walls with different cross-section shapes and core walls, further study need to be carried out to enhance this procedure for application to the design of such systems. The proposed DBSD procedures presented here are suitable for designing structures for different performance objectives, which is a step towards the performance based design of building structures.

7.1.1 Summary of DBSD for wall-frame structures

The proposed DBSD for wall-frame structures is based on the assumption that displacements in the seismic response of such structures are dominated by their first mode shape configuration. However, after the design procedure has converged a multi-mode pushover analysis is used to investigate the effects of the higher modes.

Simple empirical relations are employed to represent the deformed shape of reinforced concrete wall-frame structures in their first mode shape configuration, in order to estimate the yield displacement and ultimate displacement. Three different limits are imposed on the ultimate displacement to ensure that the design meets the performance

criteria. These limits are ductility capacity limit, drift limit, and P- Δ instability limit. Acceptable ultimate displacement is calculated so as not to exceed either of these limits.

The ductility demand in the wall-frame system is calculated based on the estimated yield and ultimate displacements. An equivalent SDOF system is developed and is used to estimate the base shear demand on the structure from an inelastic design spectrum in the A-D format for the site where the building is located. Once an estimate has been obtained for the base shear, the structural elements are designed for corresponding forces imposed on them. Moment curvature analyses are carried out for the designed elements to obtain their section properties. Based on these section properties, the displacement estimates are updated and iterations are continued until the base shear has converged.

To assess the proposed DBSD, it is applied in the seismic design of five wall-frame structures of different heights. Nonlinear time-history analyses of the response of the designed structures to twenty spectrum compatible ground motions are carried out to provide a basis for comparison of the estimated seismic demands.

7.1.2 Summary of DBSD for asymmetric plan buildings

A new DBSD procedure suitable for the seismic design of asymmetric plan building is presented for both torsionally stiff and torsionally flexible structures. This procedure is based on parametric study of torsional seismic response of asymmetric plan buildings.

Base shear torque (BST) surfaces and the response of 2DOF systems to increasing intensity ground motions are employed to study the behaviour of torsionally restrained and unrestrained systems. In addition, the behaviour of torsionally stiff, torsionally flexible and torsionally similar systems is investigated using modal decomposition of the response of such systems at their flexible edge, at the center of mass and at the stiff edge.

Rotational component of the elastic mode shape when normalized by the translational component is called angle of twist. It is shown that this parameter can be used to provide a conservative estimate of the seismic response of asymmetric plan buildings. The angle of twist for the first mode shape is used in the DBSD of torsionally stiff structures. For torsionally flexible structures, the angles of twist for both the first and the second mode should be considered in the DBSD.

The proposed DBSD for asymmetric plan buildings is applied in the seismic design of two 12-storey torsionally unbalanced systems, one being torsionally stiff and the other torsionally flexible. The buildings are assumed to be symmetric in one direction but unsymmetric in the perpendicular direction. In contrast to DBSD for wall-frame systems, both base shear and base torque demands are calculated in each iteration of design using the 2DOF system and inelastic design spectrum. The iterations of design are carried out using only the first mode for torsionally stiff system, while for torsionally flexible system both the first and the second modes are employed. The limits on ultimate displacements are similar to those for wall-frame system, however, the drift limits are evaluated at the periphery of the plan not at the location of the lateral resisting planes.

Lateral resisting planes in the symmetric direction of the plan are designed at the beginning of the DBSD for asymmetric plan buildings. The demands on these orthogonal planes are re-evaluated within the iterations for the design of the asymmetric direction and the orthogonal structural elements are re-designed if the increased demands due to rotation of the plan exceed the current capacity of the orthogonal planes.

7.2 Conclusions

The proposed DBSD procedures for both wall-frame and torsionally unbalanced structures are quite straightforward and easy to implement. Although further refinement would be needed before these procedures are ready for use in a design office, they show good promises for such application. The procedures also permit designing for different performance objectives to ensure reliable performance of structural and non-structural elements based on several local and global design criteria.

7.2.1 Concluding remarks for DBSD of wall-frame structures

It is shown that simple empirical relations can be used instead of the first mode shape of the structure to estimate the deformed shape of wall-frame-structures. This simplifies the DBSD procedure.

The DBSD of the five wall-frame structures that have been studied reveals that when unconfined concrete sections are used for the walls the ductility capacity limit may at times govern the design. Use of confined concrete at the potential hinge locations

including the base of the wall and column sections, which would increase the ductility capacity of the system, would improve the performance of such structures. It should however be noted that the full ductility capacity of confined concrete as provided in the codes could rarely be mobilized since the code prescribed drift limits and the limits to preclude P- Δ instability would start to govern.

Multi-mode pushover analyses of wall-frame structures show that higher modes make significant contributions to the storey shears, but have negligible effect on the displacements and inter-storey drift ratios.

Nonlinear dynamic analyses illustrate that the displacement and inter-storey responses of wall-frame structures have greater dispersion as compared to the storey shear responses. The proposed DBSD for wall-frame systems estimates the storey shear quite accurately all along the height of the structure. However, the displacements are over-estimated, especially for taller buildings. Inter-storey drift ratios are slightly under-estimated at the upper levels, but over-estimated at the lower levels; nevertheless they are quite accurate around the point of inflection where the maximum inter-storey drifts are expected.

7.2.2 Concluding remarks related to DBSD of asymmetric plan buildings

The two case studies of the torsionally stiff and torsionally flexible systems showed that the estimated global yield displacement, obtained from the equivalent yield displacements of resisting planes when transferred to the center of mass using the

proposed angle of twist, is very close to the yield displacements obtained from the pushover analysis.

For torsionally stiff system, the ultimate displacement is controlled by the instability limit, while the ductility and the drift limits allow greater acceptable ultimate displacements. However, for torsionally flexible system the ultimate displacement is controlled by the drift limits.

In the case of torsionally flexible system, the acceptable ultimate displacement in the second mode is less than that in the first mode, however, the acceptable ductility demand in the first mode is smaller than that in the second mode ductility and is very close to one. Therefore, the base shear and base torques on the structure in the first mode are greater and govern the design.

The realized ductility in both torsional systems are less than two, which indicates that the designed torsionally unbalanced systems are not expected to dissipate as much energy due to inelastic behaviour, when compared to symmetrical systems.

Dynamic response of the designed torsionally stiff system to spectrum compatible ground motions showed that the maximum displacement occurs at the flexible edge and the assumption that the response of torsionally stiff system will be dominated by the first mode is valid. When comparing the results of multi-mode pushover analyses with the nonlinear time-history analyses, it is seen that the base shear, roof displacement,

maximum twist in the plan and maximum inter-storey drifts are estimated quite accurately.

Nonlinear time-history analyses of torsionally flexible system showed that the estimated base shears are quite accurate while the displacements and inter-storey drift estimates are conservative.

7.3 Recommendations for future research

The present study and other previous studies in the field have addressed the displacement-based design of symmetric concrete and steel frame buildings, symmetric and unsymmetric concrete shear wall buildings, and symmetric wall-frame buildings. These studies need to be further refined before they provide a robust method for design office use. Related to the present work the following issues merit further study

- Nonlinear response analyses show that in the proposed DBSD the displacements are generally overestimated. A parametric study may be carried out to introduce correction factors for displacement estimates of wall-frame structures

- Studies may be carried out to verify that the proposed method could be extended to the design of structures having walls with a cross-section other than rectangular and/or core walls. The application of the method to the design of doubly unsymmetric structures also needs to be studied. Work needs to be done to extend the method for application in the design of buildings with irregularity along the height

- Work may be carried out to develop application of the DBSD to buildings incorporating passive dampers

A. Case study 12-storey wall frame structure

A.1 Problem definition

The plan view of the twelve storey reinforced concrete building is shown in Figure A.1. The building is 48 m by 24 m. The first storey is 4.85 m high, the other stories are 3.65 m each. The structural framing consists of 200 mm RC slab. The lateral resistance in the North-South direction is provided by two 6-meter shear walls and 2 frames. All columns are assumed to be 700 mm by 700 mm. The beams are 400 mm wide by 600 mm deep. The shear walls are assumed to be 6000 mm by 400 mm thick. The superimposed dead load plus floor and roof self weight on all floors and the roof is 5.8 kN/m². The live load is 2.4 kN/m². The snow load on roof is 2.2 kN/m². The strength of concrete is 30 MPa and the steel yield strength is 400 MPa

A.2 Gravity Load Calculations

The self weight of structural components are calculated as follows

$$\text{Floor columns} \quad \frac{24 \times 0.7 \times 0.7 \times 24 \times 3.45}{48 \times 24} = 0.845 \text{ kN/m}^2$$

$$\text{1st level columns} \quad \frac{24 \times 0.7 \times 0.7 \times 24 \times 4.45}{48 \times 24} = 1.09 \text{ kN/m}^2$$

$$\text{Roof columns} \quad \frac{24 \times 0.7 \times 0.7 \times 24 \times 1.725}{48 \times 24} = 0.423 \text{ kN/m}^2$$

Floor walls
$$\frac{12 \times 0.4 \times 24 \times 3.45}{48 \times 24} = 0.345 \text{ kN/m}^2$$

1st level wall
$$\frac{12 \times 0.4 \times 24 \times 4.45}{48 \times 24} = 0.445 \text{ kN/m}^2$$

Roof walls
$$\frac{12 \times 0.4 \times 24 \times 1.725}{48 \times 24} = 0.1725 \text{ kN/m}^2$$

North-south beams
$$\frac{2 \times (24 - 3 \times 0.7) \times 0.4 \times 0.4 \times 24}{48 \times 24} = 0.146 \text{ kN/m}^2$$

East-west beams
$$\frac{4 \times (48 - 5 \times 0.7 - 2 \times 0.4) \times 0.4 \times 0.4 \times 24}{48 \times 24} = 0.583 \text{ kN/m}^2$$

The inertial masses assigned to individual floors are calculated as follows:

Roof dead load $0.25 \times 2.2 + 0.423 + 0.1725 + 0.146 + 0.583 + 5.8 = 7.675 \text{ kN/m}^2$

Total roof load 841.6 kN

Roof mass 901.3 tonne

Floor dead load $0.845 + 0.345 + 0.729 + 5.8 = 7.719 \text{ kN/m}^2$

Total floor load 8892.3 kN

Floor mass 906.5 tonne

| | |
|----------------------------------|---|
| 1 st level dead load | $1.09+0.445+0.729+5.8 = 8.064 \text{ kN/m}^2$ |
| Total 1 st level load | 9289.7 kN |
| 1 st level mass | 947 tonne |
| | |
| Total dead load | $8841.6 + 88923.0 + 9289.7 = 107054.3 \text{ kN}$ |
| Total mass | $901.3 + 9065.0 + 947.0 = 10913.3 \text{ tonne}$ |

A.3 Gravity Load on lateral resisting elements

Assuming that the slab is one-way, the tributary areas or width for gravity loads on columns, walls and beams are determined and are given in Table A.1. The self weights of one storey height of columns and walls are as follows:

$$\text{Typical floor column: } 0.7 \times 0.7 \times 24 \times 3.45 = 40.57 \text{ kN}$$

$$\text{First floor column: } 0.7 \times 0.7 \times 24 \times 4.65 = 54.68 \text{ kN}$$

$$\text{Typical floor wall: } 6.0 \times 0.4 \times 24 \times 3.45 = 198.72 \text{ kN}$$

$$\text{First floor wall: } 6.0 \times 0.4 \times 24 \times 4.65 = 267.84 \text{ kN}$$

The calculated axial forces on walls and columns are shown in Table A.2 through Table A.4. In these tables an entry against floor *i* gives the load at the base of that floor.

The gravity load combination of D+0.5L produces axial loads of 5903.6 kN, 3222.9 kN, and 7856.4 kN at the base of interior columns, exterior columns and the walls, respectively. Assuming that the slab is one way, fixed end forces and moments produced by the gravity load combination D+0.5L on the floor beams is calculated.

$$\text{Tributary area for each beam : } 8 \times 24 = 192 \text{ m}^2.$$

$$\text{Live load reduction factor } 0.3 + \sqrt{\frac{9.8}{192}} = 0.5259$$

$$\text{Floor level load including slab dead load and live load: } 5 \times 2.4 \times 0.5259 + 5.8 = 6.431 \text{ kN/m}^2$$

$$\text{Load per unit length including self weight } 6.431 \times 8 + 24 \times 0.4 \times 0.4 = 55.29 \text{ kN/m}$$

$$\text{Fixed end reaction: } 0.5 \times 55.29 \times 8 = 221.2 \text{ kN}$$

$$\text{Fixed end moment: } 55.29 \times 64/12 = 294.9 \text{ kNm}$$

The fixed end reactions and moments for the gravity load combination D+0.5L on the roof beams are calculated as follows

Floor dead load, slab live and snow load: $0.25 \times 2.2 + 5.8 = 6.35$
kN/m²

Load per unit length including self weight: $6.35 \times 8 + 24 \times 0.4 \times 0.4 = 54.64$
kN/m

Fixed end reaction: $0.5 \times 54.64 \times 8 = 218.56$ kN

Fixed end moment: $54.64 \times 64/12 = 291.41$ kNm

To determine the P-Delta effect in modal pushover, and dynamic analysis, we need the total gravity loads on the entire building produced by the combination D+0.5L. Part of this load has been applied in the analysis as distributed beam load. In determining the remaining load we take the live load reduction factor corresponding to the total area:

$$48 \times 24 = 1152. \text{ m}^2$$

$$\text{LLRF} = 0.3 + \sqrt{\frac{9.8}{1152}} = 0.392$$

Additional gravity load combination D+0.5L for first floor, typical floor, and roof floor levels are calculated as shown in Table A.5 through Table A.7.

A.4 Preliminary design

A.4.1 Inflection height estimate

Assuming the contribution ratio of the frames, α , in resisting the lateral loads we find that

$$\begin{cases} V_{frames} = \alpha V_b \\ V_{walls} = (1 - \alpha) \times V_b \end{cases}$$

where the V_b is the base shear. Assuming triangular distribution, the lateral load at i^{th} floor, f_i , of an n -storey building will be

$$f_i = \frac{2 \times i}{n(n+1)} V_b$$

Therefore the storey shear can be obtained as

$$V_i = \left[1 - \frac{i(i-1)}{n(n+1)} \right] V_b$$

The inflection height is the height where the moment in the wall becomes zero, therefore taking the moment of the lateral load and the contribution of the frames which is represented by a point load at the top of the wall we will have

$$\sum_{i=1}^m \left[\frac{2(n-i+1)}{n(n+1)} [x - (i-1) \times h_i] V_b - \alpha V_b x \right] = 0$$

where m is the number of storeys above the inflection point, and x is the distance from inflection point to the roof, which should be $(m-1) \times h_i \leq x \leq m \times h_i$, therefore, inflection height h_e is

$$h_e = H - x$$

where H is the total height. For the 12-storey building and assigning 35% of the base shear to be resisted by the frame, the inflection height works out to 30.6 m. Here it is assumed that the point of inflection at the moment when the wall base reaches yield is at 0.6755 of the total height (floor level 8), giving

$$h_e = 0.6755H = 30.40 \text{ m}$$

The yield curvature can be obtained from the empirical expression given as:

$$\varphi_y = \frac{1.8\epsilon_y}{l_w} = \frac{1.8 \times 0.002}{6} = 0.0006 \text{ 1/m}$$

The lateral displacements at base yield are obtained by assuming that the moment varies in the shape of a triangle from zero at h_e to a maximum at the base, and that for $h >$

h_e the moment can be taken as negligible. The displacements are then obtained from Equation 2.2. The maximum storey drift at yield is at the height of h_e and is given by

$$\theta_y = \frac{\varphi_y h_e}{2} = \frac{0.0006 \times 30.40}{2} = 0.00912$$

Assuming that the maximum storey drift should not exceed 0.025, the limit on plastic drift is given by

$$\theta_p = 0.025 - \theta_y = 0.01588$$

The total displacement at level i is given by

$$\Delta_{ui} = \Delta_{yi} + (h_i - l_p/2) \times \theta_p$$

where l_p is the plastic hinge length. Assuming $l_p = 0.5 l_w$ the storey level displacements are calculated and are shown in Table A.8.

The inter-storey yield rotation of the frames is obtained from

$$\theta_{fy} = \frac{0.5 \varepsilon_y l_b}{D_b} = \frac{0.5 \times 0.002 \times 8}{0.6} = 0.0133$$

The corresponding yield displacement at roof is given by

$$\Delta_{fyr} = H \times \theta_{fy} = 0.6 \text{ m}$$

We now assume that 65% of the base shear will be resisted by the shear walls and the remaining by the two frames. The stiffness of the walls and frames is thus obtained from

$$k_w = \frac{0.65V_b}{\Delta_{yr}} = 2.044V_b$$

$$k_f = \frac{0.35V_b}{\Delta_{fyr}} = 0.5833V_b$$

The yield displacement of the wall frame system is given by

$$\Delta_y = \frac{\sum V}{\sum k} = \frac{V_b}{2.044V_b + 0.5833V_b} = 0.381 \text{ m}$$

Ductility demand is obtained from the roof displacements

$$\mu = \frac{\Delta_{ur}}{\Delta_y} = \frac{1.0087}{0.381} = 2.65$$

We assume the displacement shape as being equal to Δ_u normalized so that the displacement at roof is 1. Thus we have

$$\varphi^T = [0.0594, 0.1297, 0.2057, 0.2865, 0.3711, 0.4585, 0.5479, 0.6382, 0.7286, 0.8191, 0.9095, 1.0000]$$

The properties of the SDOF are given by

$$\Gamma = \frac{\varphi^T \mathbf{M} \mathbf{1}}{\varphi^T \mathbf{M} \varphi} = 1.4564$$

$$M^* = 0.7441 \times 10913.3 = 8120.6 \text{ tonne}$$

The ultimate and yield displacements of the SDOF system are

$$\delta_u = \frac{\Delta_{ur}}{\Gamma} = 0.693$$

$$\delta_y = \frac{\Delta_y}{\Gamma} = 0.262$$

A.4.2 Demand and capacity diagrams

The elastic spectrum is obtained from the design spectrum for 10% chance of exceedance in 50 years in LA and is shown in Figure A.2. It should be mentioned that for periods greater than 4 second the spectral acceleration is assumed to decay inversely with respect to period.

The elastic and inelastic spectra, the latter for ductility of 2.65, are plotted in Figure A.3. The inelastic spectrum is entered with the ultimate displacement calculated above to obtain the spectral acceleration from which the design base shear is obtained as follows

$$V_b = 0.031g \times M^* = 0.031 \times 9.81 \times 8120.6 = 2469.55 \text{ kN}$$

A.4.3 Lateral loads

We distribute the base shear along the height in proportion to $\mathbf{M}\varphi$, where \mathbf{M} is the mass matrix and φ is the vector of ultimate storey displacements calculated earlier. The floor level forces are shown in Column 2 of Table A.9. Of the total base shear of 2469.55 kN, 35% or 864.3 kN is assigned to the frames. Based on our assumption that frame shear is constant across the height, the frames carry a single lateral force of 864.3 at the roof level. The balance of the forces is carried by the walls; they are shown in Column 3 of Table A.9. The wall shears and moments are shown in Columns 4 and 5, respectively. The shear and moment distributions are also shown in Figure A.4 and Figure A.5, respectively

From Figure A.5, inflection height is seen to be 32.0 meter, and the base moment on each wall is 20,367 kNm. We need to design the wall to withstand this moment in combination with the axial load. The axial force due to the combination D+0.5L works out to 7856.35 kN. We assume that the concrete is unconfined and $\varepsilon_{cu} = 0.004$. The minimum reinforcement in the wall with two layers of 100 mm² at 200 mm spacing gives

a resisting moment of 26,310 kNm, yield curvature of $\varphi_y = 5.924 \times 10^{-4}$ per m, and ultimate curvature of $\varphi_u = 4.017 \times 10^{-3}$ per m (see Figure A.6).

The corresponding value of θ_p is:

$$\theta_p = (\varphi_u - \varphi_y) \times l_p = (4.017 \times 10^{-3} - 5.924 \times 10^{-4}) \times 3.0 = 0.01027$$

This plastic rotation is less than plastic rotation calculated based on the 0.025 inter-storey drift at the base of the wall earlier, therefore the ductility capacity governs.

A.5 Second iteration

The new yield and ultimate displacements obtained based on the new plastic rotation, yield curvature, and inflection height, are given in Table A.10. The stiffness of the walls and frames are obtained from

$$k_w = \frac{0.65V_b}{\Delta_{yr}} = \frac{0.65V_b}{0.3254} = 1.997V_b$$

$$k_f = \frac{0.35V_b}{\Delta_{fyr}} = \frac{0.35V_b}{0.6} = 0.5833V_b$$

The yield displacement of the wall frame system is given by

$$\Delta_y = \frac{\sum V}{\sum k} = \frac{V_b}{1.997V_b + 0.5833V_b} = 0.3875 \text{ m}$$

Ductility demand is obtained from the roof displacements

$$\mu = \frac{\Delta_{ur}}{\Delta_y} = \frac{0.7722}{0.3875} = 1.993$$

The properties of the SDOF obtained from φ equal to the normalized ultimate displacement that is shown in Table A.10, are given by

$$\Gamma = \frac{\varphi^T \mathbf{M} \mathbf{1}}{\varphi^T \mathbf{M} \varphi} = 1.4622$$

$$M^* = 0.732 \times 10913.3 = 7988.5 \text{ tonne}$$

The ultimate and yield displacements of the SDOF system are

$$\delta_u = \frac{\Delta_{ur}}{\Gamma} = 0.528$$

$$\delta_y = \frac{\Delta_y}{\Gamma} = 0.265$$

A.5.1 Demand and capacity diagrams

The elastic and inelastic spectra, the latter for ductility of 1.993, are plotted in Figure A.7. For the calculated ultimate displacement of SDOF, the design base shear is obtained from the following (see Figure A.7)

$$V_b = 0.0552 \times 9.81 \times 7988.5 = 4325.86 \text{ kN}$$

A.5.2 Lateral loads

We distribute the new base shear along the height in proportion to $\mathbf{M}\varphi$, where \mathbf{M} is the mass matrix and φ is the vector of ultimate storey displacements calculated from Table A.10. The floor level forces are shown in Column 2 of Table A.11. Of the total base shear of 4325.86 kN, 35% or 1514.05 kN is assigned to the frames. The balance of the lateral forces are carried by the walls; they are shown in Column 3 of Table A.11. The wall shears and moments are shown in Columns 4 and 5, respectively.

The base moment on each wall is 36,174.7 kNm. The wall is designed with three layers of 2000 mm² on each edge and vertical distribution steel consisting of two layers of 100 mm² bars spaced at 200 mm. This gives a resisting moment of 38,003 kNm. The yield curvature is 5.988×10^{-4} per m, while the curvature at a concrete strain of 0.004 is 4.00×10^{-3} per m. The effective moment of inertia is $0.3598 I_g$. The moment curvature relationship is shown in Figure A.8. The corresponding value of θ_p is obtained from

$$\theta_p = (\varphi_u - \varphi_y) \times l_p = (4.0 \times 10^{-3} - 5.988 \times 10^{-4}) \times 3.0 = 0.0102$$

A.6 Subsequent iterations

The new yield and ultimate displacements obtained for plastic rotation of 0.0102 are given in Table A.12. The stiffness of the walls and frames are thus obtained from

$$k_w = \frac{0.65V_b}{\Delta_{yr}} = 1.976V_b$$

$$k_f = \frac{0.35V_b}{\Delta_{fyr}} = 0.5833V_b$$

The yield displacement of the wall frame system is given by

$$\Delta_y = \frac{\sum V}{\sum k} = \frac{V_b}{1.976V_b + 0.5833V_b} = 0.3907 \text{ m}$$

Ductility demand is obtained from the roof displacements

$$\mu = \frac{\Delta_{ur}}{\Delta_y} = \frac{0.7726}{0.3907} = 1.977$$

The properties of the SDOF are given by

$$\Gamma = \frac{\varphi^T \mathbf{M} \mathbf{1}}{\varphi^T \mathbf{M} \varphi} = 1.4625$$

$$M^* = 0.73147 \times 10913.3 = 7982.75 \text{ tonne}$$

The ultimate displacement of the SDOF system is

$$\delta_u = \frac{\Delta_{ur}}{\Gamma} = 0.528$$

$$\delta_y = \frac{\Delta_y}{\Gamma} = 0.267$$

A.6.1 Demand and capacity diagrams

The elastic and inelastic spectra, the latter for ductility of 1.977, are plotted in Figure A.9.

The design base shear is then obtained from the following

$$V_b = 0.0557 \times 9.81 \times 7982.75 = 4361.9 \text{ kN}$$

The difference between this base shear and the previous one is less than 1%. The iterations may be assumed to have converged.

A.7 Pushover analysis

The lateral load of 1526.66 kN is carried equally by the two frames. An elastic analysis is now carried out for a single frame subjected to a lateral load of 763.33 kN at roof level, and gravity load combination D+0.5L applied as fixed end reaction, and fixed end moment at the ends of the beams calculated earlier for typical floor beams and roof beams.

On the basis of this analysis we set the beam moment capacity as 955 kNm. The column base moment capacity is set as 955 kNm. In the analysis other sections of the column are given large moment capacity, so that they remain elastic. The moments of inertia for beams and columns are set as 50% of the gross moment of inertia. The base moment capacity of the wall is set as 38003 kNm and the moment of inertia as 0.36 times the gross moment of inertia.

A pushover analysis is now carried out with and without considering the P- Δ effect. An idealized bilinear curve gives a yield displacement equal to 0.37 meter, the ultimate displacement based on 5 percent decrease in the maximum base shear is 1.045 meter, and the maximum shear capacity 4328.8 kN is achieved at roof displacement of 0.63 m, see Figure A.10.

As shown in Figure A.11 and Figure A.12 the 0.025 drift occurs first at storey 7 at a roof displacement of 1.05m. The ultimate displacement is the least of the ultimate displacement based on ductility capacity of the wall, 5% decrease in maximum shear strength due to P- Δ effect, and 0.025 drift limit.

For the 6 meter wall shown in Figure A.8 the yield curvature is 5.988×10^{-4} per m, and the curvature at a concrete strain of 0.004 is 4.00×10^{-3} /m. The yield displacement of the wall is at the displacement at first yield in the wall. The ultimate displacement at the limit of ductility is calculated as follows

$$\begin{aligned}\Delta_{ul} &= \Delta_{yu} + (h_i - l_p/2)(\varphi_u - \varphi_y) \times l_p \\ &= 0.29 + (45 - 3/2)(4.00 \times 10^{-6} - 5.988 \times 10^{-7}) \times 3000 = 0.734 \text{ m}\end{aligned}$$

Therefore the ductility capacity governs. Ductility demand is obtained from the roof displacements

$$\mu = \frac{\Delta_{ur}}{\Delta_y} = \frac{0.734}{0.37} = 1.984$$

The dynamic properties of the system for equivalent SDOF system for first mode are:

$$T_1 = 4.15 \text{ sec}$$

$$\begin{aligned}\varphi_1^T &= [0.024, 0.069, 0.132, 0.210, 0.298, 0.394, 0.495, 0.597, 0.700, 0.801, 0.901, \\ &1.000]\end{aligned}$$

$$\Gamma_1 = \frac{\varphi_1^T \mathbf{M} \mathbf{1}}{\varphi_1^T \mathbf{M} \varphi_1} = 1.459$$

$$M_l^* = 0.68054 \times 10913.3 = 7426.94 \text{ tonne}$$

$$\delta_{u1} = \frac{\Delta_{ur}}{\Gamma_1} = 0.503$$

$$\delta_{y1} = \frac{\Delta_y}{\Gamma_1} = 0.2536$$

A.7.1 Demand and capacity diagrams

The elastic and inelastic spectra for ductility of 1.984 are plotted in Figure A.13. The design base shear based on the first mode shape is obtained from the following

$$V_b = 0.0581g \times M^* = 0.0581 \times 9.81 \times 7426.94 = 4233.07 \text{ kN}$$

This base shear demand of 4233.07 kN is 2.26 percent less than the maximum base shear capacity of 4328.8 kN, thus the design is satisfactory.

A.8 Multi-mode pushover analysis

The first mode mass participation is 68.05% of total mass, therefore higher modes should be considered as they may contribute to structural response. We carry out a multi mode pushover analysis to investigate the higher mode contribution. The first mode pushover is carried out to the maximum target displacement of 0.73 m as calculated earlier. It is assumed that the structure remains elastic for higher modes, however this assumption will be verified during the pushover analysis for each mode. Therefore, the target displacement for pushover analysis is obtained from elastic design spectrum.

$$T_2 = 0.825 \text{ sec}$$

$$\varphi^T_2 = [-0.123, -0.319, -0.536, -0.721, -0.832, -0.840, -0.734, -0.519, -0.210, 0.165, 0.576, 1.000]$$

$$M^*_2 = 0.17677 \times 10913.3 = 1929.14 \text{ tonne}$$

$$\Gamma_2 = 0.6856$$

From elastic design spectrum shown in Figure A.2, displacement of SDOF system having a period of 0.825 second is obtained and then the demand roof displacement is calculated,

$$\delta(0.825) = S_a(0.825) \times (0.825)^2 / 4\pi^2 = 0.776 \times 9.81 \times (0.825)^2 / 4\pi^2 = 0.1312 \text{ m}$$

$$\Delta_{\text{roof}}^2 = 0.1312 \times 0.6856 = 0.09 \text{ m}$$

Similarly for mode 3 we have,

$$T_3 = 0.31 \text{ sec}$$

$$\varphi^T_3 = [0.334, 0.744, 1.000, 0.952, 0.589, 0.031, -0.519, -0.857, -0.846, -0.465, 0.194, 0.985]$$

$$\mathbf{M}^*{}_3 = 0.0656 \times 10913.3 = 715.9 \text{ tonne}$$

$$\Gamma_3 = 0.367$$

$$\delta(0.31) = S_a(0.31) \times (0.31)^2 / 4\pi^2 = 1.065 \times 9.81 \times (0.31)^2 / 4\pi^2 = 0.0254 \text{ m}$$

$$\Delta^{\text{roof}}{}_3 = 0.0254 \times 0.367 \times 0.985 = 0.0092 \text{ m}$$

For the first 3 modes effective modal masses add up to 92.29% of the total mass, and it seems no additional modes need to be included. For each of these three modes a pushover analysis using the force distribution proportional to $\mathbf{M}\varphi$ is carried out.

Second mode pushover analysis shows that the structure becomes inelastic at roof displacement of 0.056 m. In order to capture the response of structure in second mode, we determine the displacement at the fifth floor level. This displacement increases monotonically with the lateral load. On the other hand roof displacement is observed to change direction as the structure is pushed under second mode load distribution. The first estimate of target displacement for fifth floor is obtained based on the elastic deformed shape of structure under lateral loading of $\mathbf{M}\varphi_2$:

$$\Delta^{5\text{th}}{}_2 = \Delta^{\text{roof}}{}_2 \times \varphi_2^{5\text{th}} = 0.09 \times 0.832 = 0.075 \text{ m}$$

Now we carry out the pushover analysis to the fifth floor target displacement of 0.075. The pushover curve for second mode is shown in Figure A.14. The wall yields at fifth floor displacement of 0.042 m. We transform the pushover curve to equivalent SDOF space by dividing the base by M_2^*g and the fifth floor displacement by $\Gamma_2\phi_2^{5th}$. The target displacement is obtained iteratively by using the demand capacity diagram to find the performance point (see Figure A.15). The target displacement at fifth floor works out to $\delta_u\Gamma_2\phi_2^{5th} = 0.1245 \times 0.6856 \times 0.832 = 0.071$ m, and the second mode ductility is 1.7.

The third mode analysis shows that the structure remains elastic as expected. In order to investigate the higher mode effect further, fourth mode pushover analysis is also carried out. The dynamic parameters of the fourth mode are:

$$T_4 = 0.16 \text{ sec}$$

$$\phi^T_4 = [-0.562, -1.000, -0.870, -0.186, 0.605, 0.965, 0.649, -0.113, -0.777, -0.851, -0.216, 0.847]$$

$$M_4^* = 0.0331 \times 10913.3 = 361.2 \text{ tonne}$$

$$\Gamma_4 = 0.2591$$

$$\delta(0.159) = S_a(0.16) \times (0.16)^2 / 4\pi^2 = 1.07 \times 9.81 \times (0.16)^2 / 4\pi^2 = 0.0068 \text{ m}$$

$$\Delta_{\text{roof}}^{\text{roof}} = 0.0067 \times 0.2591 \times 0.847 = 0.0015 \text{ m}$$

The target displacement for these four modes can be combined to calculate maximum roof displacement as:

$$\Delta_u^{\text{roof}} = \sqrt{(\Delta_1^{\text{roof}})^2 + (\Delta_2^{\text{roof}})^2 + (\Delta_3^{\text{roof}})^2 + (\Delta_4^{\text{roof}})^2} = 0.7322 \text{ m}$$

It should be mentioned that the second mode target displacement at roof level is 0.056 m, which is the maximum roof displacement at the yield of the wall, after the yielding the roof displacement decreases as we push the structure. The estimate of ultimate roof displacement in our last iteration was 0.7726 m, which is quite close to 0.7322 m.

A.1.1 Results and design check

Table A.13 and Table A.14 show the section shears and inter-storey drifts for the first four modes, square root of sum of squares (SRSS) of the first 3 and 4 modes, and the difference between the latter two. Columns (3) and (4) in Table A.13 show the significance of higher mode participation in storey shears. Adding mode 4, which has a mass participation factor of 3.31% of total mass, increases the storey shear as much as 14.22 and 13.062% in 8th and 9th storey; and 10.07% and 11.61% in the 5th and 12th storey, respectively. On the other hand, higher modes have negligible effect on the inter-storey drifts, and drifts can be estimated quite accurately by considering the first mode only.

A.8.1.1 Walls

Table A.16 shows the moment in the wall along the height. The wall yields at the base in the mode 1 and 2 pushover analyses. The corresponding inelastic rotations at the base are 0.0102, and 0.0017. In order to find the maximum ultimate curvature demand, the total curvature demand of the wall for each mode should be calculated. For the first and second modes we have:

$$\varphi_u^1 = \varphi_y + \varphi_{id}^1 = \varphi_y + \frac{\theta_{id}^1}{l_p} = 5.97 \times 10^{-7} + \frac{0.0102}{3000} = 3.997 \times 10^{-6} \text{ 1/mm}$$

$$\varphi_u^2 = \varphi_y + \varphi_{id}^2 = \varphi_y + \frac{\theta_{id}^2}{l_p} = 5.97 \times 10^{-7} + \frac{0.0017}{3000} = 1.164 \times 10^{-6} \text{ 1/mm}$$

For the third and fourth modes since the wall has not yielded the ultimate curvature is obtained from moment curvature relationship for the wall. For the moment of 22030 kNm in the 3rd mode (Table A.16) the curvature works out to 3.47×10^{-7} 1/mm, and for the 4th mode moment of 8755 kNm (Table A.16) to 1.37×10^{-7} 1/mm, respectively. Since the gravity load curvature for the wall is zero the maximum ultimate curvature is obtained by taking the SRSS of the ultimate curvature for each mode:

$$\varphi_u = \sqrt{(\varphi_u^1)^2 + (\varphi_u^2)^2 + (\varphi_u^3)^2 + (\varphi_u^4)^2} = 4.18 \times 10^{-6} \text{ 1/mm}$$

Although ultimate curvature demand is slightly more than the ultimate curvature capacity of the wall which is 4.00×10^{-6} 1/mm, the design is considered satisfactory.

A.8.1.2 Beams

We need to ensure that the local ductility demands in the beams do not exceed the ductility capacity. Figure A.16 and Figure A.17 show the moment curvature relations for the roof and floor beams with yield curvatures of 5.935×10^{-6} per mm and 7.526×10^{-6} per mm respectively. In the roof beams, the ultimate curvature corresponding to 0.004 strain in the concrete is 5.64×10^{-5} per mm therefore, the local ductility capacity for roof beams equals 9.5. Similarly for the floor beams, the ultimate curvature corresponding to 0.004 strain of concrete is 3.124×10^{-5} and the local ductility capacity works out to 4.15.

Maximum negative and positive inelastic rotations of plastic hinge of the floor beams, and corresponding bending moments for the first four modes and gravity loads are shown in Table A.17 and Table A.18. In order to find the curvature demand in the beams, plastic hinge length in the beams is needed. The plastic hinge length of beams is calculated as:

$$l_p = 0.05z + 0.5d = 0.05 \times 4000 + 0.5 \times 550 = 475 \text{ mm}$$

We will check the seventh floor beam, which has the greatest inelastic rotation in the first mode, and the roof beams.

A.8.1.2.1 Roof beam

The maximum ultimate curvature demand is calculated by taking the sum of gravity curvature and SRSS of the ultimate curvature demand in each mode without the gravity effect. From the moment curvature relation in Figure A.16 for roof beams, the corresponding curvature for gravity moment of 317.2 kNm is 3.983×10^{-6} 1/mm. The ultimate curvature demand of each mode is calculated as follows

$$\varphi_u^1 = \varphi_y + \varphi_{id}^1 = \varphi_y + \frac{\theta_{id}^1}{l_p} = 5.936 \times 10^{-6} + \frac{0.0197}{475} = 4.741 \times 10^{-5} \text{ 1/mm}$$

$$\varphi_u^2 = \varphi_y + \varphi_{id}^2 = \varphi_y + \frac{\theta_{id}^2}{l_p} = 5.936 \times 10^{-6} + \frac{0.0032}{475} = 1.267 \times 10^{-5} \text{ 1/mm}$$

$$M_u^3 = 393.1 \text{ kNm} \Rightarrow \varphi_u^3 = 4.94 \times 10^{-6} \text{ 1/mm}$$

$$M_u^4 = 320.2 \text{ kNm} \Rightarrow \varphi_u^4 = 4.03 \times 10^{-6} \text{ 1/mm}$$

The maximum ultimate curvature demand is given by

$$\begin{aligned} \varphi_{total} &= \varphi_{Grav} + \sqrt{(\varphi_u^1 - \varphi_{Grav})^2 + (\varphi_u^2 - \varphi_{Grav})^2 + (\varphi_u^3 - \varphi_{Grav})^2 + (\varphi_u^4 - \varphi_{Grav})^2} \\ &= 4.828 \times 10^{-5} \text{ 1/mm} \end{aligned}$$

The local ductility demand works out to $4.828 \times 10^{-5} / 5.936 \times 10^{-6} = 8.13$ which is less than the ductility capacity of 9.5.

A.8.1.2.2 Floor beams

From Figure A.17, the gravity curvature corresponding to moment of 313.1 kNm is 2.48×10^{-6} , therefore the maximum ultimate curvature demand in the 7th floor for each mode is calculated as follows

$$\varphi_u^1 = \varphi_y + \varphi_{id}^1 = \varphi_y + \frac{\theta_{id}^1}{l_p} = 7.526 \times 10^{-6} + \frac{0.0087}{475} = 2.584 \times 10^{-5} \text{ 1/mm}$$

$$M_u^2 = 438.2 \text{ kNm} \Rightarrow \varphi_u^2 = 3.44 \times 10^{-6} \text{ 1/mm}$$

$$M_u^3 = 381.9 \text{ kNm} \Rightarrow \varphi_u^3 = 3.00 \times 10^{-6} \text{ 1/mm}$$

$$M_u^4 = 330.9 \text{ kNm} \Rightarrow \varphi_u^4 = 2.54 \times 10^{-6} \text{ 1/mm}$$

The maximum ultimate curvature demand will be:

$$\begin{aligned}\varphi_{total} &= \varphi_{Grav} + \sqrt{(\varphi_u^1 - \varphi_{Grav})^2 + (\varphi_u^2 - \varphi_{Grav})^2 + (\varphi_u^3 - \varphi_{Grav})^2 + (\varphi_u^4 - \varphi_{Grav})^2} \\ &= 2.587 \times 10^{-5} \text{ 1/mm}\end{aligned}$$

The local ductility demand work out to $2.587 \times 10^{-5} / 7.526 \times 10^{-6} = 3.437$ which is less than local ductility capacity of 4.15. Therefore the beam designs are satisfactory.

A.8.1.3 Columns

Moment curvature relation of the interior column with 12M25 for axial load of 5903.55 kN is shown in Figure A.18. We check for the base of the columns. In the first mode pushover analysis, bases of all four columns yield. The maximum inelastic rotation

of plastic hinge at the base of columns, and corresponding bending moments for the first four modes and gravity loads are shown in Table A.19. The plastic hinge length of column is calculated as

$$l_p = 0.05z + 0.5d = 0.05 \times 2425 + 0.5 \times 560 = 401.25 \text{ mm, Say } 400 \text{ mm.}$$

From the moment curvature relation in Figure A.18, the curvature for gravity moment of 51.0 kNm is 1.0×10^{-7} . The ultimate curvature demand in each mode is calculated as

$$\varphi_u^1 = \varphi_y + \varphi_{id}^1 = \varphi_y + \frac{\theta_{id}^1}{l_p} = 7.72 \times 10^{-6} + \frac{0.00683}{400} = 2.479 \times 10^{-5} \text{ 1/mm}$$

$$M_u^2 = 522.1 \text{ kNm} \Rightarrow \varphi_u^2 = 1.044 \times 10^{-6} \text{ 1/mm}$$

$$M_u^3 = 146.3 \text{ kNm} \Rightarrow \varphi_u^3 = 2.926 \times 10^{-7} \text{ 1/mm}$$

$$M_u^4 = 51.0 \text{ kNm} \Rightarrow \varphi_u^4 = 1.0 \times 10^{-7} \text{ 1/mm}$$

The maximum ultimate curvature demand is given by

$$\begin{aligned} \varphi_{total} &= \varphi_{Grav} + \sqrt{(\varphi_u^1 - \varphi_{Grav})^2 + (\varphi_u^2 - \varphi_{Grav})^2 + (\varphi_u^3 - \varphi_{Grav})^2 + (\varphi_u^4 - \varphi_{Grav})^2} \\ &= 2.481 \times 10^{-5} \text{ 1/mm} \end{aligned}$$

which is greater than the curvature at concrete strain of 0.004. UBC 1997 allows up to 1.5% of concrete strain for well confined concrete. Therefore we need to provide enough confinement for first storey columns to satisfy the local ductility limit. Assuming the confined concrete for the column core, and unconfined concrete for column cover, the moment curvature relation for interior column obtained using program OpenSees (Mazzoni et al. (2007)) is presented in Figure A.19. The ultimate curvature capacity is much more than the total curvature demand, therefore the design is satisfactory.

A.9 Dynamic analysis

In order to verify the accuracy of the design process, we run time history analysis of the designed structure for 20 ground motion records developed by Somerville et al. (1997) that are compatible to the uniform hazard spectrum with 10 % chance of exceedance in 50 years for Los Angeles. The ground motions and their scaling factors are the same as those explained in Chapter 3.

Twenty nonlinear time history analyses have been carried out for the ground motions described. Figure A.21 shows the distribution of storey shears and their average. Maximum base shear at the base of structure is 13,769.6 kN which is quite close to 13,202.0 kN estimated by the proposed design procedure. The kink in the average storey shear between 8th storey and 11th storey is due to wall frame interaction. Figure A.22 shows the accuracy of the multi-modal pushover estimates of the storey shears when compared to the average results of nonlinear time history analyses. It is also shown that

four modes SSRS combination gives very close results to time history analyses. However, first mode storey shears estimates significantly underestimate the actual shears.

Figure A.23 shows the storey drift ratios. As expected the behaviour of the structure is controlled by the wall, and the drifts increase along the height of structure. It is interesting to mention that the drifts increase linearly between first floor and eleventh floor. The drift ratios show much greater disperses than the storey shears. It is also the case for lateral displacement profile (see Figure A.24).

The storey drift ratios as well as the lateral displacements at the roof level -as shown in Figure A.25 and Figure A.26, respectively- are estimated accurately by multi-modal pushover analyses and are close to the results of nonlinear time history analyses. However, they are overestimated at the lower floor levels, and the overestimation is greater for the lowest floor levels. In both Figure A.25 and Figure A.26 the difference between first mode estimates and four modes SSRS combinations are very small, which shows that the higher modes make only small contribution to displacements and drift ratios estimates.

Table A.1: Tributary areas for gravity loads on columns, walls and beams

| Columns, tributary area, m ² | | Beams, | Walls, |
|---|----------|---------------------|--------------------------------|
| interior | exterior | tributary width , m | tributary area, m ² |
| 64 | 32 | 8 | 64 |

Table A.2: Axial gravity forces in an interior column

| Floor level | Dead load, kN/m ² | Dead load Floor + column kN | Cumulative Dead kN | Cumulative tributary area, m ² | LLRF type B | Cumulative Live Load kN | Reduced Live Load kN |
|-------------|------------------------------|-----------------------------|--------------------|---|-------------|-------------------------|----------------------|
| 12 | 7.079 | 493.6 | 493.6 | 0 | 0 | 0 | 0 |
| 11 | 6.529 | 458.4 | 952.1 | 64 | 0.691 | 153.6 | 106.1 |
| 10 | 6.529 | 458.4 | 1410.5 | 128 | 0.577 | 307.2 | 177.3 |
| 9 | 6.529 | 458.4 | 1868.9 | 192 | 0.526 | 460.8 | 242.4 |
| 8 | 6.529 | 458.4 | 2327.3 | 256 | 0.496 | 614.4 | 304.7 |
| 7 | 6.529 | 458.4 | 2785.8 | 320 | 0.475 | 768 | 364.8 |
| 6 | 6.529 | 458.4 | 3244.2 | 384 | 0.46 | 921.6 | 423.9 |
| 5 | 6.529 | 458.4 | 3702.6 | 448 | 0.448 | 1075.2 | 481.7 |
| 4 | 6.529 | 458.4 | 4161.0 | 512 | 0.438 | 1228.8 | 538.2 |
| 3 | 6.529 | 458.4 | 4619.5 | 576 | 0.43 | 1382.4 | 594.4 |
| 2 | 6.529 | 458.4 | 5077.9 | 640 | 0.424 | 1536 | 651.3 |
| 1 | 6.529 | 472.6 | 5550.4 | 704 | 0.418 | 1689.6 | 706.3 |

Table A.3: Axial gravity forces in an exterior column

| Floor level | Dead load, kN/m ² | Dead load Floor + column kN | Cumulative Dead kN | Cumulative tributary area, m ² | LLRF type B | Cumulative Live Load kN | Reduced Live Load kN |
|-------------|------------------------------|-----------------------------|--------------------|---|-------------|-------------------------|----------------------|
| 12 | 7.079 | 267.1 | 267.1 | 0 | 0 | 0 | 0 |
| 11 | 6.529 | 249.5 | 516.6 | 32 | 0.8534 | 76.8 | 65.5 |
| 10 | 6.529 | 249.5 | 766.1 | 64 | 0.6913 | 153.6 | 106.2 |
| 9 | 6.529 | 249.5 | 1015.6 | 96 | 0.6195 | 230.4 | 142.7 |
| 8 | 6.529 | 249.5 | 1265.1 | 128 | 0.5767 | 307.2 | 177.2 |
| 7 | 6.529 | 249.5 | 1514.6 | 160 | 0.5475 | 384 | 210.2 |
| 6 | 6.529 | 249.5 | 1764.1 | 192 | 0.5259 | 460.8 | 242.3 |
| 5 | 6.529 | 249.5 | 2013.6 | 224 | 0.5092 | 537.6 | 273.7 |
| 4 | 6.529 | 249.5 | 2263.1 | 256 | 0.4957 | 614.4 | 304.5 |
| 3 | 6.529 | 249.5 | 2512.6 | 288 | 0.4845 | 691.2 | 334.9 |
| 2 | 6.529 | 249.5 | 2762.1 | 320 | 0.475 | 768 | 364.8 |
| 1 | 6.529 | 263.6 | 3025.7 | 352 | 0.4669 | 844.8 | 394.4 |

Table A.4: Axial gravity forces on a wall

| Floor level | Dead load, kN/m ² | Dead load Floor + column kN | Cumulative Dead kN | Cumulative tributary area, m ² | LLRF type B | Cumulative Live Load kN | Reduced Live Load kN |
|-------------|------------------------------|-----------------------------|--------------------|---|-------------|-------------------------|----------------------|
| 12 | 7.079 | 651.8 | 651.8 | 0 | 0 | 0 | 0 |
| 11 | 6.529 | 616.6 | 1268.4 | 64 | 0.691 | 153.6 | 106.1 |
| 10 | 6.529 | 616.6 | 1884.9 | 128 | 0.577 | 307.2 | 177.3 |
| 9 | 6.529 | 616.6 | 2501.5 | 192 | 0.526 | 460.8 | 242.4 |
| 8 | 6.529 | 616.6 | 3118.1 | 256 | 0.496 | 614.4 | 304.7 |
| 7 | 6.529 | 616.6 | 3734.7 | 320 | 0.475 | 768 | 364.8 |
| 6 | 6.529 | 616.6 | 4351.2 | 384 | 0.46 | 921.6 | 423.9 |
| 5 | 6.529 | 616.6 | 4967.8 | 448 | 0.448 | 1075.2 | 481.7 |
| 4 | 6.529 | 616.6 | 5584.4 | 512 | 0.438 | 1228.8 | 538.2 |
| 3 | 6.529 | 616.6 | 6201.0 | 576 | 0.43 | 1382.4 | 594.4 |
| 2 | 6.529 | 616.6 | 6817.5 | 640 | 0.424 | 1536 | 651.3 |
| 1 | 6.529 | 685.7 | 7503.2 | 704 | 0.418 | 1689.6 | 706.3 |

Table A.5: Gravity load calculation of roof level for P-Δ analysis

| Roof | Total D + 0.5L load, kN | Already accounted for, kN |
|--|---|---------------------------|
| Columns | $24 \times 40.57 =$ | 973.68 |
| Walls | $2 \times 198.72 =$ | 397.44 |
| Slab | $5.8 \times 24 \times 48 =$ | 6681.60 |
| Snow | $0.25 \times 2.2 \times 24 \times 48 =$ | 633.60 |
| East-West beams | $0.583 \times 24 \times 48 =$ | 671.62 |
| North-South beams | $24 \times 2 \times 0.4 \times 0.4 \times 24 =$ | 184.32 |
| | Total = | 10084.2 kN |
| | | Total = 2865.1 kN |
| Remaining portion of load combination D +0.5L for roof level = 6919.5 kN | | |

Table A.6: Gravity load calculation of a typical floor level for P-Δ analysis

| Typical Floor | Total D + 0.5L load, kN | Already accounted for, kN |
|--|---|---|
| Columns | $24 \times 40.57 =$ | 973.68 |
| Walls | $2 \times 198.72 =$ | 397.44 |
| Slab | $5.8 \times 24 \times 48 =$ | 6681.60 |
| Live | $0.5 \times 0.392 \times 2.4 \times 24 \times 48 =$ | 541.90 |
| East-West beams | $0.583 \times 24 \times 48 =$ | 671.62 |
| North-South beams | $24 \times 2 \times 0.4 \times 0.4 \times 24 =$ | 184.32 |
| | | $24 \times 2 \times 0.4 \times 0.4 \times 24 =$ |
| | | 184.32 |
| Total = | 9450.6 kN | Total = |
| | | 2653.9 kN |
| Remaining portion of load combination D+0.5L for a typical floor = 6796.7 kN | | |

Table A.7: Gravity load calculation of first floor level for P- Δ analysis

| First Floor | Total D + 0.5L load, kN | Already accounted for, kN |
|----------------------|---|---|
| Columns | $24 \times 54.68 =$ | 1312.32 |
| Walls | $2 \times 267.84 =$ | 535.68 |
| Slab | $5.8 \times 24 \times 48 =$ | 6681.60 |
| Live | $0.5 \times 0.392 \times 2.4 \times 24 \times 48 =$ | 541.90 |
| East-West beams | $0.583 \times 24 \times 48 =$ | 671.62 |
| North-South beams | $24 \times 2 \times 0.4 \times 0.4 \times 24 =$ | 184.32 |
| | | $24 \times 2 \times 0.4 \times 0.4 \times 24 =$ |
| | Total= | 9927.4 kN |
| | | Total = |
| | | 2653.9 kN |
| | Remaining portion of load combination D +0.5L for first floor = | 7273.6 kN |

Table A.8: Yield and ultimate displacements of the wall

| Floor level | Yield displacement, Δ_{wy} , m | Ultimate displacement, Δ_u , m |
|-------------|---------------------------------------|---------------------------------------|
| 1 | 0.0067 | 0.0599 |
| 2 | 0.0197 | 0.1308 |
| 3 | 0.0384 | 0.2075 |
| 4 | 0.0619 | 0.2890 |
| 5 | 0.0893 | 0.3743 |
| 6 | 0.1195 | 0.4625 |
| 7 | 0.1517 | 0.5527 |
| 8 | 0.1848 | 0.6438 |
| 9 | 0.2181 | 0.7350 |
| 10 | 0.2514 | 0.8263 |
| 11 | 0.2847 | 0.9175 |
| 12 | 0.3180 | 1.0087 |

Table A.9: Lateral forces, and the actions in the wall

| Floor level | Lateral force kN | Lateral force on walls | Shear on the walls kN | Moments on the walls kNm |
|----------------|------------------------|---------------------------------|--------------------------------|-----------------------------------|
| | | kN | | |
| 0 | 0.0 | 0.0 | 1605.25 | 40733.7 |
| 1 | 24.9 | 24.9 | 1605.25 | 32948.3 |
| 2 | 52.1 | 52.1 | 1580.3 | 27180.1 |
| 3 | 82.6 | 82.6 | 1528.3 | 21601.9 |
| 4 | 115.0 | 115.0 | 1445.7 | 16325.2 |
| 5 | 149.0 | 149.0 | 1330.7 | 11468.3 |
| 6 | 184.1 | 184.1 | 1181.7 | 7155.2 |
| 7 | 220.0 | 220.0 | 997.6 | 3514.0 |
| 8 | 256.2 | 256.2 | 777.6 | 675.7 |
| 9 | 292.5 | 292.5 | 521.4 | -1227.3 |
| 10 | 328.9 | 328.9 | 228.9 | -2062.7 |
| 11 | 365.1 | 365.1 | -100.0 | -1697.7 |
| 12 | 399.2 | -465.1 | -465.1 | 0.0 |

Table A.10: Displacements at the yield of wall and at ultimate, in m

| Floor level | Yield displacement | Ultimate displacement |
|-------------|--------------------|-----------------------|
| 1 | 0.0066 | 0.0410 |
| 2 | 0.0195 | 0.0914 |
| 3 | 0.0382 | 0.1476 |
| 4 | 0.0618 | 0.2086 |
| 5 | 0.0894 | 0.2737 |
| 6 | 0.1200 | 0.3419 |
| 7 | 0.1529 | 0.4122 |
| 8 | 0.1871 | 0.4839 |
| 9 | 0.2216 | 0.5559 |
| 10 | 0.2562 | 0.6280 |
| 11 | 0.2908 | 0.7001 |
| 12 | 0.3254 | 0.7722 |

Table A.11: Lateral forces, and the actions in the wall

| Floor level | Lateral force kN | Lateral | Shear on the walls kN | Moments on the walls kNm |
|----------------|------------------------|----------------------------|--------------------------------|-----------------------------------|
| | | force on walls kN | | |
| 0 | 0.0 | 0.0 | 2811.81 | 72349.4 |
| 1 | 39.8 | 39.8 | 2811.81 | 58712.1 |
| 2 | 85.0 | 85.0 | 2772.0 | 48594.3 |
| 3 | 137.2 | 137.2 | 2687.0 | 38786.7 |
| 4 | 193.9 | 193.9 | 2549.9 | 29479.8 |
| 5 | 254.4 | 254.4 | 2355.9 | 20880.7 |
| 6 | 317.7 | 317.7 | 2101.5 | 13210.3 |
| 7 | 383.1 | 383.1 | 1783.7 | 6699.6 |
| 8 | 449.7 | 449.7 | 1400.6 | 1587.4 |
| 9 | 516.8 | 516.8 | 950.9 | -1883.2 |
| 10 | 583.7 | 583.7 | 434.1 | -3467.7 |
| 11 | 650.8 | 650.8 | -149.6 | -2921.5 |
| 12 | 713.6 | -800.4 | -800.4 | 0.0 |

Table A.12: Displacements at the yield of wall and at ultimate, in m

| Floor level | Yield displacement | Ultimate displacement |
|-------------|--------------------|-----------------------|
| 1 | 0.0067 | 0.0409 |
| 2 | 0.0197 | 0.0911 |
| 3 | 0.0386 | 0.1472 |
| 4 | 0.0624 | 0.2083 |
| 5 | 0.0903 | 0.2734 |
| 6 | 0.1213 | 0.3416 |
| 7 | 0.1545 | 0.4121 |
| 8 | 0.1891 | 0.4839 |
| 9 | 0.2240 | 0.5560 |
| 10 | 0.2590 | 0.6282 |
| 11 | 0.2940 | 0.7004 |
| 12 | 0.3289 | 0.7726 |

Table A.13: Multi-modal pushover analysis section shears, in kN

| (1) Storey | (2) Mode 1 | (3) Mode 2 | (4) Mode 3 | (5) Mode 4 | (6) SRSS 3 modes | (7) SRSS 4 modes | difference (6) and (7) % |
|---------------|------------------|------------------|------------------|------------------|------------------------|------------------------|--------------------------------|
| 1 | 4329.0 | 9003.4 | 7581.2 | 4126.8 | 12541.0 | 13202.5 | 5.28 |
| 2 | 4289.4 | 8630.2 | 6351.6 | 2552.4 | 11542.2 | 11821.0 | 2.42 |
| 3 | 4204.8 | 7704.0 | 3729.6 | 129.1 | 9536.3 | 9537.2 | 0.01 |
| 4 | 4068.0 | 6157.6 | 205.6 | 2462.0 | 7382.9 | 7782.6 | 5.41 |
| 5 | 3874.4 | 4064.2 | 3149.2 | 2960.8 | 6437.9 | 7086.1 | 10.07 |
| 6 | 3620.2 | 1648.4 | 5224.8 | 1338.5 | 6566.7 | 6701.7 | 2.06 |
| 7 | 3302.4 | 790.5 | 5334.0 | 1249.2 | 6323.2 | 6445.4 | 1.93 |
| 8 | 2919.2 | 2921.6 | 3505.2 | 2989.6 | 5417.0 | 6187.2 | 14.22 |
| 9 | 2469.0 | 4428.6 | 485.0 | 2686.6 | 5093.5 | 5758.6 | 13.06 |
| 10 | 1951.6 | 5038.4 | 2496.4 | 603.0 | 5952.0 | 5982.5 | 0.51 |
| 11 | 1366.9 | 4559.2 | 4135.0 | 1679.1 | 6305.0 | 6524.7 | 3.49 |
| 12 | 715.0 | 2886.8 | 3451.2 | 2258.2 | 4555.8 | 5084.8 | 11.61 |

Table A.14: Multi-modal pushover analysis, inter-storey drifts

| (1) Storey | (2) Mode 1 | (3) Mode 2 | (4) Mode 3 | (5) Mode 4 | (6) SRSS 3 modes | (7) SRSS 4 modes | difference (6) and (7) % |
|---------------|---------------|---------------|---------------|---------------|------------------------|------------------------|--------------------------------|
| 1 | 0.01163 | 0.00295 | 0.00065 | 0.00022 | 0.01201 | 0.01201 | 0.02 |
| 2 | 0.01382 | 0.00435 | 0.00106 | 0.00023 | 0.01452 | 0.01453 | 0.01 |
| 3 | 0.01526 | 0.00454 | 0.00066 | 0.00007 | 0.01594 | 0.01594 | 0.00 |
| 4 | 0.01635 | 0.00393 | 0.00013 | 0.00036 | 0.01681 | 0.01682 | 0.02 |
| 5 | 0.01710 | 0.00270 | 0.00094 | 0.00041 | 0.01733 | 0.01734 | 0.03 |
| 6 | 0.01755 | 0.00105 | 0.00145 | 0.00019 | 0.01764 | 0.01764 | 0.01 |
| 7 | 0.01774 | 0.00153 | 0.00143 | 0.00017 | 0.01786 | 0.01786 | 0.00 |
| 8 | 0.01773 | 0.00308 | 0.00088 | 0.00040 | 0.01802 | 0.01802 | 0.03 |
| 9 | 0.01758 | 0.00438 | 0.00002 | 0.00035 | 0.01811 | 0.01812 | 0.02 |
| 10 | 0.01735 | 0.00531 | 0.00098 | 0.00004 | 0.01817 | 0.01817 | 0.00 |
| 11 | 0.01712 | 0.00584 | 0.00171 | 0.00033 | 0.01817 | 0.01817 | 0.02 |
| 12 | 0.01697 | 0.00603 | 0.00205 | 0.00055 | 0.01813 | 0.01814 | 0.05 |

Table A.15: Multi-modal pushover analysis, wall shear forces in kN

| (1) Storey | (2) Mode 1 | (3) Mode 2 | (4) Mode 3 | (5) Mode 4 | (6) SRSS 3 modes | (7) SRSS 4 modes | difference (6) and (7) % |
|---------------|------------------|------------------|------------------|------------------|------------------------|------------------------|--------------------------------|
| 1 | 1711.0 | 4153.0 | 3733.0 | 2033.0 | 5840.4 | 6184.1 | 5.89 |
| 2 | 1940.0 | 4144.0 | 3075.0 | 1243.0 | 5512.9 | 5651.3 | 2.51 |
| 3 | 1604.0 | 3584.0 | 1809.0 | 60.1 | 4323.2 | 4323.7 | 0.01 |
| 4 | 1511.0 | 2847.0 | 106.8 | 1195.0 | 3224.9 | 3439.2 | 6.64 |
| 5 | 1345.0 | 1858.0 | 1500.0 | 1435.0 | 2740.7 | 3093.6 | 12.88 |
| 6 | 1149.0 | 749.3 | 2489.0 | 648.2 | 2842.0 | 2915.0 | 2.57 |
| 7 | 917.2 | 346.7 | 2537.0 | 604.1 | 2719.9 | 2786.2 | 2.44 |
| 8 | 656.5 | 1278.0 | 1666.0 | 1444.0 | 2200.0 | 2631.5 | 19.62 |
| 9 | 419.7 | 1908.0 | 238.6 | 1297.0 | 1968.1 | 2357.1 | 19.76 |
| 10 | 179.8 | 2105.0 | 1152.0 | 294.4 | 2406.3 | 2424.3 | 0.75 |
| 11 | 357.0 | 1829.0 | 1919.0 | 805.4 | 2674.9 | 2793.5 | 4.43 |
| 12 | 726.6 | 823.3 | 1444.0 | 1041.0 | 1814.1 | 2091.6 | 15.30 |

Table A.16: Multi-modal pushover analysis wall moments in kN.m

| (1) Storey | (2) Mode 1 | (3) Mode 2 | (4) Mode 3 | (5) Mode 4 | (6) SRSS 3 modes | (7) SRSS 4 modes | difference (6) and (7) % |
|-------------------|---------------|---------------|---------------|------------------|------------------------|------------------------|--------------------------------|
| 1 | 38000.0 | 38000.0 | 22030.0 | 8755.0 | 38430.0 | 38430.0 | 0.00 |
| 2 | 31230.0 | 18230.0 | 7305.0 | 5643.0 | 36891.9 | 37320.9 | 1.16 |
| 3 | 24190.0 | 10350.0 | 13910.0 | 5643.0 | 29761.8 | 30292.1 | 1.78 |
| 4 | 18710.0 | 20740.0 | 14300.0 | 5423.0 | 31380.0 | 31845.1 | 1.48 |
| 5 | 13870.0 | 27520.0 | 14300.0 | 4177.0 | 33973.8 | 34229.6 | 0.75 |
| 6 | 9551.0 | 30260.0 | 8821.0 | 6543.0 | 32934.8 | 33578.4 | 1.95 |
| 7 | 5836.0 | 30260.0 | 9522.0 | 6543.0 | 32255.2 | 32912.1 | 2.04 |
| 8 | 2784.0 | 28990.0 | 15600.0 | 4338.0 | 33038.3 | 33321.9 | 0.86 |
| 9 | 3912.0 | 24320.0 | 16480.0 | 5665.0 | 29637.1 | 30173.6 | 1.81 |
| 10 | 3955.0 | 17360.0 | 16480.0 | 6740.0 | 24261.1 | 25179.9 | 3.79 |
| 11 | 3955.0 | 9679.0 | 12270.0 | 6740.0 | 16120.7 | 17473.0 | 8.39 |
| 12 | 2652.0 | 3005.0 | 5269.0 | 3800.0 | 6620.1 | 7633.2 | 15.30 |
| Hinge rotation | 0.0102 | 0.0017 | 0.0000 | 0.0000 | | | |

Table A.17: Maximum negative moments in kN.m and inelastic hinge rotations¹ in storey beams

| (1) Storey | (2) Mode 1 | (3) Mode 2 | (4) Mode 3 | (5) Mode 4 | (6) Gravity |
|---------------|-------------------|---------------|---------------|---------------|----------------|
| 1 | 955.0 (0.0017) | 523.6 | 351.9 | 297.1 | 297.1 |
| 2 | 955.0 (0.0038) | 548.7 | 347.7 | 294.7 | 294.8 |
| 3 | 955.0 (0.0058) | 543.0 | 314.2 | 310.6 | 297.8 |
| 4 | 955.0 (0.0071) | 494.4 | 302.6 | 326.4 | 302.8 |
| 5 | 955.0 (0.0080) | 416.5 | 306.4 | 324.9 | 306.6 |
| 6 | 955.0 (0.0085) | 321.6 | 309.8 | 310.2 | 310.1 |
| 7 | 955.0 (0.0087) | 312.8 | 312.8 | 312.8 | 313.1 |
| 8 | 955.0 (0.0085) | 315.1 | 315.1 | 315.1 | 315.5 |
| 9 | 955.0 (0.0083) | 317.5 | 345.9 | 317.5 | 317.9 |
| 10 | 955.0 (0.0079) | 317.1 | 393.6 | 325.2 | 317.4 |
| 11 | 955.0 (0.0076) | 325.5 | 436.0 | 352.7 | 327 |
| 12 | 477.5 (0.0197) | 291.6 | 393.1 | 320.2 | 317.2 |

¹ Inelastic hinge rotation values are in parentheses

Table A.18: Maximum positive moments in kN.m and inelastic hinge rotations² in storey beams

| (1) Storey | (2) Mode 1 | (3) Mode 2 | (4) Mode 3 | (5) Mode 4 | (6) Gravity |
|---------------|------------------|---------------|---------------|---------------|-------------------|
| 1 | 297.1 | 297.1 | 297.1 | 313 | 297.1 |
| 2 | 294.8 | 294.7 | 294.7 | 300.6 | 294.8 |
| 3 | 297.8 | 297.7 | 297.7 | 297.7 | 297.8 |
| 4 | 302.8 | 302.6 | 334.1 | 302.6 | 302.8 |
| 5 | 306.6 | 306.4 | 377.4 | 306.4 | 306.6 |
| 6 | 310.1 | 346.3 | 395.5 | 309.8 | 310.1 |
| 7 | 313.1 | 438.2 | 381.9 | 330.9 | 313.1 |
| 8 | 315.5 | 520.9 | 341.5 | 339.0 | 315.5 |
| 9 | 317.9 | 586.2 | 317.5 | 330.1 | 317.9 |
| 10 | 317.4 | 625.6 | 317.1 | 317.1 | 317.4 |
| 11 | 327.0 | 656.0 | 325.5 | 325.5 | 327 |
| 12 | 317.2 | 477.5 | 291.6 | 291.6 | 317.2 (0.0032) |

² Inelastic hinge rotation values are in parentheses

Table A.19: Maximum moments in kN.m and inelastic hinge rotation³ at the base of columns

| (1) Column | (2) Mode 1 | (3) Mode 2 | (4) Mode 3 | (5) Mode 4 | (6) Gravity |
|---------------|---------------|---------------|---------------|---------------|----------------|
| | 955.0 | 522.1 | 146.3 | 51.0 | 51.0 |
| Base | | (0.0068) | | | |

³ Inelastic hinge rotation values are in parentheses

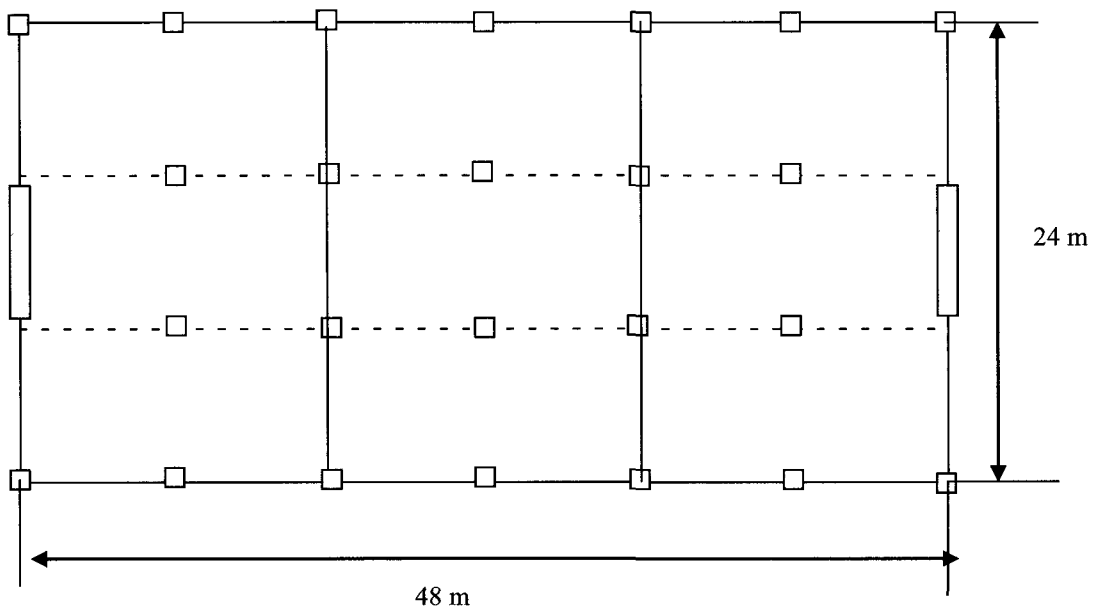


Figure A.1: Plan view of frame wall building

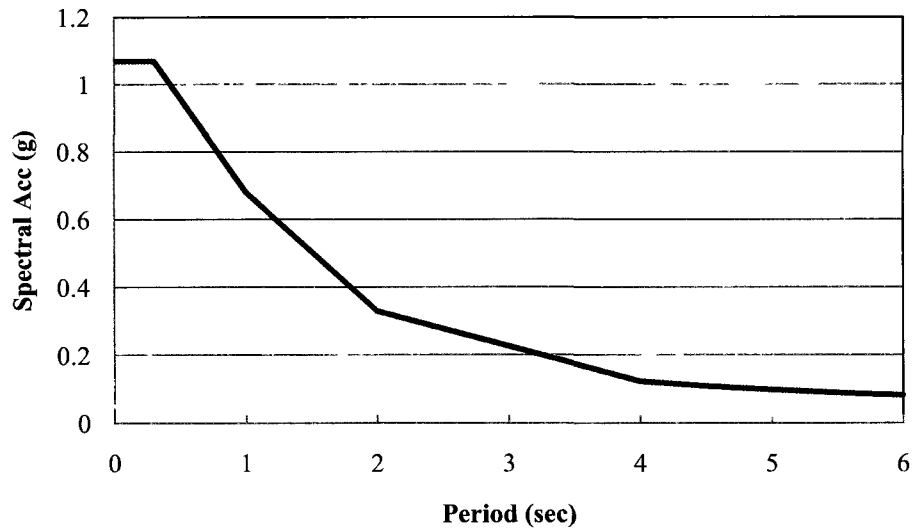


Figure A.2: Design spectrum for LA

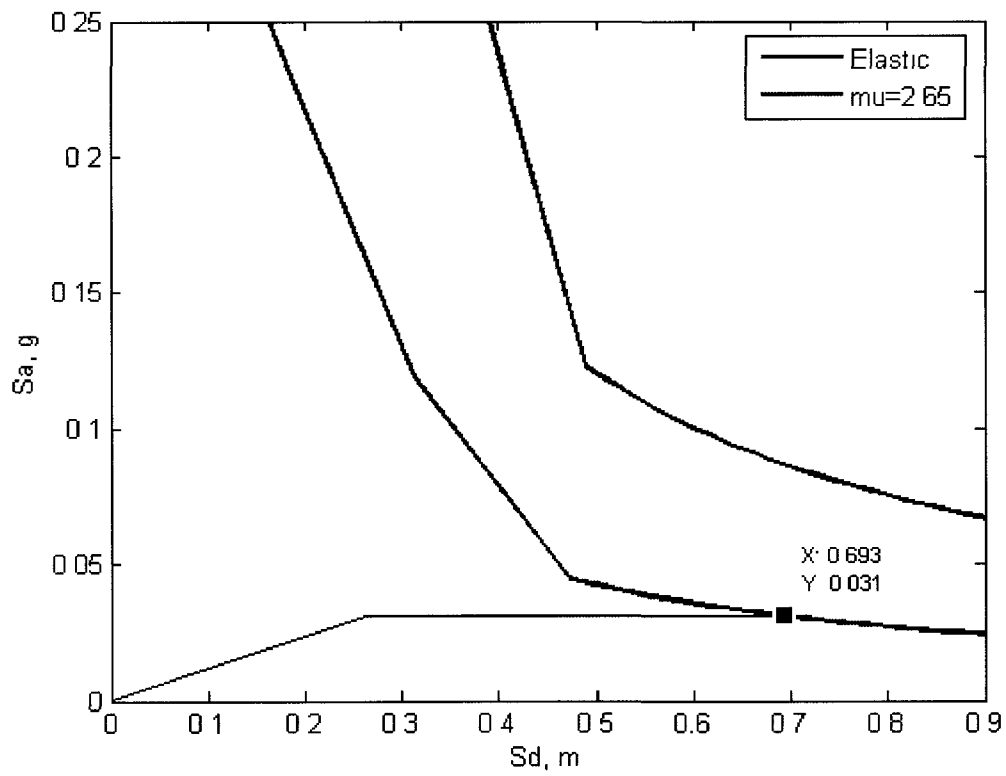


Figure A.3: Capacity and demand diagrams

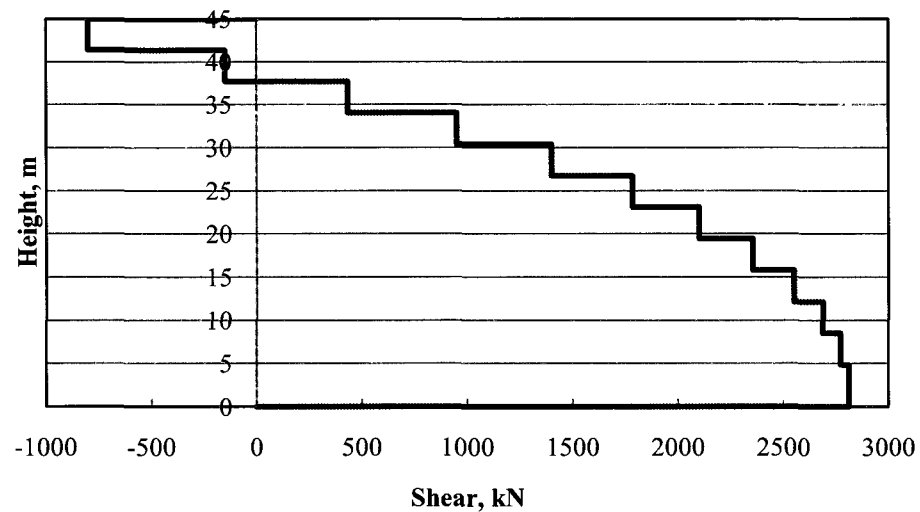


Figure A.4: Total shear in the two walls

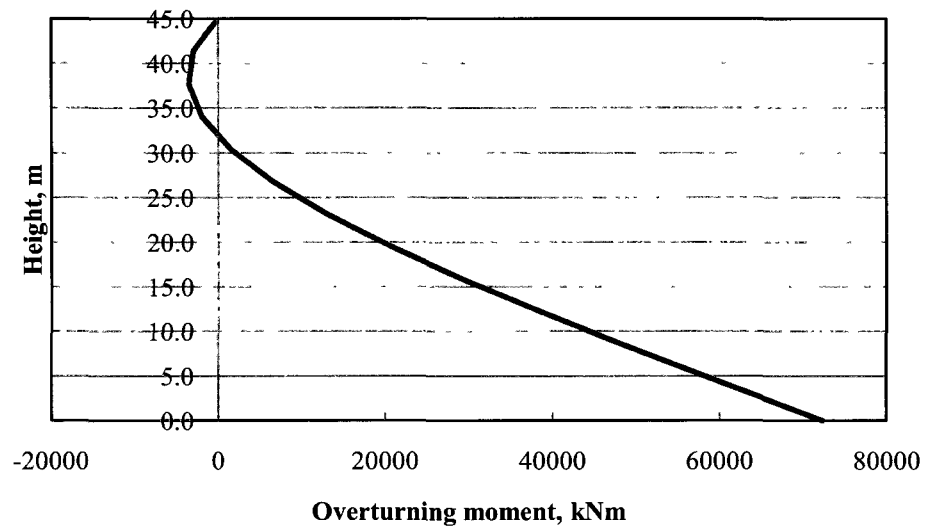


Figure A.5: Total overturning moment in the two walls

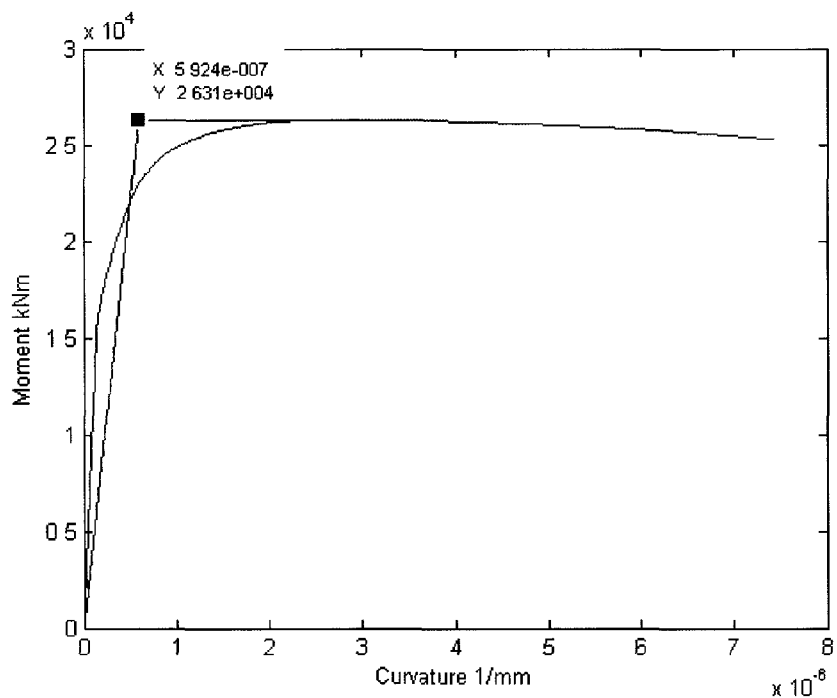


Figure A.6: Moment curvature relation for 6-meter wall

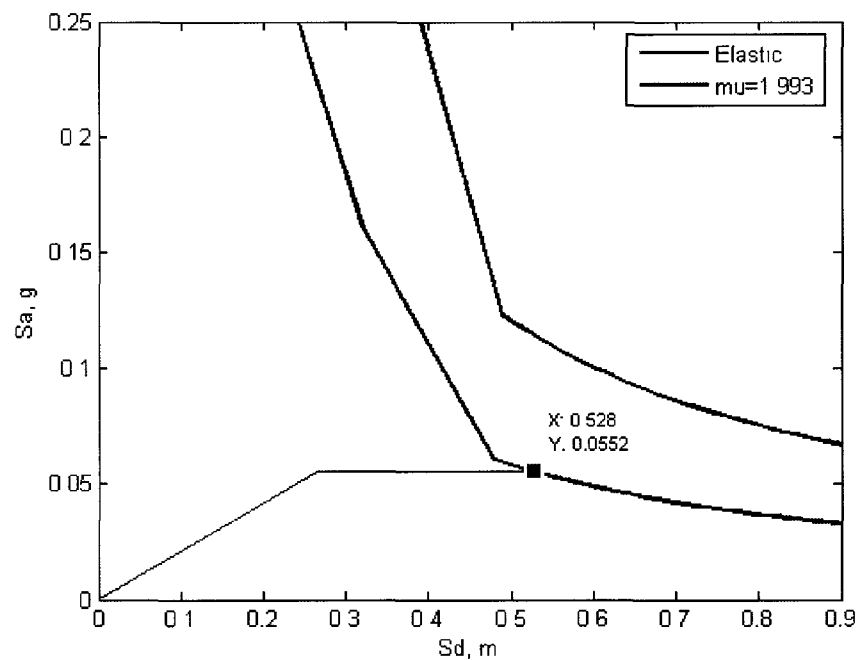


Figure A.7: Demand capacity diagram

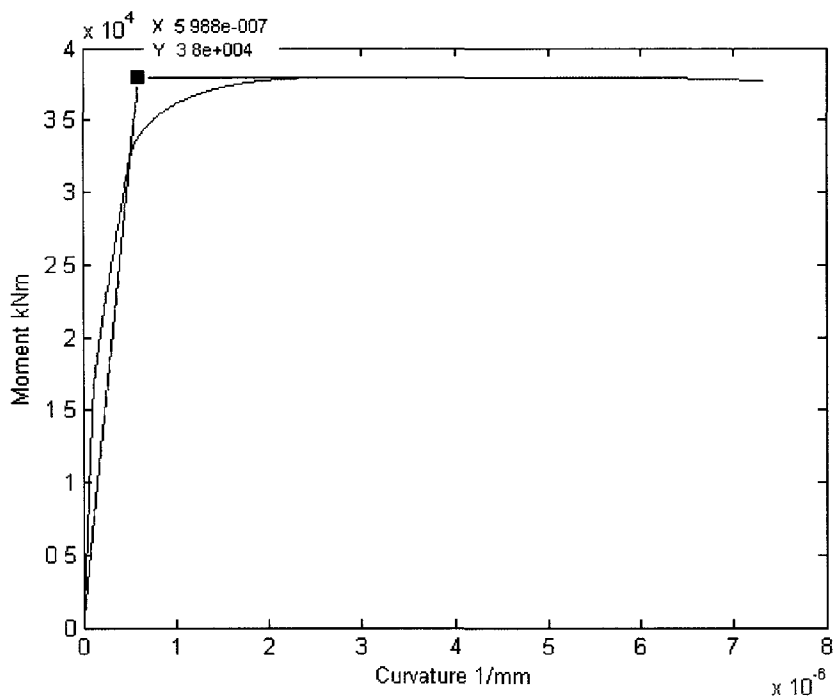


Figure A.8: Moment-curvature relationship for 6-meter wall

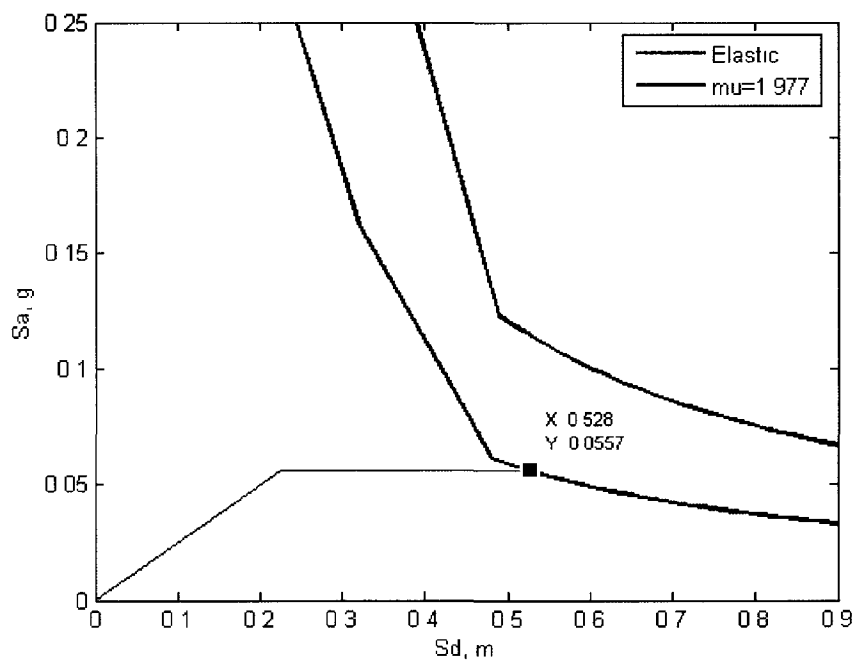


Figure A.9: Demand capacity diagrams

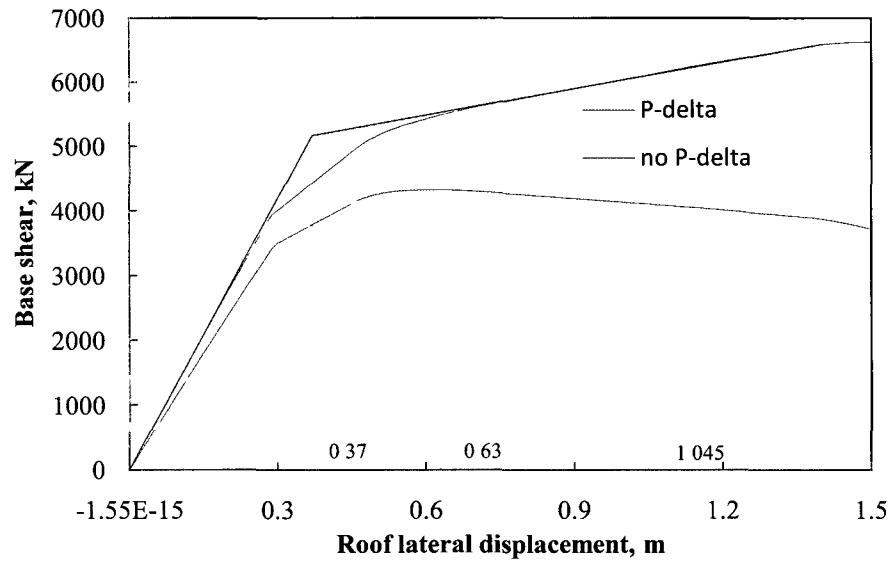


Figure A.10: Pushover curves with and without P- Δ effect

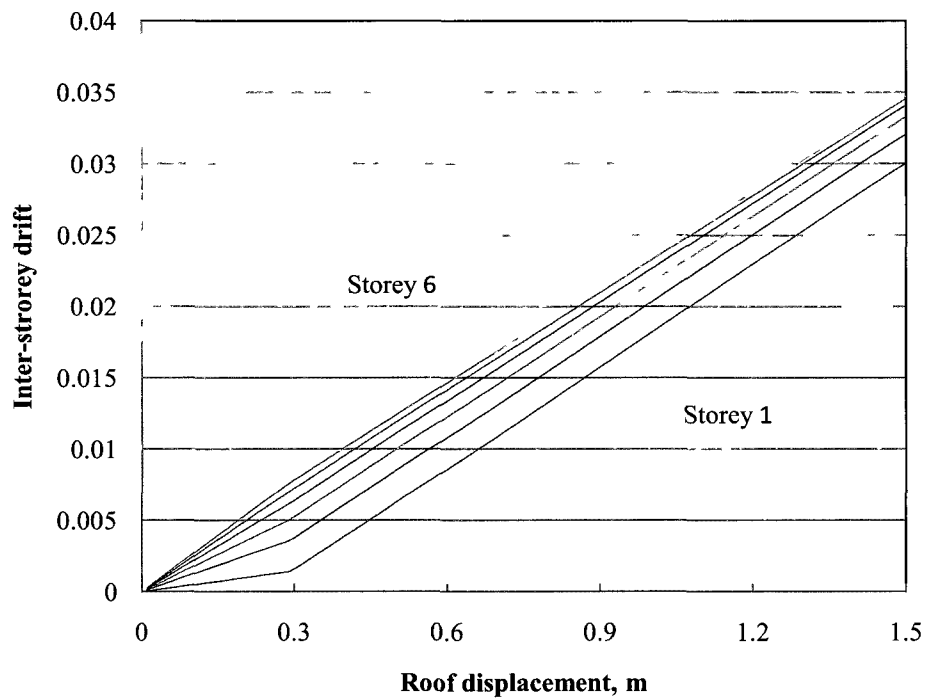


Figure A.11: Inter-storey drifts storey 1 to 6

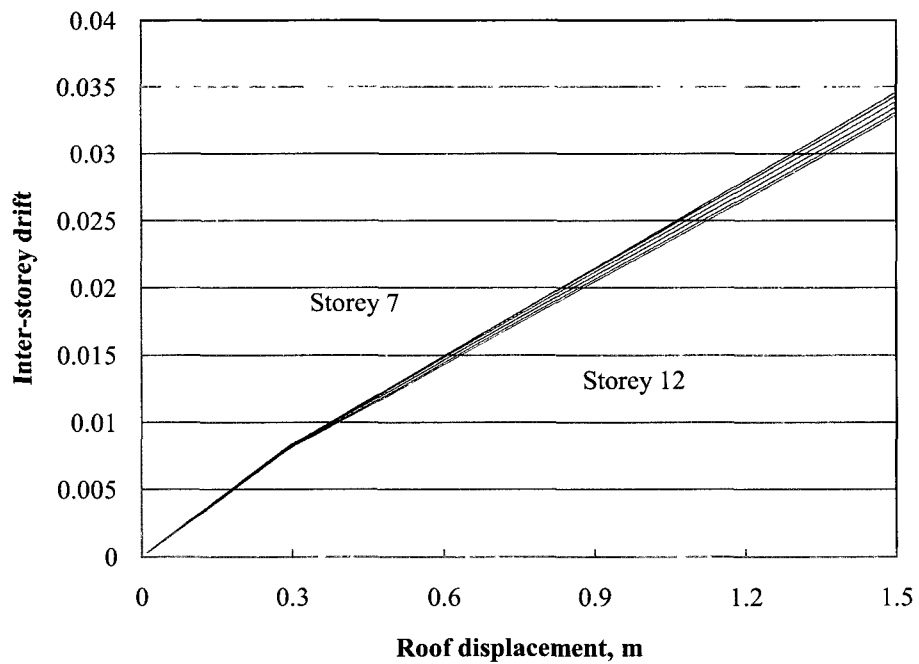


Figure A.12: Inter-storey drifts storey 7 to 12

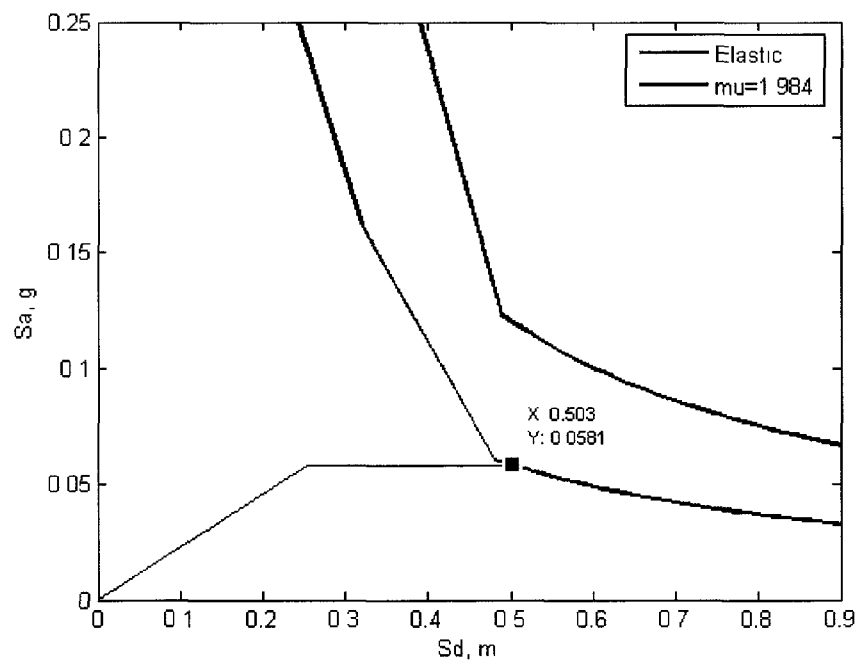


Figure A.13: Demand capacity diagram

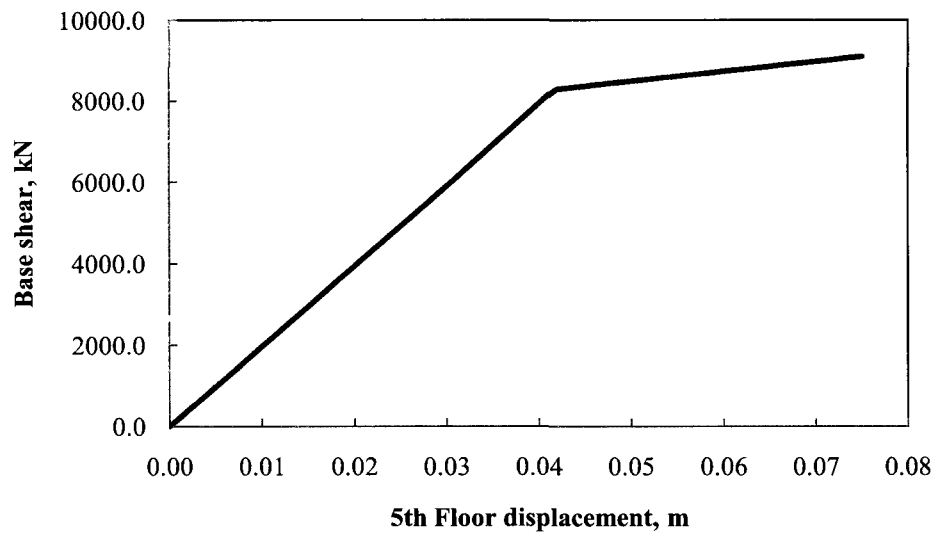


Figure A.14: Second mode pushover curve

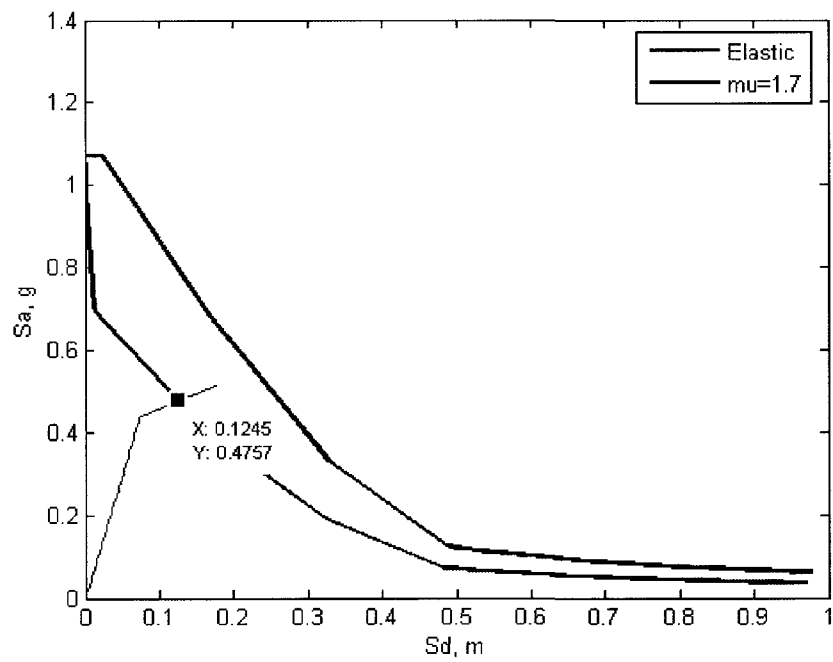


Figure A.15: Demand capacity diagram for second mode

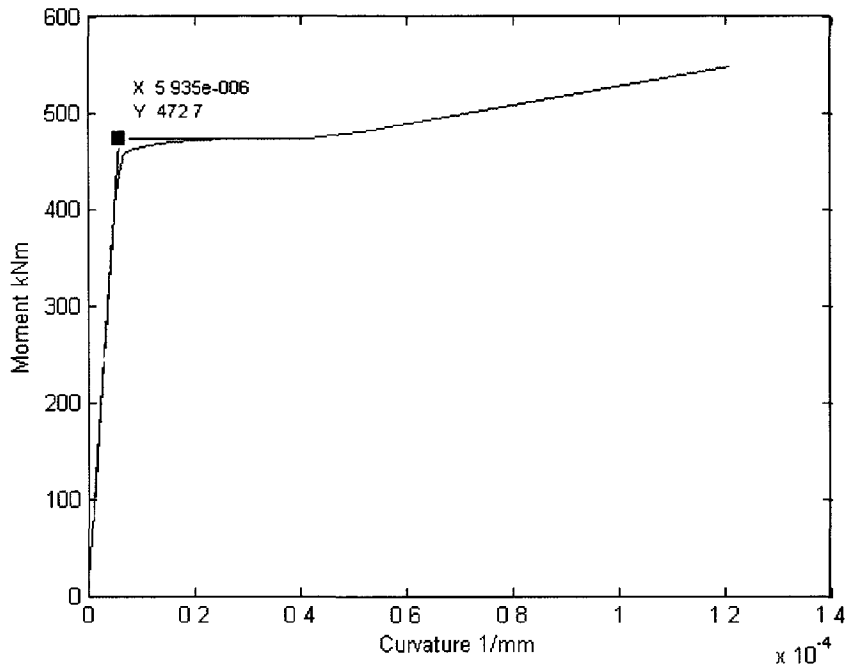


Figure A.16: Moment curvature relation of roof beams

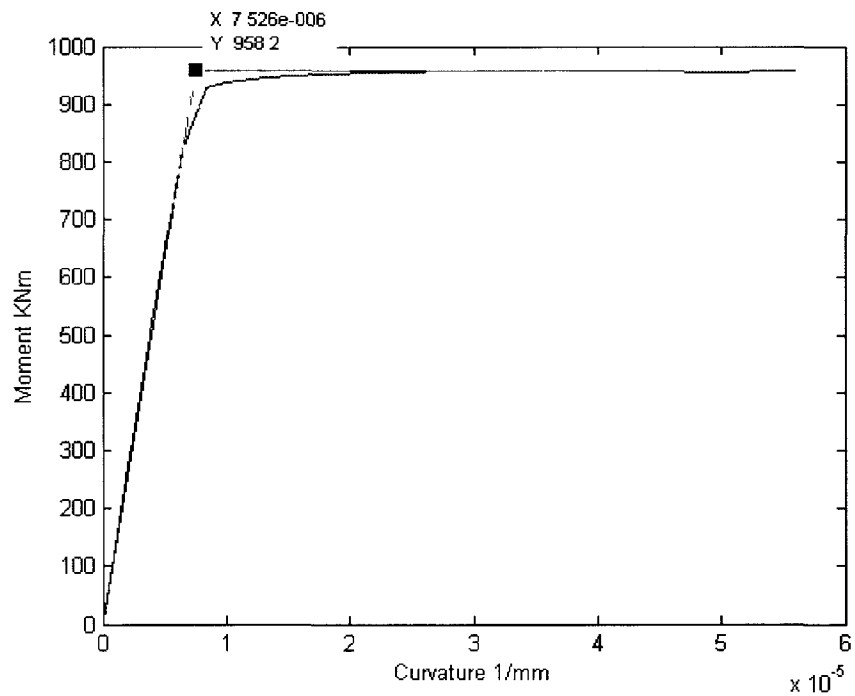


Figure A.17: Moment curvature relation of floor beams

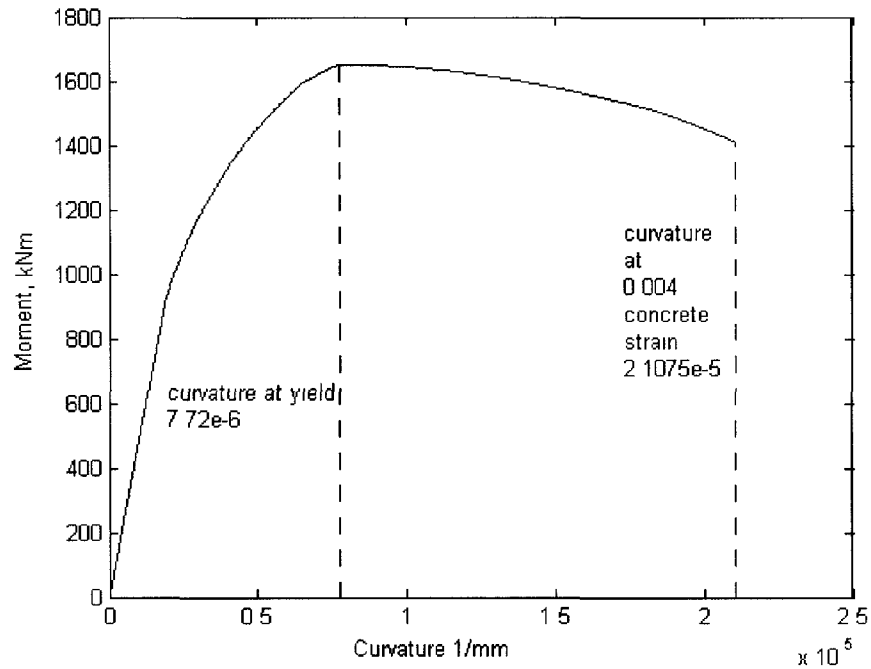


Figure A.18: Moment curvature relation for unconfined interior column

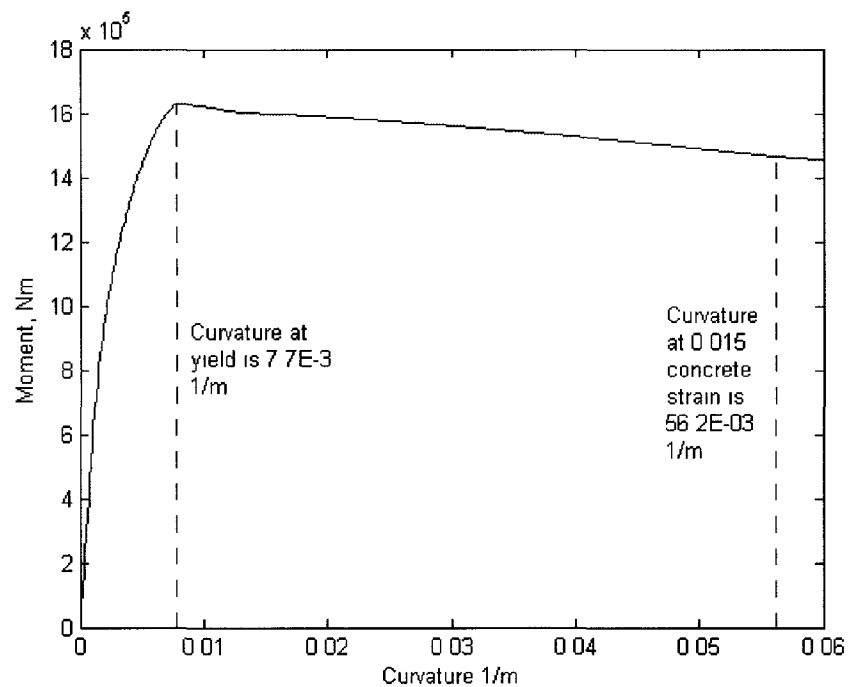


Figure A.19: Moment curvature relation for confined interior column

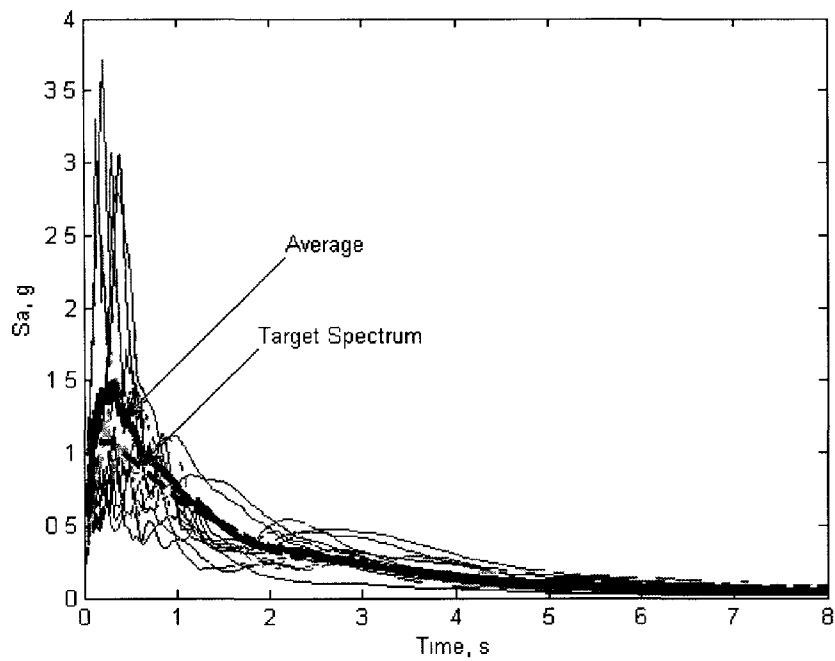


Figure A.20: Response spectra for 20 ground motions and the design spectrum

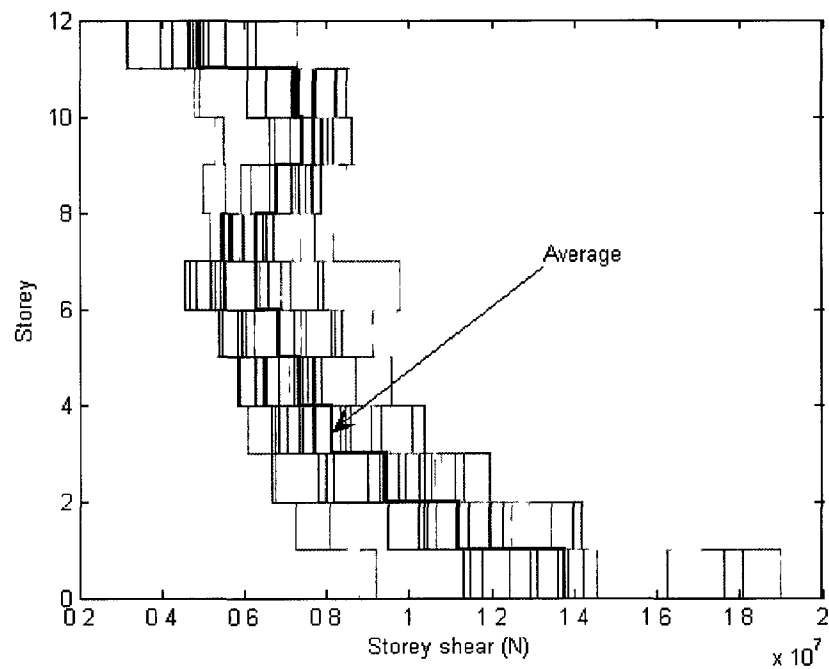


Figure A.21: Storey shears obtained from 20 dynamic analyses and their average

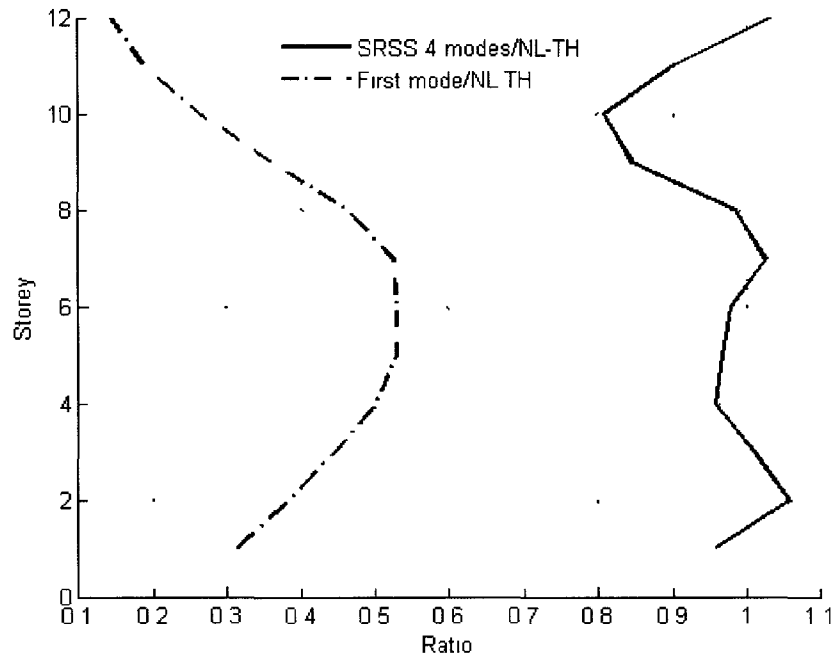


Figure A.22: Comparison of the modal and first mode base shears with the results of nonlinear time history analyses (NL-TH)

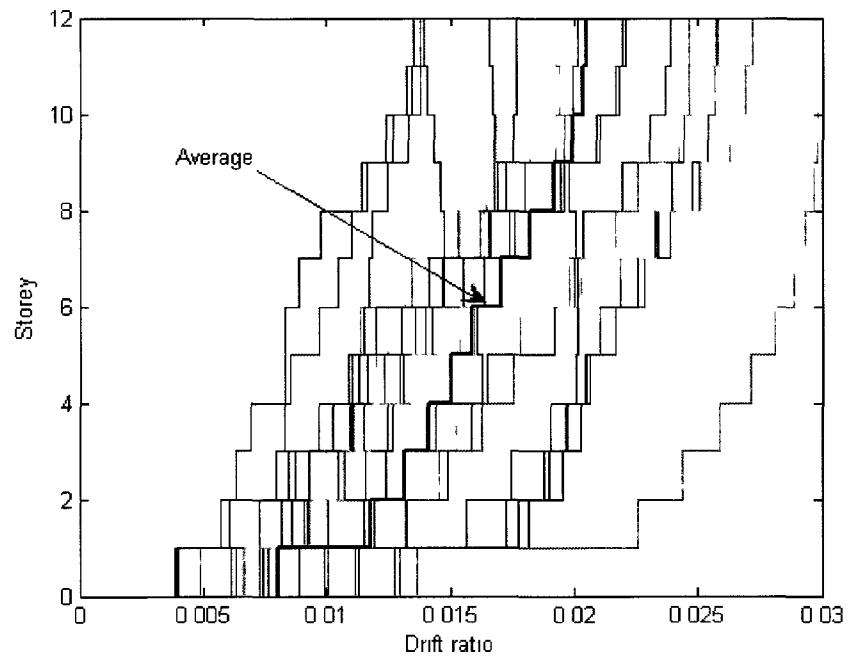


Figure A.23: Storey drift ratios obtained from 20 dynamic analyses and their average

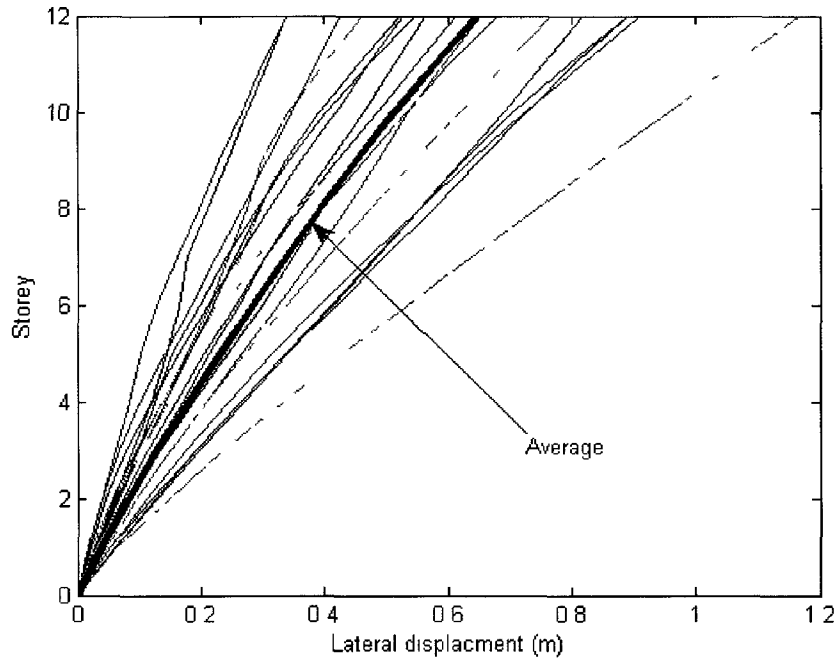


Figure A.24: Displacement profiles obtained from 20 dynamic analyses and their average

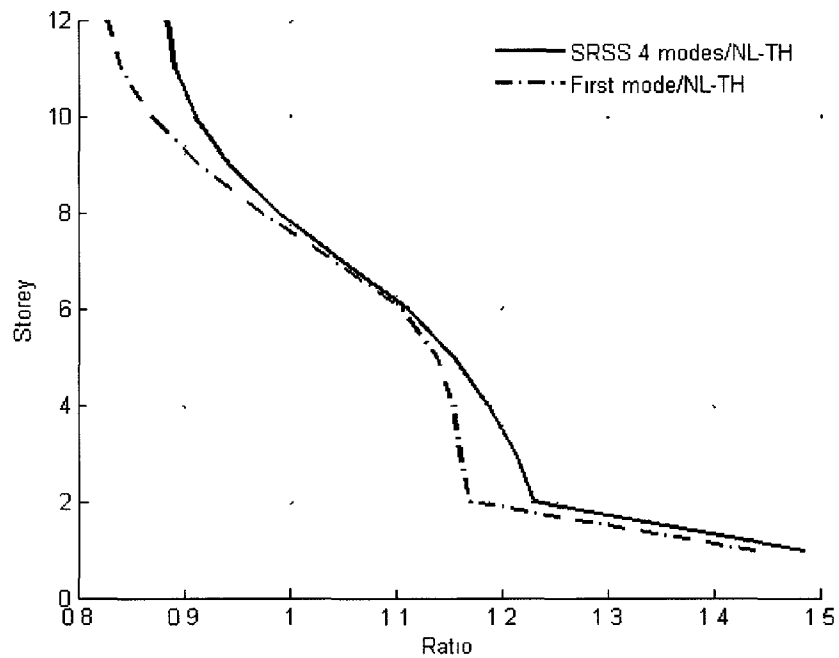


Figure A.25: Comparison of the modal and first mode inter-storey drifts with the results of nonlinear time history analyses (NL-TH)

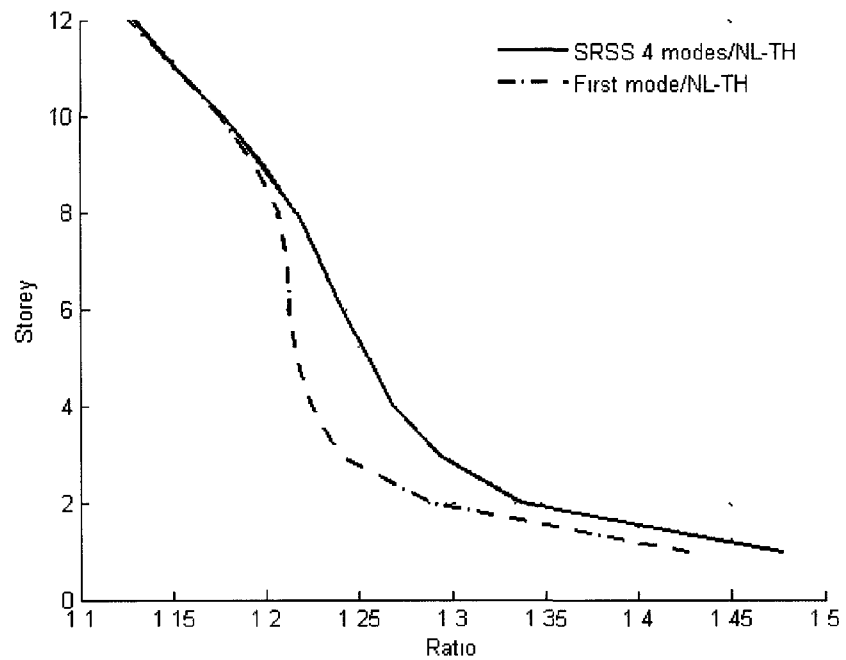


Figure A.26: Comparison of the modal and first mode displacements with the results of nonlinear time history analyses (NL-TH)

B. Supplemental data on multi-mode pushover and nonlinear time-history analyses

This appendix supplements Chapter 3 on DBSD of wall-frame structures.

Supplemental data for 6, 9, 15, and 20-storey buildings are presented.

Table B.1: Multi-modal pushover analysis section shears, in kN

| (1) | (2) | (3) | (4) | (5) | (6) | (7) | difference |
|--------|--------|--------|--------|--------|--------------|--------------|---------------|
| Storey | Mode 1 | Mode 2 | Mode 3 | Mode 4 | SRSS 3 modes | SRSS 4 modes | (6) and (7) % |
| 1 | 3409.8 | 6827 | 2988 | 256.6 | 8194.8 | 8198.8 | 0.05 |
| 2 | 3323.8 | 5341 | 659 | 156.9 | 6325.2 | 6327.1 | 0.03 |
| 3 | 3093.2 | 2384 | 1939.1 | 193.0 | 4360.0 | 4364.3 | 0.10 |
| 4 | 2666.8 | 1067 | 2078.4 | 186.6 | 3545.4 | 3550.3 | 0.14 |
| 5 | 2018.0 | 3437.0 | 232.0 | 169.7 | 3992.4 | 3996.0 | 0.09 |
| 6 | 1134.1 | 3328.8 | 1892.7 | 184.5 | 3993.7 | 3997.9 | 0.11 |

Table B.2: Multi-modal pushover analysis, wall shear forces in kN

| (1) | (2) | (3) | (4) | (5) | (6) | (7) | difference |
|--------|--------|--------|--------|--------|--------------|--------------|---------------|
| Storey | Mode 1 | Mode 2 | Mode 3 | Mode 4 | SRSS 3 modes | SRSS 4 modes | (6) and (7) % |
| 1 | 1168.0 | 3267.0 | 1462.0 | 125.8 | 3765.0 | 3767.1 | 0.06 |
| 2 | 1336.0 | 2550.0 | 317.7 | 76.4 | 2896.3 | 2897.3 | 0.03 |
| 3 | 959.8 | 1125.0 | 935.1 | 93.7 | 1749.6 | 1752.1 | 0.14 |
| 4 | 737.1 | 489.7 | 1003.0 | 91.0 | 1337.6 | 1340.7 | 0.23 |
| 5 | 449.5 | 1597.0 | 112.1 | 82.5 | 1662.8 | 1664.9 | 0.12 |
| 6 | 203.9 | 1404.0 | 885.9 | 88.2 | 1672.6 | 1674.9 | 0.14 |

Table B.3 Multi-modal pushover analysis, inter-storey drifts

| (1) Storey | (2) Mode 1 | (3) Mode 2 | (4) Mode 3 | (5) Mode 4 | (6) | (7) | difference (6) and (7) % |
|---------------|---------------|---------------|---------------|---------------|-----------------|-----------------|-----------------------------|
| | | | | | SRSS 3 modes | SRSS 4 modes | |
| 1 | 0.01736 | 0.00192 | 0.00026 | 0.00001 | 0.01747 | 0.01747 | 0.00 |
| 2 | 0.01947 | 0.00236 | 0.00006 | 0.00002 | 0.01962 | 0.01962 | 0.00 |
| 3 | 0.02050 | 0.00112 | 0.00037 | 0.00002 | 0.02053 | 0.02053 | 0.00 |
| 4 | 0.02096 | 0.00122 | 0.00036 | 0.00001 | 0.02100 | 0.02100 | 0.00 |
| 5 | 0.02104 | 0.00277 | 0.00011 | 0.00001 | 0.02122 | 0.02122 | 0.00 |
| 6 | 0.02097 | 0.00355 | 0.00055 | 0.00003 | 0.02127 | 0.02127 | 0.00 |

Table B.4 Multi-modal pushover analysis wall moments in kNm

| (1) Storey | (2) Mode 1 | (3) Mode 2 | (4) Mode 3 | (5) | | (7) SRSS 4 modes | difference (6) and (7) % |
|-------------------|---------------|---------------|---------------|-----------|-----------------|---------------------|-----------------------------|
| | | | | Mode 4 | SRSS 3 modes | | |
| 1 | 16520.0 | 16520.0 | 4819.0 | 309.7 | 16520.0 | 16520.0 | 0.00 |
| 2 | 12210.0 | 8633.0 | 3432.0 | 309.7 | 15342.5 | 15345.6 | 0.02 |
| 3 | 7410.0 | 12740.0 | 3432.0 | 311.0 | 15132.6 | 15135.8 | 0.02 |
| 4 | 4210.0 | 12740.0 | 3643.0 | 311.0 | 13903.4 | 13906.8 | 0.03 |
| 5 | 1729.0 | 10950.0 | 3643.0 | 322.0 | 11668.9 | 11673.3 | 0.04 |
| 6 | 744.3 | 5123 | 3233 | 322.0 | 6103.4 | 6111.9 | 0.14 |
| Hinge rotation | 0.0158 | 0.0007 | | | | | |

Table B.5 Multi-modal pushover analysis section shears, in kN

| (1) | (2) | (3) | (4) | (5) | (6) SRSS | (7) SRSS | difference (6) and (7) |
|--------|--------|--------|--------|--------|----------|----------|---------------------------|
| Storey | Mode 1 | Mode 2 | Mode 3 | Mode 4 | 3 modes | 4 modes | % |
| 1 | 3829.4 | 7817 | 5593 | 3644.0 | 10346.2 | 10969.1 | 6.02 |
| 2 | 3794.4 | 7162 | 3792 | 1005.4 | 8948.1 | 9004.4 | 0.63 |
| 3 | 3698.2 | 5634 | 521.3 | 2114.0 | 6759.8 | 7082.6 | 4.78 |
| 4 | 3515.6 | 3297 | 2730.2 | 2625.6 | 5539.0 | 6129.8 | 10.67 |
| 5 | 3229.8 | 552.2 | 4172.8 | 61.4 | 5305.5 | 5305.9 | 0.01 |
| 6 | 2829.2 | 2017.4 | 3041.0 | 2611.8 | 4617.6 | 5305.0 | 14.89 |
| 7 | 2307.4 | 3788.8 | 146.1 | 2356.0 | 4438.5 | 5025.1 | 13.21 |
| 8 | 1662.0 | 4237.6 | 2546.0 | 438.8 | 5215.5 | 5233.9 | 0.35 |
| 9 | 893.62 | 3023.6 | 2984.4 | 2254.2 | 4341.4 | 4891.7 | 12.68 |

Table B.6 Multi-modal pushover analysis, inter-storey drifts

| (1) | (2) | (3) | (4) | (5) | (6) SRSS | (7) SRSS | difference (6) and (7) % |
|--------|---------|---------|---------|---------|----------|----------|-----------------------------|
| Storey | Mode 1 | Mode 2 | Mode 3 | Mode 4 | 3 modes | 4 modes | |
| 1 | 0.01459 | 0.00245 | 0.00049 | 0.00019 | 0.01480 | 0.01480 | 0.01 |
| 2 | 0.01672 | 0.00352 | 0.00058 | 0.00006 | 0.01709 | 0.01709 | 0.00 |
| 3 | 0.01797 | 0.00319 | 0.00001 | 0.00026 | 0.01825 | 0.01825 | 0.01 |
| 4 | 0.01876 | 0.00199 | 0.00069 | 0.00030 | 0.01888 | 0.01888 | 0.01 |
| 5 | 0.01915 | 0.00046 | 0.00099 | 0.00000 | 0.01918 | 0.01918 | 0.00 |
| 6 | 0.01921 | 0.00209 | 0.00068 | 0.00030 | 0.01933 | 0.01934 | 0.01 |
| 7 | 0.01903 | 0.00347 | 0.00007 | 0.00026 | 0.01935 | 0.01935 | 0.01 |
| 8 | 0.01873 | 0.00436 | 0.00085 | 0.00009 | 0.01925 | 0.01925 | 0.00 |
| 9 | 0.01845 | 0.00473 | 0.00130 | 0.00040 | 0.01909 | 0.01909 | 0.02 |

Table B.7 Multi-modal pushover analysis, wall shear forces in kN

| (1) | (2) | (3) | (4) | (5) | (6) | (7) | difference |
|--------|--------|--------|--------|--------|-----------------|-----------------|------------------|
| Storey | Mode 1 | Mode 2 | Mode 3 | Mode 4 | SRSS 3 modes | SRSS 4 modes | (6) and (7) % |
| 1 | 1461.0 | 3689.0 | 2749.0 | 1792.0 | 4827.0 | 5148.9 | 6.67 |
| 2 | 1633.0 | 3433.0 | 1838.0 | 489.1 | 4222.6 | 4250.8 | 0.67 |
| 3 | 1360.0 | 2644.0 | 257.6 | 1028.0 | 2984.4 | 3156.5 | 5.77 |
| 4 | 1223.0 | 1538.0 | 1312.0 | 1277.0 | 2362.7 | 2685.7 | 13.67 |
| 5 | 996.8 | 274.4 | 2004.0 | 30.0 | 2255.0 | 2255.2 | 0.01 |
| 6 | 738.0 | 918.4 | 1459.0 | 1267.0 | 1875.3 | 2263.2 | 20.68 |
| 7 | 446.4 | 1692.0 | 77.4 | 1143.0 | 1751.6 | 2091.5 | 19.41 |
| 8 | 237.6 | 1878.0 | 1209.0 | 213.4 | 2246.1 | 2256.2 | 0.45 |
| 9 | 1055 | 1074.0 | 1342.0 | 1068.0 | 2016.8 | 2282.1 | 13.16 |

Table B.8 Multi-modal pushover analysis wall moments in kNm

| (1) Storey | (2) Mode 1 | (3) Mode 2 | (4) Mode 3 | (5) Mode 4 |
|----------------|------------|------------|------------|------------|
| 1 | 26320.0 | 26320.0 | 12580.0 | 6074.0 |
| 2 | 20830.0 | 8817.0 | 7460.0 | 4403.0 |
| 3 | 15040.0 | 13750.0 | 8400.0 | 4403.0 |
| 4 | 10790.0 | 19370.0 | 8400.0 | 4013.0 |
| 5 | 7011.0 | 20300.0 | 3706.0 | 4122.0 |
| 6 | 3815.0 | 20300.0 | 9031.0 | 4122.0 |
| 7 | 3391.0 | 16950.0 | 9314.0 | 4677.0 |
| 8 | 3850.0 | 10770.0 | 9314.0 | 4677.0 |
| 9 | 3850.0 | 3921 | 4899 | 3898.0 |
| Hinge rotation | 0.0131 | 0.0012 | | |

Table B.9 Multi-modal pushover analysis section shears, in kN

| (1) Storey | (2) Mode 1 | (3) Mode 2 | (4) Mode 3 | (5) Mode 4 | (6) SRSS 3 modes | (7) SRSS 4 modes | difference |
|---------------|---------------|---------------|---------------|---------------|---------------------|---------------------|------------------|
| | | | | | | | (6) and (7) % |
| 1 | 5207.8 | 9404 | 9107 | 5302.0 | 14089.3 | 15053.9 | 6.85 |
| 2 | 5194.2 | 9175 | 8250 | 4104.2 | 13387.4 | 14002.4 | 4.59 |
| 3 | 5156.6 | 8586 | 6278.4 | 1731.3 | 11820.4 | 11946.5 | 1.07 |
| 4 | 5084.2 | 7552 | 3279.4 | 1113.9 | 9676.3 | 9740.2 | 0.66 |
| 5 | 4968.2 | 6075.2 | 218.0 | 3267.6 | 7851.0 | 8503.9 | 8.32 |
| 6 | 4803.0 | 4231.0 | 3486.4 | 3799.8 | 7288.7 | 8219.7 | 12.77 |
| 7 | 4582.8 | 2149.6 | 5798.4 | 2505.2 | 7697.0 | 8094.5 | 5.16 |
| 8 | 4305.4 | 1.2 | 6640.6 | 7.1 | 7914.2 | 7914.2 | 0.00 |
| 9 | 3968.6 | 2029.4 | 5846.4 | 2513.6 | 7351.8 | 7769.6 | 5.68 |
| 10 | 3572.2 | 3745.6 | 3652.8 | 3882.2 | 6335.1 | 7430.0 | 17.28 |
| 11 | 3116.4 | 4971.6 | 650.2 | 3472.6 | 5903.5 | 6849.1 | 16.02 |
| 12 | 2602.0 | 5560.6 | 2356.0 | 1512.2 | 6575.8 | 6747.5 | 2.61 |
| 13 | 2030.2 | 5404.6 | 4509.2 | 1005.7 | 7325.6 | 7394.3 | 0.94 |
| 14 | 1402.6 | 4434.6 | 5089.0 | 2749.8 | 6894.3 | 7422.4 | 7.66 |
| 15 | 721.46 | 2619.6 | 3630.2 | 2589.6 | 4534.4 | 5221.8 | 15.16 |

Table B.10 Multi-modal pushover analysis, inter-storey drifts

| (1) Storey | (2) Mode 1 | (3) Mode 2 | (4) Mode 3 | (5) Mode 4 | (6) SRSS 3 modes | (7) SRSS 4 modes | difference % (6) and (7) |
|---------------|---------------|---------------|---------------|---------------|------------------------|------------------------|--------------------------------|
| 1 | 0.01197 | 0.00318 | 0.00099 | 0.00038 | 0.01243 | 0.01243 | 0.05 |
| 2 | 0.01474 | 0.00523 | 0.00187 | 0.00054 | 0.01576 | 0.01576 | 0.06 |
| 3 | 0.01662 | 0.00595 | 0.00166 | 0.00021 | 0.01773 | 0.01773 | 0.01 |
| 4 | 0.01807 | 0.00581 | 0.00081 | 0.00030 | 0.01900 | 0.01900 | 0.01 |
| 5 | 0.01911 | 0.00494 | 0.00038 | 0.00071 | 0.01974 | 0.01975 | 0.06 |
| 6 | 0.01976 | 0.00347 | 0.00156 | 0.00080 | 0.02012 | 0.02014 | 0.08 |
| 7 | 0.02006 | 0.00161 | 0.00239 | 0.00053 | 0.02027 | 0.02027 | 0.03 |
| 8 | 0.02005 | 0.00102 | 0.00267 | 0.00001 | 0.02025 | 0.02025 | 0.00 |
| 9 | 0.01979 | 0.00290 | 0.00229 | 0.00051 | 0.02013 | 0.02014 | 0.03 |
| 10 | 0.01933 | 0.00462 | 0.00135 | 0.00079 | 0.01992 | 0.01993 | 0.08 |
| 11 | 0.01873 | 0.00606 | 0.00005 | 0.00069 | 0.01969 | 0.01970 | 0.06 |
| 12 | 0.01807 | 0.00722 | 0.00131 | 0.00025 | 0.01950 | 0.01951 | 0.01 |
| 13 | 0.01742 | 0.00795 | 0.00247 | 0.00033 | 0.01931 | 0.01931 | 0.01 |
| 14 | 0.01685 | 0.00828 | 0.00321 | 0.00082 | 0.01905 | 0.01907 | 0.09 |
| 15 | 0.01646 | 0.00833 | 0.00352 | 0.00107 | 0.01878 | 0.01881 | 0.16 |

Table B.11 Multi-modal pushover analysis, wall shear forces in kN

| (1) Storey | (2) Mode 1 | (3) Mode 2 | (4) Mode 3 | (5) Mode 4 | (6) SRSS 3 modes | (7) SRSS 4 modes | difference (6) and (7) % |
|---------------|---------------|---------------|---------------|---------------|------------------------|------------------------|--------------------------------|
| 1 | 2081.0 | 4287.0 | 4466.0 | 2600.0 | 6531.0 | 7029.5 | 7.63 |
| 2 | 2304.0 | 4326.0 | 3939.0 | 1978.0 | 6288.0 | 6591.7 | 4.83 |
| 3 | 1932.0 | 3894.0 | 2996.0 | 838.5 | 5279.4 | 5345.6 | 1.25 |
| 4 | 1880.0 | 3384.0 | 1561.0 | 529.7 | 4174.0 | 4207.5 | 0.80 |
| 5 | 1755.0 | 2678.0 | 83.5 | 1558.0 | 3202.9 | 3561.7 | 11.20 |
| 6 | 1596.0 | 1843.0 | 1607.0 | 1810.0 | 2920.0 | 3435.5 | 17.65 |
| 7 | 1397.0 | 933.2 | 2674.0 | 1191.0 | 3158.0 | 3375.1 | 6.88 |
| 8 | 1165.0 | 62.2 | 3054.0 | 3.5 | 3269.3 | 3269.3 | 0.00 |
| 9 | 904.8 | 807.2 | 2681.0 | 1190.0 | 2942.4 | 3174.0 | 7.87 |
| 10 | 623.7 | 1479.0 | 1674.0 | 1834.0 | 2319.2 | 2956.7 | 27.49 |
| 11 | 360.1 | 1918.0 | 311.7 | 1639.0 | 1976.2 | 2567.5 | 29.92 |
| 12 | 139.1 | 2074.0 | 1036.0 | 715.1 | 2322.5 | 2430.1 | 4.63 |
| 13 | 445.6 | 1867.0 | 1960.0 | 458.6 | 2743.3 | 2781.4 | 1.39 |
| 14 | 547.3 | 1434.0 | 2205.0 | 1276.0 | 2686.6 | 2974.2 | 10.71 |
| 15 | 2041 | 63.5 | 1220.0 | 1097.0 | 2378.7 | 2619.5 | 10.12 |

Table B.12 Multi-modal pushover analysis wall moments in kNm

| (1) Storey | (2) Mode 1 | (3) Mode 2 | (4) Mode 3 | (5) Mode 4 |
|----------------|------------|------------|------------|------------|
| 1 | 48190.0 | 48190.0 | 32000.0 | 13600.0 |
| 2 | 40180.0 | 27430.0 | 10340.0 | 6228.0 |
| 3 | 31800.0 | 12860.0 | 14970.0 | 9289.0 |
| 4 | 24900.0 | 14920.0 | 20670.0 | 9289.0 |
| 5 | 18990.0 | 24700.0 | 20670.0 | 7356.0 |
| 6 | 13620.0 | 31430.0 | 20360.0 | 4937.0 |
| 7 | 8826.0 | 34830.0 | 14500.0 | 9284.0 |
| 8 | 4650.0 | 34920.0 | 6407.0 | 9296.0 |
| 9 | 7801.0 | 34920.0 | 16190.0 | 9296.0 |
| 10 | 10050.0 | 31970.0 | 22300.0 | 4953.0 |
| 11 | 11140.0 | 26570.0 | 23440.0 | 7724.0 |
| 12 | 11140.0 | 19570.0 | 23440.0 | 10330.0 |
| 13 | 11070.0 | 12000 | 19660 | 10330.0 |
| 14 | 9445.0 | 5188 | 12500 | 8660.0 |
| 15 | 7449.0 | 231.8 | 4454 | 4004.0 |
| Hinge rotation | 0.0102 | 0.0015 | | |

Table B.13 Multi-modal pushover analysis section shears, in kN

| (1) Storey | (2) Mode 1 | (3) Mode 2 | (4) Mode 3 | (5) Mode 4 | (6) SRSS 3 modes | (7) SRSS 4 modes | difference (6) and (7) % |
|---------------|---------------|---------------|---------------|---------------|---------------------|---------------------|--------------------------------|
| 1 | 6415.6 | 11682 | 11340 | 6954.8 | 17499.5 | 18830.9 | 7.61 |
| 2 | 6408.4 | 11554 | 10843 | 6199.2 | 17092.3 | 18181.8 | 6.37 |
| 3 | 6388.0 | 11215 | 9615.2 | 4502.2 | 16094.6 | 16712.4 | 3.84 |
| 4 | 6348.0 | 10590 | 7548.6 | 1988.2 | 14471.9 | 14607.8 | 0.94 |
| 5 | 6283.2 | 9650.0 | 4762.0 | 825.0 | 12461.0 | 12488.3 | 0.22 |
| 6 | 6188.4 | 8390.6 | 1537.7 | 3264.2 | 10538.6 | 11032.6 | 4.69 |
| 7 | 6060.8 | 6843.6 | 1745.9 | 4717.0 | 9306.8 | 10433.9 | 12.11 |
| 8 | 5896.8 | 5062.8 | 4673.4 | 4817.8 | 9068.9 | 10269.2 | 13.24 |
| 9 | 5693.4 | 3122.6 | 6866.2 | 3560.8 | 9450.4 | 10099.0 | 6.86 |
| 10 | 5449.4 | 1115.5 | 8042.4 | 1299.9 | 9778.6 | 9864.6 | 0.88 |
| 11 | 5164.0 | 858.1 | 8055.6 | 1334.9 | 9607.1 | 9699.4 | 0.96 |
| 12 | 4835.0 | 2695.6 | 6927.6 | 3621.8 | 8867.6 | 9578.8 | 8.02 |
| 13 | 4463.4 | 4294.0 | 4842.4 | 4933.4 | 7861.9 | 9281.6 | 18.06 |
| 14 | 4048.2 | 5558.4 | 2126.4 | 4921.8 | 7197.6 | 8719.5 | 21.14 |
| 15 | 3590.4 | 6403.8 | 797.4 | 3607.4 | 7384.8 | 8218.8 | 11.29 |
| 16 | 3090.4 | 6761.0 | 3457.8 | 1380.9 | 8198.7 | 8314.1 | 1.41 |
| 17 | 2549 | 6578.6 | 5405.8 | 1090.0 | 8888.1 | 8954.7 | 0.75 |
| 18 | 1966.3 | 5818.0 | 6248.0 | 3037.4 | 8760.9 | 9272.5 | 5.84 |
| 19 | 1343.6 | 4461.0 | 5702.6 | 3765.0 | 7363.8 | 8270.5 | 12.31 |
| 20 | 681.56 | 2497.8 | 3606.2 | 2795.8 | 4439.4 | 5246.4 | 18.18 |

Table B.14 Multi-modal pushover analysis, inter-storey drifts

| (1) Storey | (2) Mode 1 | (3) Mode 2 | (4) Mode 3 | (5) Mode 4 | (6) SRSS 3 modes | (7) SRSS 4 modes | difference (6) and (7) % |
|---------------|---------------|---------------|---------------|---------------|------------------------|------------------------|--------------------------------|
| 1 | 0.00940 | 0.00243 | 0.00066 | 0.00027 | 0.00973 | 0.00973 | 0.04 |
| 2 | 0.01124 | 0.00390 | 0.00139 | 0.00049 | 0.01198 | 0.01199 | 0.08 |
| 3 | 0.01257 | 0.00467 | 0.00155 | 0.00041 | 0.01349 | 0.01350 | 0.05 |
| 4 | 0.01369 | 0.00500 | 0.00133 | 0.00015 | 0.01463 | 0.01463 | 0.01 |
| 5 | 0.01461 | 0.00492 | 0.00082 | 0.00018 | 0.01544 | 0.01544 | 0.01 |
| 6 | 0.01534 | 0.00449 | 0.00011 | 0.00049 | 0.01599 | 0.01600 | 0.05 |
| 7 | 0.01591 | 0.00374 | 0.00065 | 0.00067 | 0.01635 | 0.01637 | 0.08 |
| 8 | 0.01630 | 0.00274 | 0.00135 | 0.00067 | 0.01659 | 0.01660 | 0.08 |
| 9 | 0.01655 | 0.00156 | 0.00187 | 0.00050 | 0.01673 | 0.01674 | 0.04 |
| 10 | 0.01666 | 0.00040 | 0.00213 | 0.00018 | 0.01680 | 0.01680 | 0.01 |
| 11 | 0.01665 | 0.00161 | 0.00209 | 0.00018 | 0.01686 | 0.01686 | 0.01 |
| 12 | 0.01654 | 0.00281 | 0.00175 | 0.00049 | 0.01686 | 0.01687 | 0.04 |
| 13 | 0.01634 | 0.00392 | 0.00115 | 0.00066 | 0.01684 | 0.01685 | 0.08 |
| 14 | 0.01608 | 0.00491 | 0.00037 | 0.00065 | 0.01681 | 0.01683 | 0.07 |
| 15 | 0.01578 | 0.00572 | 0.00049 | 0.00045 | 0.01679 | 0.01680 | 0.04 |
| 16 | 0.01546 | 0.00635 | 0.00133 | 0.00012 | 0.01676 | 0.01676 | 0.00 |
| 17 | 0.01515 | 0.00677 | 0.00204 | 0.00026 | 0.01672 | 0.01672 | 0.01 |
| 18 | 0.01487 | 0.00702 | 0.00256 | 0.00061 | 0.01664 | 0.01666 | 0.07 |
| 19 | 0.01466 | 0.00714 | 0.00287 | 0.00084 | 0.01655 | 0.01657 | 0.13 |
| 20 | 0.01453 | 0.00715 | 0.00298 | 0.00095 | 0.01646 | 0.01649 | 0.17 |

Table B.15 Multi-modal pushover analysis, wall shear forces in kN

| (1) Storey | (2) Mode 1 | (3) Mode 2 | (4) Mode 3 | (5) Mode 4 | (6) SRSS 3 modes | (7) SRSS 4 modes | difference (6) and (7) % |
|---------------|---------------|---------------|---------------|---------------|------------------------|------------------------|--------------------------------|
| 1 | 2433.0 | 5437.0 | 5621.0 | 3447.0 | 8190.0 | 8885.8 | 8.50 |
| 2 | 2928.0 | 5620.0 | 5286.0 | 3038.0 | 8252.2 | 8793.7 | 6.56 |
| 3 | 2497.0 | 5281.0 | 4681.0 | 2208.0 | 7485.7 | 7804.5 | 4.26 |
| 4 | 2437.0 | 4953.0 | 3660.0 | 974.4 | 6623.2 | 6694.5 | 1.08 |
| 5 | 2281.0 | 4459.0 | 2307.0 | 397.5 | 5514.3 | 5528.6 | 0.26 |
| 6 | 2137.0 | 3840.0 | 754.8 | 1583.0 | 4458.9 | 4731.6 | 6.11 |
| 7 | 2006.0 | 3103.0 | 815.4 | 2287.0 | 3783.9 | 4421.3 | 16.85 |
| 8 | 1852.0 | 2277.0 | 2207.0 | 2333.0 | 3672.3 | 4350.7 | 18.47 |
| 9 | 1676.0 | 1398.0 | 3242.0 | 1723.0 | 3908.2 | 4271.1 | 9.29 |
| 10 | 1480.0 | 526.9 | 3791.0 | 628.4 | 4103.6 | 4151.5 | 1.17 |
| 11 | 1263.0 | 350.1 | 3790.0 | 643.1 | 4010.2 | 4061.5 | 1.28 |
| 12 | 1027.0 | 1129.0 | 3254.0 | 1744.0 | 3594.1 | 3994.9 | 11.15 |
| 13 | 803.4 | 1786.0 | 2274.0 | 2372.0 | 3001.1 | 3825.3 | 27.46 |
| 14 | 609.8 | 2281.0 | 1007.0 | 2365.0 | 2566.9 | 3490.3 | 35.97 |
| 15 | 405.9 | 2578.0 | 345.5 | 1732.0 | 2632.5 | 3151.2 | 19.70 |
| 16 | 189.2 | 2648.0 | 1562.0 | 667.2 | 3080.2 | 3151.6 | 2.32 |
| 17 | 409 | 2475.0 | 2435.0 | 510.3 | 3496.0 | 3533.1 | 1.06 |
| 18 | 745.2 | 2008.0 | 2764.0 | 1425.0 | 3496.7 | 3775.9 | 7.98 |
| 19 | 1050 | 1396.0 | 2494.0 | 1768.0 | 3044.9 | 3521.0 | 15.64 |
| 20 | 1646 | 176.3 | 1190.0 | 1193.0 | 2038.7 | 2362.1 | 15.86 |

Table B.16 Multi-modal pushover analysis wall moments in kNm

| (1) Storey | (2) Mode 1 | (3) Mode 2 | (4) Mode 3 | (5) Mode 4 |
|----------------|------------|------------|------------|------------|
| 1 | 80630.0 | 80630.0 | 53180.0 | 23630.0 |
| 2 | 72080.0 | 54360.0 | 25910.0 | 6917.0 |
| 3 | 61500.0 | 35210.0 | 10470.0 | 12230.0 |
| 4 | 52740.0 | 16830.0 | 23830.0 | 15790.0 |
| 5 | 44730.0 | 19780.0 | 32250.0 | 15790.0 |
| 6 | 37400.0 | 33800.0 | 35000.0 | 14340.0 |
| 7 | 30500.0 | 45120.0 | 35000.0 | 8557.0 |
| 8 | 24050.0 | 53440.0 | 32030.0 | 8307.0 |
| 9 | 18110.0 | 58540.0 | 23970.0 | 14590.0 |
| 10 | 12700.0 | 60390.0 | 12140.0 | 16890.0 |
| 11 | 7858.0 | 60390.0 | 15530.0 | 16890.0 |
| 12 | 8970.0 | 59110.0 | 27410.0 | 14540.0 |
| 13 | 11790.0 | 54990 | 35710 | 8176.0 |
| 14 | 13630.0 | 48470 | 39380 | 9114.0 |
| 15 | 14400.0 | 40140 | 39380 | 15440.0 |
| 16 | 14400.0 | 30730 | 38120 | 17870.0 |
| 17 | 14060.0 | 21070 | 32420 | 17870.0 |
| 18 | 12560.0 | 12030 | 23540 | 16010.0 |
| 19 | 9843.0 | 4706 | 13450 | 10810.0 |
| 20 | 6009.0 | 643.4 | 4344 | 4355.0 |
| Hinge rotation | 0.0083 | 0.0014 | | |

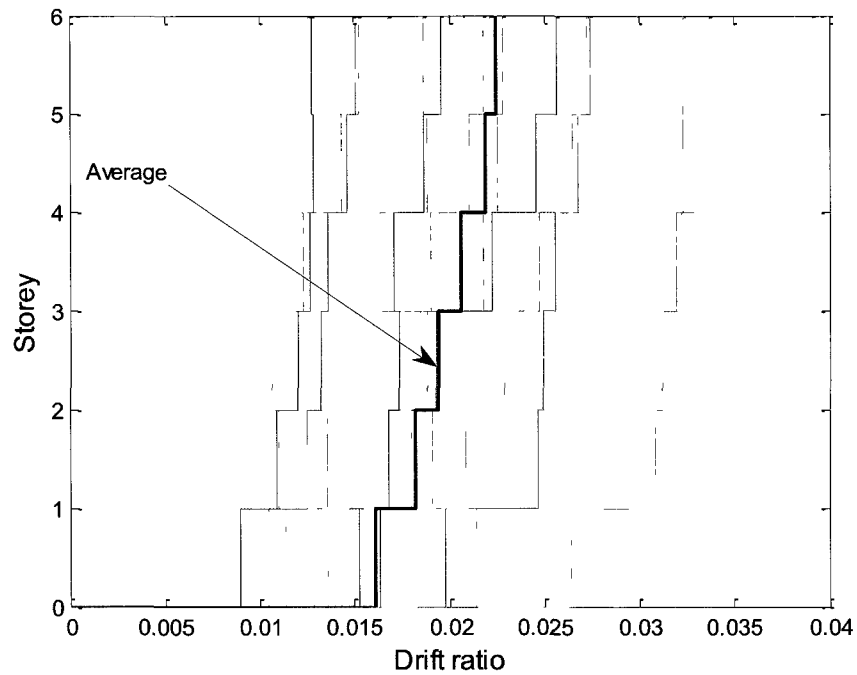


Figure B.1 Storey drift ratios obtained from 20 dynamic analyses and their average for 6-storey building

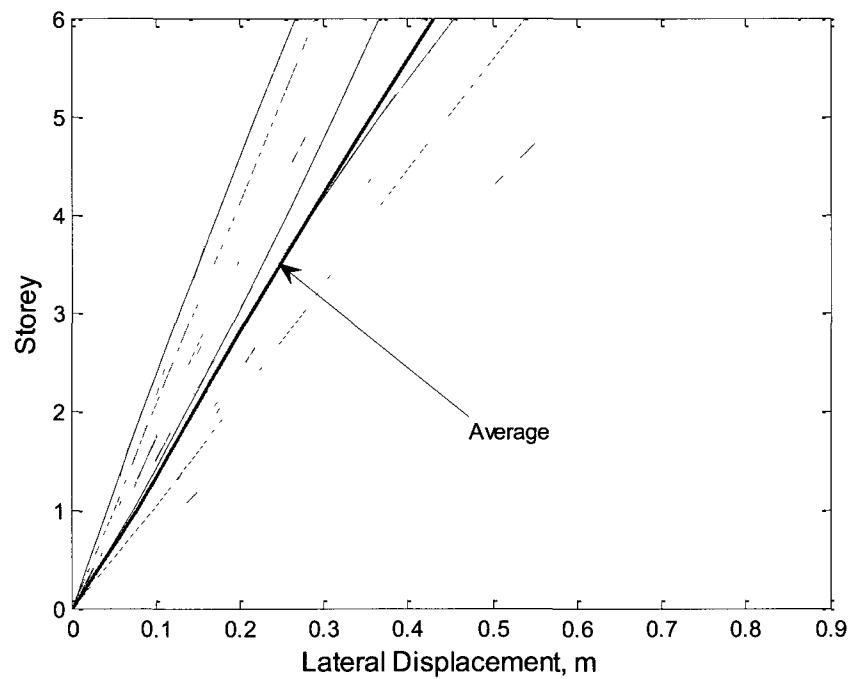


Figure B.2 Displacement profiles obtained from 20 dynamic analyses and their average for 6-storey building

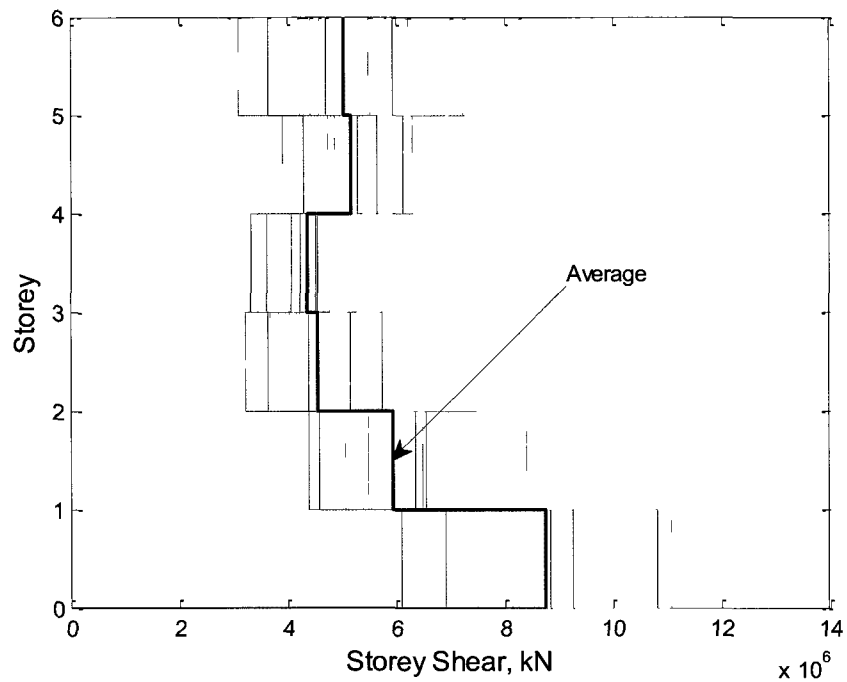


Figure B.3 Storey shears obtained from 20 dynamic analyses and their average for 6-storey building

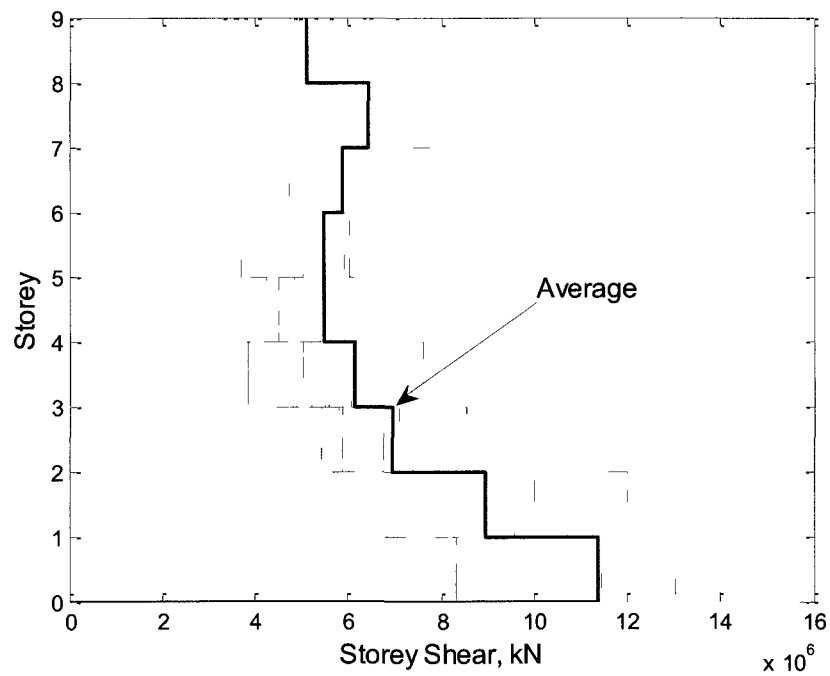


Figure B.4 Storey shears obtained from 20 dynamic analyses and their average for 9-storey building

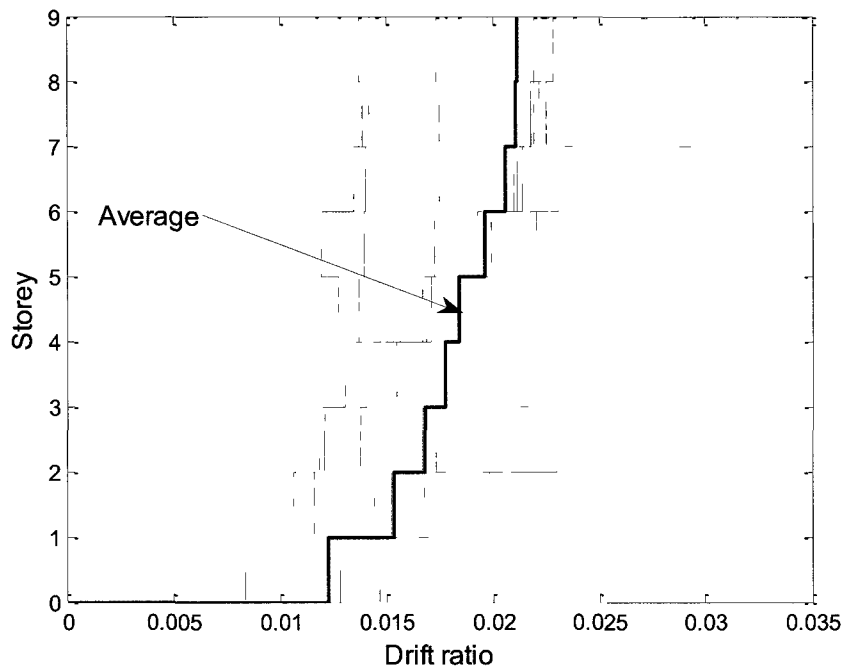


Figure B.5 Storey drift ratios obtained from 20 dynamic analyses and their average for 9-storey building

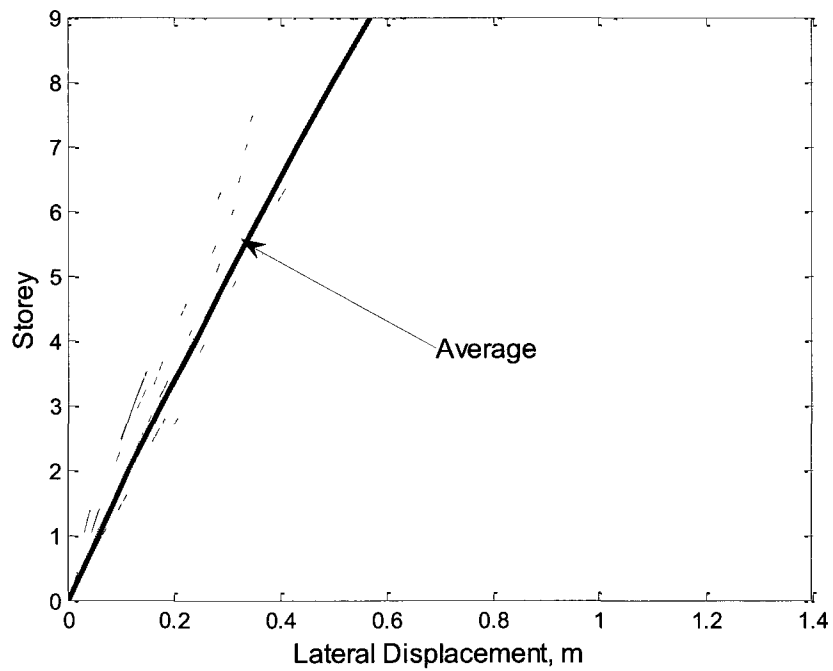


Figure B.6 Displacement profiles obtained from 20 dynamic analyses and their average for 9-storey building

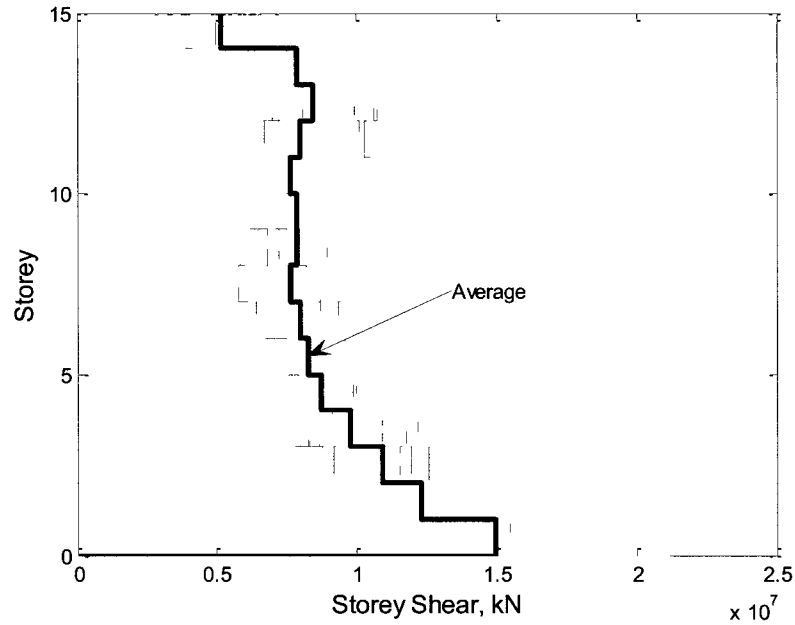


Figure B.7 Storey shears obtained from 20 dynamic analyses and their average for 15-storey building

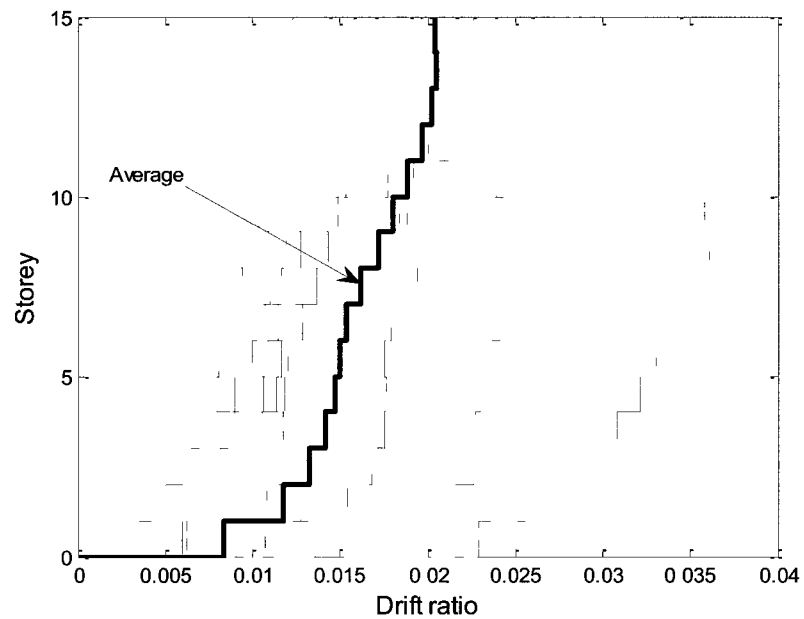


Figure B.8 Storey drift ratios obtained from 20 dynamic analyses and their average for 15-storey building

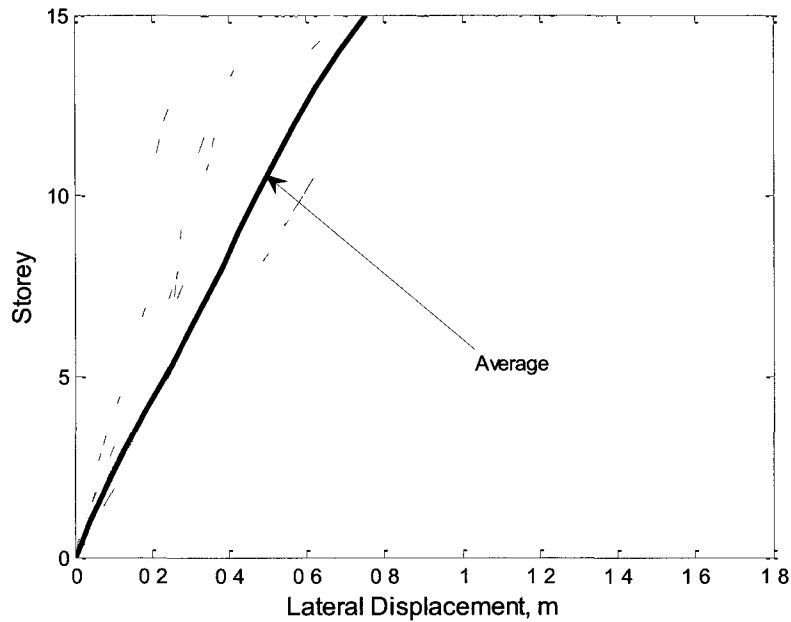


Figure B.9 Displacement profiles obtained from 20 dynamic analyses and their average for 15-storey building

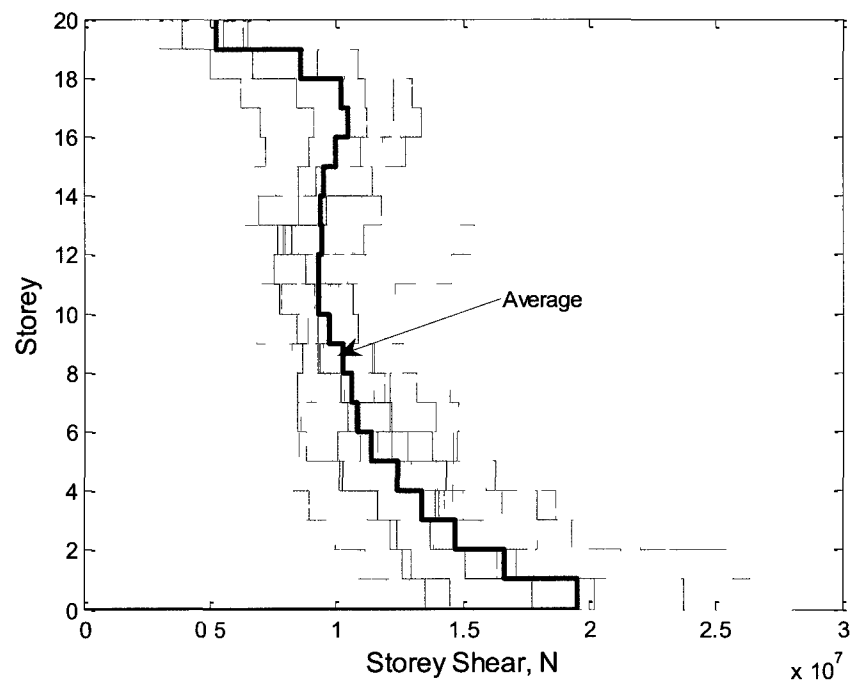


Figure B.10 Storey shears obtained from 20 dynamic analyses and their average for 20-storey building

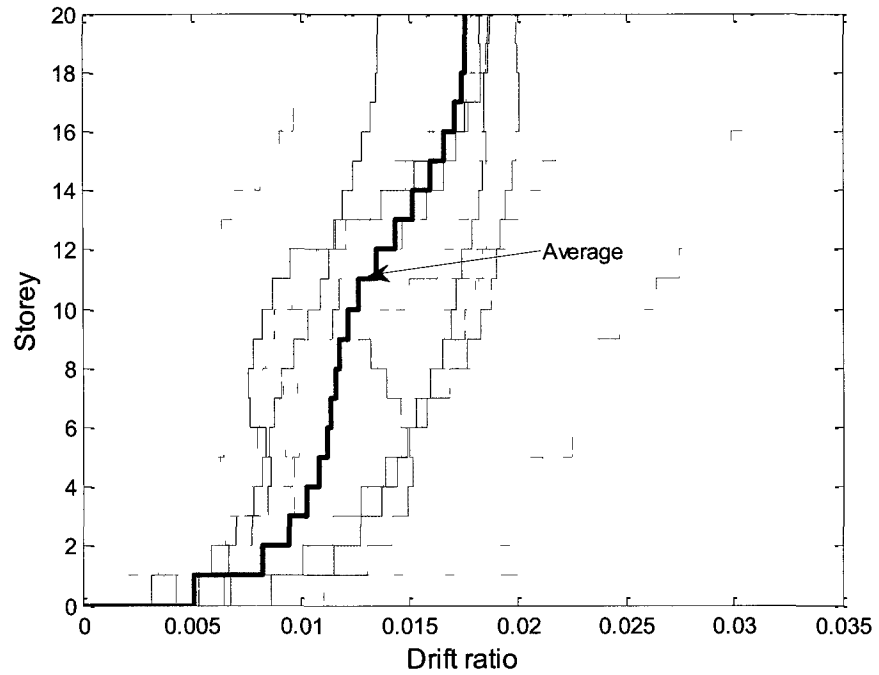


Figure B.11 Storey drift ratios obtained from 20 dynamic analyses and their average for 20-storey building

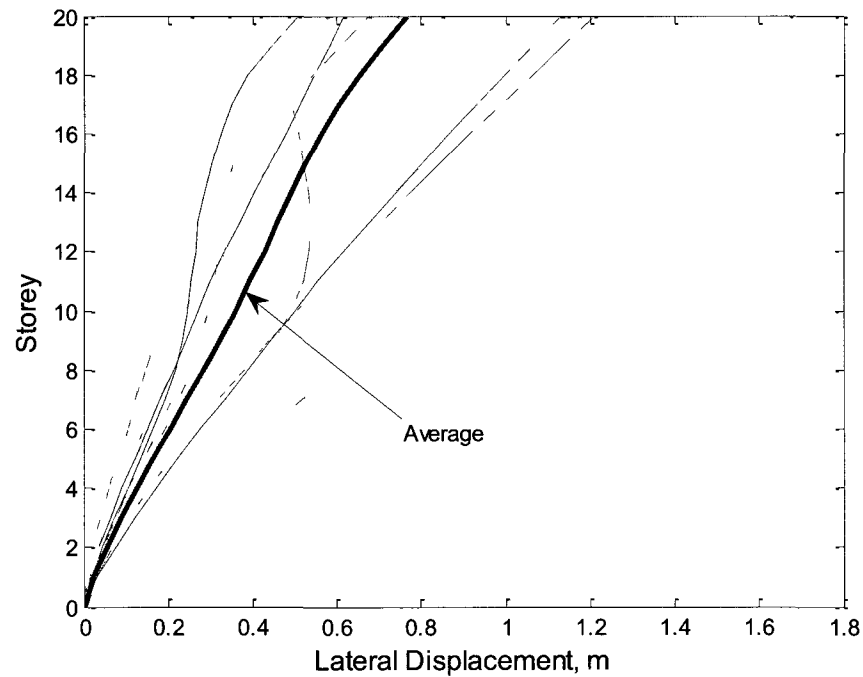


Figure B.12 Displacement profiles obtained from 20 dynamic analyses and their average for 20-storey building

C. Case studies for DBSD of asymmetric plan buildings

C.1 Torsionally stiff system

Consider the 12 storey system located in Vancouver (Ladner), whose plan is shown in Figure C.1. The floor dimension is 36 meter along the X axis, and 24 meter along the Y axis. The first storey is 4.85 m in height and the rest are 3.65 m high. The structural framing consists of 200 mm thick RC flat slab on 500 mm by 500 mm RC columns. The lateral resistance is provided by two 6.0 m by 0.4 m walls in the X direction and three walls in the Y direction. Of the Y direction walls the west and center walls are 5.0 m by 0.4 m, while the east wall is 7.0 m by 0.4 m. Floor dead load is 5.8 kPa, the live load is assumed to be 2.4 kPa, and the snow load is considered to be 2.2 kPa. The ultimate strength of concrete is assumed to be 30 MPa and the yield strength of the reinforcing, steel is taken as 400MPa. The modulus of elasticity of concrete is assumed to be 24,500 MPa.

Using the D+0.25S load case the first floor mass works out to 675.3 tonne and its mass moment of inertia as 105,347.2 tonne.m². The typical floors have a mass of 650.94 tonne with mass moment of inertia of 101,546 tonne.m²; the roof mass is 629.32 tonne and its mass moment of inertia is 98,174.1 tonne.m². The gravity loads at the base of each wall for D+0.5L+0.25S are shown in Table C.1. These loads will be used in the design of the walls sections.

C.1.1 Design of orthogonal planes

C.1.1.1 Yield and ultimate displacements

In the present study the orthogonal walls are assumed to be 6 meter in length. The ductility demand imposed on these walls by the code-prescribed drift limit is calculated as follows:

Wall yield curvature $\varphi_y = \frac{2.0\epsilon_y}{l_w} = 0.000667 \text{ } 1/\text{m}$

Roof level drift at yield $\theta_y = \varphi_y H/2 = 0.015$

Limit on plastic rotation $\theta_p = 0.025 - \theta_y = 0.01$

Wall yield displacement at roof $\Delta_y = \frac{\varphi_y H^2}{3} = 0.45 \text{ m}$

Total displacement at the roof level $\Delta_u = \Delta_y + (H - l_p/2) \times \theta_p = 0.885 \text{ m}$

Ductility demand $\mu = \frac{\Delta_u}{\Delta_y} = 1.967$

Displacement at level i $\Delta_{ui} = \Delta_{yi} + (h_i - l_p/2) \times \theta_p$

In the above, h_i is the height above base to level i , $H=45 \text{ m}$ is the total height of the building and l_p is the length of the plastic hinge of the wall assumed as being located at the base of the wall and having a length equal to half of the length of the wall. For preliminary design, we assume the displacement shape φ as being equal to Δ_{ui} normalized

so that the displacement at roof is 1. Using this deformed shape the properties of the SDOF can be obtained:

Participation factor

$$\Gamma = \frac{\varphi^T \mathbf{M} \mathbf{1}}{\varphi^T \mathbf{M} \varphi} = 1.523$$

Modal mass

$$M^* = \frac{(\varphi^T \mathbf{M} \mathbf{1})^2}{\varphi^T \mathbf{M} \varphi} = 0.697 M_i = 5448.1 \text{ tonne}$$

Ultimate displacement of SDOF

$$\delta_u = \frac{\Delta_u}{\Gamma} = 0.581$$

Yields displacement of SDOF

$$\delta_y = \frac{\Delta_y}{\Gamma} = 0.2954$$

C.1.1.2 Demand and capacity diagrams

The elastic design spectrum is obtained from the uniform hazard spectrum for 2% chance of exceedance in 50 years for Vancouver, which is provided in NBCC 2005. It should be mentioned that for periods greater than 4 second the spectral acceleration is assumed to decay inversely with period. The elastic and inelastic spectra, the latter for ductility of 1.967, are plotted in Figure C.2 in the acceleration-displacement format. The inelastic spectrum is entered with the ultimate displacement calculated above to obtain the spectral acceleration from which the design base shear is obtained as follows

$$V_b = 0.0275 g \times M^* = 0.0275 \times 9.81 \times 5448.1 = 1469.7 \text{ kN}$$

We distribute this base shear along the height in proportion to $\mathbf{M}\varphi$, where \mathbf{M} is the mass matrix and φ is the vector of ultimate storey displacements calculated earlier. These forces induce a moment of 24,290 kN.m at the base of each 6.0 m wall. We need to design the wall to withstand this moment in combination with the axial load.

The axial force due to the combination D+0.5L works out to 6074.3 kN. The minimum reinforcement in the wall with two layers of 100 mm^2 at 200 mm spacing and 2 layers of 800 mm^2 at each edge, gives a resisting moment of 25,050 kNm, yield curvature of $\varphi_y = 5.77 \times 10^{-4}$ per m, ultimate curvature at the concrete strain of 0.004, as $\varphi_u = 4.851 \times 10^{-3}$ per m, and the effective moment of inertia as 24.61% of the gross moment of inertia. The corresponding value of θ_p is:

$$\theta_p = (\varphi_u - \varphi_y) \times l_p = (0.004851 - 0.000577) \times 3.0 = 0.01282$$

The limit on plastic rotation works out to

$$\theta_p = 0.025 - \frac{\varphi_y H}{2} = 0.012$$

The limit on plastic rotation based on ductility limit is greater than plastic rotation at the base of the wall calculated for 0.025 inter-storey drift limit, therefore the drift limit governs. We will assume that the 6-m wall as designed is adequate and will continue further design process with 6-m orthogonal walls.

C.1.2 Design of planes along the axis of unsymmetry

After the orthogonal planes have been designed, planes along the axis of asymmetry can be designed according to the proposed procedure. The first step is to estimate the yield and ultimate displacements of the resisting planes.

C.1.2.1 Yield and ultimate displacements

The yield displacement of each wall can be obtained using the same empirical relations as presented earlier. Note that the calculations for 5-m wall represent both the center and the flexible walls while the 7-m wall is for the stiff wall.

Yield curvature of 5-m wall

$$\varphi_y = \frac{2.0\epsilon_y}{l_w} = 0.0008 \text{ } 1/\text{m}$$

Roof level yield displacement of 5-m wall

$$\Delta_y = \frac{\varphi_y H^2}{3} = 0.54 \text{ } \text{m}$$

Yield curvature of 7-m wall

$$\varphi_y = \frac{2.0\epsilon_y}{l_w} = 0.000571 \text{ } 1/\text{m}$$

Roof level yield displacement of 7-m wall

$$\Delta_y = \frac{\varphi_y H^2}{3} = 0.386 \text{ } \text{m}$$

Ultimate displacement of each wall can be estimated using the code-prescribed drift limit at the preliminary design stage as follows:

Plastic rotation of 5-m wall

$$\theta_p = 0.025 - \frac{\varphi_y H^2}{2} = 0.007$$

$$\text{Roof level ultimate displacement of 5-m wall} \quad \Delta_u = \Delta_y + (H - l_p/2) \times \theta_p = 0.846 \text{ m}$$

$$\text{Plastic rotation of 7-m wall} \quad \theta_p = 0.025 - \frac{\varphi_y H^2}{2} = 0.012$$

$$\text{Roof level ultimate displacement of 7-m wall} \quad \Delta_u = \Delta_y + (H - l_p/2) \times \theta_p = 0.911 \text{ m}$$

It may be noted that at this stage the limit on ultimate displacement as imposed by the other two criteria: (1) ductility capacity, and (2) stability under P–Δ effect is not available, therefore, the preliminary design will be carried out only for the ultimate displacement dictated by the code-prescribe drift limit.

C.1.2.2 Equivalent 2DOF system

In order to construct the equivalent 2DOF system, an eigenvalue problem needs to be solved to determine the mode shapes. The stiffness of the planes along the axis of asymmetry is unknown at the preliminary design stage; however, one can estimate the relative stiffness of different elements according to their relative strength. Here it is assumed that the base shear is distributed proportional to the length of the walls, therefore, 30 percent of the total base shear along the Y axis is assigned to each of the 5-m walls and 40 percent of the total base shear to the 7-m wall. Based on this assumption, the relative stiffnesses of the 7-m wall and 5-m walls will be related to the square of their length. Initial values of stiffnesses relative to the 6-m orthogonal wall are assigned on the same basis, and these relative stiffnesses are used to find the mode shapes. The first mode shape is obtained as follows:

$$\phi_1 = [0.000368, 0.001078, 0.002108, 0.003412, 0.004946, 0.006668, 0.008536, 0.010512, 0.012565, 0.014664, 0.016787, 0.018918, -0.000007706, -0.000023, -0.000044, -0.000072, -0.000104, -0.00014, -0.000179, -0.000221, -0.000264, -0.000308, -0.000353, -0.000398]^T$$

It should be mentioned that in the mode shape presented here the first twelve values are the components of the mode shape in the Y direction and the next twelve are the rotational components with counter-clockwise direction considered positive. The angle of twist Ψ_1 for the first mode determined from the first mode shape is calculated at the roof level as $-0.000398 / 0.018918$ which works out to -0.021 . Note that for torsionally stiff system only the first mode is used as the design mode. The equivalent yield and ultimate displacements at the centre of mass that correspond to the similar parameters for the edge walls are now obtained according to Equations (5.15) and (5.17) and are shown in Table C.2, where Δ_y^* and Δ_u^* denote the equivalent yield and ultimate displacements at the center of mass. For example, the equivalent yield and ultimate displacements at the center of mass for the 5-m wall are obtained from:

Equivalent yield displacement of flexible wall $\Delta_y^* = \frac{0.54}{1 + (-18) \times (-0.021)} = 0.392$

Equivalent ultimate displacement of flexible wall $\Delta_u^* = \frac{0.846}{1 + (-18) \times (-0.021)} = 0.614$

Note that while the yield and ultimate displacements of flexible and center walls are the same, their equivalent yield and ultimate displacements at the center of mass are

different. Next, the global yield displacement is calculated from the Δ_y^* values for individual walls as follows:

$$\text{Global yield displacement} \quad \Delta_y = \frac{\sum V}{\sum k} = \frac{1}{0.3/0.392 + 0.3/0.54 + 0.4/0.620} = 0.509 \text{ m}$$

The global ultimate displacement will be the minimum of the equivalent ultimate displacements for three walls as entered in Table 1.2 (0.614, 0.846, 1.465) that is 0.614 m. The corresponding ductility is given by:

$$\text{Ductility demand} \quad \mu = \frac{\Delta_u}{\Delta_y} = 1.207$$

The ultimate and yield displacement of the equivalent 2DOF system can be obtained from the first mode shape as:

$$\text{Participation factor} \quad \Gamma_1 = \frac{\varphi_{y1}^T \mathbf{m} \mathbf{1}}{\varphi_1^T \mathbf{M} \varphi_1} = 1.488$$

$$\text{Modal mass} \quad M_1^* = \frac{(\varphi_{y1}^T \mathbf{m} \mathbf{1})^2}{\varphi_1^T \mathbf{M} \varphi_1} = 5118.52 \text{ tonne}$$

$$\text{Ultimate displacement of SDOF} \quad \delta_{u1} = \frac{\Delta_u}{\Gamma_1} = \frac{0.614}{1.488} = 0.4126$$

$$\text{Yield displacement of SDOF} \quad \delta_{y1} = \frac{\Delta_y}{\Gamma_1} = \frac{0.509}{1.488} = 0.3421$$

where ϕ_{y1} is the lateral component of the first mode shape.

C.1.2.3 Capacity demand diagram

The inelastic spectrum shown in Figure C.3 is entered with the ultimate displacement calculated above to obtain the spectral acceleration from which the design base shear and base torque are obtained as follows:

$$V_b = 0.06474 g \times M_1^* = 3250.77 \text{ kN}$$

$$T_b = 0.06474 g \times I_{O1}^* = 10659.06 \text{ kNm}$$

Forty percent of this base shear is assigned to 7-m wall and the rest equally to the two 5-m walls. Based on this assignment the moment demand at the base of 7-m wall works out to 43,885.4 kNm and at the base of 5-m walls to 32,914.0 kNm. We design the walls for these base moments acting together with the axial loads due to gravity. The details of the design are shown in the Table C.3. Minimum distributed reinforcement is found to be 200 mm² every 200 mm which is shown as 200@200 in Table C.3 and the concentrated reinforcements at the edge of the walls are expressed in mm². The elastic parameters entered in Table C.3 are based on moment-curvature analyses of the wall sections; I_e is the effective moment of inertia and I_g is the gross moment of inertia.

The demand torque and the additional torque due to asymmetry caused by the assignment of base shear to 5-m and 7-m walls, as shown in Figure C.4, are to be resisted

by the orthogonal walls. The shear demand on each of the orthogonal walls can be calculated as:

$$\text{Shear demand} = [10659.06 + (0.4 - 0.3) \times 3250.77 \times 18]/24 = 687.94 \text{ kN}$$

This shear demand on the orthogonal walls causes a base moment of 23,217.8 kNm, which is smaller than the current capacity of the orthogonal walls that is 25,050 kNm. Therefore, the orthogonal walls do not need to be re-designed.

C.1.2.4 First iteration

The yield and ultimate displacements of the walls as well as their equivalent values at the center of mass are updated according to results of moment-curvature analysis of wall sections and the new angle of twist of $\Psi_1=0.0243$ obtained from the eigenvalue analysis of the structure. Such an analysis is carried out with the new values of the effective section moments of inertia as shown in Table C.4. The corresponding global yield displacement is calculated as:

$$\text{Global yield displacement } \Delta_y = \frac{\sum V}{\sum k} = \frac{1}{0.3/0.335 + 0.3/0.504 + 0.4/0.582} = 0.459 \text{ m}$$

The ultimate displacement as governed by ductility capacity is the minimum of those determined for the three walls, that is 0.673 meter. The limiting values of the

ultimate displacement as governed by P–Δ stability and code-prescribed drift limit are presented in the following section.

C.1.2.5 Pushover analysis

A pushover analysis is now carried out with lateral forces and torques applied at the center of mass using the first mode load shape. Figure C.5 shows the resulting pushover curves with and without the P–Δ effect. Total base shear goes up to 2806 kN at the global yield displacement of 0.445 meter; which is close to our estimate of 0.459 meter. The 95 percent decay in the base shear is reached at roof displacement of 0.549 meter which is assumed to be the ultimate displacement to prevent P–Δ instability.

The equivalent ultimate displacement at the center of mass based on drift limit works out to 0.557 meter, where the roof at the flexible side reaches the 2.5% limit first. Therefore, among the ductility limit, drift limit and the stability limit; the ultimate displacement of the structure is controlled by the stability limit which is 0.549 meter.

C.1.2.6 Equivalent 2DOF system

The next step is to construct the equivalent 2DOF system. The dynamic properties of the system are as follows:

Ductility demand

$$\mu = \frac{\Delta_u}{\Delta_y} = \frac{0.549}{0.445} = 1.234$$

Participation factor

$$\Gamma_1 = \frac{\varphi_{y1}^T \mathbf{m} \mathbf{1}}{\varphi_1^T \mathbf{M} \varphi_1} = 1.363$$

Modal mass

$$M_1^* = \frac{(\varphi_{y1}^T \mathbf{m} \mathbf{1})^2}{\varphi_1^T \mathbf{M} \varphi_1} = 4677.7 \text{ tonne}$$

Ultimate displacement of SDOF

$$\delta_{u1} = \frac{\Delta_u}{\Gamma_1} = \frac{0.549}{1.363} = 0.403$$

Yields displacement of SDOF

$$\delta_{y1} = \frac{\Delta_y}{\Gamma_1} = \frac{0.445}{1.363} = 0.326$$

The inelastic spectrum as shown in Figure C.6 is entered with the ultimate displacement calculated above to obtain the spectral acceleration from which the design base shear is obtained as follows

$$V_b = 0.0646 g \times M_1^* = 2964.38 \text{ kN}$$

$$T_b = 0.0646 g \times I_{O1}^* = 11241.6 \text{ kNm}$$

Forty percent of this base shear is assigned to 7-m wall and the rest equally to the 5-m walls. Based on this assignment the moment demand at the base of 7-m wall works out to 40,019 kNm and at the base of 5-m walls to 30,014 kNm. We design the walls for these base moments in association with the axial loads due to gravity. The details of the design are shown in the Table C.5.

The demand torque and the additional torque caused by the assignment of base shear to 5-m and 7-m walls must be resisted by the orthogonal walls. The resulting shear demand on each of the orthogonal walls is calculated as follows:

$$\text{Shear demand} = [11241.6 + (0.4 - 0.3) \times 2964.38 \times 18]/24 = 690.73 \text{ kN}$$

This shear demand causes a base moment of 23,312 kNm, which is smaller than the current capacity of the orthogonal walls, 25,050 kNm. Therefore, the orthogonal walls do not need to be re-designed.

C.1.2.7 Second iteration

The updated value of the yield and ultimate displacements of the walls and their equivalent values at the center of mass for the first mode angle of twist of $\Psi_1=0.0236$ are calculated and are shown in Table C.6. The global yield displacement of the system is obtained from:

$$\text{Global yield displacement } \Delta_y = \frac{\sum V}{\sum k} = \frac{1}{0.3/0.334 + 0.3/0.502 + 0.4/0.574} = 0.456 \text{ m}$$

The ultimate displacement as governed by the ductility capacity is the minimum of those for the three walls, which is 0.690 meter.

C.1.2.8 Pushover analysis

We run a pushover analysis for lateral forces and torques applied at the center of mass, using the first mode load shape. Figure C.7 shows the resulting pushover curves with and without the P–Δ effect. Total base shear goes up to 2586 kN at the global yield displacement of 0.445 meter. The 5 percent decay in the base shear is traced at roof displacement of 0.594 meter. The ultimate displacement at the center of mass based on the code-prescribed drift limit works out to 0.709 meter, where the roof of the flexible side reaches the limit first.

Among the ductility limit, drift limit and the stability limit (0.690, 0.709, 0.594); the ultimate displacement of the structure is controlled by the stability limit which is 0.594 meter.

C.1.2.9 Equivalent 2DOF system

Based on the updated values of the ultimate and yield displacement new estimate for system ductility is obtained and the dynamic properties of the equivalent 2DOF system are updated as follow:

Ductility demand

$$\mu = \frac{\Delta_u}{\Delta_y} = \frac{0.594}{0.445} = 1.335$$

Participation factor

$$\Gamma_1 = \frac{\varphi_{yl}^T \mathbf{m1}}{\varphi_1^T \mathbf{M} \varphi_1} = 1.370$$

Modal mass

$$M_1^* = \frac{(\varphi_{y1}^T \mathbf{m} \mathbf{1})^2}{\varphi_1^T \mathbf{M} \varphi_1} = 4701.9 \text{ tonne}$$

Ultimate displacement of SDOF

$$\delta_{u1} = \frac{\Delta_u}{\Gamma_1} = \frac{0.594}{1.370} = 0.434$$

Yields displacement of SDOF

$$\delta_{y1} = \frac{\Delta_y}{\Gamma_1} = \frac{0.445}{1.370} = 0.325$$

New inelastic spectrum is constructed as shown in Figure C.8. The spectrum is entered at the ultimate displacement as calculated above, to estimate the spectral acceleration from which the design base shear is obtained as follows:

$$V_b = 0.0553g \times M_1^* = 2550.75 \text{ kN}$$

$$T_b = 0.0553g \times I_{O1}^* = 9373.74 \text{ kNm}$$

This demand base shear of 2550.75kN is very close to base shear capacity of 2586 kN, therefore the design is assumed to have converged.

C.2 Torsion flexible system

Consider the 12 storey building located in Vancouver (Ladner), whose plan is shown in Figure C.9. This building is similar to the torsionally stiff system respecting all the dimensions, applied gravity loads, and material properties. However, the edge walls are located closer to the center of the mass, so that the torsional stiffness is reduced and the structure becomes torsionally flexible.

The floor masses and mass moments of inertia are also the same as for the torsionally stiff building for the load case of D+0.25S. The gravity loads at the base of each wall for D+0.5L+0.25S are shown in Table C.7 and have been calculated on the basis of the tributary areas of individual walls.

C.2.1 Design of orthogonal planes

The initial design of the orthogonal planes is identical to that for the torsionally stiff system presented in Section C.1.1 and the design base shear is found to be 1469.7 kN. This design base shear induces a moment demand of 24,290 kN.m when distributed in proportion to $M\phi$ along the height. We need to design the wall to withstand this moment in combination with the axial load.

The axial force on each of the orthogonal walls due to the combination D+0.5L is different from that for torsionally stiff system and works out to 5173.43 kN. The minimum distributed reinforcement in the wall consists of two layers of 100 mm^2 at 200 mm spacing. Concentrated reinforcement consists of 2 layers of 1200 mm^2 at each edge. This reinforcement gives a resisting moment of 24,720 kNm, yield curvature of $\phi_y = 5.653 \times 10^{-4}$ per m, ultimate curvature at the concrete strain of 0.004 of $\phi_u = 5.404 \times 10^{-3}$ per m, and effective moment of inertia equal to 24.79% of the gross moment of inertia. The corresponding value of θ_p is:

$$\theta_p = (\phi_u - \phi_y) \times l_p = (0.005404 - 0.0005653) \times 3.0 = 0.0145$$

The limit on plastic rotation works out to

$$\theta_p = 0.025 - \frac{\varphi_y H}{2} = 0.0123$$

The plastic rotation based on ductility capacity is greater than the plastic rotation calculated for 0.025 inter-storey drift limit, therefore the latter governs. We will therefore assume that the 6-m wall is adequate as designed and will continue further design process with 6-m orthogonal walls.

C.2.2 Design of planes along the axis of unsymmetry

C.2.2.1 Yield and ultimate displacements

The yield displacement of each wall can be obtained using the same empirical relations as employed earlier. Note that the calculations for 5-m wall represent both the center and the flexible walls while the 7-m wall is for the stiff wall.

Yield curvature of 5-m wall

$$\varphi_y = \frac{2.0\epsilon_y}{l_w} = 0.0008 \text{ } 1/\text{m}$$

Roof level yield displacement of 5-m wall

$$\Delta_y = \frac{\varphi_y H^2}{3} = 0.54 \text{ } \text{m}$$

Yield curvature of 7-m wall

$$\varphi_y = \frac{2.0\epsilon_y}{l_w} = 0.000571 \text{ } 1/\text{m}$$

Roof level yield displacement of 7-m wall

$$\Delta_y = \frac{\varphi_y H^2}{3} = 0.386 \text{ } \text{m}$$

At this preliminary design stage, the ultimate displacement of each wall can be estimated using the code-prescribed drift limit as follows:

Plastic rotation of 5-m wall

$$\theta_p = 0.025 - \frac{\varphi_y H^2}{2} = 0.007$$

Roof level ultimate displacement of 5-m wall $\Delta_u = \Delta_y + (H - l_p/2) \times \theta_p = 0.846 \text{ m}$

Plastic rotation of 7-m wall

$$\theta_p = 0.025 - \frac{\varphi_y H}{2} = 0.012$$

Roof level ultimate displacement of 7-m wall $\Delta_u = \Delta_y + (H - l_p/2) \times \theta_p = 0.911 \text{ m}$

C.2.2.2 Equivalent yield and ultimate displacements

In order to construct the equivalent 2DOF system, an eigenvalue problem needs to be solved and mode shapes determined. The stiffness of the planes along the axis of asymmetry is unknown at the preliminary design stage, but one can estimate the relative stiffness of different elements according to their relative strength. Here it is assumed that 30 percent of the total base shear along the Y axis is assigned to each of the 5-m walls and 40 percent of the total base shear to the 7-m wall. Based on this assumption, the relative stiffnesses of the 7-m wall and 5-m walls will be related to the square of their length. Initial values of stiffnesses relative to the 6-m orthogonal wall are assumed to find the mode shapes.

The angles of twist Ψ_1 and Ψ_2 based on modal analysis are found to be -0.0586 and 0.1094 for first and second modes, respectively. The deformed configuration based on

normalized mode shapes at roof level is shown in Figure C.12. As observed from that figure, the first mode imposes larger relative displacement demand on the flexible side and the second mode causes larger relative displacement demand on the stiff side of the plan.

The yield and ultimate displacements at the center of mass that correspond to the similar displacements of the edge walls are determined according to the procedure described earlier, and are shown in Table C.8. It will be noted that for the flexible plane the ultimate displacement is controlled by the first mode, while the displacement for the stiff plane is controlled by the second mode. The ultimate displacement corresponding to the code-prescribed limit should be selected such that the inter-storey drift ratio does not exceed 0.025 on the edges of the building. This displacement is calculated based on the drift ratio at the roof level using an appropriate mode shape from Equations (5.18) and (5.19). The second mode governs for the stiff edge, which reaches the drift limit when the displacement at the center of mass is 0.2717 m. The first mode shape governs for the flexible side edge, which reaches the drift limit of 0.025 when the displacement at the center of mass is 0.3925 m.

The ductility demand related to the flexible plane based on first mode =

$$\frac{0.3925}{0.368} = 1.07$$

The ductility demand related to the stiff plane based on the second mode =

$$\frac{0.2717}{0.206} = 1.32$$

Two design base shears will be calculated for the first two modes and the structure will be designed for the greater of the two.

C.2.2.3 Equivalent 2DOF system for the first mode

Dynamic properties of equivalent 2DOF system for the first mode shape are calculated as follows:

Participation factor

$$\Gamma_1 = \frac{\varphi_{y1}^T \mathbf{m1}}{\varphi_1^T \mathbf{M} \varphi_1} = 0.9893$$

Modal mass

$$M_1^* = \frac{(\varphi_{y1}^T \mathbf{m1})^2}{\varphi_1^T \mathbf{M} \varphi_1} = 3326.1 \text{ tonne}$$

Ultimate displacement of SDOF

$$\delta_{ul} = \frac{\Delta_u}{\Gamma_1} = 0.3967$$

Yields displacement of SDOF

$$\delta_{yl} = \frac{\Delta_y}{\Gamma_1} = 0.372$$

The inelastic spectrum for the ductility corresponding to the first mode is shown in Figure C.13 and it is entered with the ultimate displacement calculated above to obtain the spectral acceleration from which the design base shear and base torque are obtained as follows:

$$V_{bl} = 0.0755 \times 9.81 \times 3326.1 = 2,463.5 \text{ kN}$$

$$T_{bl} = 0.0755 \times 9.81 \times -30415 = -22,527 \text{ kNm}$$

C.2.2.4 Equivalent 2DOF system for the second mode

Dynamic properties of equivalent 2DOF system for the second mode shape are calculated as follows:

Participation factor

$$\Gamma_2 = \frac{\varphi_{y2}^T \mathbf{m} \mathbf{1}}{\varphi_2^T \mathbf{M} \varphi_2} = 0.5196$$

Modal mass

$$M_2^* = \frac{(\varphi_{y2}^T \mathbf{m} \mathbf{1})^2}{\varphi_2^T \mathbf{M} \varphi_2} = 1782.9 \text{ tonne}$$

Ultimate displacement of SDOF

$$\delta_{u2} = \frac{\Delta_u}{\Gamma_2} = 0.523$$

Yields displacement of SDOF

$$\delta_{y2} = \frac{\Delta_y}{\Gamma_2} = 0.398$$

The design base shear and base torque are obtained from the spectral acceleration that is found by entering the ultimate displacement calculated above in the inelastic spectrum for the ductility corresponding to the second mode shown in Figure C.14, as:

$$V_{b2} = 0.0467 \times 9.81 \times 1782.9 = 816.79 \text{ kN}$$

$$T_{b2} = 0.0467 \times 9.81 \times 30415 = 13,934 \text{ kNm}$$

The first mode design shear and torque are much greater than the second mode; therefore the structure will be designed for the first mode base shear and torque demand.

C.2.2.5 First iteration

Forty percent of the design base shear is assigned to 7-m wall and the rest is assigned equally to the two 5-m walls. Based on this assignment the moment demand at the base of 7-m wall works out to be 33,257.25 kNm and at the base of 5-m walls to be 24,942.9 kNm. We design the walls for these base moments accompanied by the axial loads due to gravity. The details of the design are shown in the Table C.9. The demand torque and the additional torque due to asymmetry of assigning base shear are to be resisted by the orthogonal walls. Therefore the shear demand on each of the orthogonal walls is calculated from:

$$\text{Shear demand} = [22527 + (0.4 - 0.3) * 2463.5 * 8]/24 = 1020.7 \text{ kN}$$

This shear demand causes a base moment of 34448.9 kN, which is greater than the current capacity of the orthogonal walls therefore, they need to be re-designed. The revised design of the orthogonal walls is also shown in Table C.9 and Figure C.15.

Having the properties of all five walls, the periods and angles of twist for the first two modes are determined and are shown in Table C.10. Based on the updated estimates of the angles of twist and walls section properties, yield and ultimate displacements of the walls and their equivalents at the center of mass are calculated as shown in Table C.11.

C.2.2.6 Pushover analysis

Pushover analyses for the first two modes are carried out next for lateral forces and torques applied at the center of mass to obtain the ultimate displacements based on code-prescribed drift limit and the limit to prevent global instability under P-Δ effect. The first mode pushover shows that the flexible edge reaches the drift limit for a displacement of 0.43 at the center of mass. The second mode pushover indicates that stiff edge reaches the drift limit of 0.025 when the displacement at the center of mass is 0.30.

Figure C.16 shows the pushover curves for the first two modes with and without the P-Δ effects. In the first mode, the ultimate displacement for 5% decrease in shear capacity due to P-Δ effect is 0.61 m, while in the second mode the capacity drops by 5% at a displacement of 0.77 m at the center of mass.

The ultimate displacement for the first mode is the least of (0.601, 0.43, 0.61), while the ultimate displacement for the second mode is the least of (0.484, 0.30, 0.77). It will be noted that for both modes the drift limit governs the ultimate displacements. From Figure C.16 it is seen that the yield displacement for first mode is 0.42 m, while it is 0.25 for the second mode.

$$\text{The ductility demand for the first mode} = \frac{0.43}{0.42} = 1.023$$

$$\text{The ductility demand for the second mode} = \frac{0.30}{0.25} = 1.20$$

Two design base shears will be calculated, one for each of the first two modes and the structural elements will be designed for the effect of the greater of the two.

C.2.2.7 Equivalent 2DOF system for the first mode

Dynamic properties of equivalent 2DOF system for the first mode shape are calculated as follows:

Participation factor

$$\Gamma_1 = \frac{\varphi_{y1}^T \mathbf{m} \mathbf{1}}{\varphi_1^T \mathbf{M} \varphi_1} = 1.0062$$

Modal mass

$$M_1^* = \frac{(\varphi_{y1}^T \mathbf{m} \mathbf{1})^2}{\varphi_1^T \mathbf{M} \varphi_1} = 3452.6 \text{ tonne}$$

Ultimate displacement of SDOF

$$\delta_{u1} = \frac{\Delta_u}{\Gamma_1} = 0.427$$

Yields displacement of SDOF

$$\delta_{y1} = \frac{\Delta_y}{\Gamma_1} = 0.417$$

The spectral acceleration for the first mode is determined from the inelastic spectrum curve shown in Figure C.17. The design base shear and base torque are then calculated as follows:

$$V_{b1} = 0.0735 \times 9.81 \times 3452.6 = 2,489.44 \text{ kN}$$

$$T_{b1} = 0.0735 \times 9.81 \times -29868 = -21,535.9 \text{ kNm}$$

C.2.2.8 Equivalent 2DOF system for the second mode

Dynamic properties of equivalent 2DOF system for the second mode shape are calculated as follows:

Participation factor

$$\Gamma_2 = \frac{\varphi_{y2}^T \mathbf{m1}}{\varphi_2^T \mathbf{M} \varphi_2} = 0.4827$$

Modal mass

$$M_2^* = \frac{(\varphi_{y2}^T \mathbf{m1})^2}{\varphi_2^T \mathbf{M} \varphi_2} = 1656.3 \text{ tonne}$$

Ultimate displacement of SDOF

$$\delta_{u2} = \frac{\Delta_u}{\Gamma_2} = 0.6215$$

Yields displacement of SDOF

$$\delta_{y2} = \frac{\Delta_y}{\Gamma_2} = 0.5179$$

The spectral acceleration for the second mode is determined from the inelastic spectrum curve shown in Figure C.18. The design base shear and base torque are then calculated as follows:

$$V_{b2} = 0.0432 \times 9.81 \times 1656.3 = 701.93 \text{ kN}$$

$$M_{b2} = 0.0432 \times 9.81 \times 29868 = 12657.82 \text{ kNm}$$

The first mode design shear and torque are much greater than those in the second mode. Also they are very close to those determined in the last iteration, the difference being about 1 percent in shear and 4 percent in the torque. The design may therefore be assumed to have converged.

Table C.1: Axial loads due to the gravity load combination D+0.5L+0.25S

| | 7 m stiff | 5m center | 5m flexible | 6m orthogonal |
|-------------------------|------------|------------|-------------|---------------|
| Loads at the base level | 6506.32 kN | 9281.43 kN | 5688.4 kN | 6074.32 |

Table C.2: Ultimate and yield displacements of walls and equivalent values at the mass center

| Parameter | 5-m Flexible | 5-m Center | 7-m Stiff |
|-----------------|--------------|------------|-----------|
| ϕ_y 1/m | 8E-04 | 8E-04 | 5.71E-4 |
| Δ_y m | 0.540 | 0.540 | 0.385 |
| Δ_u m | 0.846 | 0.846 | 0.911 |
| Δ_{y*} m | 0.392 | 0.540 | 0.620 |
| Δ_{u*} m | 0.614 | 0.846 | 1.465 |

Table C.3: Details of the design of the walls

| | 5-m Flexible | 5-m Center | 7-m Stiff |
|-----------------|---|-----------------------------------|-----------------------------------|
| Axial load (kN) | 5688.4 | 9281.43 | 6506.32 |
| Reinforcements | <u>2 layers of 3700 + 1 layer of 2800 + 200@200</u> | <u>2 layers of 3000 + 200@200</u> | <u>2 layers of 3000 + 200@200</u> |
| ϕ_y | 7.136E-04 | 7.465E-04 | 4.849E-04 |
| ϕ_u | 5.151E-03 | 3.652E-03 | 4.39E-03 |
| I_e/I_g | 0.4645 | 0.4345 | 0.3216 |
| M_y (kNm) | 33,840 | 33,110 | 43,680 |

Table C.4: Wall yield and ultimate displacements as governed by ductility capacity

| Parameter | 5-m Flexible | 5-m Center | 7-m Stiff |
|----------------|--------------|------------|-----------|
| ϕ_y 1/m | 7.14E-04 | 7.47E-04 | 4.85E-04 |
| ϕ_u 1/m | 5.15E-03 | 3.65E-03 | 4.39E-03 |
| Δ_y m | 0.482 | 0.504 | 0.327 |
| Δ_u m | 0.967 | 0.822 | 0.918 |
| Δ^*_y m | 0.335 | 0.504 | 0.582 |
| Δ^*_u m | 0.673 | 0.822 | 1.632 |

Table C.5: Details of the design of walls

| | 5-m Flexible | 5-m Center | 7-m Stiff |
|-----------------|-----------------------------------|-----------------------------------|-----------------------------------|
| Axial load (kN) | 5688.4 | 9281.43 | 6506.32 |
| Reinforcements | <u>200@200 + 2 layers of 4000</u> | <u>200@200 + 2 layers of 2400</u> | <u>200@200 + 2 layers of 2400</u> |
| ϕ_y | 7.051E-04 | 7.433E-04 | 4.891E-04 |
| ϕ_u | 5.336E-03 | 3.651E-03 | 4.397E-03 |
| I_e/I_g | 0.4284 | 0.4069 | 0.2956 |
| M_y (kNm) | 30,830 | 30,880 | 40,500 |

Table C.6: Walls yield and ultimate displacements

| Parameter | 5-m Flexible | 5-m Center | 7-m Stiff |
|----------------|--------------|------------|-----------|
| ϕ_y 1/m | 7.05E-04 | 7.43E-04 | 4.89E-04 |
| ϕ_u 1/m | 5.34E-03 | 3.65E-03 | 4.40E-03 |
| Δ_y m | 0.476 | 0.502 | 0.330 |
| Δ_u m | 0.982 | 0.820 | 0.922 |
| Δ^*_y m | 0.334 | 0.502 | 0.574 |
| Δ^*_u m | 0.690 | 0.820 | 1.602 |

Table C.7: Axial load produced by gravity load combination D+0.5L+0.25S

| | 7-m Stiff | 5-m Center | 5-m Flexible | 6-m Orthogonal |
|-------------------|-----------|------------|--------------|----------------|
| Loads at the base | 8304.36 | 7638.84 | 7486.44 | 5173.43 |

Table C.8: Equivalent ultimate and yield displacements of the walls at C.M

| | Parameter | 5-m Flexible | 5-m Center | 7-m Stiff |
|--------|----------------|--------------|------------|-----------|
| | ϕ_y 1/m | 8.00E-04 | 8.00E-04 | 5.71E-04 |
| | Δ_y m | 0.540 | 0.540 | 0.385 |
| | Δ_u m | 0.846 | 0.846 | 0.911 |
| mode 1 | Δ^*_y m | 0.368 | 0.540 | 0.726 |
| | Δ^*_u m | 0.576 | 0.846 | 1.715 |
| mode 2 | Δ^*_y m | 4.327 | 0.540 | 0.206 |
| | Δ^*_u m | 6.781 | 0.846 | 0.486 |

Table C.9: Details of the design of the walls

| | 5-m Flexible | 5-m Center | 7-m Stiff | 6-m Orth. |
|-----------------|---|---|----------------|---|
| Axial load (kN) | 7486.44 | 7638.84 | 8304.36 | 5173.43 |
| Reinforcements | <u>2 layers of 2000</u> <u>+ 200@200</u> | <u>2 layers of 2400</u> <u>+ 200@200</u> | <u>200@200</u> | <u>2 layers of 3400</u> <u>+ 200@200</u> |
| ϕ_y | 7.28E-04 | 7.26E-04 | 5.00E-04 | 5.66E-04 |
| ϕ_u | 4.34E-03 | 4.28E-03 | 3.71E-03 | 5.363E-03 |
| M_y (kNm) | 26,600 | 26,850 | 33,620 | 34,620 |

Table C.10: First and second mode angles of twist and periods

| | Mode 1 | Mode 2 |
|-----------------------|---------|--------|
| Angle of twist Ψ | -0.0555 | 0.1156 |
| Period (sec) | 4.613 | 3.999 |

Table C.11: Yield and ultimate displacements as governed by the ductility capacity

| Parameter | 5-m Flexible | 5-m Center | 7-m Stiff |
|--------------|----------------|------------|-----------|
| ϕ_y 1/m | 7.28E-04 | 7.26E-04 | 5.00E-04 |
| ϕ_u 1/m | 4.34E-03 | 4.28E-03 | 3.71E-03 |
| Δ_y m | 0.491 | 0.490 | 0.338 |
| Δ_u m | 0.868 | 0.869 | 0.932 |
| mode 1 | Δ_y^* m | 0.340 | 0.490 |
| | Δ_u^* m | 0.601 | 0.869 |
| mode 2 | Δ_y^* m | 6.535 | 0.490 |
| | Δ_u^* m | 11.549 | 0.869 |
| | | | 0.484 |

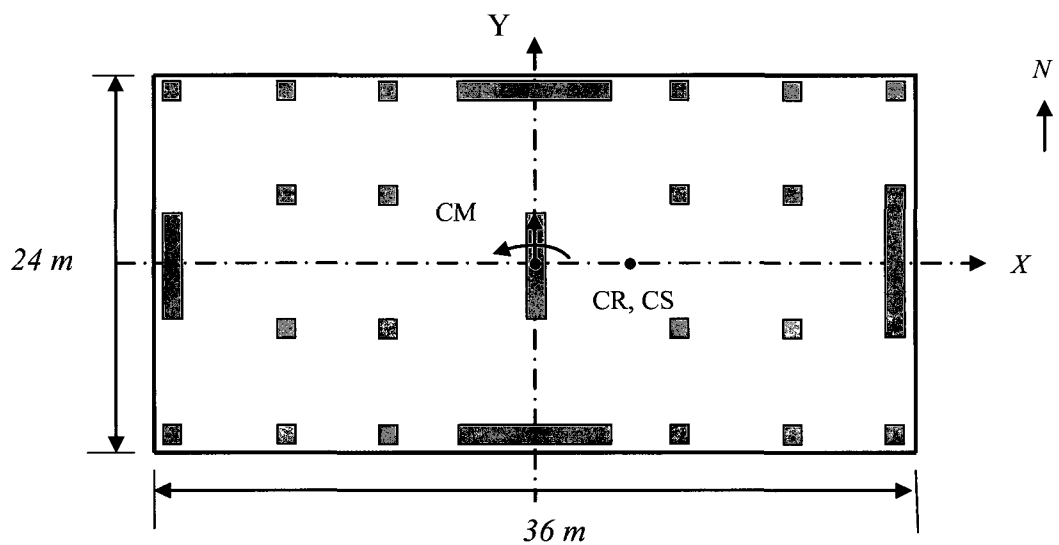


Figure C.1: Plan layout of torsionally stiff system

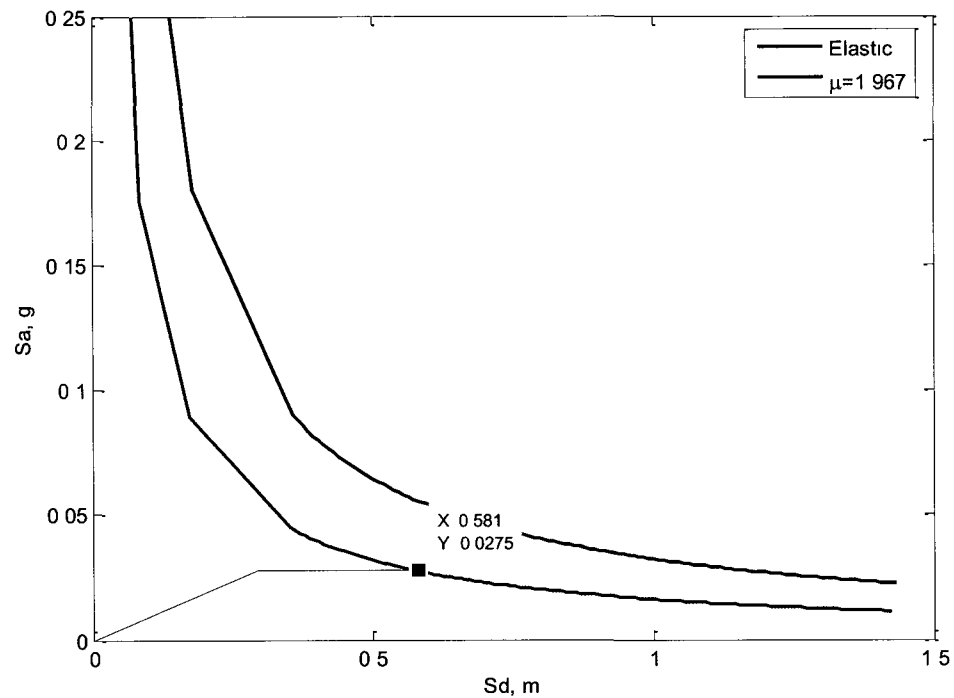


Figure C.2: Capacity and demand diagrams

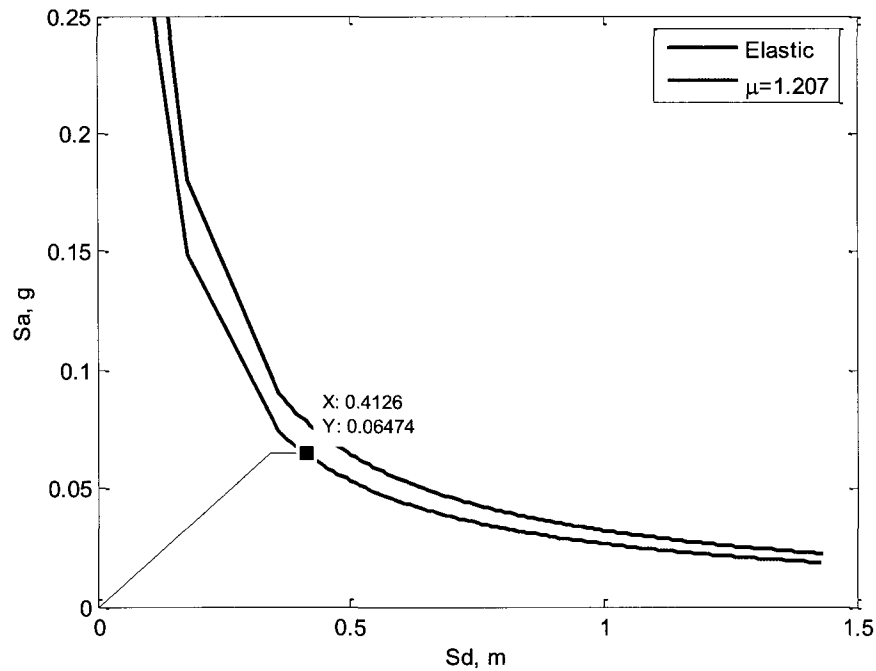


Figure C.3: Capacity and demand diagrams

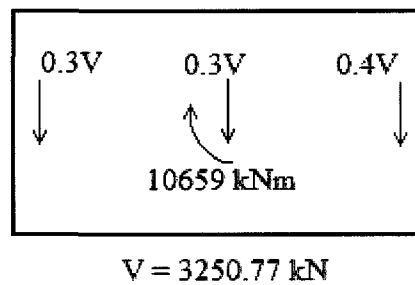


Figure C.4: Distribution of base shear among the resisting planes

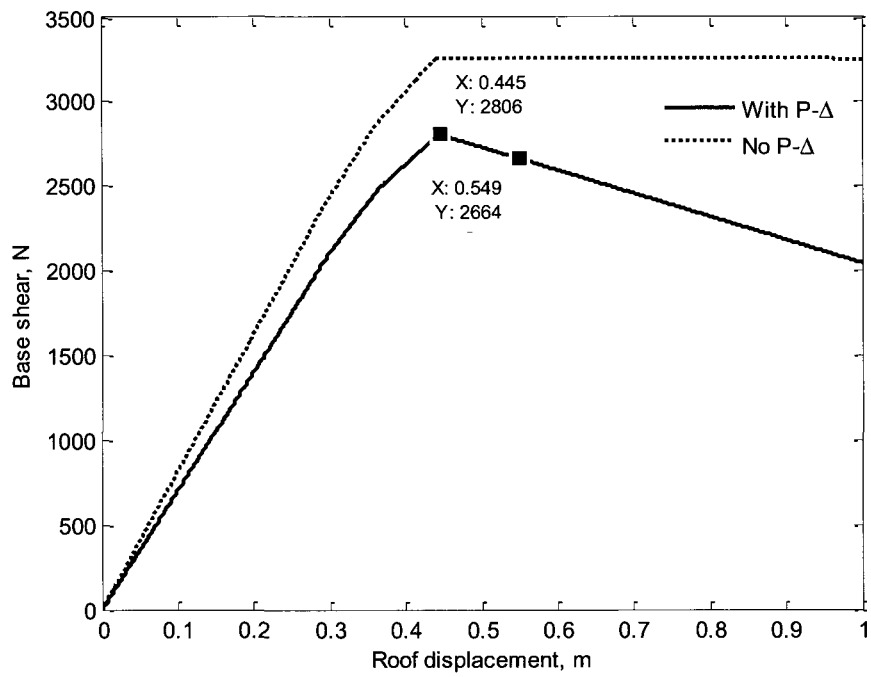


Figure C.5: First mode pushover curves

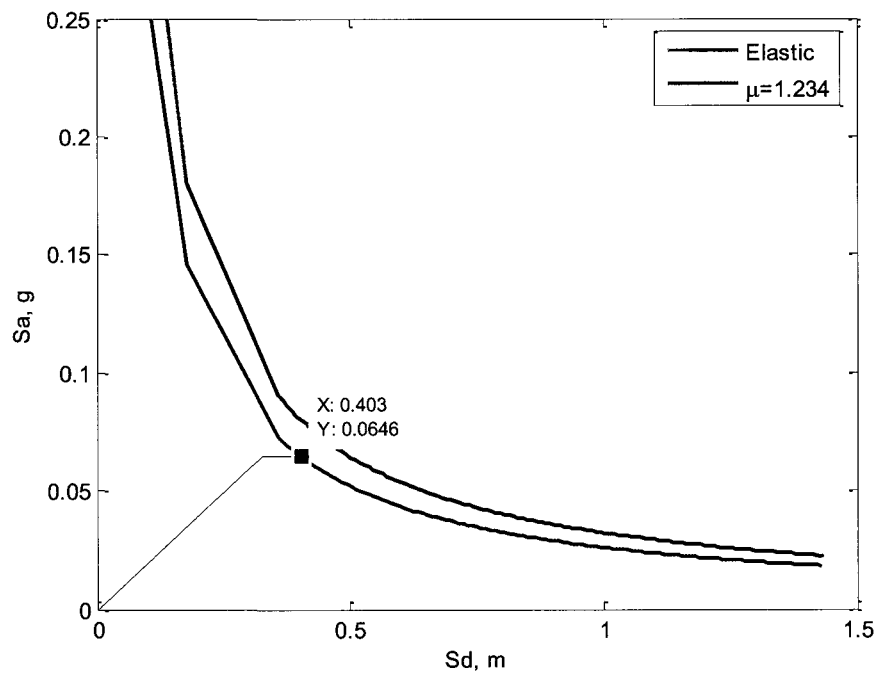


Figure C.6: Capacity and demand diagrams

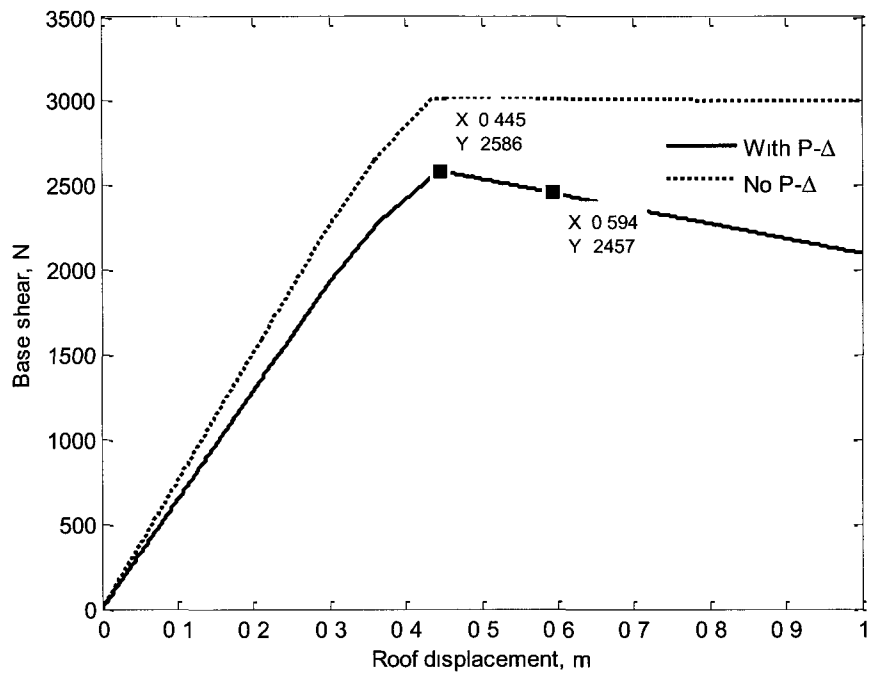


Figure C.7: pushover curves

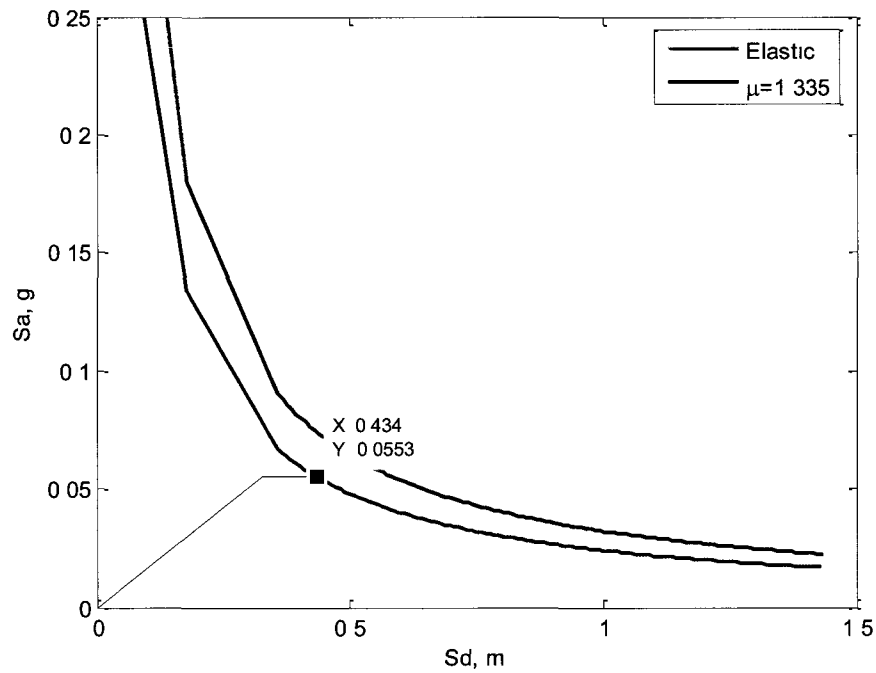


Figure C.8: Capacity and demand diagrams

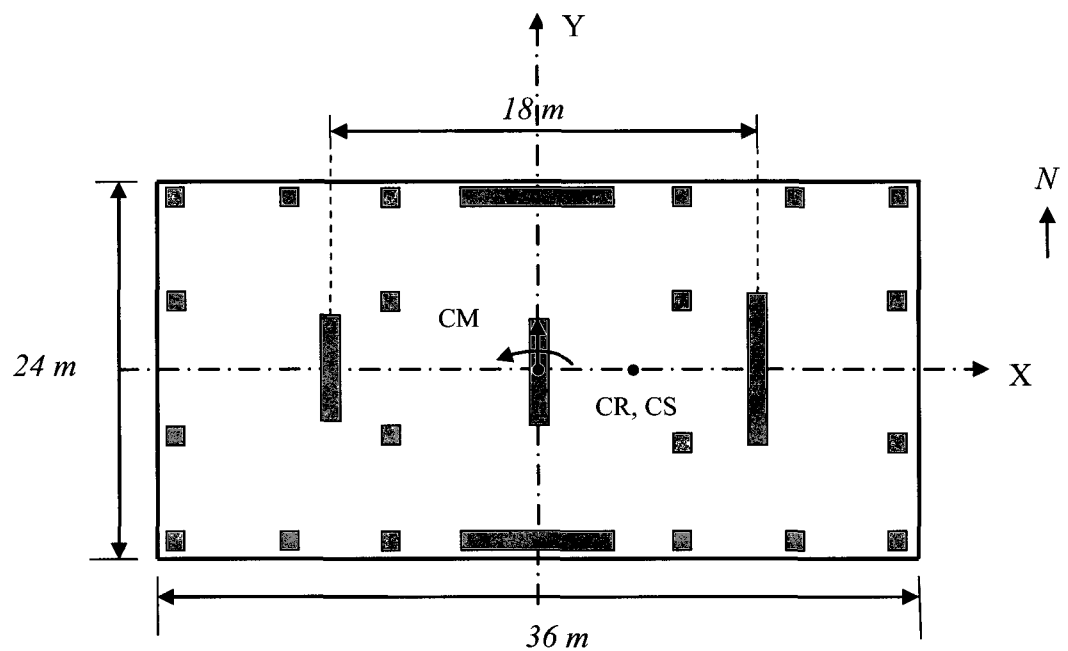


Figure C.9: Plan view of torsionally flexible system

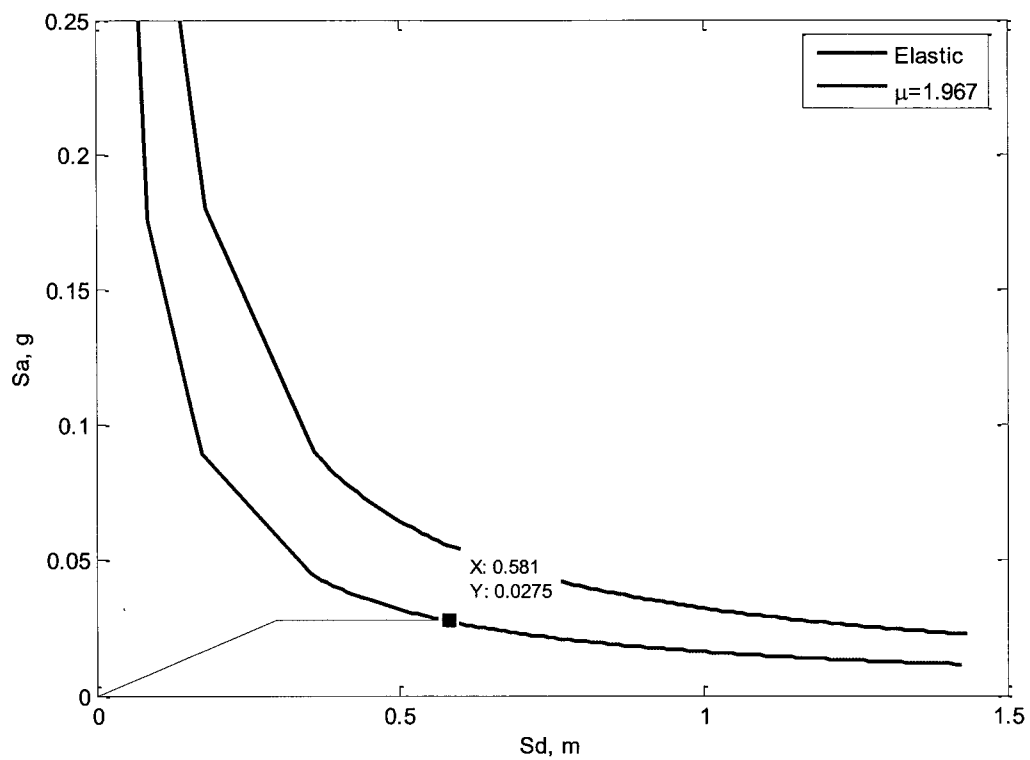


Figure C.10: Capacity and demand diagrams

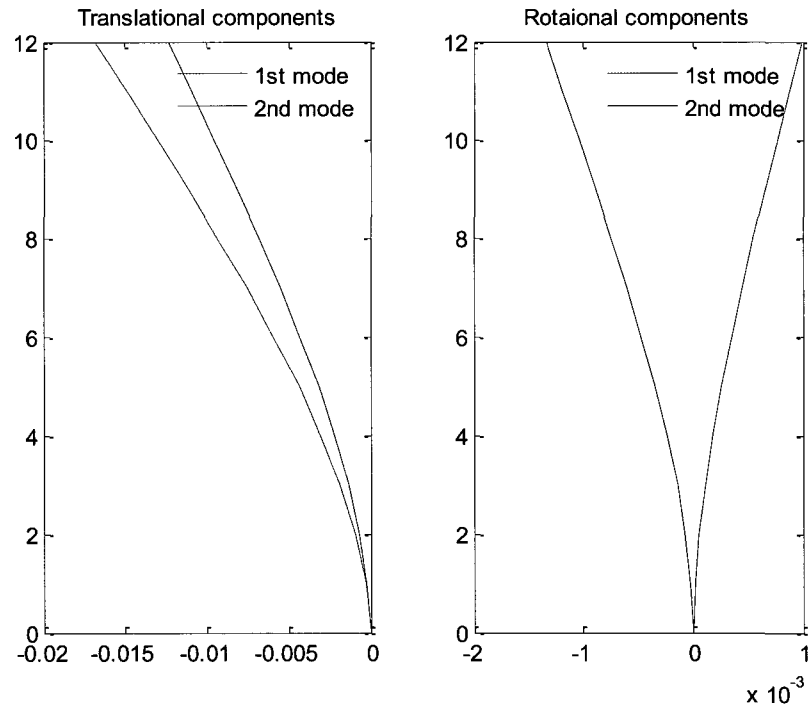


Figure C.11: Translational and torsional components of the first two modes

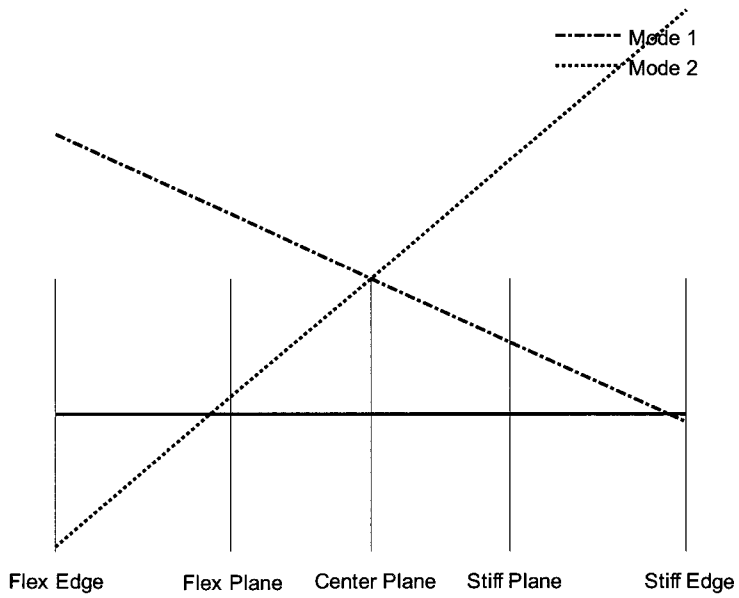


Figure C.12: Displacement configurations based on normalized mode shape at roof level

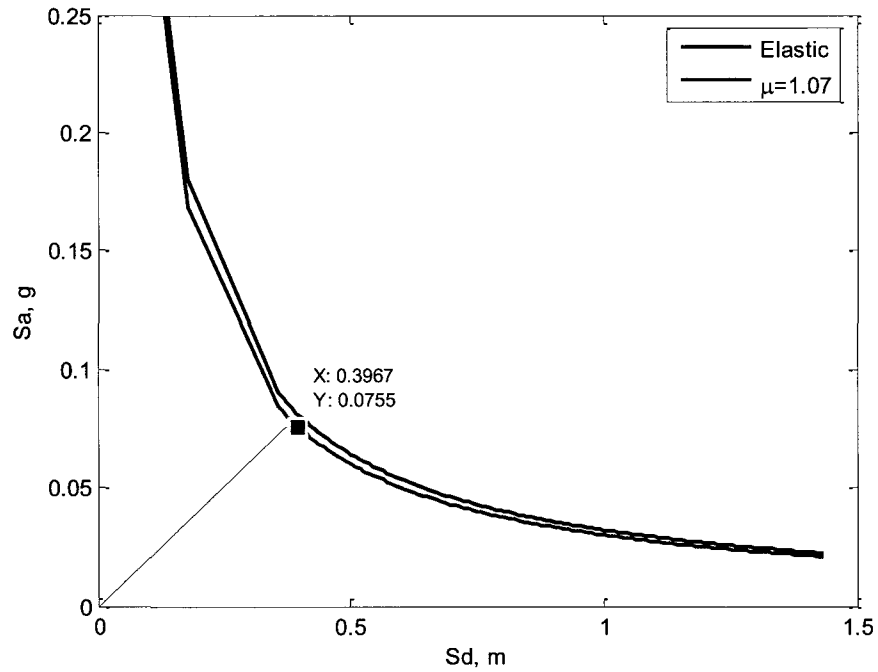


Figure C.13: Capacity and demand diagrams for the first mode

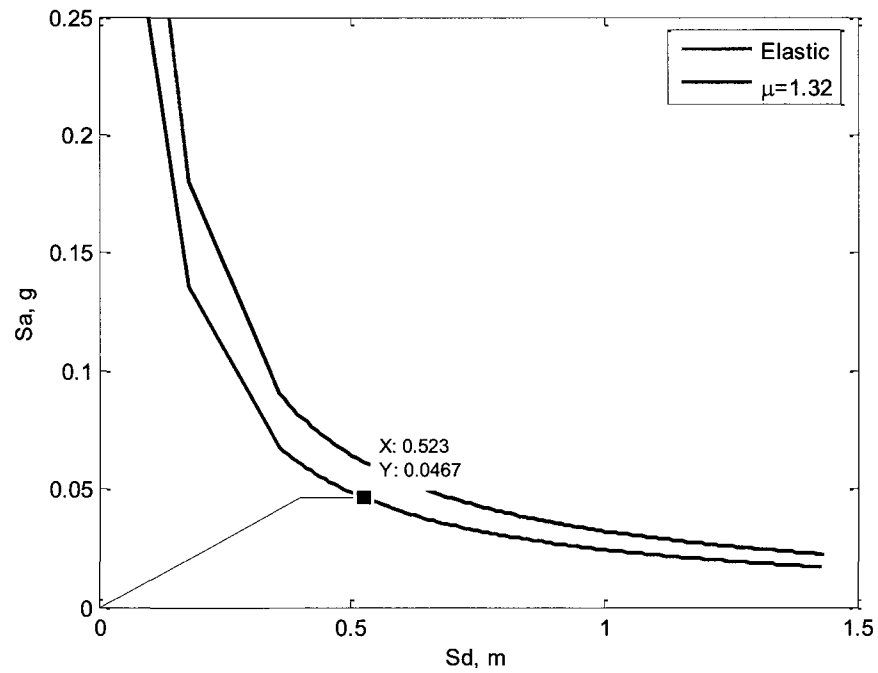


Figure C.14: Capacity and demand diagrams for the second mode

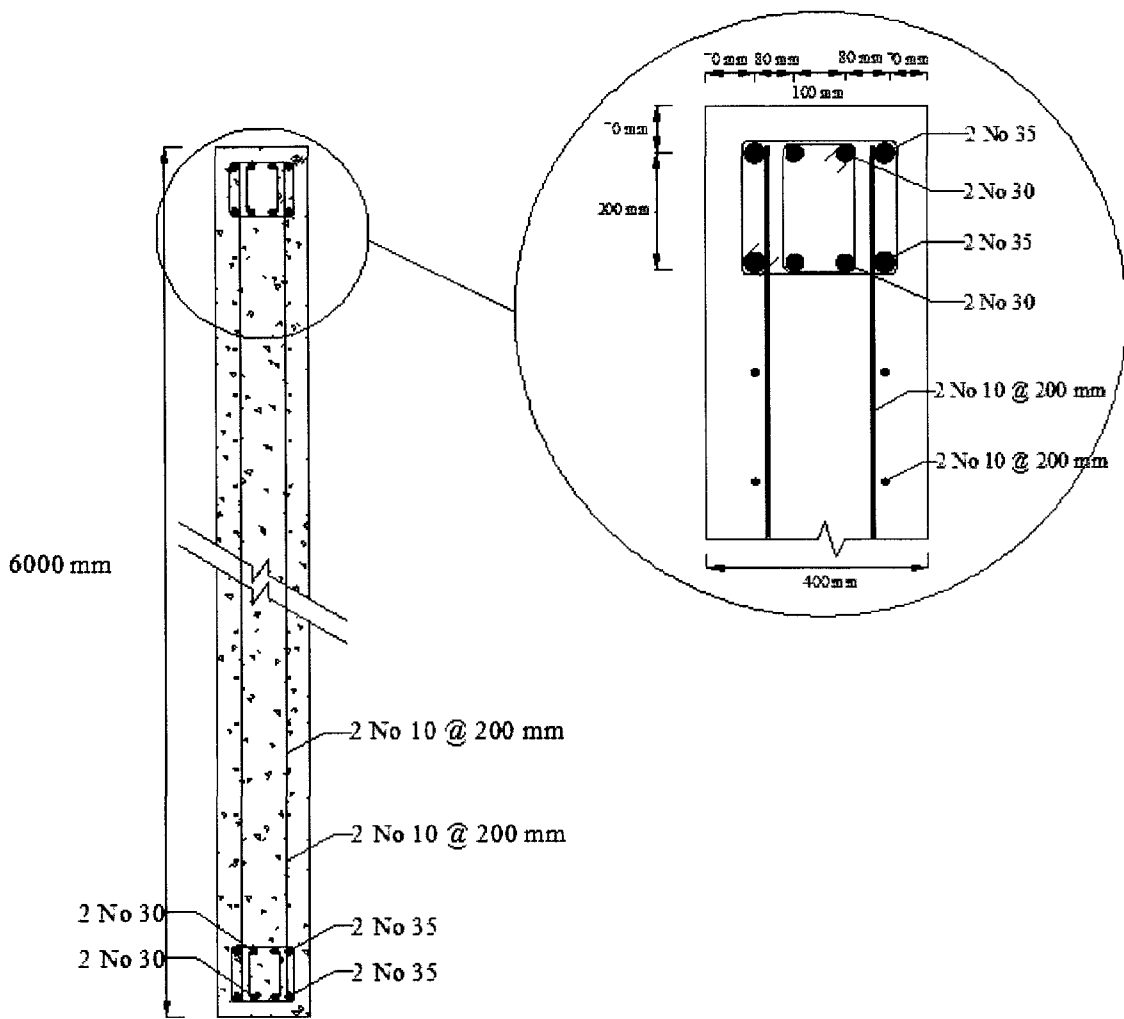


Figure C.15: Details of re-designed longitudinal reinforcements of 6-m orthogonal walls for torsionally flexible building

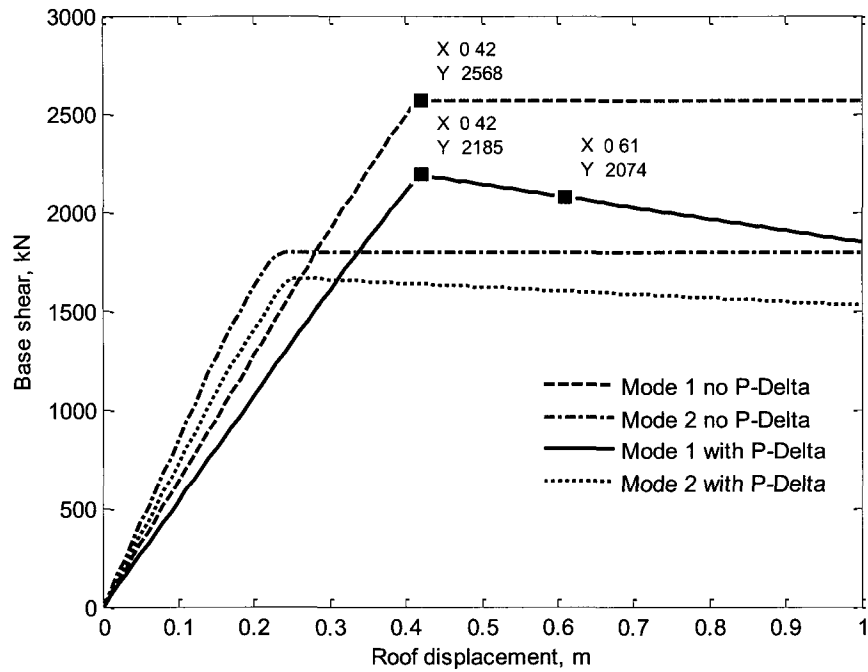


Figure C.16: Pushover curves with and without $P-\Delta$ for the first two modes

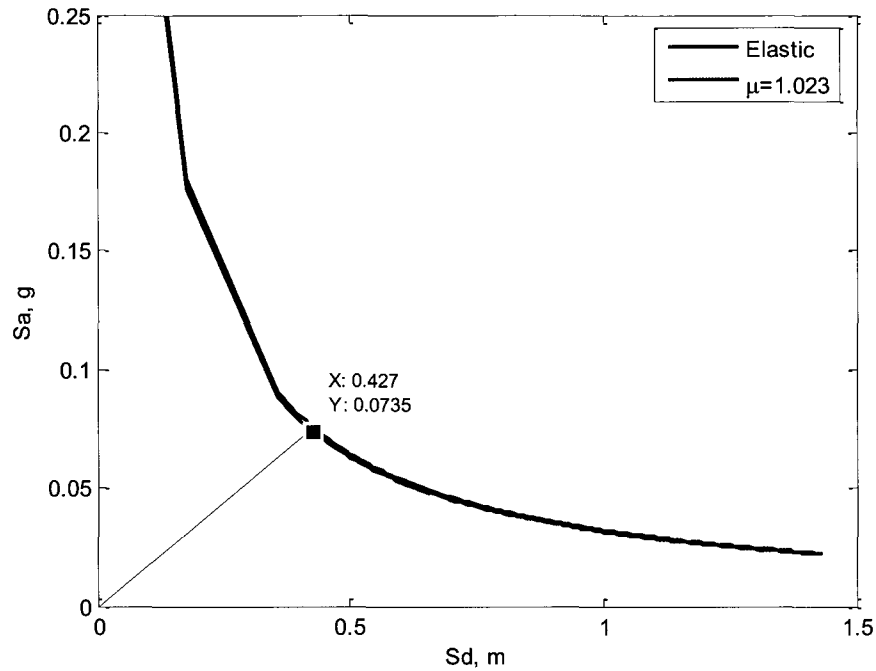


Figure C.17: Capacity and demand diagrams for the first mode

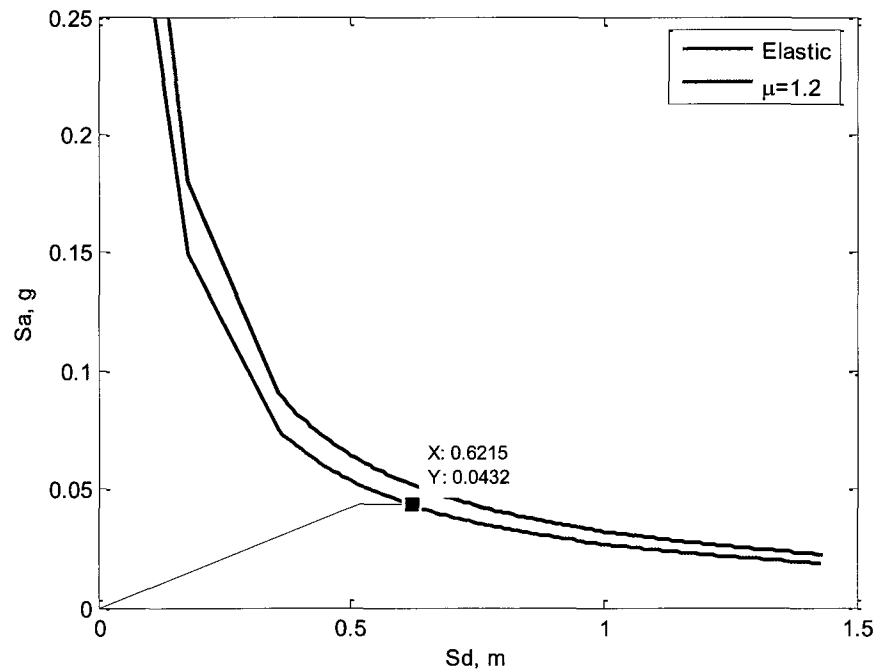


Figure C.18: Capacity and demand diagrams for the second mode

References

- Aschheim, M. (2002). "Seismic Design Based on the Yield Displacement." *Earthquake Spectra*, 18(4), 581-600.
- ATC-40. (1996). *Seismic Evaluation and Retrofit of Concrete Buildings*. Seismic Safety Commission, State of California, USA.
- Atkinson, G. M. (2009). "Earthquake time histories compatible with the 2005 National building code of Canada uniform hazard spectrum." *Canadian Journal of Civil Engineering*, 36(6), 991-1000.
- Aziminejad, A., Moghadam, A., and Tso, W. (2008). "A new methodology for designing multi-story asymmetric buildings" *14 th World Conference on Earthquake Engineering: Innovation Practice Safety*, International Association for Earthquake Engineering.
- Canadian Commission on Fire and Building Codes, (2005). The National Building Code of Canada, National Research Council of Canada, Ottawa, Canada.
- Castillo, R., Carr, A., and Restrepo, J. (2001). "The rotation of asymmetric plan structures." *Proceedings of Conference of the New Zealand Society for Earthquake Engineering* .
- Chopra, A. K., and Goel, R. K. (2004). "A modal pushover analysis procedure to estimate seismic demands for unsymmetric-plan buildings." *Earthquake Eng.Struct.Dyn.*, 33 903-928.

Chopra, A. K., and Goel, R. K. (2003). "Direct Displacement - Based Design: Use of Inelastic vs. Elastic Design Spectra." *Earthquake Spectra*, 17 47.

Chopra, A. K., and Goel, R. K. (2002). "A modal pushover analysis procedure for estimating seismic demands for buildings." *Earthquake Eng.Struct.Dyn.*, 31(3), 561-582.

Chopra, A. K., and Goel, R. K. (2000). "Evaluation of NSP to Estimate Seismic Deformation: SDF Systems." *J.Struct.Eng.*, 126(4), 482-490.

Chopra, A. K., and Goel, R. K. (1999). "Capacity-demand-diagram methods for estimating seismic deformation of inelastic structures: SDF systems." *University of California, Berkeley*.

Comartin, C. (2004). "A summary of FEMA 440: improvement of nonlinear static seismic analysis procedures." *Proc. of 13th World Conference on Earthquake Engineering, Vancouver, Canada*

De La Llera, and Chopra, A. K. (1995). "Understanding the inelastic seismic behaviour of asymmetric-plan buildings." *Earthquake Eng.Struct.Dyn.*, 24(4), 549-572.

De Stefano, M., and Pintucchi, B. (2010). "Predicting torsion - induced lateral displacements for pushover analysis: Influence of torsional system characteristics." *Earthquake Eng.Struct.Dyn.*, 39(12), 1369-1394.

De Stefano, M., and Pintucchi, B. (2008). "A review of research on seismic behaviour of irregular building structures since 2002." *Bulletin of Earthquake Engineering*, 6(2), 285-308.

Elrodesly, A. (2008). "Displacement based seismic design of reinforced concrete shear wall buildings." *M.A.Sc Thesis, Carleton University, Ottawa, Canada*.

Fajfar, P. (2000). "A Nonlinear Analysis Method for Performance-Based Seismic Design." *Earthquake Spectra*, 16(3), 573-592.

Fajfar, P. (1999). "Capacity spectrum method based on inelastic demand spectra." *Earthquake Eng.Struct.Dyn.*, 28(9), 979-993.

Fajfar, P., and Gaspersic, P. (1996). "The N 2 method for the seismic damage analysis of RC buildings." *Earthquake Eng.Struct.Dyn.*, 25(1), 31-46.

Fajfar, P., Marusic, D., and Perus, I. (2005). "Torsional effects in the pushover-based seismic analysis of buildings." *J.Earthquake Eng.*, 9(6), 831-854.

FEMA 273. (1997). "NEHRP Guidelines for the Seismic Rehabilitation of Buildings," *Federal Emergency Management Agency: Washington, DC, USA*.

FEMA 356. (2000). "Commentary for the seismic rehabilitation of buildings, FEMA-356." *Federal Emergency Management Agency, USA*.

Ghorbanie-Asl, M. (2007). "Performance based seismic design of building structures." *PhD Thesis, Carleton University, Ottawa, Canada*.

Humar, J., and Ghorbanie-Asl, M. (2005). "A new displacement based design method for buildings." *Proceedings of the 33rd CSCE Annual Conference: Gateway to Excellence*, Toronto, Canada.

Humar, J., and Ghorbanie-Asl, M. (2006). A practical method of displacement-based seismic design. *Eighth U.S. national Conference on Earthquake Engineering, San Francisco, California*.

Humar, J., Ghorbanie-Asl, M., and Pina, F. (2006). Displacement-based design of structures with significant higher mode contribution. *First European Conference on Earthquake Engineering and Seismology, Geneva, Switzerland*.

Humar, J., Elrodesley, A., and Fazileh, F. (2010). Displacement-based design of torsionally stiff unsymmetrical shear wall buildings. *Annual Conference, Canadian Society of Civil Engineering, Winnipeg, Canada*.

Humar, J., Mahgoub, M., and Ghorbanie-Asl, M. (2006). "Effect of second-order forces on seismic response." *Can.J.Civ.Eng./Rev.can.Genie Civ.*, 33(6), 692-706.

Humar, J., and Kumar, P. (1999). "Effect of orthogonal inplane structural elements on inelastic torsional response." *Earthquake Eng.Struct.Dyn.*, 28(10), 1071-1097.

Humar, J., and Kumar, P. (1998). "Torsional motion of buildings during earthquakes. II. Inelastic response." *Canadian Journal of Civil Engineering*, 25(5), 917-934.

Iwan, W. D., Huang, C. T., and Guyader, A. C. (2000). "Important features of the response of inelastic structures to near-field ground motion." *Auckland, New Zealand: New Zealand Society for Earthquake Engineering.*

Krawinkler, H., and Nassar, A. A. (1992). "Seismic design based on ductility and cumulative damage demands and capacities." *Nonlinear Seismic Analysis and Design of Reinforced Concrete Buildings*, 23-40.

Mattock, A. (1967). "Discussion of" Rotational capacity of reinforced concrete beams," by WG Corley." *Journal of the Structural Division*, 519-522.

Mazzoni, S., MacKenna, F., and Fenves, G. (2007). "OpenSees command language manual, PEER." *University of California, Berkeley, CA, USA.*

Myslimaj, B. (2005). "A design-oriented approach to strength distribution in single-story asymmetric systems with elements having strength-dependent stiffness." *Earthquake Spectra*, 21 197.

Myslimaj, B., and Tso, W. (2002). "A strength distribution criterion for minimizing torsional response of asymmetric wall - type systems." *Earthquake Eng.Struct.Dyn.*, 31(1), 99-120.

Newmark, N. M., and Hall, W. J. (1982). "Earthquake Spectra and Design." *Engineering Monographs on Earthquake Criteria, Structural Design, and Strong Motion Records*, Berkeley, CA: *Earthquake Engineering Research Institute*, | c1982, .

Paulay, T. (2002a). "A Displacement-Focused Seismic Design of Mixed Building Systems." *Earthquake Spectra*, 18(4), 689-718.

Paulay, T. (2002b). "An estimation of displacement limits for ductile systems." *Earthquake Eng.Struct.Dyn.*, 31(3), 583-600.

Paulay, T. (2001a). "A Re-definition of the Stiffness of Reinforced Concrete Elements and its Implications in Seismic Design." *Struct.Eng.Int.*, 11(1), 36-41.

Paulay, T. (2001b). "Seismic response of structural walls: recent developments", *Canadian Journal of Civil Engineering*, 28(6), 922-937.

Paulay, T. (2000). "A simple displacement compatibility-based design strategy for reinforced concrete buildings." *Proceedings of the 12th World Conference on Earthquake Engineering, Auckland, New Zealand, Paper*, .

Paulay, T. (1998). "Torsional Mechanisms in Ductile Building Systems." *Earthquake Eng.Struct.Dyn.*, 27(10), 1101-1121.

Perus, I., and Fajfar, P. (2005). "On the inelastic torsional response of single-storey structures under bi-axial excitation." *Earthquake Eng.Struct.Dyn.*, 34(8), 931-941.

Peruš, I., and Fajfar, P. (2002). *On inelastic seismic response of an asymmetric single-storey structures under bi-axial excitation*.

Pettinga, D., Pampanin, S., Christopoulos, C., Carr, A., and Castillo, R. (2008). "Experimental investigation into residual displacements due to inelastic torsional

response" *14 th World Conference on Earthquake Engineering: Innovation Practice Safety*, International Association for Earthquake Engineering, .

Pettinga, J., Priestley, M., Pampanin, S., and Christopoulos, C. (2006). "Accounting for the effects on residual deformations due to torsional response.".

Pina Burgos, F.E. (2006). "Displacement-based seismic design of shear wall buildings." *M.A.Sc Thesis, Carleton University, Ottawa, Canada.*

Prakash, V., Powell, G., and Campbell, S. (1993). "DRAIN 2D User Guide V 1.10." *University of California at Berkeley, CA.*

Priestley, M. (2003). *Myths and Fallacies in Earthquake Engineering, Revisited*. IUSS Press.

Priestley, M. K., MJ. (2000). "Direct displacement-based seismic design of concrete buildings." *Bulletin of the New Zealand National Society for Earthquake Engineering*, 33(4), 421-444.

Priestley, M., Calvi, G., and Kowalsky, M. (2007). *Direct displacement-based seismic design*. IUSS Press, Pavia, Italy, .

Priestley, M., and Kowalsky, M. (1998). "Aspects of drift and ductility capacity of rectangular cantilever structural walls." *Bulletin of the New Zealand National Society for Earthquake Engineering*, 31(2), 73-85.

Priestley, M., and Kowalsky, M. (1998). "Aspects of drift and ductility capacity of rectangular cantilever structural walls." *Bulletin of the New Zealand National Society for Earthquake Engineering*, 31(2), 73-85.

Rutenberg, A. (1992). "Nonlinear response of asymmetric building structures and seismic codes: a state of the art review." *Nonlinear Seismic Analysis and Design of Reinforced Concrete Buildings*, 281–305.

Rutenberg, A. "EAEE Task Group (TG) 8: Behaviour of irregular and complex structures, asymmetric structures—Progress since 1998." *proceeding of 12th European Conference on Earthquake Engineering, London, UK.*

SEAOC. (1995). "Performance-based seismic engineering Vision 2000 Report." *Structural Engineers Association of California, Sacramento, California.*

Somerville, P. G., Venture, S. A. C. J., and Woodward-Clyde Federal Services (Firm). (1997). *Development of ground motion time histories for phase 2 of the FEMA/SAC steel project.* SAC Joint Venture.

Sommer, A., and Bachmann, H. (2005). "Seismic behavior of asymmetric RC wall buildings: principles and new deformation - based design method." *Earthquake Eng.Struct.Dyn.*, 34(2), 101-124.

Sullivan, T., Priestley, M., and Calvi, G. (2006). "Direct displacement-based design of frame-wall structures." *J.Earthquake Eng.*, 10 91-124.

Trombetti, T., and Conte, J. (2005). "New insight into and simplified approach to seismic analysis of torsionally coupled one-story, elastic systems." *J.Sound Vibrat.*, 286(1-2), 265-312.

Vamvatsikos, D., and Cornell, C. A. (2002). "Incremental dynamic analysis." *Earthquake Eng.Struct.Dyn.*, 31(3), 491-514.

Vidic, T., Fajfar, P., and Fischinger, M. (1994). "Consistent inelastic design spectra: Strength and displacement." *Earthquake Eng.Struct.Dyn.*, 23(5), 507-521.

Xue, Q. (2001). "A direct displacement-based seismic design procedure of inelastic structures." *Eng.Struct.*, 23(11), 1453-1460.

Xue, Q., and Chen, C. C. (2003). "Performance-based seismic design of structures: a direct displacement-based approach." *Eng.Struct.*, 25(14), 1803-1813.

Yavari, S. (2001). "Design of Concrete Shear Wall Buildings for Earthquake Induced Torsion." *M.A.Sc. Thesis, Carleton University, Ottawa, Canada*